cGMP Signaling as a Molecular Target for Central Adaptation in Age-Related Cochlear Synaptopathy

Dissertation

der Mathematisch-Naturwissenschaftlichen Fakultät

der Eberhard Karls Universität Tübingen

zur Erlangung des Grades eines

Doktors der Naturwissenschaften

(Dr. rer. nat.)

vorgelegt von

Dila Calis

aus Izmir, Türkei

Tübingen

2024

Gedruckt mit Genehmigung der Mathematisch-Naturwissenschaftlichen Fakultät der Eberhard Karls Universität Tübingen.

Tag der mündlichen Qualifikation:	26.06.2024
Dekan:	Prof. Dr. Thilo Stehle
1. Berichterstatterin:	Prof. Dr. Marlies Knipper
2. Berichterstatter:	Prof. Dr. Peter Ruth
3. Berichterstatter:	Prof. Dr. Harald Schmidt

Acknowledgments

It does not kill you, but it does not make you stronger either, hearing loss…

Table of Contents

Abbreviations

ABR, auditory brainstem response

ACTH, adrenocorticotropic hormone

AMPA, a-amino-3-hydroxy-5-methyl-4-isoxazole propionic acid

ANP, atrial natriuretic peptide

Arc/Arg3.1, activity-regulated cytoskeleton-associated protein

ASSR, auditory steady-state response

AVP, arginine vasopressin

BDNF, brain-derived neurotrophic factor

BK channels, large conductance Ca^{2+}- and voltage-activated K^{+} channels

BNP, B-type natriuretic peptide,

Ca^{2+}, calcium

CaMKII, Ca2+ /calmodulin-dependent protein

cAMP, cyclic adenosine monophosphate

cGK, cGMP-dependent protein kinase

cGMP, cyclic guanosine monophosphate

CNP, C-type natriuretic peptide

CRE, cAMP response element

CREB, cAMP response element binding protein

CRF, corticotropin-releasing factor

Epac, exchange protein activated by cAMP

GC-A, guanylyl cyclase-A

GR, glucocorticoid receptors

GRE, glucocorticoid-responsive elements

GTP, guanosine triphosphate

HPA, hypothalamic-pituitary-adrenal axis

K^{+}, potassium

LTCC, L-type calcium channels

LTD, long-term depression

LTP, Long-term potentiation

mPFC, medial prefrontal cortex

MR, mineralocorticoid receptor

NMDA, N-methyl-D-aspartate

NO, nitric-oxide

NO-GC, soluble guanylyl cyclase

NPRs, natriuretic peptide receptors

PDE, phosphodiesterase

pGC, particulate guanylyl cyclase

PKA, protein kinase A

PKG, protein kinase G

Pkg1, cGMP-dependent protein kinase 1

PPF, paired-pulse facilitation

PV, parvalbumin

PVN, paraventricular nucleus

sAC, soluble adenylyl cyclase

SGN, spiral ganglion neurons

SNR, signal-to-noise ratio

SR, spontaneous rate

tAC, transmembrane adenylyl cyclase

TrkB, tropomyosin receptor kinase B

Zusammenfassung

Altersbedingter Hörverlust entsteht graduell über Jahre als Folge sich ansammelnder umweltbedintger Lärmbelastung. Cochleäre Synaptopathie entsteht durch die Schädigung der Synapse zwischen Haarzellen in der Cochlea und Hörnervenfasern. Diese Schädigung kann zu Hörproblemen, insbesondere in lauten Umgebungen führen. Dieser Zustand kann zu altersbedingtem Hörverlust beitragen und wird mit einer Beeinträchtigung der auditiven Wahrnehmung in Verbindung gebracht. Vor allem die zeitliche Verarbeitung des Hörens, die für das Verstehen von Sprache, insbesondere in komplexen Hörumgebungen, entscheidend ist, ist beeinträchtigt. Cochleäre Synaptopathie kann zu Defiziten der zeitlichen Auflösung führen, wenn die verringerte auditorische Eingangsaktivität nicht in höheren auditorischen Zentren (Mittelhirn) kompensiert werden kann. Ob cochleräre Synaptopathie kompensiert werden kann ist sehr von der individuellen Kompensationsfähigkeit abhängig, ist sie hoch sprechen wir von „*high compensators*“, ist sie niedrig von „*low compensators*“. In unseren Studien wollten wir die zugrundeliegenden Mechanismen für zentrale auditorische Kompensation identifizieren. Da zentrale auditorische Kompensation einen gedächtnisabhängigen Anpassungsprozess erfordert, haben wir die Wirkung eines PDE9A-Hemmers untersucht, der, über die Erhöhung des cGMP Spiegels, positiv auf kognitive Prozesse einwirkt. Diese Studien wurden an mittelalten (9 - 14 Monate) Mäusen durchgeführt. Wir konnten beobachten das *high compensators* im Gegensatz zu *low compensators* einen erhöhten Kortikosteronspiegel als Reaktion auf Stress (Vehikelinjektionen) aufweisen. Bei *high compensators* führte diese Stressreaktion zu mehreren negativen Effekten bei der Hörverarbeitung. Es kam zu Beeinträchtigungen der Funktion der inneren Haarzellen, des LTP und der BDNF-Expression, die bei *low compensators* nicht beobachtet wurden. Die Behandlung mit einem PDE9A-Hemmer kehrte die negativen Effekte von Stress bei *high compensators* um, führte aber bei *low compensators* nicht zu einer Verbesserung der Ausgangslage. Auch auf zeitliche Kodierung. die bei *low compensators* weniger präzise als bei *high compensators* war, hatte der PDE9A-Hemmer keinen Effekt. Des Weiteren wurden LTP-Messungen durchgeführt und Änderungen der synaptischen Dornfortsätze analysiert. Die Ergebnisse aus beiden Analysen bestätigten, dass *low compensators* eine geringere Anpassungsfähigkeit haben *high compensators*, aber nicht *low compensators*, wiesen eine Anpassung des LTD und eine erhöhte Anzahl von anpassungsfähigen Dornfortsätzen auf. Sowohl LTD als auch die Veränderung der Dornfortsätze konnten durch Stress beeinträchtigt werden, was durch die Behandlung mit einem PDE9A-Hemmer verhindert wurden. Wir konnten zeigen, dass die Fähigkeit zur zentralen Kompensation von cochleärer Synaptopathie von Glukokortikoid und cGMP abhängt. Wir vermuten daher, dass eine gedämpfte Stressrektion zum Fehlen des Kompensationsmechanismus führen kann, was möglicherweise ein Baustein bei der Verbindung von Hörverlust und Demenz sein könnte. Zusätzlich untersuchten wir die Rolle der Stressrezeptoren MR und GR für die Modulation der Stressreaktion, insbesondere bei auditorischer Verarbeitung und synaptischer Plastizität im Hippocampus. Wir konnten zeigen, dass MR-cKO-Mäuse in der Lage waren, eine veränderte Aktivität des Hörnervs zentral zu kompensieren, während dies bei GR-cKO-Mäusen nicht der Fall war. Zusätzlich untersuchten wir die Expression von cGMP-Generatoren (GC-A, NO-GC) und Arc, als Regulator der synaptischen Plastizität. Die

Veränderungen des LTPs sowohl bei MR cKO- als auch bei GR cKO-Mäusen standen in engem Zusammenhang mit ihrer zentralen Kompensationsfähigkeit, was auf einen postsynaptischen Mechanismus hindeutet. Die Deletion von MR beeinflusst die Expression von GR, NO-GC und Arc, die alle an der Regulierung der Kompensationsfähigkeit beteiligt sind. Die GC-A-Expression und das ABR-Wellen-IV/I-Verhältnis, als Maß der Kompensation, waren bei MR cKO-Mäusen, mit erhöhter GR-Expression, erhöht, während sie bei GR cKO-Mäusen, mit beeinträchtigter GR-Expression, niedriger oder unverändert waren. Dies deutet darauf hin, dass GR-abhängige Prozesse LTP und auditorische neuronale Verstärkung über GC-A beeinflussen könnten. Schließlich untersuchten wir in Zusammenhang mit synaptischer Plastizität im Hippocampus die Rolle von Ca^{2+}- und spannungsaktivierten K^+-Kanälen mit großer Leitfähigkeit (BK-Kanäle), insbesondere während Lernprozessen und Gedächtnisbildung. Hierfür wurde BK gezielt in CA1-Pyramidenneuronen deletiert. Unsere Ergebnisse zeigten, eine Beeinträchtigung von elektrisch und chemisch induziertem LTP in BK cKOs im Vergleich zu Kontrollen. Zusätzlich wurden Beeinträchtigungen bei der Gedächtnisbildung und -abruf im Morris-Wasser-Labyrinth gezeigt. Außerdem wurde eine veränderte Dynamik im intrazellulären K^+ und Ca^{2+} durch Plastizitätsänderungen nach LTP beobachtet. Diese Ergebnisse deuten darauf hin, dass BK-Kanäle eine wichtige Rolle bei LTP im Hippocampus spielen, indem sie den Kaliumausstrom ermöglichen, der für die Induktion von LTP entscheidend ist und wesentlich zu Lernen und Gedächtnisbildung beiträgt.

Summary

Age-related hearing loss may gradually occur over the years due to adverse effects of accumulated environmental or occupational noise exposure. Cochlear synaptopathy is a condition where the synapses between the hair cells in the cochlea and the auditory nerve fibers are damaged. This damage can lead to difficulties in hearing, especially in noisy environments. This condition can contribute to age-related hearing loss and has been linked with impaired auditory perception and temporal auditory processing, which is crucial for understanding speech, particularly in complex listening environments. However, cochlear synaptopathy does not necessarily lead to temporal resolution deficits when the reduced auditory input is compensated by midbrain responses (neural gain). Individuals may vary in their ability to compensate for cochlear synaptopathy with *low compensators* showing reduced central compensation abilities and *high compensators* exhibiting robust compensation. In our studies, we aimed to identify the underlying mechanisms for central auditory compensation. Given that central auditory compensation needs a memory-dependent adaptation process, we investigated a cognitive enhancer, a PDE9A inhibitor. PDE9A inhibitor is suggested to have positive effects on learning and memory by increasing cGMP levels. To test this, we used an animal model involving middle-aged mice. During these studies, we observed that *high compensators* had elevated corticosterone levels in response to stress (vehicle injections) while *low compensators* did not show this response. In *high compensators,* stress led to several negative effects on auditory processing, inner hair cell function, LTP, and BDNF expression which were not observed in *low compensators*. Treatment with PDE9A inhibitor reversed the negative effects of stress in *high compensators* but did not show improvements in *low compensators*. On the other hand, temporal coding in *low compensators* was less precise than in *high compensators* which were not improved by the treatment with PDE9A inhibitor. Further analysis of LTD measurement and the dendritic spine remodeling confirmed that *low compensators* have reduced capacity for developing adaptation *high compensators*, but not *low compensators*, exhibited LTD adjustment and higher amount of learning spines which were also impaired through vehicle injection and prevented by PDE9A inhibitor treatment. We could show that the ability to centrally compensate for cochlear synaptopathy is a mechanism dependent on glucocorticoid and cGMP. Hence, we suggest that a blunted stress response can lead to a failure in this compensation mechanism, potentially contributing to the link between hearing loss and dementia. Further, we investigated the role of stress receptors MR and GR in the modulation of the stress response, particularly in auditory processing and hippocampal synaptic plasticity. We could reveal that MR cKO mice were able to compensate for reduced auditory nerve activity in the higher auditory pathway, while GR cKO mice were not. Additionally, we checked for the expression of cGMP generators and Arc for the synaptic plasticity regulator. Changes in LTP in both MR cKO and GR cKO mice were more closely related to their central compensation capacity, indicating a postsynaptic mechanism. The deletion of MR influences the expression of GR, NO-GC, and Arc, all of which are involved in the regulation of auditory pathway compensation. The GC-A expression and ABR Wave IV/I ratio, as a measure for compensation, were enhanced in MR cKO mice, that have elevated GR, but were lower or unchanged in GR cKO mice with impaired GR expression. This suggests that GR-

dependent processes might influence LTP and auditory neural gain through GC-A. Finally, for the hippocampal synaptic plasticity, we investigated the role of large conductance Ca^{2+}- and voltage-activated K^+ channels (BK channels) in cognitive functions. Particularly in learning and memory by specifically deleting BK in CA1 pyramidal neurons. Our results revealed impaired electrical and chemical LTP in cKO brain slices compared to controls in addition to impaired memory acquisition and retrieval in the Morris Water Maze and altered dynamics of intracellular K^+ and Ca^{2+} concentration during synaptic plasticity events in LTP. These findings suggest that BK channels play an important role in hippocampal LTP by mediating potassium outflow which is crucial for the induction of LTP and significantly contributes to learning and memory.

List of Publications in the Thesis

*Equal Contribution

a) Accepted Papers

Savitska, D., Hess, M**., Calis, D.**, Marchetta, P., Harasztosi, C., Fink, S., Eckert, P., Ruth, P., Rüttiger, L., Knipper, M., & Singer, W. (2022). Stress Affects Central Compensation of Neural Responses to Cochlear Synaptopathy in a cGMP-Dependent Way. Frontiers in neuroscience, 16, 864706.

Calis, D.*, Hess, M.*, Marchetta, P., Singer, W., Modro, J., Nelissen, E., Prickaerts, J., Sandner, P., Lukowski, R., Ruth, P., Knipper, M., & Rüttiger, L. (2023). Acute deletion of the central MR/GR steroid receptor correlates with changes in LTP, auditory neural gain, and GC-A cGMP signaling. Frontiers in molecular neuroscience, 16, 1017761.

Pham, T., Hussein, T., **Calis, D**., Bischof, H., Skrabak, D., Cruz Santos, M., Maier, S., Spähn, D., Kalina, D., Simonsig, S., Ehinger, R., Groschup, B., Knipper, M., Plesnila, N., Ruth, P., Lukowski, R., & Matt, L. (2023). BK channels sustain neuronal Ca^{2+} oscillations to support hippocampal long-term potentiation and memory formation. Cellular and molecular life sciences: CMLS, 80(12), 369.

b) Manuscript in Preparation

Calis, D., Hess, M., Harasztosi, C., Fink, S., Jacob, MH., Ruth, P., Rüttiger, L., Knipper, M., & Singer, W. Plastic dendritic spines and subsequent structural modifications support central auditory adaptation in response to age-related cochlear synaptopathy.

Personal Contribution to the Studies

*Equal Contribution

a) Accepted Papers

Savitska, D., Hess, M**., Calis, D.**, Marchetta, P., Harasztosi, C., Fink, S., Eckert, P., Ruth, P., Rüttiger, L., Knipper, M., & Singer, W. (2022). Stress Affects Central Compensation of Neural Responses to Cochlear Synaptopathy in a cGMP-Dependent Way. Frontiers in neuroscience, 16, 864706.

My contribution to this study: I ran two cohorts of mice in which I performed pre-post ABR and ASSR measurements and collected pre-post blood from the tail vein of mice. I did the 10 days of treatment with a PDE9A inhibitor or vehicle. Further, I did the brain and cochlea collection. I analyzed in vitro electrophysiology measurements data of long-term potentiation, paired-pulse facilitation, and input-output relation and prepared the manuscript figures and statistics. I also performed 2 sets of ELISA blood corticosterone assays and further did statistical analysis and prepared figures for the publication. Finally, I contributed to the writing of the manuscript for the results and methods section.

Calis, D.*, Hess, M.*, Marchetta, P., Singer, W., Modro, J., Nelissen, E., Prickaerts, J., Sandner, P., Lukowski, R., Ruth, P., Knipper, M., & Rüttiger, L. (2023). Acute deletion of the central MR/GR steroid receptor correlates with changes in LTP, auditory neural gain, and GC-A cGMP signaling. Frontiers in molecular neuroscience, 16, 1017761.

My part in this study was to analyze in vitro electrophysiology measurements data of long-term potentiation, and paired-pulse facilitation, input-output relation and prepare the manuscript figures and statistics. Further, I contributed to the manuscript writing: methods and results sections as well as the reviewing processes of the manuscript submission.

Pham, T., Hussein, T., **Calis, D**., Bischof, H., Skrabak, D., Cruz Santos, M., Maier, S., Spähn, D., Kalina, D., Simonsig, S., Ehinger, R., Groschup, B., Knipper, M., Plesnila, N., Ruth, P., Lukowski, R., & Matt, L. (2023). BK channels sustain neuronal Ca^{2+} oscillations to support hippocampal long-term potentiation and memory formation. Cellular and molecular life sciences: CMLS, 80(12), 369.

In this study, I performed the cLTP recording in both WT and cKO mice and further analyzed the data of long-term potentiation, paired-pulse facilitation, and input-output relation and prepared the manuscript figures and statistics.

b) Manuscript in Preparation

Calis, D., Hess, M., Harasztosi, C., Fink, S., Jacob, MH., Ruth, P., Rüttiger, L., Knipper, M., & Singer, W. Plastic dendritic spines and subsequent structural modifications support central auditory adaptation in response to age-related cochlear synaptopathy.

For this study, I performed pre-post ABR and ASSR measurements. I performed the drug treatment with a PDE9A inhibitor or vehicle. After post hearing measurements I performed LTP-LTD recording or

Golgi-Cox staining or tissue fixation for histology from the brain. I also collected cochlea from these mice. Further, I analyzed pre-post ABR and ASSR data, in vitro electrophysiology data and I applied the Golgi-Cox impregnated brain sectioning and mounting and later imaging and dendritic spines analysis. Finally, I did the statistical analysis and the figures for the manuscript in addition to writing the manuscript.

1. Introduction

According to the World Report on Hearing 2021 by the WHO (Organization, 2021), more than 1.5 billion people experience hearing loss to a certain degree. This number is expected to rise to 2.5 billion by 2050 in industrialized countries (Fortunato et al., 2016). Typically, hearing loss could occur due to acoustic trauma, ototoxic drug treatments, and co-morbid diseases like hypertension and diabetes (Cruickshanks et al., 2003). But in most cases, hearing loss occurs following cumulative exposure to environmental or occupational noise (Gourevitch et al., 2014) which makes it a disease that progresses slowly and mostly remains undetected for long periods (Li-Korotky, 2012).

All sensory systems can be affected gradually as individuals get older; however, hearing is the most severely affected sensory system among others, in humans (Bowl & Dawson, 2019; Jafari et al., 2019). Furthermore, age-related hearing loss, also referred to as presbycusis, has been reported as the third leading cause of disability in older adults and the most relevant risk factor for cognitive decline and dementia (Azeem et al., 2023; Livingston et al., 2017; Loughrey et al., 2018). It has been reported that after a hearing loss greater than 25 dB, the chance of developing dementia increases by 20% for every 10 dB increase in hearing loss (Fortunato et al., 2016; Lin et al., 2011). Currently, hearing loss constitutes 8% of global dementia incidences (Brewster et al., 2022; Huang et al., 2023), therefore it is important to recognize age-related hearing loss as early as possible and to start treatment in time since it appears as the largest modifiable risk factor for dementia (Brewster et al., 2022; Huang et al., 2023; Livingston et al., 2017).

One of the most visible impacts of hearing impairment can be noticed in the verbal communication of an individual (Howarth & Shone, 2006; Jafari et al., 2019; Rutherford et al., 2018). Especially, older people often report difficulties in speech understanding particularly in complex listening environments such as in the presence of noise, even though they still have normal hearing thresholds (Bharadwaj et al., 2014; Sergeyenko et al., 2013). The underlying reason is commonly attributed to cochlear synaptopathy (Sergeyenko et al., 2013) which is an irreversible structural abnormality characterized by the synaptic degeneration of the auditory nerve fibers from the inner hair cells which takes place progressively over years (Bharadwaj et al., 2014; Kujawa & Liberman, 2009). This is why, until now reliable markers for the onset of hearing loss are not really established since many patients remain with a normal hearing threshold when the cochlear synaptopathy has already started.

1.1. Cochlear synaptopathy progressively modifies central auditory processing

Sound waves are received and translated into an electrical signal starting from the outer ear through the middle ear and the sensory hair cells in the organ of Corti. There are two types of sensory cells: outer hair cells and inner hair cells (Dallos, 1986). Outer hair cells amplify the sound-induced vibrations, hence increase the cochlea sensitivity and frequency selectivity. Inner hair cells convert the sound waves into electrical signals and form synapses to the auditory nerve fibers (Kandel, 2013).

Sound-induced vibrations in the cochlea cause the inner hair cells to deflect, which opens mechanically gated ion channels (Katrin Amunts, 2012). The influx of ions, mainly potassium (K^+) and calcium (Ca^{2+}), generates an electrical signal. This acoustic information is later, captured by the auditory nerve via specialized synaptic structures found in inner hair cells, called ribbon synapses (Moser et al., 2006). They allow for the rapid and sustained release of neurotransmitters, which is crucial for depolarization of the auditory nerve fibers and processing the ongoing and complex stimuli of acoustic information (see for review (Malmierca, 2003)). Auditory nerve fibers can be classified based on their spontaneous rate (SR) response to sound levels. Low SR fibers are activated at high sound pressure levels, while high SR fibers are activated close to the hearing threshold (Liberman, 1980). The functional specialization of auditory nerve fibers allows the auditory system to effectively code sound over a broad dynamic range of sound levels (Bharadwaj et al., 2014; Liberman, 1980).

The auditory nerve bifurcates and projects various neurons in the cochlear nuclei in the brainstem (dorsal and ventral cochlear nuclei). From the cochlear nuclei, axons of the bushy cells cross to the opposite side (contralaterally) and some stay on the same side (ipsilaterally), they project to the superior olivary complex to support the sound localization. Axons from the superior olivary complex ascend to the nucleus of the lateral lemniscus. The lateral lemniscus fibers continue to ascend to the inferior colliculus, an essential midbrain relay station in the auditory pathway. From the inferior colliculus, fibers ascend to the medial geniculate body of the thalamus, which is the main auditory relay station of the thalamus. Neurons from the medial geniculate body project to the primary auditory cortex located in the temporal lobe. The primary auditory cortex is where the conscious perception of sound begins and is responsible for the basic processing of sound frequency (pitch), intensity (loudness), and duration (Kandel, 2013; Malmierca, 2003).

The sound-evoked neural activity in the ascending auditory pathway can be measured by subcutaneous scalp electrodes, as the auditory brainstem response (ABR) (Kujawa & Liberman, 2009; Rumschlag & Razak, 2021). These auditory-evoked potentials can be represented as electrical potential waves along the auditory pathway. The ABR wave amplitudes reflect the summed activity of neurons with the first ABR peak (ABR wave-I) showing the response of the auditory nerve, the later waves arising from the cochlear nucleus (wave-II), the superior olivary complex (wave-III), and the forth peak (wave-IV) representing inferior colliculus (Melcher & Kiang, 1996). Apart from this, sound-evoked potentials can also be elicited by continuous, e.g. amplitude modulated sounds which are used to assess the temporal processing (Schrode & Bee, 2015). In response to this, uditory nerve fibers typically exhibit a tendency to fire at a given phase of the stimulus cycle (Kiang et al., 1965; Rose et al., 1967), reflected as steady-state auditory evoked responses (ASSR). Hence, the magnitude of the ASSR represents the capacity of tracking temporal fluctuations of the stimuli and therefore, is suggested as a required feature for speech understanding (Gall et al., 2011; Mann et al., 2005).

Poor speech discrimination in noisy backgrounds is often observed in age-related hearing loss (McClaskey et al., 2019; Shaddock Palombi et al., 2001; Walton, 2010). This might be due to the weakened ability to temporally process acoustic signals. The impaired processing of temporal cues is

seen in both humans (Delano et al., 2020) and animal models and is associated with cochlear synaptopathy (Ruttiger et al., 2013; Sergeyenko et al., 2013). Cochlear synaptopathy can result from noise damage (Liberman & Kiang, 1978) or aging over the years (Bramhall et al., 2015; Konrad-Martin et al., 2012). The ABR wave-I amplitude reduction, as mentioned, can indicate this synaptopathy (Bramhall et al., 2021; Earl & Chertoff, 2010; Kujawa & Liberman, 2009). Contrarily, even with normal audiometric thresholds, older adults may struggle to understand speech in noise (Fullgrabe et al., 2014), which suggests that the speech understanding problems are not solely related to the ability to detect sound (threshold sensitivity) but also to the integrity of the auditory nerve fibers (Bramhall et al., 2015). This loss can degrade the timing information necessary for speech discrimination, making it difficult to follow conversations with background noise (McClaskey et al., 2019).

When hearing loss occurs, slowly over a long period of time, the brain may adapt to the reduced sensory input. It has been recently documented that the loss in auditory input (reduced ABR wave-I) in the periphery can be compensated via progressively amplified midbrain responses with a stronger ABR wave IV response, also known as neural gain. The similar effect can be detected both in humans (Delano et al., 2020; McClaskey et al., 2019) and rodents (Eckert et al., 2021; Matt et al., 2018; Ruttiger et al., 2013). Notably, it had been observed that in cases where the reduced auditory input was compensated, also the temporal processing was preserved since the temporal cues can be properly coded (Chambers et al., 2016). It has been suggested that the restoration of the midbrain-derived ABR wave-IV and the preserved physiological response to amplitude modulated sound might be linked with the central auditory adaptation (Schrode & Bee, 2015). Indeed, this refers to the ability of the brain to reorganize in order to compensate for injury or to adjust to new situations (Bellistri et al., 2013) (see Chapter 1.4 for more details).

1.2. Influence of stress response on auditory function

The most fundamental mechanism inducing learning and adaption in the central nervous system is the “stress” response. Stress is a biological response to both temporary or prolonged threats (Herman et al., 2016). It activates the body's sympathetic nervous system, triggering the 'fight or flight' response, and releases hormones like corticosterone in rodents (cortisol in humans) via the hypothalamic-pituitary-adrenal (HPA) axis (Figure 1) (de Kloet et al., 2005). When encountered with a stressful situation, a chain of reactions is initiated with the secretion of the corticotropin-releasing factor (CRF) and arginine vasopressin (AVP) from the paraventricular nucleus (PVN) of the hypothalamus. Later, CRF and AVP lead to the release of adrenocorticotropic hormone (ACTH) from the pituitary gland stimulating the production and the release of corticosteroids from the adrenal cortex (Godoy et al., 2018; Joels & Baram, 2009; Spencer & Deak, 2017).

There are two different receptors that bind corticosteroids: mineralocorticoid receptors (MR) and glucocorticoid receptors (GR). They differ in their binding-affinity such that: MR has a 10-fold higher affinity than GR (Reul & Kloet, 1985), hence they coordinate different stages of the stress response

(Figure 1, right panel) (Herman et al., 2016; van Bodegom et al., 2017). MR-dominated action mediates the appraisal step by inducing alertness and optimizes stress-coping (Berger et al., 2006; ter Horst et al., 2012) while consecutively, the GR-mediated step promotes memory consolidation and behavioral adaptation (de Kloet et al., 2019). Both receptors are highly expressed throughout the brain, abundantly in the hippocampus and medial prefrontal cortex (mPFC) (Han et al., 2005; Spencer & Deak, 2017), which are critical brain regions for reasoning and adaptive behavior, and provide the negative feedback on the PVN to reset the HPA-axis activity (Figure 1, left panel) (de Kloet et al., 2019; Herman et al., 2016). However, when the stressful situation stays persistent, the inhibitory control on PVN may not function which overloads the stress system (Berger et al., 2017). It was shown that cortico-limbic structures including the mPFC and the hippocampus undergo structural and functional changes under chronic stress exposure. These changes are linked to the reduced dendritic arborization of neurons (Han & Nestler, 2017; Zhu et al., 2007), impaired induction of LTP in the hippocampus (Joels & Karst, 2012; Yuen et al., 2012), deficits in learning and memory (Herbert et al., 2006), increased anxiety and depressive-like behaviors (Allen & Badcock, 2003; Lambert & Kinsley, 2011).

Interestingly, corticosterone treatment is the most common therapy used in clinics for sudden hearing loss (El Sabbagh et al., 2017; Hobson et al., 2016) although the mechanism of action is not fully known. Contrarily, chronic stress may exacerbate the symptoms of hearing problems, like tinnitus symptoms (Canlon et al., 2013; Kraus & Canlon, 2012; Mazurek et al., 2015). In that regard, long-term stress can make it harder to process complex sounds, therefore understanding speech patterns or adapting to the hearing loss, yet the exact underlying mechanism of how stress may hamper auditory processing remains elusive.

In fact, noise level of 85 dB SPL and above may induce the release of stress hormones (Burow et al., 2005). After exposure of short duration, the GRs can restore the stress response back to baseline by negative feedback on the HPA axis. Prolonged high intensity noise exposure, however, can lead to persistent corticosterone elevation and also upregulation of GRs (Hayes et al., 2019). This may potentially compromise the stress response (Hébert & Lupien, 2007) and contribute to cognitive deficits, especially by impairing the hippocampal function. In line with these observations, mice and rats when exposed to acoustic trauma for a longer period, displayed elevated corticosterone levels for several weeks (Shukla et al., 2019), loss in the hippocampal neurogenesis (Liu et al., 2016; Newman et al., 2015) and learning deficiency in Morris Water Maze (Liu et al., 2016; Matt et al., 2018) as well as deficits in the memory consolidation (Manohar et al., 2020). Intense noise exposure caused a reduction in hippocampal LTP (Cunha et al., 2018; Matt et al., 2018) indicating altered synaptic plasticity as a possible functional origin for the observed memory deficits (Yu et al., 2011).

MR and GR are also expressed in cochlea including hair cells or spiral ganglion neurons (SGN) (Shimazaki et al., 2002; ten Cate et al., 1993). Recently, several studies highlighted the protective effect of not MR but particularly GR against acoustic trauma by either endogenous or administered elevation of corticosterone levels in animal models (Singer, Kasini, et al., 2018; Tahera et al., 2006). Marchetta et al., (2022) showed in more detail the individual impact of central MR and GR on auditory

nerve processing. The mouse lines used in this study enabled a selective deletion of MR and/or GR only in the forebrain, leaving their expression in the cochlea intact. They documented that MR reduces the number of IHC ribbons and auditory nerve responses while GR disrupts the auditory nerve fiber synchrony, indicating a top-down modulation of the auditory system (Marchetta et al., 2022).

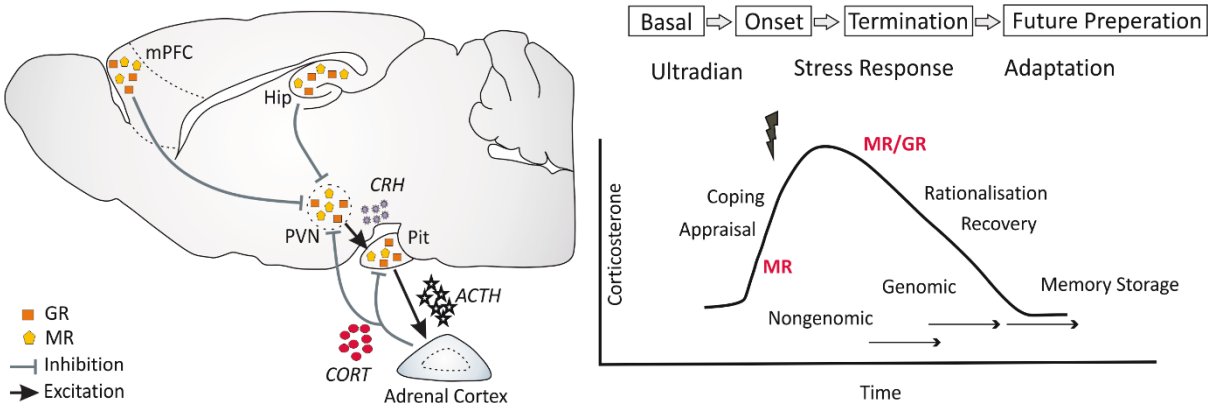

Figure.1 | Hypothalamic-pituitary-adrenal (HPA) axis (left panel) and the trajectory of the information processing (right panel). Left panel: psychological stressors or ascending brain-stem pathways that convey visceral and sensory stimuli activate the HPA axis. Upon HPA axis activation CRH and AVP are produced in PVN which induces the synthesis of ACTH from the pituitary gland. ACTH, then, stimulates the secretion of corticosterone (in rats and mice) and cortisol (in humans) from the adrenal cortex. Right panel: the inverted U-shaped response to stress. The MR- and GR- mediated actions are involved in a particular stage of information processing over time. The MR is mostly responsible for the maintenance of the stress-related neural circuits and is implicated in the appraisal of sensory information, whereas the GR-mediated actions lead to the dampening of the stress reaction and homeostasis and are involved in the storage of information for future use. Initially, MR homodimers are involved but, with the progressive increase in stress hormone concentrations, MR-GR heterodimers, GR-GR homodimers, and complexes of MR/GR monomers are formed and act as transcription factor of specific sets of genes. CRH, corticotropin-releasing hormone; PVN, paraventricular nucleus; Pit, pituitary gland; ACTH, adrenocorticotropic hormone; CORT, corticosterone; Hip, hippocampus; mPFC, medial prefrontal cortex (Figure is adapted from (van Bodegom et al., 2017) & (de Kloet et al., 2019)).

1.3. Cyclic guanosine monophosphate (cGMP) signaling in auditory plasticity

The cyclic guanosine monophosphate (cGMP) is a second messenger signaling molecule that has a crucial role and is involved in various physiological processes spanning from smooth muscle relaxation to synaptic plasticity (Kleppisch & Feil, 2009; Potter, 2011). The cGMP signaling cascade (Figure 2, right panel) is typically initiated by the binding of extracellular ligands, such as natriuretic peptides to their respective membrane-spanning natriuretic peptide receptors (NPRs) or by nitric oxide (NO) through soluble guanylyl cyclase (NO-GC/sGC) (Friebe & Koesling, 2003; Kuhn, 2009). There are three types of natriuretic peptides: atrial natriuretic peptide (ANP), B-type natriuretic peptide (BNP), C-type natriuretic peptide (CNP) and they bind to three particulate guanylyl cyclase p(GC) receptors: ANP and

BNP stimulate the GC-A (NPR-A) and CNP binds to GC-B (NPR-B) whereas NPR-C is a clearance receptor which controls the local concentration of natriuretic peptides through degradation (see Review (Potter et al., 2006)). On the other hand, NO diffuses into the cell and activates NO-GC (Murad et al., 1978). Once the receptors are activated, guanosine triphosphate (GTP) is converted into cGMP. cGMP diffuses and activates cGMP-gated ion channels, protein kinase G (PKG; or cGMP-dependent protein kinase (cGK)), and phosphodiesterases (PDEs) (Kemp-Harper & Feil, 2008).

Recently, the impact of the cGMP signaling on the auditory system has been documented (see Review (Eckert et al., 2021)). From the upstream regulators of the pathway, GC-A was revealed to have a protective function such that a deletion of GC-A exhibits greater vulnerability of hair cells to hidden hearing loss or noise- and age-dependent hearing loss, and this effect was associated with GC-A expression in spiral ganglia and outer hair cells but not in inner hair cells (Marchetta, Möhrle, et al., 2020). Also, GC-B deleted mice exhibited compromised auditory processing, determined by elevated audiometric thresholds, delayed sound-evoked auditory brainstem responses, and loss of the temporal precision of auditory processing, as indicated by the pre-pulse inhibition of the acoustic startle response (Wolter et al., 2018). In contrast, NO-GC isoforms and cGMP responses were identified in inner hair cells but not in outer hair cells, specifying a hair cell-specific expression and function. Further, the deletion of one of the two isoforms of NO-GC (NO-GC1 or NO-GC2) in mice protected against the loss of noise-induced ABR threshold and wave-I amplitude compared to WT mice following acoustic trauma (Mohrle et al., 2017).

Moreover, from the cGMP effectors, mice with a deletion of the gene encoding *Pkg1* (cGMP-dependent protein kinase type I, Prkg1), displayed more vulnerability to and less recovery from acoustic trauma compared to WT mice suggesting the endogenous protective function of the cGMP-Prkg1 signaling pathway in which this effect was confirmed by the administration of the PDE5 inhibitors (Vardenafil) before acoustic overstimulation (Jaumann et al., 2012) highlighting the therapeutic potential of cGMP signaling for noise damages.

PDEs are the enzymes that modulate the intracellular level of cGMP by hydrolyzing cGMP via breaking the phosphodiester bond (Bender & Beavo, 2006). The PDE family consists of 11 isoforms of PDEs (Figure 2) that include more than one gene product that also has multiple splice variants (Bender & Beavo, 2006) specifically localized in subcellular compartments (Keravis & Lugnier, 2012). Additionally, PDEs vary in substrate specificity such that only PDE5, PDE6 and PDE9 specifically hydrolyses cGMP (Calamera et al., 2022; Kokkonen & Kass, 2017; Kukreja et al., 2012). Besides the many other cellular functions counting cardiovascular homeostasis, cellular growth, and contractility or inflammation, the interest in the role of PDEs in enhancing cognitive performances has been growing lately (Argyrousi et al., 2020; Blokland et al., 2006) and accordingly inhibition of PDEs has been suggested as a new therapeutic approach for cognitive dysfunction and learning and memory problems (Prickaerts et al., 2002; Reneerkens et al., 2009).

Among other PDEs, PDE9A has been demonstrated to have the highest affinity to cGMP (Fisher et al., 1998; Soderling et al., 1998). It is abundantly expressed throughout the brain, particularly in the

hippocampal CA1 region (Andreeva et al., 2001; Van Staveren et al., 2003). In addition, PDE9A inhibitor has been identified to regulate cGMP signaling independent of NO signaling in both cardiac tissue (Lee et al., 2015) and the brain (Harms et al., 2019). These observations may suggest that the PDE9A function could be considered specific to the pGC/cGMP signaling cascade. Given that among the cGMP generators described above, the GC-A deletion generated a hearing phenotype, thus the inhibition of PDE9A may stand out as a molecular tool that is specific to a GC-A generated cGMP pool for combatting noise-induced or age-related hearing loss.

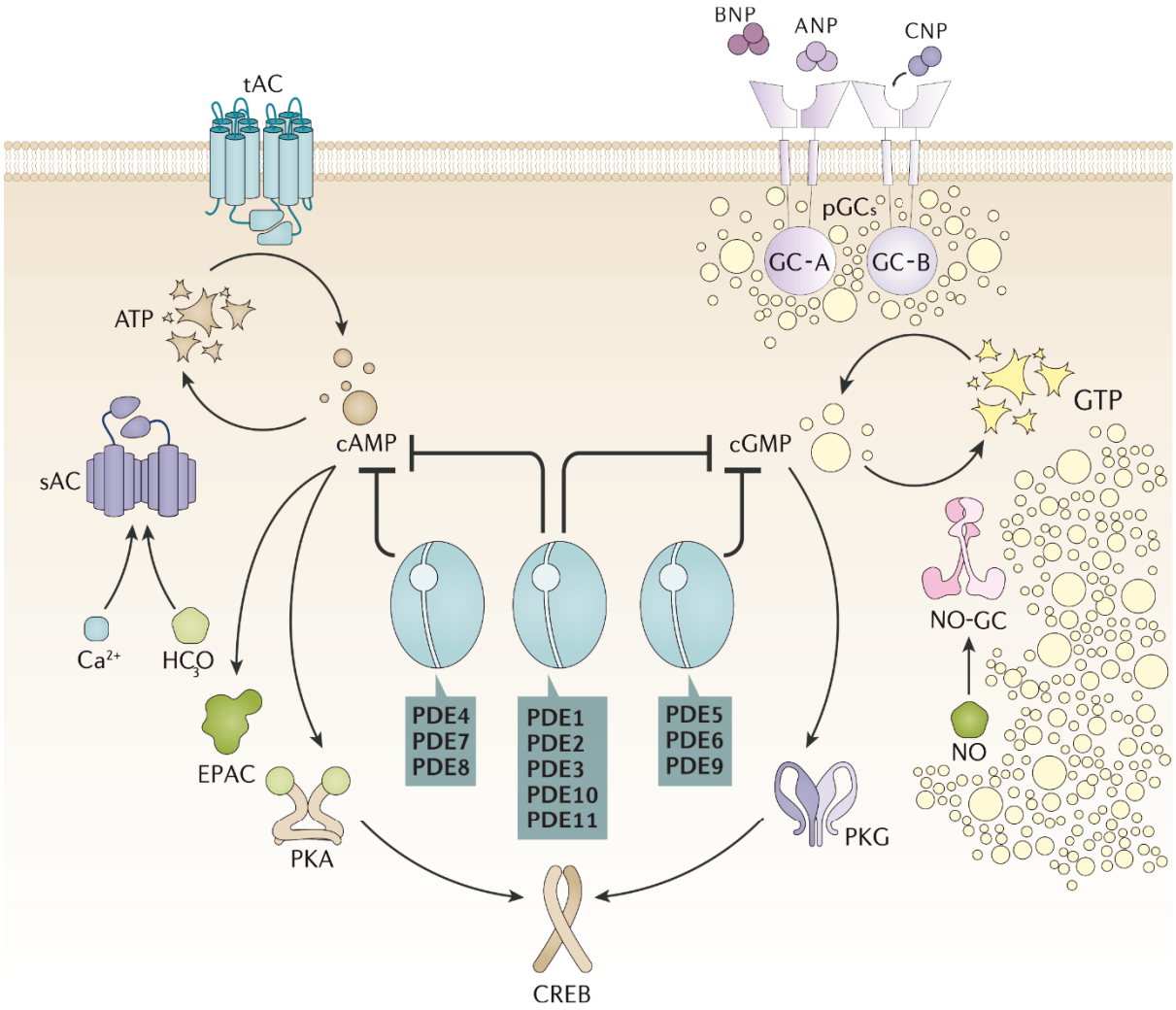

Figure.2 | The canonical cyclic nucleotide signaling pathways (cAMP and cGMP). Briefly, cAMP (left panel) is also a second messenger and synthesized by transmembrane adenylyl cyclases (tACs) that are regulated by G-protein coupled receptors (not shown here) as well as soluble adenylyl cyclases (sACs) that are activated by bicarbonate and calcium. cGMP (right panel) is synthesized by particulate guanylyl cyclases (pGCs: GC-A & GC-B) that are activated by natriuretic peptides: ANP, BNP, and CNP, might be located close to the membrane, and soluble guanylyl cyclases (sGCs) that are activated by nitric oxide (NO), possibly distributed broadly in the intracellular domain. cGMP only stimulates protein kinase G (PKG), whereas cAMP activates protein kinase A (PKA), exchange protein activated by cAMP (Epac). Ultimately, both cAMP and cGMP signaling through PKA and PKG respectively, leads to phosphorylation of the transcription factor cAMP response element binding protein (CREB). Phosphorylated CREB (p-CREB) can bind to the cAMP response element (CRE) and initiates the transcription of specific genes, coding e.g. AMPA receptors or BDNF (not shown here). Termination of

the signaling pathway occurs via the degradation of the cyclic nucleotides by substrate specific phosphodiesterases (PDEs). (Figure is adapted from (Baillie et al., 2019) and (Kemp-Harper & Feil, 2008))

1.4. The role of synaptic plasticity in central auditory adaptation

Synaptic plasticity is a crucial feature of the brain that occurs upon neuronal activity from experiences to alter neural circuit function and thus impact thoughts, feelings, and behavior. This usually takes place due to the change in synaptic strength in response to use or disuse (Hebb, 2005). Synaptic plasticity is long-term potentiation (LTP) or long-term depression (LTD) which can either promote or dampen synaptic transmission, respectively (Citri & Malenka, 2008; Lynch et al., 2007). This mechanism has been suggested as the biological substrate for learning and memory and is more extensively studied in the hippocampus although similar forms of synaptic changes have also been observed in other brain regions (Citri & Malenka, 2008). The process of LTP can be initiated by high-frequency stimulation which releases glutamate neurotransmitters from the pre-synapse (Jackman & Regehr, 2017). Subsequently, with the membrane depolarization and the binding of glutamate activates N-methyl-D-aspartate (NMDA) receptors and a-amino-3-hydroxy-5-methyl-4-isoxazole propionic acid (AMPA) receptors. This allows the influx of Ca^{2+} ions into the post-synapse (Bliss et al., 2018; Citri & Malenka, 2008; Lynch et al., 2007). The increase in the Ca^{2+} concentration facilitates intracellular enzymes including Ca^{2+} /calmodulin-dependent protein kinase II (CaMKII) (Lisman et al., 2012) and phosphorylation of additional AMPA receptors (Diering & Huganir, 2018; Ferretti et al., 2015) followed by their insertion to the post-synaptic membrane (Penn et al., 2017). Hence, the initiation of these series of events of LTP is tightly bound to the influx of the Ca^{2+} and membrane depolarization. Regarding this, large conductance Ca^{2+}- and voltage-activated K^+ channels (BK) are sensitive to the intracellular Ca^{2+} levels (Berkefeld & Fakler, 2013; Shah et al., 2021; Vandael et al., 2010); their activation can lead to K^+ efflux, which in turn can affect the membrane potential and thus the driving force for Ca^{2+} entry into the neuron (Hu et al., 2001). In this way, BK channels determine the repolarization and after-hyperpolarization phases of the action potential (Hu et al., 2001; Storm, 1987) which is crucial for the induction and regulation of LTP.

The neuronal activity and activation of NMDA receptor-dependent signaling triggers the synthesis of proteins modulating the synaptic function: as the activity-regulated cytoskeleton-associated protein (Arc/Arg3.1) (Bramham et al., 2008) and brain-derived neurotrophic factor (BDNF) (Hartmann et al., 2001; Zheng et al., 2012). Arc is an immediate-early gene and is rapidly induced upon synaptic activity (Bramham et al., 2008). Once transcribed, Arc mRNA is transported to dendrites (Hedde et al., 2021) where it is involved in the trafficking and degradation of AMPA receptors (Penn et al., 2017; Sumi & Harada, 2020). Thus, by influencing AMPA receptor dynamics, Arc can contribute to the enhancement (LTP) or weakening (LTD) of synaptic transmission (Bramham et al., 2008; Tzingounis & Nicoll, 2006). On the other hand, BDNF is a protein that belongs to the neurotrophin family of growth factors, which are involved in the survival, development, and function of neurons (Leal et al., 2017). It is synthesized in the neuron as a precursor protein (proBDNF) and then cleaved to form mature BDNF. It is released

from neurons in an activity-dependent manner and exerts its effects primarily by binding to specific receptors on the cell surface called TrkB (tropomyosin receptor kinase B) and $p75^{NTR}$ (Chao, 2003; Leal et al., 2017). It is known to promote synaptic plasticity by facilitating LTP via TrkB signaling (Bramham & Messaoudi, 2005; Minichiello et al., 2002) or LTD via $p75^{NTR}$ (Rosch et al., 2005) as well as structural changes, such as the growth of new dendritic spines (Kolb, 2008). Regarding synaptic plasticity, dendritic spines are small, protruding structures that come off the dendrites of neurons (Bonhoeffer & Yuste, 2002). They are the primary postsynaptic targets for excitatory synaptic inputs in the central nervous system and are thought to be a physical manifestation of synaptic plasticity (Bosch et al., 2014).

These neuronal plasticity mechanisms are also required when hearing loss occurs. In that case, the brain needs to change how it processes auditory information by adjusting neural gain to adapt to the loss in the auditory input. Over time, this can lead to more long-term changes in central auditory plasticity. In support of these, several lines of research have shown diminished expression levels of activity-dependent BDNF and Arc (Ruttiger et al., 2007; Singer et al., 2013) or reduced number of dendritic spines (Dong et al., 2018; Zhao et al., 2018) in hippocampal and cortical brain regions as well as lack of LTP recruitment (Eckert et al., 2021; Matt et al., 2018) from cortical and hippocampal brain regions due to noise-induced or age-related hearing loss.

An increasing line of evidence has documented that inhibition of PDE9A (PDE9A inhibitor) has a pro-cognitive effect in animal models. Intracellular localization was described in neuronal cell bodies and primary dendrites (Dorner-Ciossek et al., 2017). The enhanced synaptic plasticity by PDE9A inhibitor has been shown via electrophysiology recordings, under different stimulation paradigms to increase LTP in healthy rodents, particularly in aged rats (van der Staay et al., 2008), and in a dose-dependent way (Hutson et al., 2011; Kroker et al., 2014; Rosenbrock et al., 2019). In addition, PDE9A inhibitor has been revealed to improve memory performance in a variety of behavioral paradigms including T-Maze, object recognition tasks, or social recognition (van der Staay et al., 2008). Finally, it was also found that PDE9A inhibitor reversed the drug-induced memory impairment in animal models (Vardigan et al., 2011 2011) as well as the auditory gating deficits (Kleiman et al., 2010), suggesting that it may ameliorate auditory information processing (Dorner-Ciossek et al., 2017). Likewise, the electrophysiological and behavioral findings, PDE9A inhibitor was reported to increase the neurite growth and number of synapses in an in-vitro model (Hutson et al., 2011) and attenuated the loss of spines in hippocampus in a transgenic mouse-model (Kleiman et al., 2010), and in addition, to increase synaptic calcium activity, hence elevate activity-dependent synaptic plasticity in cortical region (Lai et al., 2018).

2. Objectives

In this study, it was primarily aimed to investigate central auditory adaptation mechanisms in response to age-related cochlear synaptopathy. It has been previously described that mammals can adapt to loss in the auditory input by compensating within the ascending auditory pathway. Thus, they can be classified as *low compensators* or *high compensators* by calculating their ABR IV/I ratio. In addition, it was also documented that in *high compensators*, the temporal auditory processing was preserved which was attributed to a better cognitive ability defined by higher levels of LTP, recruitment of activity-dependent BDNF, and parvalbumin-positive labeling. Additionally, also the performance in Morris Water Maze was better in *high compensators*. In Savitska et al., (2022), we first investigated if *low compensators* phenotype could be improved in the direction of *high compensators* by modulating their compensatory mechanisms in middle-aged (9-14.7 months old) mice. For this, we targeted the intracellular cyclic guanosine monophosphate (cGMP) levels by administering PDE9A inhibitor for 10 days which was extensively shown to enhance cognition, LTP, and synaptic plasticity, compared to a group administered with vehicle. Given the fact that high stress level over a long period has deteriorating effects on hearing function and cognition, we also assessed their blood corticosterone level upon the 10 days of treatment.

Furthermore, we investigated the impact of individual stress receptors: mineralocorticoid receptor (MR) and glucocorticoid receptor (GR) on central auditory compensation mechanisms (Calis et al., 2023). For this, we used a tamoxifen-inducible CreERT2/loxP system to generate mice with a single or combined deletion of central MR and GR in the brain, while preserving the expression of cochlear MR and GR. Next, in order to assess the compensation capacity, we analyzed the ABR wave IV/I ratio. Additionally, we studied the pre- and post-synaptic plasticity changes by paired-pulse facilitation (PPF) and LTP recording from acute hippocampal slices. Further, as a regulatory marker for AMPA receptor trafficking at the synapses, we examined the Arc expression level. In order to identify the role of cGMP signaling under different stress activities for central neural gain, we also analyzed NO-GC and GC-A expression levels by in situ hybridization from the hippocampal CA1 region.

In the next step (Calis et al, in preparation), in addition to ABR wave amplitude, to assess the accuracy of the spike timing which is required for precise temporal processing, we also assessed the ABR wave latencies between *low* and *high compensators* and their response to 10 days of treatment. Further, in order to study synaptic plasticity as a means of the adaptation process, which is suggested to be the underlying ability to define *high compensators*, we recorded LTD in response to low-frequency stimulation, following LTP recording. Moreover, we applied Golgi-Cox staining to investigate the dendritic spine remodeling which indicates a structural correlate of synaptic plasticity and learning and memory.

Finally, in another line of study (Pham et al., 2023), the role of the big conductance potassium (BK) channels in synaptic plasticity was examined. BK channel are ubiquitously expressed in various cell types and mutations in BK coding genes have been found to be involved in cognitive impairments (Miller et al., 2021). For this, the BK channels were deleted specifically in the CA1 region of the

hippocampus in mice and further, electrophysiological LTP upon high-frequency stimulation and chemical LTP with forskolin, rolipram, picrotoxin cocktail, were performed in the CA1 region of the mice, in addition to the behavioral paradigms and Ca^{2+} and K^{+} imaging protocols.

3. Results

3.1. Stress response determines the central adaption in response to reduced auditory input in a cGMP-dependent way

It has been previously well characterized that loss in auditory input due to cochlear synaptopathy can be centrally compensated (Mohrle et al., 2016; Ruttiger et al., 2013). This mechanism helps to preserve good temporal auditory processing detected by ASSRs and is linked to better cognitive capacity and synaptic plasticity (Eckert et al., 2021; Matt et al., 2018). In this study (Savitska et al., 2022) we investigated the potential underlying factors determining the capacity of the central compensation response to the reduced auditory input. We first analyzed the hearing function of the middle-aged (9–14.7 months, Figure 1, white circles (Savitska et al., 2022)) and old (15.2–22.7 months, Figure 1, black circles (Savitska et al., 2022)) mice by click stimulus-evoked ABR. Next, we calculated the ABR wave IV/I ratio as a measure of central compensation, for the individual mouse and plotted it as a function of ABR wave I strength (average of the three highest wave amplitude values (Figure 1F (Savitska et al., 2022)). Subsequently, mice were classified, as either *low compensators* or *high compensators* according to the inserted power function ($y = a^{*}x^{b}$) as a regression line (Figure 1F (Savitska et al., 2022)). *Low* and *high compensators* did not show a difference in thresholds for click and noise-burst or 11 kHz pure-tone stimuli (Figure 2A, B, C (Savitska et al., 2022). In contrast, the pure-tone stimuli of increasing frequencies (2–32 kHz, half-octave steps), revealed that *low compensators* had a loss in threshold in comparison to *high compensators* (Figure 2D, (Savitska et al., 2022)). Further, to get insight into temporal resolution, ASSR was assessed in response to amplitude modulated tones. Confirming our previous findings (Marchetta, Savitska, et al., 2020), *low compensators* have significantly poorer temporal resolution compared to *high compensators* (Figure 2E, (Savitska et al., 2022)).

Later, a set of mice from *low* and *high compensators* were treated either with PDE9A inhibitor or vehicle for 10 days. Given that stress may compromise hearing function as well as central neuronal activity, we analyzed blood corticosterone levels at pre- and post-treatment. We observed that *low compensators* have lower blood corticosterone levels than *high compensators*. Following 10 days of treatment regardless of substance, *high compensators* but not *low compensators*, showed significantly increased corticosterone levels (Figure 3, (Savitska et al., 2022)). This indicates that not a PDE9A inhibitor per se but rather the injection itself is stressful for *high compensators*.

Keeping the difference in stress response in mind, we examined the click ABRs and ASSRs in response to treatment *high compensator* treated with vehicle a had significant decrease in ABR wave-I amplitude and signal-to-noise ratio (SNR) of ASSR while PDE9A inhibitor prevented this loss (Figure

4A, B; Figure 5A, B (Savitska et al., 2022)). *Low compensators*, with no alteration in their stress level, showed no difference in ABR wave-I amplitude (Figure 4C, D (Savitska et al., 2022)) and ASSRs (Figure 5C, D (Savitska et al., 2022)) in response to either vehicle or PDE9A inhibitor treatment. These may indicate that the synchronous response of the auditory nerve and temporal coding of the sound can be maintained if the stress axis and cGMP signaling remains sensitive over age which could possibly be impaired in *low compensators*.

As a metric for the auditory nerve coupling to inner hair cells determining the auditory nerve response amplitude, the number of CtBP2/RIBEYE-immunopositive dots opposing neurofilament-200 positive auditory fibers was quantified. Not on the apical turn but particularly in the medial/midbasal turn of the cochlea we observed that only *high compensators* treated with vehicle had a reduced number in inner hair cell ribbon number which is not present after PDE9A inhibitor treatment (Figure 4E, F, G (Savitska et al., 2022)). Consistently, these findings reflect the ABR wave-I amplitude results which were reduced in *high compensators* with the vehicle and preserved with PDE9A inhibitor while there was no change in *low compensators*. Hence this may suggest that the injection itself exerts a stressful effect and disrupts the discharge rate of auditory nerve response which can be prevented by PDE9A inhibitor only in *high compensators* but not *in low compensators*.

Since it has been suggested that the central synaptic plasticity favors the auditory compensation mechanisms (Eckert et al., 2021; Matt et al., 2018), we assessed the synaptic plasticity in the hippocampus. As documented before (Eckert et al., 2021) *low compensators* had lower LTP than *high compensators* (Figure 6C, (Savitska et al., 2022). In response to treatment with either vehicle or PDE9A inhibitor*, low compensators* did not exhibit any alteration in LTP. In contrast, *high compensators* displayed a significant reduction in their LTP after vehicle treatment which could be prevented by PDE9A inhibitor administration. In addition, we studied the activity-dependent changes in *Bdnf* exon-IV and -VI expression tagged by bi-cistronic expression of CFP or YFP, respectively (Figure 7A, (Savitska et al., 2022)) as well as parvalbumin (PV) protein staining (Singer, Manthey, et al., 2018). *Low compensators* tend to have lower CFP (not significant) and YFP (significant) expression in comparison to *high compensators* (Figure 7H, I (Savitska et al., 2022)). Upon treatment *low compensators* did not show any alteration in their CFP or YFP expression (Figure 7H, I (Savitska et al., 2022)). By contrast, *high compensators* treated with PDE9A inhibitor had significantly increased CFP and YFP expression in comparison to those treated with vehicle (Figure 7H, I (Savitska et al., 2022)). Similarly, PV expression was not different between *high* and *low compensators*, and no alteration in response to treatment was depicted in *low compensators* whereas *high compensators* treated with PDE9A inhibitor showed a significantly higher PV expression in comparison to the vehicle treated group.

These results suggest that when the stress response is insufficient, not only are animals left unable to develop auditory adaptation for age-related cochlear synaptopathy, but they are also unable to benefit from PDE9A inhibitor treatment.

3.2. Central MR/GR steroid receptors provide means of top-down control for auditory neural gain via elevating LTP, and GC-A cGMP signaling

Considering that stress response has a determining role in central auditory plasticity processes (Savitska et al., 2022), in the next step, we specifically examined the role of mineralocorticoid (MR) and glucocorticoid receptors (GR) in synaptic plasticity and auditory neural gain. Three tamoxifen-inducible conditional knockout mouse lines in which MR and/or GR were deleted under the CaMKIIα promoter were generated as previously described (MRGR^{TMX}cKO, MR^{TMX}cKO, GR^{TMX}cKO (Marchetta et al., 2022)). Previously, global, or conditional deletion of MR led to an increase in the GR expression level (Berger et al., 2006; Erdmann et al., 2007). In our mouse-line MR deletion also induced a higher expression level of GR in the hippocampus compared to their WT control while GR deletion did not significantly influence MR expression (Figure 1A, B, (Calis et al., 2023)). Therefore, the phenotype of MR^{TMX}cKOs mice can be attributed not only to the absence of MR but also to induced GR function. Following, we analyzed the ratio of ABR wave-IV to wave-I amplitude in order to assess how the central neural gain activity is altered under disrupted stress response in these mouse lines. Our findings showed that MR^{TMX}cKOs mice could amplify the reduced auditory nerve response by an increase in central auditory response in comparison to WTs, while GR deletion resulted in a reduction of neural gain (Figure 2A, B left panel, (Calis et al., 2023)). Finally, the absence of both MR and GR displayed no change in ABR wave IV/I ratio (Figure 2C left panel, (Calis et al., 2023)), indicating a counterbalanced effect of individual stress receptors on central neural responses. Due to a possible link between central auditory compensation and synaptic plasticity as previously described (Eckert et al., 2021; Matt et al., 2018), we assessed the hippocampal LTP in these mouse lines. Like in their auditory compensation, the MR^{TMX}cKOs had significantly higher LTP in comparison to their WT controls while GR^{TMX}cKOs had a trend towards lower LTP in comparison to their WT controls (Figure 2A, B right panel, (Calis et al., 2023)). In contrast, MRGR^{TMX}cKOs had significantly lower LTP in comparison to their WT controls (Figure 2C right panel, (Calis et al., 2023)). In addition, we assessed the pre-synaptic function by performing PPF recording, which is an indicator of the neurotransmitter release probability, hence determining the post-synaptic responses (Jackman & Regehr, 2017; Yang et al., 2019). MR^{TMX}cKO mice had a significantly lower PPF, while GR^{TMX}cKO mice did not have a significant difference, likewise, MRGR^{TMX}cKO mice when compared to their respective controls (Figure 3A, B, (Calis et al., 2023)). Given that different compensation ability as observed in *low* and *high compensators*, is controlled by the HPA axis activity in a cGMP signaling dependent way (Savitska et al., 2022), we analyzed the expression of the upstream generators of the cGMP. Additionally, we examined the expression of Arc which is involved in AMPA receptor trafficking and required for LTP recruitment. MR^{TMX}cKOs exhibited significantly higher levels of NO-GC, Arc, and GC-A mRNA in comparison to their WT controls (Figure 4A, (Calis et al., 2023)). Interestingly GR^{TMX}cKOs also had significantly higher levels of NO-GC mRNA but showed no significant differences in levels of Arc and GC-A mRNA in comparison to their WT controls (Figure 4B, (Calis et al., 2023)). MRGR^{TMX}cKO displayed significantly higher levels of NO-GC and Arc mRNA, but the GC-A expression levels in the MRGR^{TMX}cKO were significantly diminished (Figure 4B, (Calis et al., 2023)). Apart from regulating the HPA-axis, MR and GR also execute genomic

activity by acting as transcription factors. Upon observing altered expression patterns in NO-GC and GC-A, we analyzed MR/GR-specific binding motifs (GRE sequences) in the genes encoding NO-GC (i.e., *Gucy1a1, Gucy1a2, Gucy1b1*) and GC-A (*Npr1*). Among these, only NO-GC encoding genes *Gucy1a1* and *Gucy1a2*, were identified to contain a conserved GRE sequence. It was found in the regulatory regions of the intron between exons 3 and 4 respectively (Supplementary Figures 5 and 6 (Calis et al., 2023)).

These findings indeed reveal the multifaceted impact of individual stress receptors on cGMP signaling and synaptic plasticity. When the stress axis undergoes GR-dominated state, it further induces the cGMP signaling regulators by increasing expression levels of NO-GC, GC-A, and Arc in the hippocampus. These features might be functionally translated to elevated LTP and auditory neural gain, supporting the previous view that auditory compensation requires a memory-dependent amplification process which can be promoted by cGMP signaling.

3.3. Plastic dendritic spines and subsequent structural modifications support central adaptation in response to age-related cochlear synaptopathy

As previously described *low* and *high compensators* differ in terms of many aspects of their hearing function. In this study, after classifying middle-aged mice (10-16 months old) as *low* and *high compensators* (Figure 3A, (Calis, in preparation)), we also assessed the latency of ABR waves -I & -IV, in addition to ABR wave amplitudes. While ABR amplitudes indicate the summed activity of neurons along the auditory pathway, ABR wave latency shows the spike timing of the sound-evoked activity of neurons, relative to the stimulus onset. Thus, accurate coding of the stimulus onset is critical to generate sound-evoked spikes, to resolve the temporal features in the signal, in higher levels of auditory nuclei. The comparison of ABR wave-I amplitudes between *low* and *high compensators* showed significant interaction in their growth function (Figure 3B, (Calis, in preparation)). Specifically, while *high compensators* produced a graded ABR response with increasing sound intensity, *low compensators* showed a higher level of wave-I amplitude close to the hearing threshold but not with a higher (>50 dB relative to threshold) sound pressure level. This suggests that *low* and *high compensators* already differ at the auditory nerve level in terms of sound coding. Further, *low compensators* had significantly lower ABR wave-IV amplitude than *high compensators* (Figure 3C, (Calis, in preparation)) which may explain the smaller ABR IV/I ratio. Consistently, *low compensators* also had significantly poorer ASSR representing temporal resolution than *high compensators* (Figure 3D, (Calis, in preparation)). Besides, *low compensators* tended to have shorter ABR wave-I latency (not significant, $p=0.09$) in the level range (>25 dB, <50 dB relative to threshold) where ABR wave-I amplitude was larger (Figure 3E, (Calis, in preparation)) and shorter ABR wave-IV latency (not significant, $p=0.06$) (Figure 3F, (Calis, in preparation)).

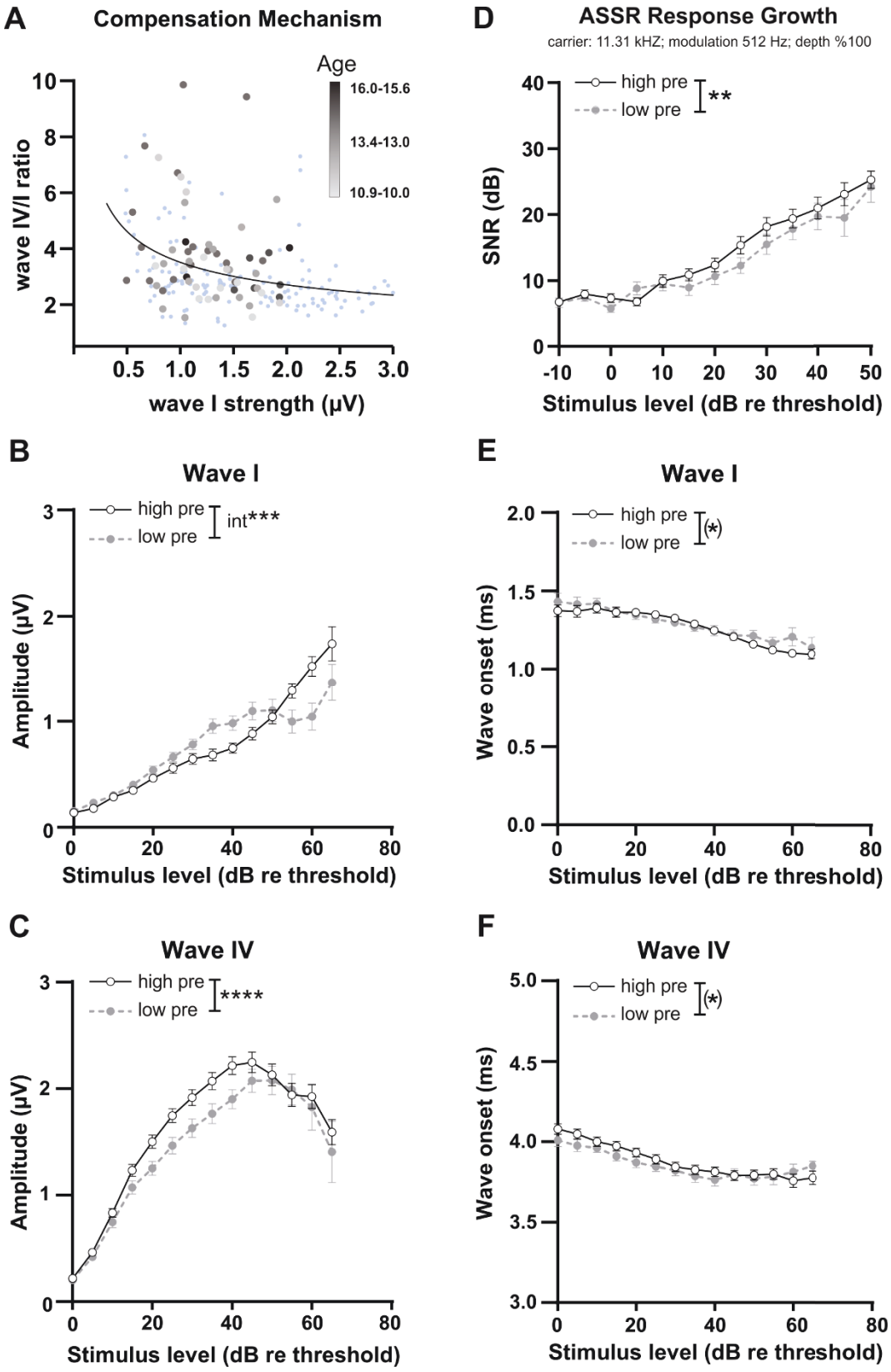

Figure.3 | The hearing phenotype of middle-aged *low* and *high compensators* before treatment. (A) ABR wave-IV/I amplitude ratio plotted as a function of ABR wave-I strength for individual mice, representing animals with reduced ABR wave-I (ABR wave I strength < 2.0 µV) subdivided along the black regression line according to their central compensation capacity into *low compensators* (below

the line) and *high compensators* (above the line). **(B)** *Low* and *high compensators* respond differently at different sound intensities > 25dB (significant interaction). **(C)** *Low compensators* had significantly lower wave-IV amplitude than *high compensators*. **(D)** ASSR of *low compensators* was significantly decreased in comparison to *high compensators*. Both ABR wave-I **(E)** and -IV **(F)** latency tend to be shortened in *low compensators* in comparison to *high compensators*. Mean ± SEM. 2-way ANOVA, *p <0.05, **p <0.01, ***p <0.001, ****p <0.0001, $^{(*)}$ trend p <0.1.

Following the characterization of *low* and *high compensators* in terms of their auditory processing before treatment we assessed their auditory processing after 10 days of PDE9A inhibitor treatment. We confirmed our previous findings (Savitska et al., 2022) in which *low compensators* did not show any alteration in their ABR wave-I amplitudes in response to either vehicle or PDE9A inhibitor. In contrast, *high compensator* treated with vehicle had a significant loss in the ABR wave-I amplitude while PDE9A inhibitor treatment prevented this loss (data not shown here).

Spike timing analysis revealed that *low compensators* had significantly shortened ABR wave-I and -IV latency with both vehicle and PDE9A inhibitor treatment (Figure 4A, B & Figure 5A, B, (Calis, in preparation)). In *high compensators* only, vehicle treatment accelerated the ABR wave-I and -IV latency (Figure 4C & 5C, (Calis, in preparation)) whereas PDE9A inhibitor preserved latencies against this acceleration (Figure 4D & 5D, (Calis, in preparation)). These findings show that in response to treatment, the synchronous auditory neuronal responses might be not affected when the stress axis is impaired like in *low compensators*; yet, the accurate spike generation and onset coding of the sound was degraded due to injection stress which can be only prevented in *high compensators* with PDE9A inhibitor.

Given that the variance in the coding of the stimulus onset may compromise temporal auditory resolution we further analyzed ASSR to amplitude modulated sounds. ASSR analysis showed *that low compensators* did not respond to vehicle treatment (Figure 6A, (Calis, in preparation)). In contrast, with PDE9A inhibitors they exhibited a loss in their temporal resolution (Figure 6B, (Calis, in preparation)) *high compensators* when administered with vehicle had a loss in their ASSR response (Figure 6C, (Calis, in preparation)), but this effect has been counteracted by PDE9A inhibitor treatment (Figure 6D, (Calis, in preparation)).

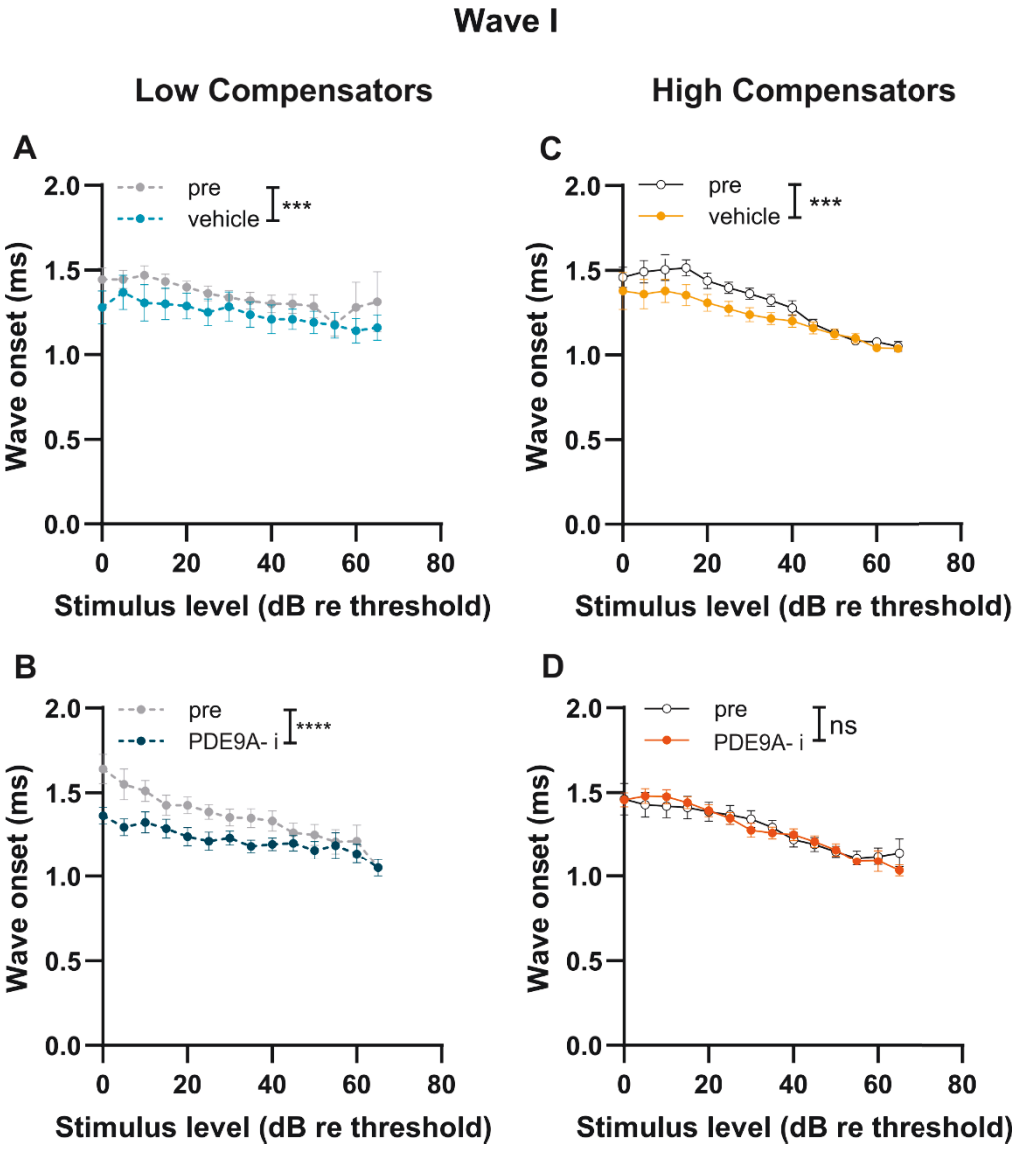

Figure.4 | ABR wave-I latency in *low* and *high compensators* before and after treatment with vehicle or PDE9A inhibitor (PDE9A- i). *Low compensators* when treated with vehicle **(A)** or PDE9A inhibitor **(B)** showed significantly shortened latency. Similarly, **(C)** *high compensators* administered with vehicle had reduced latency. **(D)** *high compensators* when treated with PDE9A inhibitor, showed no change of latency. Mean ± SEM. 2-way ANOVA, *p <0.05, **p <0.01, ***p <0.001, ****p <0.0001, (*) trend p <0.1.

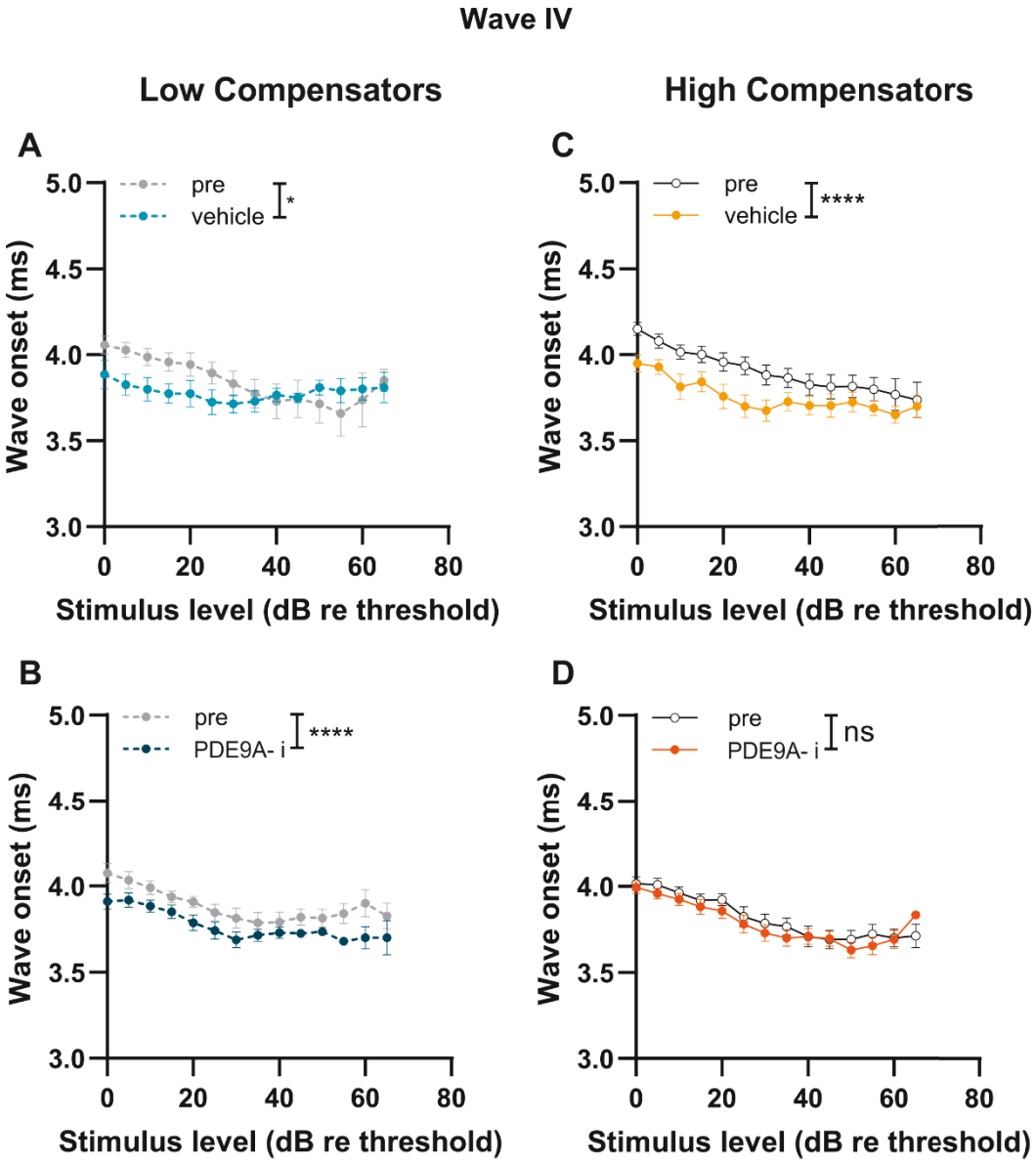

Figure.5 | ABR wave-IV latency in *low* and *high compensators* before and after treatment with vehicle or PDE9A inhibitor (PDE9A- i). *Low compensators* when treated with vehicle **(A)** or PDE9A inhibitor **(B)** showed significantly shortened latency. Similarly, **(C)** *high compensators* administered with vehicle had reduced latency. **(D)** *high compensators* when treated with PDE9A inhibitor, showed no change of latency. Mean ± SEM. 2-way ANOVA, *p <0.05, **p <0.01, ***p <0.001, ****p <0.0001, $^{(*)}$ trend p <0.1.

In order to identify the capacity for adaptation by altering the synaptic strength, we performed LTP recordings from the CA1 region of the hippocampus which were followed by LTD recordings. As we previously showed (Savitska et al., 2022), *low compensators* had lower LTP than *high compensators.* Additionally, *low compensators* did not show LTD while *high compensators* acquired LTD when presented with low-frequency stimulation (Figure 7B, (Calis, in preparation)).

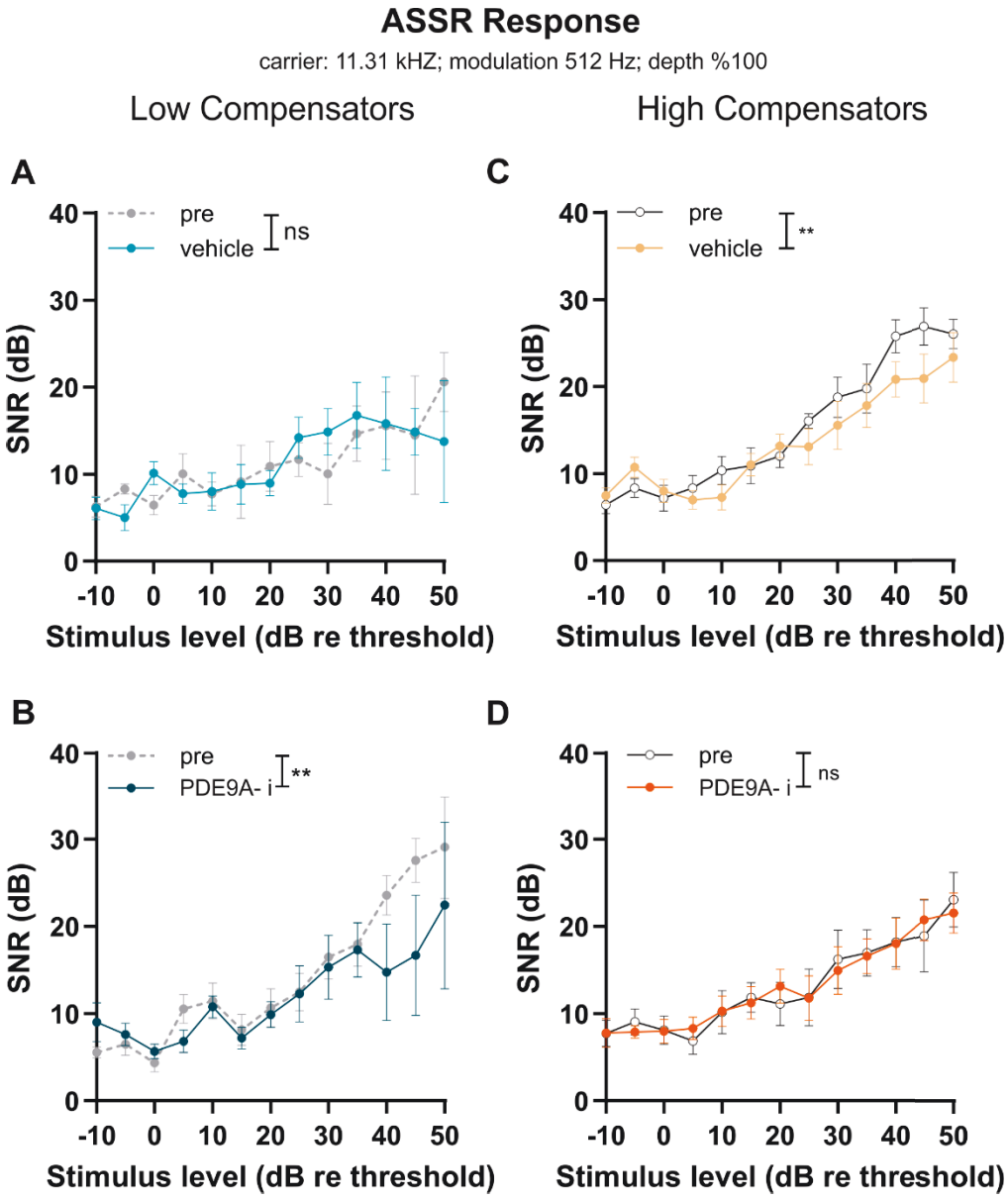

Figure.6 | Input-output relationship of auditory steady-state responses in *low* and *high compensators* treated with either vehicle or PDE9A inhibitor (PDE9A- i). (A) *Low compensators* treated with vehicle showed no change in response to treatment. **(B)** *Low compensators* treated with PDE9A inhibitor had a significant reduction in their ASSR responses. **(C)** *High compensators* when treated with vehicle showed a significant loss in their ASSR responses, however, this loss was prevented by PD9A inhibitor **(D)**. Mean ± SEM. 2-way ANOVA, *p <0.05, **p <0.01, ***p <0.001, ****p <0.0001, $^{(*)}$ trend p <0.1.

Moreover, neither vehicle treatment nor PDE9A inhibitor influenced LTP level in *low compensators*, hence either treatment did not affect their LTD (Figure 7B, blue bars, (Calis, in preparation)). In contrast, vehicle treatment significantly reduced LTP in *high compensators* in comparison to the untreated group, thus they did not have LTD. The reduction in LTP seemed to be overcome by the PDE9A inhibitor which was followed by significant LTD (Figure 7B, orange bars, (Calis, in preparation)).

As a morphological representation of synaptic plasticity and adaptation ability, we investigated dendritic spine remodeling from the CA1 region of the hippocampus. Our results revealed that *low* and *high compensators* differed in their composition of the dendritic spines. *Low compensators* had a significantly higher ratio of mushroom spines when compared to *high compensators*. Yet, *high compensators* had a higher ratio of immature spines (long-thin and thin spines) in comparison to *low compensators* (Figure 8D, (Calis, in preparation)).

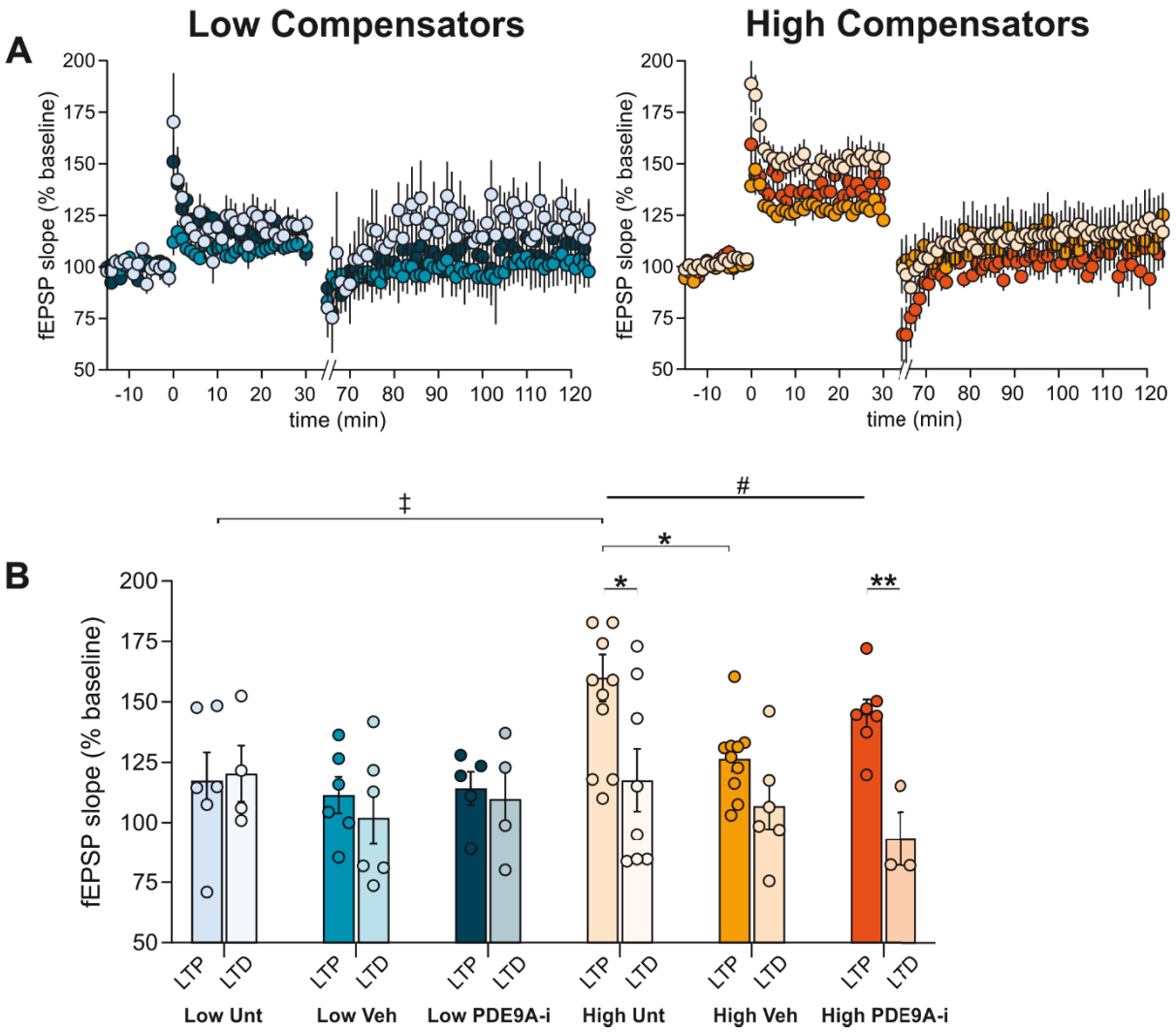

Figure.7 | Long-term potentiation (LTP) and long-term depression (LTD) of *low* and *high compensators* in response to treatment. (A) Averaged time courses of fEPSP slopes in acute coronal brain slices from *low compensators* (left panel) and *high compensators* (right panel) in all treatment groups**. (B)** The untreated *low compensators* (light blue bar) had significantly lower LTP in comparison to untreated *high compensators* (light orange bar). In addition, *low compensators* (light blue bars) did not show LTD while *high compensators* (light orange bars) showed a strong LTD. In *low compensators*, neither a vehicle (blue bar) nor PDE9A inhibitor (dark blue bar) treatment showed any effect on their already low LTP and LTD. In contrast, *high compensators* treated with a vehicle (orange bar) displayed a significant loss in LTP as well as in their LTD in comparison to their untreated controls (light orange bar). However, when treated with a PDE9A inhibitor (dark orange bar), *high compensators* had a slight

but not statistically significant elevation in their LTP, and significant LTD. Mean ± SEM. 1-way ANOVA, $^{‡}p < 0.05$, student t-test, $^{\#}p$, $*p < 0.05$, $**p < 0.01$.

In response to treatment, the results were similar to those obtained from the ABR amplitudes and LTP/LTD measurements, no alteration in their dendritic spine's composition was observed in *low compensators* (Figure 9A, (Calis, in preparation)). In contrast, *high compensators* exhibited a reduction in thin spines' ratio in response to treatment. However, the reduction in the thin spines' ratio was overcome by increasing the long-thin spines' ratio in the *high compensators* PDE9A inhibitor treated group which was not observed in the vehicle treated group (Figure 9B, (Calis, in preparation)).

Taken together, accurate onset coding may be a prerequisite to generate synchronous neuronal responses at different sound intensities and amplitude-modulated tones. The precise coding of the stimulation onset promotes the input gain to the ascending auditory pathway even in situations of cochlear synaptopathy. This compensation of a reduced auditory input may support the adaptive capacity of memory-dependent brain regions, identified in the present studies by LTP/LTD adjustment and dendritic spine remodeling in mice with *high compensation* capacity.

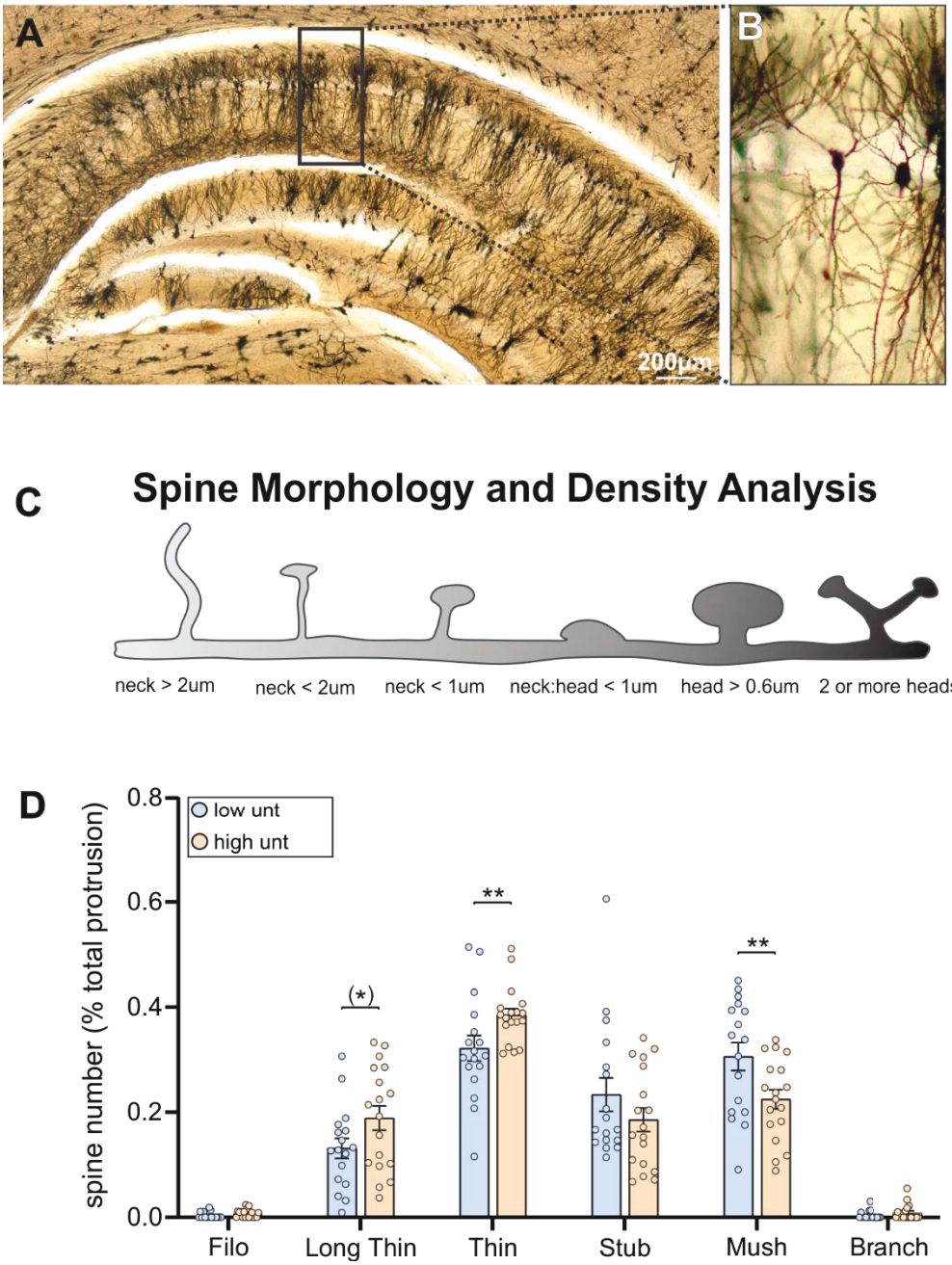

Figure.8 | Dendritic spine morphology analysis between *low* (blue) and *high compensators* (light orange). (A) Representative image of the CA1 region of the hippocampus from a Golgi-Cox impregnated mouse brain and **(B)** Magnification of uninterrupted pyramidal neuron in which the dendritic spine analysis was performed. **(C)** Abstract scheme of common dendritic spine types. Dendritic spines undergo maturation from left to right: from longer and thinner with small heads to shorter and wider heads. Their geometric characteristics, listed below each type, are used for objective identification and classification. **(D)** *Low* and *high compensators* exhibit differences in the dendritic spine composition. *Low compensators* had a significantly higher proportion of mushroom shape (mush) spines than *high compensators*. *High compensators* exhibited a significantly higher proportion of long-thin and thin spines than *low compensators*. Mean ± SEM. student t-test, *p <0.05, **p <0.01, $^{(*)}$ trend p <0.1.

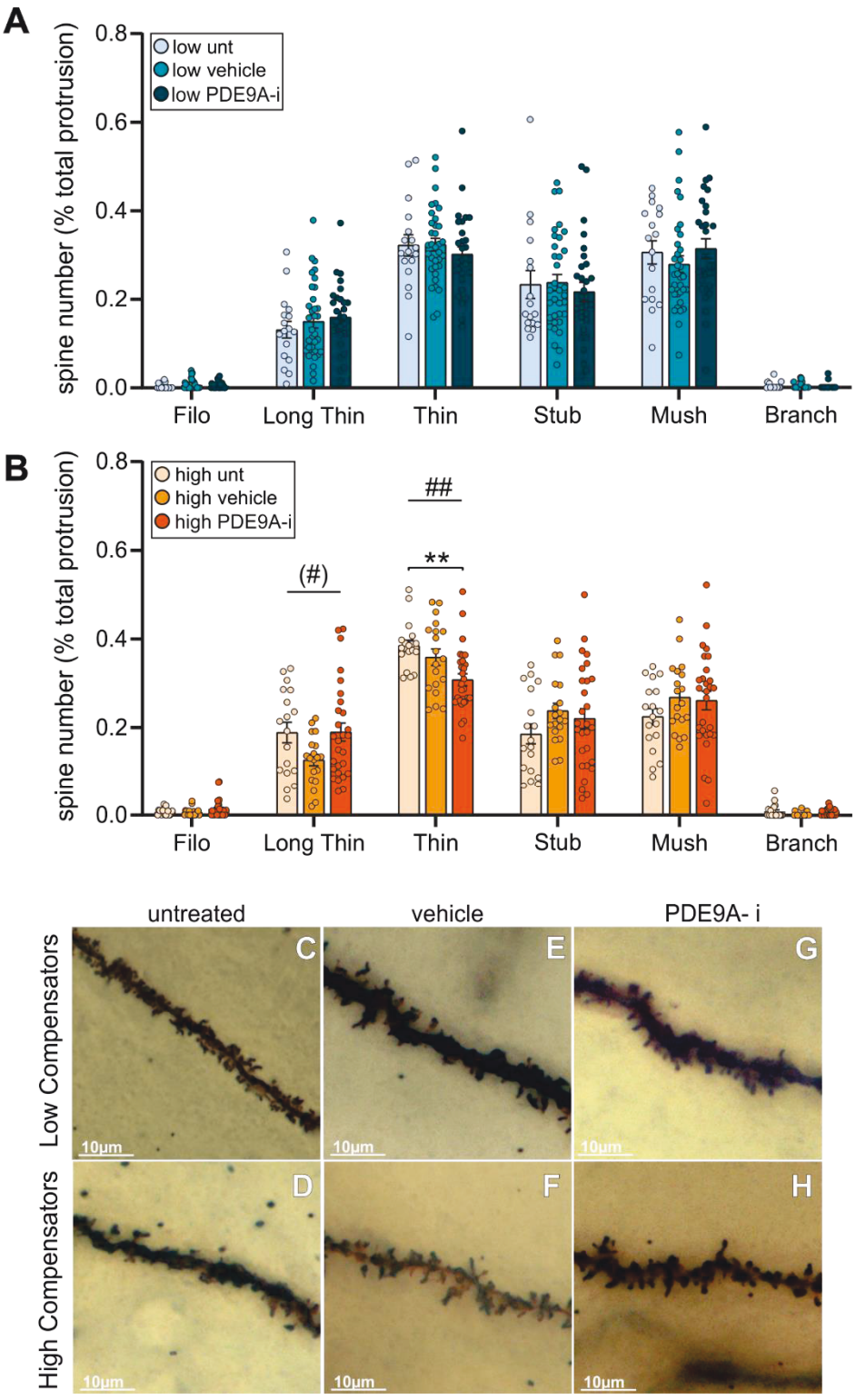

Figure.9 | Dendritic spine morphology analysis between *low* and *high compensators* in response to vehicle or PDE9A inhibitor treatment. (A) *Low compensators* did not show modifications in their dendritic spine distribution in response to either vehicle (blue) or PDE9A inhibitor (dark blue) treatment. **(B)** *High compensator* with vehicle treatment (orange) exhibited a reduction in the long-thin and thin spines. Treatment with a PDE9A inhibitor *high compensators* (dark orange) had a significant loss in their thin spines, however, this decrease was substituted by the increase in the long-

thin spines proportion. Representative images for *high compensators* **(C**, **E**, **G)** and *high compensators* **(D**, **F**, **G)**. Mean ± SEM. 1-way ANOVA $^{\#\#}$p, **p <0.01, $^{(\#)}$ trend p <0.1.

3.4. BK channels are required for Ca^{2+} oscillations to assist hippocampal long-term potentiation and memory formation

Large conductance Ca^{2+}- and voltage-activated K^+ channels (BK) are expressed throughout the brain and alteration in their function has been associated with cognitive impairments (Laumonnier et al., 2006; Miller et al., 2021). In this study (Pham et al., 2023), the role of BK channels in regulating Ca^{2+} oscillations involved in LTP, and memory formation was investigated. For this, a specific mouse model was used in which BK channels were exclusively deleted from the CA1 region of the hippocampus. In order to achieve this, a T29-1 transgenic subline in which *Cre* recombinase was expressed under the CaMKIIα promoter in CA1 pyramidal neurons (Tsien et al., 1996) was crossed with mice heterozygous for the floxed ($BK^{f/+}$; B6-$Kcnma1^{tm2.1Ruth}$) or the BK KO allele ($BK^{-/+}$; (B6-$Kcnma1^{tm1Ruth}$) (Sausbier et al., 2006). Subsequently, they were intercrossed with floxed BK ($BK^{f/f}$) mice, hence, as a result, CA1 specific conditional BK KOs were generated. CA1 specific BK deleted mice (Figure 1A, B, C (Pham, 2023)), exhibited a loss in memory acquisition and retrieval, revealed by the Morris Water Maze (Figure 2A, B (Pham, 2023)). Under *in vitro* cLTP protocol from hippocampal neurons, it was observed that intracellular K^+ concentration was reduced while L-Type Ca^{2+} channel- and NMDA receptor-dependent Ca^{2+} oscillation frequencies were increased (Figures 4 & 5, (Pham, 2023)). This feature is compromised when BK function was inhibited either pharmacologically or by genetic deletion (Figure 4 & 5, (Pham, 2023)). The translocation of AMPA receptors to the post-synapse is crucial for acquiring LTP. This requires the Glu1A phosphorylation at the S845 site of the AMPA receptor (Ferretti et al., 2015; Zhang & Abdullah, 2013). In the BK conditional KOs mice, Glu1A phosphorylation at the S845 site did not occur (Figure 3A, C, (Pham, 2023)). Overall, these findings highlighted the significance of BK-mediated K^+ outflow to support postsynaptic Ca^{2+} activity, which is required for hippocampal LTP, as well as learning and memory.

4. Discussion

Hearing loss has consistently been linked to accelerated cognitive decline and increased risk of developing dementia (Azeem et al., 2023; Griffiths et al., 2020). Age-related hearing loss can be commonly observed in adults due to accumulated noise damage to the cochlea (Cunningham & Tucci, 2017; Gourevitch et al., 2014) and results in progressive, irreversible damage to the auditory nerve, decoupling it from the sensory cells within the cochlea (Wang & Puel, 2020). This impoverishes the flow of acoustic information to the brain and deprives higher-order structures of auditory information, reflected by an impaired encoding of sound, which may underlie the poor speech intelligibility observed in older adults (Delano et al., 2020; Slade et al., 2020). Nevertheless, age-related hearing loss frequently remains neglected and undiagnosed for years. This is partially because of the slow progression of the disease, but even when the hearing function is regularly tested, current audiometric screening often only examines the hearing threshold as opposed to whether patients can make judgments about the spectral or temporal content of the sound (Gomez-Alvarez et al., 2023; Rees & Malmierca, 2005). Interestingly, age-related hearing loss may slowly trigger adaptations in the brain over a long period of time, a phenomenon which can be also observed in other sensory systems (Rich & Wenner, 2007; Schrode & Bee, 2015). This adaptation can take the form of central auditory plasticity, where the brain's auditory processing centers change their sensitivity to adjust to less auditory information (Caspary et al., 2008). One way the system can adapt to these changes in input could be through enhanced neural gain from the midbrain, which compensates for a reduced auditory input resulting from age-related cochlear synaptopathy (Chambers et al., 2016). It was previously shown that compensatory mechanisms require the preservation of inhibition to regulate the timing of an excitatory neuron's output by parvalbumin (PV) expressing, fast-spiking GABAergic neurons (Roux & Buzsaki, 2015). By providing inhibitory input, they regulate the synchrony and gain in higher brain regions and are crucial for the shaping of neural responses to fast temporal modulations (Caspary et al., 2008; Deng et al., 2020; Martin del Campo et al., 2012). This compensatory neural activity can be observed both in humans (Gu et al., 2012; Schaette & McAlpine, 2011) and in animals (Heeringa & van Dijk, 2014; Ruttiger et al., 2013). This compensation seems to help maintain temporal sound coding and may therefore protect speech understanding in complex environments.

4.1. Two endophenotypes of age-related hearing loss

Indeed, we have previously described that middle-aged animals can respond to the age-related loss in the auditory input (cochlear synaptopathy) in two different ways: either with low or high capacity to compensate by amplifying their central responses (ABR wave-IV) (Eckert et al., 2021; Mohrle et al., 2016). In the present study, our focus was to identify if it was possible to rescue the *low compensators*' phenotype by pharmacologically modulating the central synaptic plasticity mechanisms. For this purpose, we reviewed our previous studies to identify a drug that could target auditory function. We previously reported that GC-A KO mice exhibited age-related hearing deficits (Marchetta, Möhrle, et al., 2020). In addition, one of the cGMP modulating drugs - PDE9A inhibitors - have been reported to

preferentially regulate nuclear- and membrane-proximal cGMP pools primarily generated by GC-A (Harms et al., 2019; Lee et al., 2015; Patel et al., 2018) as well as to have a pro-cognitive effect (van der Staay et al., 2008), we tested a PDE9A inhibitor by 10 days administration in the *low* and *high compensator* middle-aged mice.

We suggest that *low* and *high compensators* represent two endophenotypes of age-related hearing loss that determine if mice can benefit from cognitive-enhancing treatment. Our findings revealed that the poor central compensation capacity in *low compensators* was associated with lower corticosterone levels prior to any treatment (Savitska et al., 2022). As previously shown (Eckert et al., 2021), low central compensation resulted in poorer temporal auditory processing, reduced hippocampal LTP, and decreased recruitment of activity-dependent BDNF expression in hippocampal regions in comparison to *high compensators*. In response to vehicle treatment, *high compensators* exhibited elevated blood corticosterone levels which resulted in reduced ABR wave-I amplitude, fewer inner hair cell ribbons, diminished temporal processing, reduced LTP responses, and decreased activity-dependent hippocampal BDNF expression that could be preserved upon PDE9A inhibitor treatment. In contrast, the same stress exposure through injection did not have the same effect on *low compensators*, suggesting that they have a blunted stress response (Berger et al., 2017; Charles L. Raison & Andrew H. Miller, 2003; Savitska et al., 2022).

As described in Chapter 1.2, the stress axis is regulated by two receptors: MR and GR, which are also involved in learning and adaptation processes. Hence, these receptors may also tune the memory-dependent adaptation processes following cochlear synaptopathy. The different stress axis functions between *low* and *high compensators* might be linked to the recruitment of activity-dependent BDNF transcripts, given the fact that BDNF drives the phosphorylation of GRs (Jeanneteau et al., 2019). Insufficient recruitment of activity-dependent BDNF as a consequence of hampered auditory input has been previously described (Marchetta, Savitska, et al., 2020; Matt et al., 2018). Therefore, it was suggested that the differences in activity-driven GR phosphorylation (Arango-Lievano et al., 2019) underlie the differences in memory-dependent adaption processes observed between *low* and *high compensators* (Savitska et al., 2022).

In the present study, only *high compensators* treated with the PDE9A inhibitor exhibited changes in PV expression level, with an increased level in the hippocampus. Whether or not the PDE9A inhibitor is directly involved in the PV expression pattern remains to be identified. The beneficial effect observed in *high compensators* may be attributed to the accompanying increase in BDNF expression level (Xu et al., 2010). Indeed, it was documented that BDNF-TrkB signaling increases the strength and number of GABAergic terminals in cortical regions (Abidin et al., 2008; Lau et al., 2022; Rutherford et al., 1997). Hence, the activity-dependent increase in the BDNF expression, possibly through the preserved synchronous auditory nerve activity, could promote the potentiation of inhibitory neurons which subsequently leads to the better temporal resolution observed in *high compensators* treated with the PDE9A inhibitor.

In the end, our findings highlight that central compensatory mechanisms cannot be pharmacologically rescued per se but can rather be protected during middle-aged against the maladaptive changes in auditory processing occurring over aging. Finally, we need to consider individual states of stress response as well as the identification of appropriate age intervals when exploring therapeutic interventions for age-dependent cochlear synaptopathy.

4.2. MR and GR determine the compensation phenotypes together with cGMP generators

We studied the influence of the stress response itself on auditory processing. Upon observing the stress response determining effects on compensatory mechanisms, we specifically examined the role of MR and GR in regulating central compensation capacity. We aimed to identify the role of MR and GR in the normally developed adult brain, which has up until now remained elusive since global KO mouse models are lethal (Erdmann et al., 2007). Further, given that these receptors are involved in brain development in addition to learning and memory (Eachus et al., 2021; van Bodegom et al., 2017), even if the deletion of MR and GR were possible in the immature brain, doing so may compromise the development of the auditory function. We therefore used tamoxifen-inducible conditional single or combined deletion of MR and GR in forebrain regions. Our results revealed the complex, interdependent relationship between MR and GR and their action on memory-dependent adaptation processes for auditory neural gain processes as well as stress responses.

MR and GR mediate sequential stages of the stress response due to their different binding affinities. MR, with a lower affinity, is involved in the appraisal process while GR, with a higher affinity, is activated either with circadian peak or elevated stress (Berger et al., 2017; Mifsud & Reul, 2018). Our analysis of the expression level of MR and GR from hippocampal brain sections revealed that GR expression was significantly elevated in MR cKO mice in comparison to their WT control, as previously shown (Berger et al., 2006; Erdmann et al., 2007), suggesting that the MR cKO phenotype could be caused by increased GR expression levels. This GR upregulation likely occurs as a compensatory mechanism to replace the MR-control of the basal activity of the HPA-axis (de Kloet et al., 2018). Interestingly, a loss of the negative feedback of GR on the HPA axis could be observed in GR cKO mice, which exhibited significantly higher levels of blood corticosterone (Marchetta et al., 2022), as also previously shown (Erdmann et al., 2007). The phenotype of GR cKO mice should therefore be interpreted with consideration of a disinhibited HPA-axis function in addition to the loss of GR (Harris et al., 2013).

Since we were interested in the memory-dependent adaptation processes and central neural gain in the auditory system of these mice, we explored the hearing function and the hippocampal plasticity changes, as previously described (Eckert et al., 2021; Matt et al., 2018). Although the hippocampus lies outside the classical auditory pathway, it has been documented that it is dramatically affected by hearing problems (Eckert et al., 2021; Manohar et al., 2022; Matt et al., 2018). The hippocampus receives vital sensory information and, by integrating them, forms a cognitive map for top-down

control of various sensory modalities (Antunes & Malmierca, 2021; Gilbert & Sigman, 2007). In order to make use of this cognitive map, memory-dependent amplification processes need to take place. Therefore, LTP recordings from the CA1 region of the hippocampus were performed in MR and/or GR cKO mice. Most remarkably, only MR cKO mice exhibited elevated LTP, which co-occurred with enhanced auditory neural gain compared to their WT controls. The increase in LTP and auditory neural gain can be linked to the increased function and expression of GR observed in MR cKO mice.

In light of our previous findings suggesting that auditory neural gain is a stress- and cGMP-dependent process, we studied the NO-GC and GC-A expression levels from the hippocampal CA1 region. Additionally, in the same region, we explored the Arc expression levels as a marker for synaptic plasticity (Hedde et al., 2021; Tzingounis & Nicoll, 2006). While the NO-GC expression was elevated in MR, GR, and MRGR cKO mice, the GC-A and Arc expression levels were higher only when MR was deleted. This points out that enhanced auditory neural gain and LTP co-occur with elevated GC-A and Arc expression in MR cKO mice. Taken together, these findings can indeed be attributed to a higher GR expression level rather than MR deletion. When GR is deleted, mice did not exhibit an elevation in neural gain or LTP, suggesting that increased GR expression along with increased expression of GC-A and Arc may promote the neural gain and LTP via top-down facilitation mechanisms (Asilador & Llano, 2021; Suga, 2020).

Finally, given that MR and GR also exhibit a genomic function as transcription factors through binding to glucocorticoid-responsive elements (GRE), we investigated if MR and GR may regulate the transcription of cGMP generators NO-GC and GC-A and Arc. A GRE that is a potential MR-specific recognition site (van Weert et al., 2017) exists in the start codon of NO-GC (Gucy1a1). For GC-A and Arc promoter regions, no GRE motifs were found. However, the relevance of the identified motifs for NO-GC subunits should be reviewed since the NO-GC expression level was nevertheless elevated in double cKO mice. Therefore, an alternative mechanism to explain the altered expression of NO-GC, GC-A, and Arc should be revisited.

Although highly speculative, there might be a shared intracellular mechanism between stress receptors (MR & GR) and NO-GC and GC-A, such that an elevated expression of these cGMP generators might be compensatory and substitute the function of the individual stress receptors. One possibility to consider would be the activation of cAMP-response element binding protein (CREB) as a transcription factor for BDNF, which can be phosphorylated at Ser133 by cAMP and cGMP (Lueptow et al., 2016). It is well known that CREB regulates the transcription of BDNF (Guo et al., 2017; Tao et al., 1998) in response to neural activity, especially by activation of the BDNF promoter IV (Cha-Molstad et al., 2004; Hong et al., 2008; West et al., 2014). Some studies report that CREB is also involved in the transcription of TrkB (Deogracias et al., 2004; Kingsbury et al., 2003; Lonze & Ginty, 2002). Remarkably, TrkB transcription is also regulated by MR and GR (Peters et al., 2018) such that during basal HPA axis activity, with low glucocorticoid concentration, MR drives TrkB production (Stranahan et al., 2011). Last but not least, BDNF modulates and maintains its own expression via TrkB receptors through an autoregulatory loop (Esvald et al., 2020; Nakajima et al., 2015; Tuvikene et al., 2016). In this context,

it could be considered that to maintain the TrkB-BDNF signaling following the deletion of the MR/GR receptors in the adult brain, CREB as an alternative transcription factor for TrkB may be activated by an increase of the intracellular cGMP levels through elevated NO-GC and GC-A expression.

To conclude, our study highlights that stress receptors in the brain play complex roles in modulating not only the stress response but also sensory processing, neuronal plasticity, and cGMP signaling. In our model, we suggest that MR deletion leads to elevated GR expression levels, which, as a consequence, elevate GC-A and Arc expression levels in the hippocampus. These alterations may synergistically boost hippocampal LTP, thus providing a means for top-down mechanisms enabling auditory neural gain.

4.3. Plastic dendritic spines are required for memory-dependent adaption to reduced cochlear function

Finally, two endophenotypes in mice - *low* and *high compensators* - as a consequence of age-related hearing loss have been extensively described. In our recent findings, we identified that the compensation capacity becomes decisive in an age window we defined as “middle-aged”. The changes in compensation capacity during this age window also coincide with functional changes of the stress-axis. This led us to postulate that a central auditory adaption capacity that requires an appropriate stress axis drives neuronal plasticity and cGMP signaling.

In another study, we first assessed the hearing function of mice and classified them as *low* and *high compensators* then analyzed the latency of the ABR wave-I and-IV. While ABR wave amplitudes reflect the synchronous spike activity of auditory responses, the latency reflects the fine timing of when this spike occurs in response to sound stimuli. Reliable spike timing is critical for normal auditory processing (Buran et al., 2010). Our findings showed that *low compensators* tend to have shorter latency for ABR wave-I and -IV (Figure 3E, F) and had poorer temporal resolution than *high compensators*, indicated by a lower signal-to-noise ratio in ASSRs (Figure 3D). On the other hand, the auditory nerve typically responds to increasing sound levels with a gradually increasing spike rate (Schalk & Sachs, 1980); however, *low compensators* fail to respond to high sound pressure levels, with a discharge rate at which may already be saturated (Figure 3B). This failure might be due to the imprecise encoding of stimulus onset time in the auditory periphery, reflected by shortened ABR wave-I latency that later propagates to ABR wave-IV (Buran et al., 2010).

Although we have previously described the *low compensators* as unresponsive to the treatment due to their blunted stress response on the basis of ABR wave amplitudes (Savitska et al., 2022), in this second study, assessing ABR wave latencies revealed a slightly different outcome. When treated with either vehicle or PDE9A inhibitor, both ABR wave-I and -IV in *low compensators* were significantly accelerated in *high compensators*, on the other hand, exhibited a vehicle-induced shortening of the ABR wave-I and -IV latency which was prevented by the PDE9A inhibitor. The accelerated auditory nerve and midbrain responses in *low compensators* could be associated with a downregulation of inhibitory strength, as was characterized by the reduced PV expression in Savitska et al., (2022), which

could be a maladaptive plasticity change as a consequence of the decoupling of the auditory nerve (Ibrahim & Llano, 2019; Knipper et al., 2021).

Accordingly, the analysis of the ASSR showed that vehicle-treated *low compensators* do not show a treatment response and the PDE9A inhibitor made the ASSR even worse. In contrast, in *high compensators*, as shown before, vehicle treatment reduced the ASSR, which was counteracted by the PDE9A inhibitor. The synchronous response to amplitude-modulated tones and the accuracy in the spike timing relative to the stimulus onset are indicators to evaluate temporal precision (Buran et al., 2010). Precise coding of the sound is necessary for complex auditory tasks like sound localization or speech perception (Buran et al., 2010; Heil & Peterson, 2017; Walton, 2010). Considering our findings, it could be suggested that having accelerated onset coding of the sound does not necessarily mean an improvement in auditory function, since it was followed by poor ASSRs. Instead, the unreliable onset responses and poor temporal resolution would be estimates for compromised auditory processing, like difficulties in speech understanding.

As suggested before, *low* and *high compensators* differ in their adaptation capacity following cochlear synaptopathy; therefore, we performed more a more elaborated functional and structural analysis. In support of this, *low compensators* had less LTP than *high compensators*, and they did not have LTD following LTP. This unresponsiveness was also observed when they received either a vehicle or a PDE9A inhibitor. However, *high compensators* had a higher level of LTP and later were able to recruit LTD. As expected, vehicle treatment led to a loss in the LTP/LTD adjustment, while the PDE9A inhibitor prevented the stress-induced reduction in LTP and later supported the mechanisms for LTD. Indeed, hippocampal LTP is considered a model for learning ability, while LTD reflects cognitive flexibility (Collingridge et al., 2010; Nicholls et al., 2008). The activity-dependent trafficking of AMPA receptors into and out of synapses during LTP and LTD, respectively, has been postulated as the underlying mechanism (Penn et al., 2017; Sumi & Harada, 2020). The changes in the synaptic strength are followed by the modification of spine morphology (Matsuzaki et al., 2004).

Further, structural analysis of dendritic spines from the CA1 region of the hippocampus showed that *low compensators* had fewer long-thin/thin spines and more mushroom spines than *high compensators*. Mushroom spines (memory spines) are generally associated with mature and stable synaptic connections, while long and thin spines (learning spines) are more plastic and can change more readily, which might be indicative of the capacity for neuroplasticity (Berry & Nedivi, 2017; Bourne & Harris, 2007). Likewise, they did not show any modification upon treatment, while *high compensators* primarily lost long-thin/thin spines after vehicle treatment. This loss was counteracted by PDE9A inhibitor treatment, giving rise to the new protrusions elicited by the increased proportion of long-thin spines. Long and thin spines have been consistently characterized as containing a lower AMPA to NMDA ratio (Bosch et al., 2014; Matsuzaki et al., 2001), which promotes structural flexibility. Hence, upon LTP induction, learning spines are transformed into memory spines (Bourne & Harris, 2007). This is carried out by the spine neck geometry, which determines the NMDA receptor dependent Ca^{2+} signaling (Noguchi et al., 2005), where a narrow and long spine neck provides a higher

electrical resistance (Tonnesen et al., 2014), thus retaining more Ca^{2+} in their head and, in turn, locally boosts the magnitude of the post-synaptic potential (Bourne & Harris, 2007; Noguchi et al., 2005; Tonnesen et al., 2014). In light of these, the lack of LTP/LTD adjustments observed in *low compensators* could be structurally linked with their lower proportion of long-thin/thin spines. Consequently, this could also be the root of their cognitive inflexibility in which they fail to sustain adaptive behavior upon sensory deprivation due to cochlear synaptopathy (Caspary et al., 2002; Rumschlag & Razak, 2021).

Following synaptic activity, the immediate-early gene Arc expression increases, which regulates the AMPA receptor trafficking in the post-synapse (Korb & Finkbeiner, 2011; Rial Verde et al., 2006). Arc has been shown to influence spine size, such that a higher Arc expression increased the proportion of long and thin spines while reducing short and mushroom spines (Peebles et al., 2010). Hence, it could be hypothesized that *low compensators* would have a lower Arc expression level than *high compensators* in the postsynaptic spines of the CA1 region of the hippocampus, which in turn impairs their AMPA receptor trafficking (Diering & Huganir, 2018; Eckert et al., 2021; Park, 2018). A lower level of Arc expression in *low compensators* can be expected due to their low level of BNDF expression (Savitska et al., 2022), given that the transcription of Arc is tightly influenced by the TrkB-BDNF signaling (Wibrand et al., 2006; Ying et al., 2002). This is further supported by the unchanged BDNF expression level observed in *low compensators* after treatment (Savitska et al., 2022). Alternatively, both Arc (Kawashima et al., 2009) and BDNF (Guo et al., 2017; Tao et al., 1998) expression can be induced by CREB. This could indeed support the observation in *high compensators* in which the vehicle-induced loss of long-thin/thin spines was replaced by new protrusions of long-thin spines when treated with PDE9A inhibitor. It could be suggested that the stressful effect of injection may have caused a reduction in CREB-dependent signaling and thus the transcription of Arc and BDNF, leading to the loss of synaptic arborization. Increasing intracellular cGMP levels after treatment with the PDE9A inhibitor might have been protective by intervening in the corticosterone-induced loss of CREB phosphorylation (Huang et al., 2018).

4.4. BK channels and their role in synaptic plasticity

Assuming that central auditory compensatory mechanisms and memory-dependent adaptation processes are closely linked, we considered the function of BK channels as a mediator. Until now, although we have no direct evidence for a link between better cognitive capacity and auditory neural gain, we suggest that both require an LTP-dependent memory facilitation to adapt to the changes in sensory input. As previously summarized, LTP is a functional proof for synaptic plasticity which relies on NMDA receptor and L-type calcium channels (LTCC). Upon calcium influx, AMPA receptor subunits are phosphorylated and enhance synaptic transmission. BK channels may therefore support the entry of Ca^{2+} through NMDAR or LTCC. In addition, BK channels seem to have a dual role, affecting both the repolarization phase after action potentials and supporting the Ca^{2+} oscillations which are critical for LTP. These findings may suggest that BK channels are activated by Ca^{2+} entry through NMDAR and

LTCC, which leads to K^+ outflow and amplifies Ca^{2+} spiking frequency. This facilitates further Ca^{2+} entry, promoting LTP through the phosphorylation of AMPA receptors and increased synaptic efficiency. Finally, considering the critical role of BK channels in terms of cognitive function (Typlt et al., 2013), it would be interesting to re-evaluate their role under the auditory neural gain as an alternative synaptic plasticity regulator by improving cognitive outcome.

4.5. Conclusion

The results of our current studies offer valuable insights into understanding of central mechanism and whether improving adaptation can be taken as an approach to prevent or delay the sensory and cognitive deficits from age-related hearing loss. The findings highlighted the intricate relationship between stress receptors, HPA-axis reactivity, synaptic plasticity, memory function, and activity-dependent genes.

In our studies, in addition to the middle-aged mice, we initially intended to include a group of mice older than 14 months, yet it was not possible due to the limited number of animals. It should be noted that, although it was not documented in detail in the present study, old mice were more likely to be classified as *low compensators* phenotype. It might be due to the decreasing compensation capacity of ABR wave-IV with age (Eckert et al., 2021; Mohrle et al., 2016). Hence, it can be suggested that central neural gain in age-related synaptopathy can take place only a limited period during mid-life (Mohrle et al., 2016; Tune et al., 2021) and that later, old animals may develop a blunted stress response, as noted in *low compensators*, and therefore may no longer be able to benefit from the cognitive-enhancing treatment for auditory compensation. Regarding this, it would be interesting to take into account that increased synaptic plasticity and cognition upon the treatment with a PDE9A inhibitor have been documented in old rats but not in young rats. This was linked to a corrected balance of protein kinase/phosphatase activities by restoring intracellular cGMP levels which are diminished due to aging (van der Staay et al., 2008). This could suggest that for PDE inhibitors to exert an effect, it may require the organism to undergo challenges like age-dependent loss on the intracellular level or the stressful conditions observed in *high compensators*. Taken together, these emphasize the necessity of determining the critical age interval to take action in order to prevent the adversity of age-related hearing loss, by use of the cognitive enhancers. On the other hand, it was documented that the PDE9A expression was also found in the cochlea (Marchetta et al., 2022) Currently, our studies cannot reveal the role of PDE9A inhibitor from cochlea in relation to our observations in *low* and *high compensators*. When the interplay between stress receptors (MR and GR) and cGMP signaling is considered, it should be kept in mind that those receptors are also expressed in the cochlea (Marchetta et al., 2022). Therefore, future studies should reveal the origin of the effect of PDE9A inhibitor either from the brain or the auditory periphery, in addition to its interaction with the stress receptors, under age-related hearing loss.

5. References

Abidin, I., Eysel, U. T., Lessmann, V., & Mittmann, T. (2008). Impaired GABAergic inhibition in the visual cortex of brain-derived neurotrophic factor heterozygous knockout mice. *J Physiol*, *586*(7), 1885-1901. https://doi.org/10.1113/jphysiol.2007.148627

Allen, N. B., & Badcock, P. (2003). The social risk hypothesis of depressed mood: evolutionary, psychosocial, and neurobiological perspectives. *Psychological bulletin*, *129 6*, 887-913.

Andreeva, S. G., Dikkes, P., Epstein, P. M., & Rosenberg, P. A. (2001). Expression of cGMP-specific phosphodiesterase 9A mRNA in the rat brain. *J Neurosci*, *21*(22), 9068-9076. https://doi.org/10.1523/JNEUROSCI.21-22-09068.2001

Antunes, F. M., & Malmierca, M. S. (2021). Corticothalamic Pathways in Auditory Processing: Recent Advances and Insights From Other Sensory Systems. *Front Neural Circuits*, *15*, 721186. https://doi.org/10.3389/fncir.2021.721186

Arango-Lievano, M., Borie, A. M., Dromard, Y., Murat, M., Desarmenien, M. G., Garabedian, M. J., & Jeanneteau, F. (2019). Persistence of learning-induced synapses depends on neurotrophic priming of glucocorticoid receptors. *Proc Natl Acad Sci U S A*, *116*(26), 13097-13106. https://doi.org/10.1073/pnas.1903203116

Argyrousi, E. K., Heckman, P. R. A., & Prickaerts, J. (2020). Role of cyclic nucleotides and their downstream signaling cascades in memory function: Being at the right time at the right spot. *Neurosci Biobehav Rev*, *113*, 12-38. https://doi.org/10.1016/j.neubiorev.2020.02.004

Asilador, A., & Llano, D. A. (2021). Top-Down Inference in the Auditory System: Potential Roles for Corticofugal Projections [Review]. *Frontiers in Neural Circuits*, *14*. https://doi.org/10.3389/fncir.2020.615259

Azeem, A., Julleekeea, A., Knight, B., Sohail, I., Bruyns-Haylett, M., & Sastre, M. (2023). Hearing loss and its link to cognitive impairment and dementia [Review]. *Frontiers in Dementia*, *2*. https://doi.org/10.3389/frdem.2023.1199319

Baillie, G. S., Tejeda, G. S., & Kelly, M. P. (2019). Therapeutic targeting of 3',5'-cyclic nucleotide phosphodiesterases: inhibition and beyond. *Nat Rev Drug Discov*, *18*(10), 770-796. https://doi.org/10.1038/s41573-019-0033-4

Bellistri, E., Aguilar, J., Brotons-Mas, J. R., Foffani, G., & de la Prida, L. M. (2013). Basic properties of somatosensory-evoked responses in the dorsal hippocampus of the rat. *J Physiol*, *591*(10), 2667-2686. https://doi.org/10.1113/jphysiol.2013.251892

Bender, A. T., & Beavo, J. A. (2006). Cyclic nucleotide phosphodiesterases: molecular regulation to clinical use. *Pharmacol Rev*, *58*(3), 488-520. https://doi.org/10.1124/pr.58.3.5

Berger, M., Leicht, A., Slatcher, A., Kraeuter, A. K., Ketheesan, S., Larkins, S., & Sarnyai, Z. (2017). Cortisol Awakening Response and Acute Stress Reactivity in First Nations People. *Sci Rep*, *7*, 41760. https://doi.org/10.1038/srep41760

Berger, S., Wolfer, D. P., Selbach, O., Alter, H., Erdmann, G., Reichardt, H. M., Chepkova, A. N., Welzl, H., Haas, H. L., Lipp, H. P., & Schutz, G. (2006). Loss of the limbic mineralocorticoid receptor impairs behavioral plasticity. *Proc Natl Acad Sci U S A*, *103*(1), 195-200. https://doi.org/10.1073/pnas.0503878102

Berkefeld, H., & Fakler, B. (2013). Ligand-gating by Ca2+ is rate limiting for physiological operation of BK(Ca) channels. *J Neurosci*, *33*(17), 7358-7367. https://doi.org/10.1523/JNEUROSCI.5443-12.2013

Berry, K. P., & Nedivi, E. (2017). Spine Dynamics: Are They All the Same? *Neuron*, *96*(1), 43-55. https://doi.org/10.1016/j.neuron.2017.08.008

Bharadwaj, H., Verhulst, S., Shaheen, L., Liberman, M. C., & Shinn-Cunningham, B. (2014). Cochlear neuropathy and the coding of supra-threshold sound [Hypothesis and Theory]. *Frontiers in Systems Neuroscience*, *8*. https://doi.org/10.3389/fnsys.2014.00026

Bliss, T. V. P., Collingridge, G. L., Morris, R. G. M., & Reymann, K. G. (2018). Long-term potentiation in the hippocampus: discovery, mechanisms and function. *Neuroforum*, *24*(3), A103-A120. https://doi.org/doi:10.1515/nf-2017-A059

Blokland, A., Schreiber, R., & Prickaerts, J. (2006). Improving memory: a role for phosphodiesterases. *Curr Pharm Des*, *12*(20), 2511-2523. https://doi.org/10.2174/138161206777698855

Bonhoeffer, T., & Yuste, R. (2002). Spine motility. Phenomenology, mechanisms, and function. *Neuron*, *35*(6), 1019-1027. https://doi.org/10.1016/s0896-6273(02)00906-6

Bosch, M., Castro, J., Saneyoshi, T., Matsuno, H., Sur, M., & Hayashi, Y. (2014). Structural and molecular remodeling of dendritic spine substructures during long-term potentiation. *Neuron*, *82*(2), 444-459. https://doi.org/10.1016/j.neuron.2014.03.021

Bourne, J., & Harris, K. M. (2007). Do thin spines learn to be mushroom spines that remember? *Curr Opin Neurobiol*, *17*(3), 381-386. https://doi.org/10.1016/j.conb.2007.04.009

Bowl, M. R., & Dawson, S. J. (2019). Age-Related Hearing Loss. *Cold Spring Harb Perspect Med*, *9*(8). https://doi.org/10.1101/cshperspect.a033217

Bramhall, N., Ong, B., Ko, J., & Parker, M. (2015). Speech Perception Ability in Noise is Correlated with Auditory Brainstem Response Wave I Amplitude. *J Am Acad Audiol*, *26*(5), 509-517. https://doi.org/10.3766/jaaa.14100

Bramhall, N. F., McMillan, G. P., & Kampel, S. D. (2021). Envelope following response measurements in young veterans are consistent with noise-induced cochlear synaptopathy. *Hear Res*, *408*, 108310. https://doi.org/10.1016/j.heares.2021.108310

Bramham, C. R., & Messaoudi, E. (2005). BDNF function in adult synaptic plasticity: the synaptic consolidation hypothesis. *Prog Neurobiol*, *76*(2), 99-125. https://doi.org/10.1016/j.pneurobio.2005.06.003

Bramham, C. R., Worley, P. F., Moore, M. J., & Guzowski, J. F. (2008). The immediate early gene arc/arg3.1: regulation, mechanisms, and function. *J Neurosci*, *28*(46), 11760-11767. https://doi.org/10.1523/JNEUROSCI.3864-08.2008

Brewster, K. K., Deal, J. A., Lin, F. R., & Rutherford, B. R. (2022). Considering hearing loss as a modifiable risk factor for dementia. *Expert Rev Neurother*, *22*(9), 805-813. https://doi.org/10.1080/14737175.2022.2128769

Buran, B. N., Strenzke, N., Neef, A., Gundelfinger, E. D., Moser, T., & Liberman, M. C. (2010). Onset coding is degraded in auditory nerve fibers from mutant mice lacking synaptic ribbons. *J Neurosci*, *30*(22), 7587-7597. https://doi.org/10.1523/JNEUROSCI.0389-10.2010

Burow, A., Day, H. E., & Campeau, S. (2005). A detailed characterization of loud noise stress: Intensity analysis of hypothalamo-pituitary-adrenocortical axis and brain activation. *Brain Res*, *1062*(1-2), 63-73. https://doi.org/10.1016/j.brainres.2005.09.031

Calamera, G., Moltzau, L. R., Levy, F. O., & Andressen, K. W. (2022). Phosphodiesterases and Compartmentation of cAMP and cGMP Signaling in Regulation of Cardiac Contractility in Normal and Failing Hearts. *Int J Mol Sci*, *23*(4). https://doi.org/10.3390/ijms23042145

Calis, D., Hess, M., Marchetta, P., Singer, W., Modro, J., Nelissen, E., Prickaerts, J., Sandner, P., Lukowski, R., Ruth, P., Knipper, M., & Ruttiger, L. (2023). Acute deletion of the central MR/GR steroid receptor correlates with changes in LTP, auditory neural gain, and GC-A cGMP signaling. *Front Mol Neurosci*, *16*, 1017761. https://doi.org/10.3389/fnmol.2023.1017761

Canlon, B., Theorell, T., & Hasson, D. (2013). Associations between stress and hearing problems in humans. *Hear Res*, *295*, 9-15. https://doi.org/10.1016/j.heares.2012.08.015

Caspary, D. M., Ling, L., Turner, J. G., & Hughes, L. F. (2008). Inhibitory neurotransmission, plasticity and aging in the mammalian central auditory system. *J Exp Biol*, *211*(Pt 11), 1781-1791. https://doi.org/10.1242/jeb.013581

Caspary, D. M., Palombi, P. S., & Hughes, L. F. (2002). GABAergic inputs shape responses to amplitude modulated stimuli in the inferior colliculus. *Hear Res*, *168*(1-2), 163-173. https://doi.org/10.1016/s0378-5955(02)00363-5

Cha-Molstad, H., Keller, D. M., Yochum, G. S., Impey, S., & Goodman, R. H. (2004). Cell-type-specific binding of the transcription factor CREB to the cAMP-response element. *Proc Natl Acad Sci U S A*, *101*(37), 13572-13577. https://doi.org/10.1073/pnas.0405587101

Chambers, A. R., Resnik, J., Yuan, Y., Whitton, J. P., Edge, A. S., Liberman, M. C., & Polley, D. B. (2016). Central Gain Restores Auditory Processing following Near-Complete Cochlear Denervation. *Neuron*, *89*(4), 867-879. https://doi.org/10.1016/j.neuron.2015.12.041

Chao, M. V. (2003). Neurotrophins and their receptors: a convergence point for many signalling pathways. *Nat Rev Neurosci*, *4*(4), 299-309. https://doi.org/10.1038/nrn1078

Charles L. Raison, M.D. , and, & Andrew H. Miller, M.D. (2003). When Not Enough Is Too Much: The Role of Insufficient Glucocorticoid Signaling in the Pathophysiology of Stress-Related Disorders. *American Journal of Psychiatry*, *160*(9), 1554-1565. https://doi.org/10.1176/appi.ajp.160.9.1554

Citri, A., & Malenka, R. C. (2008). Synaptic plasticity: multiple forms, functions, and mechanisms. *Neuropsychopharmacology*, *33*(1), 18-41. https://doi.org/10.1038/sj.npp.1301559

Collingridge, G. L., Peineau, S., Howland, J. G., & Wang, Y. T. (2010). Long-term depression in the CNS. *Nat Rev Neurosci*, *11*(7), 459-473. https://doi.org/10.1038/nrn2867

Cruickshanks, K. J., Tweed, T. S., Wiley, T. L., Klein, B. E., Klein, R., Chappell, R., Nondahl, D. M., & Dalton, D. S. (2003). The 5-year incidence and progression of hearing loss: the epidemiology of hearing loss study. *Archives of otolaryngology--head & neck surgery*, *129 10*, 1041-1046.

Cunha, A. O. S., Ceballos, C. C., de Deus, J. L., Pena, R. F. O., de Oliveira, J. A. C., Roque, A. C., Garcia-Cairasco, N., & Leao, R. M. (2018). Intrinsic and synaptic properties of hippocampal CA1 pyramidal neurons of the Wistar Audiogenic Rat (WAR) strain, a genetic model of epilepsy. *Sci Rep*, *8*(1), 10412. https://doi.org/10.1038/s41598-018-28725-y

Cunningham, L. L., & Tucci, D. L. (2017). Hearing Loss in Adults. *N Engl J Med*, *377*(25), 2465-2473. https://doi.org/10.1056/NEJMra1616601

Dallos, P. (1986). Neurobiology of cochlear inner and outer hair cells: intracellular recordings. *Hear Res*, *22*, 185-198. https://doi.org/10.1016/0378-5955(86)90095-x

de Kloet, E. R., de Kloet, S. F., de Kloet, C. S., & de Kloet, A. D. (2019). Top-down and bottom-up control of stress-coping. *Journal of Neuroendocrinology*, *31*(3), e12675. https://doi.org/https://doi.org/10.1111/jne.12675

de Kloet, E. R., Joels, M., & Holsboer, F. (2005). Stress and the brain: from adaptation to disease. *Nat Rev Neurosci*, *6*(6), 463-475. https://doi.org/10.1038/nrn1683

de Kloet, E. R., Meijer, O. C., de Nicola, A. F., de Rijk, R. H., & Joels, M. (2018). Importance of the brain corticosteroid receptor balance in metaplasticity, cognitive performance and neuro-inflammation. *Front Neuroendocrinol*, *49*, 124-145. https://doi.org/10.1016/j.yfrne.2018.02.003

Delano, P. H., Belkhiria, C., Vergara, R. C., Martinez, M., Leiva, A., Andrade, M., Marcenaro, B., Torrente, M., Maass, J. C., & Delgado, C. (2020). Reduced suprathreshold auditory nerve responses are associated with slower processing speed and thinner temporal and parietal cortex in presbycusis. *PLoS One*, *15*(5), e0233224. https://doi.org/10.1371/journal.pone.0233224

Deng, S., Li, J., He, Q., Zhang, X., Zhu, J., Li, L., Mi, Z., Yang, X., Jiang, M., Dong, Q., Mao, Y., & Shu, Y. (2020). Regulation of Recurrent Inhibition by Asynchronous Glutamate Release in Neocortex. *Neuron*, *105*(3), 522-533 e524. https://doi.org/10.1016/j.neuron.2019.10.038

Deogracias, R., Espliguero, G., Iglesias, T., & Rodriguez-Pena, A. (2004). Expression of the neurotrophin receptor trkB is regulated by the cAMP/CREB pathway in neurons. *Mol Cell Neurosci*, *26*(3), 470-480. https://doi.org/10.1016/j.mcn.2004.03.007

Diering, G. H., & Huganir, R. L. (2018). The AMPA Receptor Code of Synaptic Plasticity. *Neuron*, *100*(2), 314-329. https://doi.org/10.1016/j.neuron.2018.10.018

Dong, Y., Guo, C. R., Chen, D., Chen, S. M., Peng, Y., Song, H., & Shi, J. R. (2018). Association between age-related hearing loss and cognitive decline in C57BL/6J mice. *Molecular medicine reports*, *18*(2), 1726-1732.

Dorner-Ciossek, C., Kroker, K. S., & Rosenbrock, H. (2017). Role of PDE9 in Cognition. *Adv Neurobiol*, *17*, 231-254. https://doi.org/10.1007/978-3-319-58811-7_9

Eachus, H., Choi, M.-K., & Ryu, S. (2021). The Effects of Early Life Stress on the Brain and Behaviour: Insights From Zebrafish Models [Review]. *Frontiers in Cell and Developmental Biology*, *9*. https://doi.org/10.3389/fcell.2021.657591

Earl, B. R., & Chertoff, M. E. (2010). Predicting auditory nerve survival using the compound action potential. *Ear Hear*, *31*(1), 7-21. https://doi.org/10.1097/AUD.0b013e3181ba748c

Eckert, P., Marchetta, P., Manthey, M. K., Walter, M. H., Jovanovic, S., Savitska, D., Singer, W., Jacob, M. H., Rüttiger, L., Schimmang, T., Milenkovic, I., Pilz, P. K. D., & Knipper, M. (2021). Deletion of BDNF in Pax2 Lineage-Derived Interneuron Precursors in the Hindbrain Hampers the Proportion of Excitation/Inhibition, Learning, and Behavior [Original Research]. *Frontiers in Molecular Neuroscience*, *14*. https://doi.org/10.3389/fnmol.2021.642679

El Sabbagh, N. G., Sewitch, M. J., Bezdjian, A., & Daniel, S. J. (2017). Intratympanic dexamethasone in sudden sensorineural hearing loss: A systematic review and meta-analysis. *Laryngoscope*, *127*(8), 1897-1908. https://doi.org/10.1002/lary.26394

Erdmann, G., Schutz, G., & Berger, S. (2007). Inducible gene inactivation in neurons of the adult mouse forebrain. *BMC Neurosci*, *8*, 63. https://doi.org/10.1186/1471-2202-8-63

Esvald, E. E., Tuvikene, J., Sirp, A., Patil, S., Bramham, C. R., & Timmusk, T. (2020). CREB Family Transcription Factors Are Major Mediators of BDNF Transcriptional Autoregulation in Cortical Neurons. *J Neurosci*, *40*(7), 1405-1426. https://doi.org/10.1523/JNEUROSCI.0367-19.2019

Ferretti, V., Perri, V., Cristofoli, A., Vetere, G., Fragapane, P., Oliverio, A., Teule, M. A., & Mele, A. (2015). Phosphorylation of S845 GluA1 AMPA receptors modulates spatial memory and structural plasticity in the ventral striatum. *Brain Struct Funct*, *220*(5), 2653-2661. https://doi.org/10.1007/s00429-014-0816-7

Fisher, D. A., Smith, J. F., Pillar, J. S., St Denis, S. H., & Cheng, J. B. (1998). Isolation and characterization of PDE9A, a novel human cGMP-specific phosphodiesterase. *J Biol Chem*, *273*(25), 15559-15564. https://doi.org/10.1074/jbc.273.25.15559

Fortunato, S., Forli, F., Guglielmi, V., Corso, E. d., Paludetti, G., Berrettini, S., & Fetoni, A. R. (2016). A review of new insights on the association between hearing loss and cognitive decline in ageing. *Acta Otorhinolaryngologica Italica*, *36*, 155 - 166.

Friebe, A., & Koesling, D. (2003). Regulation of nitric oxide-sensitive guanylyl cyclase. *Circ Res*, *93*(2), 96-105. https://doi.org/10.1161/01.RES.0000082524.34487.31

Fullgrabe, C., Moore, B. C., & Stone, M. A. (2014). Age-group differences in speech identification despite matched audiometrically normal hearing: contributions from auditory temporal processing and cognition. *Front Aging Neurosci*, *6*, 347. https://doi.org/10.3389/fnagi.2014.00347

Gall, M. D., Henry, K. S., & Lucas, J. R. (2011). Two measures of temporal resolution in brown-headed cowbirds (Molothrus ater). *Journal of Comparative Physiology A*, *198*, 61 - 68.

Gilbert, C. D., & Sigman, M. (2007). Brain states: top-down influences in sensory processing. *Neuron*, *54*(5), 677-696. https://doi.org/10.1016/j.neuron.2007.05.019

Godoy, L. D., Rossignoli, M. T., Delfino-Pereira, P., Garcia-Cairasco, N., & de Lima Umeoka, E. H. (2018). A Comprehensive Overview on Stress Neurobiology: Basic Concepts and Clinical Implications [Review]. *Frontiers in Behavioral Neuroscience*, *12*. https://doi.org/10.3389/fnbeh.2018.00127

Gomez-Alvarez, M., Johannesen, P. T., Coelho-de-Sousa, S. L., Klump, G. M., & Lopez-Poveda, E. A. (2023). The Relative Contribution of Cochlear Synaptopathy and Reduced Inhibition to Age-Related Hearing Impairment for People With Normal Audiograms. *Trends Hear*, *27*, 23312165231213191. https://doi.org/10.1177/23312165231213191

Gourevitch, B., Edeline, J. M., Occelli, F., & Eggermont, J. J. (2014). Is the din really harmless? Long-term effects of non-traumatic noise on the adult auditory system. *Nat Rev Neurosci*, *15*(7), 483-491. https://doi.org/10.1038/nrn3744

Griffiths, T. D., Lad, M., Kumar, S., Holmes, E., McMurray, B., Maguire, E. A., Billig, A. J., & Sedley, W. (2020). How Can Hearing Loss Cause Dementia? *Neuron*, *108*(3), 401-412. https://doi.org/10.1016/j.neuron.2020.08.003

Gu, J. W., Herrmann, B. S., Levine, R. A., & Melcher, J. R. (2012). Brainstem auditory evoked potentials suggest a role for the ventral cochlear nucleus in tinnitus. *J Assoc Res Otolaryngol*, *13*(6), 819-833. https://doi.org/10.1007/s10162-012-0344-1

Guo, H., Cheng, Y., Wang, C., Wu, J., Zou, Z., Niu, B., Yu, H., Wang, H., & Xu, J. (2017). FFPM, a PDE4 inhibitor, reverses learning and memory deficits in APP/PS1 transgenic mice via cAMP/PKA/CREB signaling and anti-inflammatory effects. *Neuropharmacology*, *116*, 260-269. https://doi.org/10.1016/j.neuropharm.2017.01.004

Han, F., Ozawa, H., Matsuda, K., Nishi, M., & Kawata, M. (2005). Colocalization of mineralocorticoid receptor and glucocorticoid receptor in the hippocampus and hypothalamus. *Neurosci Res*, *51*(4), 371-381. https://doi.org/10.1016/j.neures.2004.12.013

Han, M. H., & Nestler, E. J. (2017). Neural Substrates of Depression and Resilience. *Neurotherapeutics*, *14*(3), 677-686. https://doi.org/10.1007/s13311-017-0527-x

Harms, J. F., Menniti, F. S., & Schmidt, C. J. (2019). Phosphodiesterase 9A in Brain Regulates cGMP Signaling Independent of Nitric-Oxide [Original Research]. *Frontiers in Neuroscience*, *13*. https://doi.org/10.3389/fnins.2019.00837

Harris, A. P., Holmes, M. C., de Kloet, E. R., Chapman, K. E., & Seckl, J. R. (2013). Mineralocorticoid and glucocorticoid receptor balance in control of HPA axis and behaviour. *Psychoneuroendocrinology*, *38*(5), 648-658. https://doi.org/10.1016/j.psyneuen.2012.08.007

Hartmann, M., Heumann, R., & Lessmann, V. (2001). Synaptic secretion of BDNF after high-frequency stimulation of glutamatergic synapses. *EMBO J*, *20*(21), 5887-5897. https://doi.org/10.1093/emboj/20.21.5887

Hayes, S. H., Manohar, S., Majumdar, A., Allman, B. L., & Salvi, R. (2019). Noise-induced hearing loss alters hippocampal glucocorticoid receptor expression in rats. *Hear Res*, *379*, 43-51. https://doi.org/10.1016/j.heares.2019.04.013

Hebb, D. O. (2005). *The organization of behavior: A neuropsychological theory*. Psychology press.

Hébert, S., & Lupien, S. J. (2007). The sound of stress: Blunted cortisol reactivity to psychosocial stress in tinnitus sufferers. *Neuroscience Letters*, *411*, 138-142.

Hedde, P. N., Malacrida, L., Barylko, B., Binns, D. D., Albanesi, J. P., & Jameson, D. M. (2021). Membrane Remodeling by Arc/Arg3.1 [Brief Research Report]. *Frontiers in Molecular Biosciences*, *8*. https://doi.org/10.3389/fmolb.2021.630625

Heeringa, A. N., & van Dijk, P. (2014). The dissimilar time course of temporary threshold shifts and reduction of inhibition in the inferior colliculus following intense sound exposure. *Hear Res*, *312*, 38-47. https://doi.org/10.1016/j.heares.2014.03.004

Heil, P., & Peterson, A. J. (2017). Spike timing in auditory-nerve fibers during spontaneous activity and phase locking. *Synapse*, *71*(1), 5-36. https://doi.org/10.1002/syn.21925

Herbert, J., Goodyer, I. M., Grossman, A. B., Hastings, M. H., de Kloet, E. R., Lightman, S. L., Lupien, S. J., Roozendaal, B., & Seckl, J. R. (2006). Do corticosteroids damage the brain? *J Neuroendocrinol*, *18*(6), 393-411. https://doi.org/10.1111/j.1365-2826.2006.01429.x

Herman, J. P., McKlveen, J. M., Ghosal, S., Kopp, B., Wulsin, A., Makinson, R., Scheimann, J., & Myers, B. (2016). Regulation of the Hypothalamic-Pituitary-Adrenocortical Stress Response. *Compr Physiol*, *6*(2), 603-621. https://doi.org/10.1002/cphy.c150015

Hobson, C. E., Alexander, T. H., & Harris, J. P. (2016). Primary treatment of idiopathic sudden sensorineural hearing loss with intratympanic dexamethasone. *Curr Opin Otolaryngol Head Neck Surg*, *24*(5), 407-412. https://doi.org/10.1097/MOO.0000000000000288

Hong, E. J., McCord, A. E., & Greenberg, M. E. (2008). A biological function for the neuronal activity-dependent component of Bdnf transcription in the development of cortical inhibition. *Neuron*, *60*(4), 610-624. https://doi.org/10.1016/j.neuron.2008.09.024

Howarth, A., & Shone, G. R. (2006). Ageing and the auditory system. *Postgrad Med J*, *82*(965), 166-171. https://doi.org/10.1136/pgmj.2005.039388

Hu, H., Shao, L. R., Chavoshy, S., Gu, N., Trieb, M., Behrens, R., Laake, P., Pongs, O., Knaus, H. G., Ottersen, O. P., & Storm, J. F. (2001). Presynaptic Ca2+-activated K+ channels in glutamatergic hippocampal terminals and their role in spike repolarization and regulation of transmitter release. *J Neurosci*, *21*(24), 9585-9597. https://doi.org/10.1523/JNEUROSCI.21-24-09585.2001

Huang, A. R., Jiang, K., Lin, F. R., Deal, J. A., & Reed, N. S. (2023). Hearing Loss and Dementia Prevalence in Older Adults in the US. *JAMA*, *329*(2), 171-173. https://doi.org/10.1001/jama.2022.20954

Huang, X. F., Jiang, W. T., Liu, L., Song, F. C., Zhu, X., Shi, G. L., Ding, S. M., Ke, H. M., Wang, W., O'Donnell, J. M., Zhang, H. T., Luo, H. B., Wan, Y. Q., Song, G. Q., & Xu, Y. (2018). A novel PDE9 inhibitor WYQ-C36D ameliorates corticosterone-induced neurotoxicity and depression-like behaviors by cGMP-CREB-related signaling. *CNS Neurosci Ther*, *24*(10), 889-896. https://doi.org/10.1111/cns.12864

Hutson, P. H., Finger, E. N., Magliaro, B. C., Smith, S. M., Converso, A., Sanderson, P. E., Mullins, D., Hyde, L. A., Eschle, B. K., Turnbull, Z., Sloan, H., Guzzi, M., Zhang, X., Wang, A., Rindgen, D., Mazzola, R., Vivian, J. A., Eddins, D., Uslaner, J. M., . . . Parmentier-Batteur, S. (2011). The selective phosphodiesterase 9 (PDE9) inhibitor PF-04447943 (6-[(3S,4S)-4-methyl-1-(pyrimidin-2-ylmethyl)pyrrolidin-3-yl]-1-(tetrahydro-2H-pyran-4-yl)-1,5-dihydro-4H-pyrazolo[3,4-d]pyrimidin-4-one) enhances synaptic plasticity and cognitive function in rodents. *Neuropharmacology*, *61*(4), 665-676. https://doi.org/10.1016/j.neuropharm.2011.05.009

Ibrahim, B. A., & Llano, D. A. (2019). Aging and Central Auditory Disinhibition: Is It a Reflection of Homeostatic Downregulation or Metabolic Vulnerability? *Brain Sci*, *9*(12). https://doi.org/10.3390/brainsci9120351

Jackman, S. L., & Regehr, W. G. (2017). The Mechanisms and Functions of Synaptic Facilitation. *Neuron*, *94*(3), 447-464. https://doi.org/10.1016/j.neuron.2017.02.047

Jafari, Z., Kolb, B. E., & Mohajerani, M. H. (2019). Age-related hearing loss and tinnitus, dementia risk, and auditory amplification outcomes. *Ageing Res Rev*, *56*, 100963. https://doi.org/10.1016/j.arr.2019.100963

Jaumann, M., Dettling, J., Gubelt, M., Zimmermann, U., Gerling, A., Paquet-Durand, F., Feil, S., Wolpert, S., Franz, C., Varakina, K., Xiong, H., Brandt, N., Kuhn, S., Geisler, H. S., Rohbock, K., Ruth, P., Schlossmann, J., Hutter, J., Sandner, P., . . . Ruttiger, L. (2012). cGMP-Prkg1 signaling and Pde5 inhibition shelter cochlear hair cells and hearing function. *Nat Med*, *18*(2), 252-259. https://doi.org/10.1038/nm.2634

Jeanneteau, F., Borie, A., Chao, M. V., & Garabedian, M. J. (2019). Bridging the Gap between Brain-Derived Neurotrophic Factor and Glucocorticoid Effects on Brain Networks. *Neuroendocrinology*, *109*(3), 277-284. https://doi.org/10.1159/000496392

Joels, M., & Baram, T. Z. (2009). The neuro-symphony of stress. *Nat Rev Neurosci*, *10*(6), 459-466. https://doi.org/10.1038/nrn2632

Joels, M., & Karst, H. (2012). Corticosteroid effects on calcium signaling in limbic neurons. *Cell Calcium*, *51*(3-4), 277-283. https://doi.org/10.1016/j.ceca.2011.11.002

Kandel, E. R. (2013). *Principles of Neural Science, Fifth Edition*. McGraw-Hill Education. https://books.google.de/books?id=s64z-LdAIsEC

Katrin Amunts, P. M., Heidegard Hilbig, Karl Zilles,. (2012). Auditory System. In G. P. Jürgen K. Mai (Ed.), *The Human Nervous System* (Third Edition ed., pp. 1270-1300). Academic Press. https://doi.org/doi.org/10.1016/B978-0-12-374236-0.10036-7

Kawashima, T., Okuno, H., Nonaka, M., Adachi-Morishima, A., Kyo, N., Okamura, M., Takemoto-Kimura, S., Worley, P. F., & Bito, H. (2009). Synaptic activity-responsive element in the Arc/Arg3.1 promoter essential for synapse-to-nucleus signaling in activated

neurons. *Proceedings of the National Academy of Sciences*, *106*(1), 316-321. https://doi.org/doi:10.1073/pnas.0806518106

Kemp-Harper, B., & Feil, R. (2008). Meeting report: cGMP matters. *Sci Signal*, *1*(9), pe12. https://doi.org/10.1126/stke.19pe12

Keravis, T., & Lugnier, C. (2012). Cyclic nucleotide phosphodiesterase (PDE) isozymes as targets of the intracellular signalling network: benefits of PDE inhibitors in various diseases and perspectives for future therapeutic developments. *Br J Pharmacol*, *165*(5), 1288-1305. https://doi.org/10.1111/j.1476-5381.2011.01729.x

Kiang, N. Y., Pfeiffer, R. R., Warr, W. B., & Backus, A. S. (1965). Stimulus coding in the cochlear nucleus. *Trans Am Otol Soc*, *53*, 35-58. https://www.ncbi.nlm.nih.gov/pubmed/5834666

Kingsbury, T. J., Murray, P. D., Bambrick, L. L., & Krueger, B. K. (2003). Ca(2+)-dependent regulation of TrkB expression in neurons. *J Biol Chem*, *278*(42), 40744-40748. https://doi.org/10.1074/jbc.M303082200

Kleiman, R. J., Lanz, T. A., Finley, J. E., Bove, S. E., Majchrzak, M. J., Becker, S. L., Carvajal-Gonzales, S., Kuhn, A. M., Wood, K. M., Mariga, A., Nelson, F. R., Verhoest, P. R., Seymour, P. A., & Stephenson, D. T. (2010). P3-380: Dendritic spine density deficits in the hippocampal CA1 region of young Tg2576 mice are ameliorated with the PDE9A inhibitor PF-04447943. *Alzheimer's & Dementia*, *6*(4S_Part_18), S563-S564. https://doi.org/https://doi.org/10.1016/j.jalz.2010.05.1922

Kleppisch, T., & Feil, R. (2009). cGMP signalling in the mammalian brain: role in synaptic plasticity and behaviour. *Handb Exp Pharmacol*(191), 549-579. https://doi.org/10.1007/978-3-540-68964-5_24

Knipper, M., Singer, W., Schwabe, K., Hagberg, G. E., Li Hegner, Y., Ruttiger, L., Braun, C., & Land, R. (2021). Disturbed Balance of Inhibitory Signaling Links Hearing Loss and Cognition. *Front Neural Circuits*, *15*, 785603. https://doi.org/10.3389/fncir.2021.785603

Kokkonen, K., & Kass, D. A. (2017). Nanodomain Regulation of Cardiac Cyclic Nucleotide Signaling by Phosphodiesterases. *Annu Rev Pharmacol Toxicol*, *57*, 455-479. https://doi.org/10.1146/annurev-pharmtox-010716-104756

Kolb, B. G., R. (2008). Principles of neuroplasticity and behavior. In G. W. a. I. H. R. Donald T. Stuss (Ed.), *Cognitive Neurorehabilitation: Evidence and Application* (pp. 6-21). Cambridge University Press. https://doi.org/doi.org/10.1017/CBO9781316529898.003

Konrad-Martin, D., Dille, M. F., McMillan, G., Griest, S., McDermott, D., Fausti, S. A., & Austin, D. F. (2012). Age-related changes in the auditory brainstem response. *J Am Acad Audiol*, *23*(1), 18-35; quiz 74-15. https://doi.org/10.3766/jaaa.23.1.3

Korb, E., & Finkbeiner, S. (2011). Arc in synaptic plasticity: from gene to behavior. *Trends Neurosci*, *34*(11), 591-598. https://doi.org/10.1016/j.tins.2011.08.007

Kraus, K. S., & Canlon, B. (2012). Neuronal connectivity and interactions between the auditory and limbic systems. Effects of noise and tinnitus. *Hear Res*, *288*(1-2), 34-46. https://doi.org/10.1016/j.heares.2012.02.009

Kroker, K. S., Mathis, C., Marti, A., Cassel, J. C., Rosenbrock, H., & Dorner-Ciossek, C. (2014). PDE9A inhibition rescues amyloid beta-induced deficits in synaptic plasticity and cognition. *Neurobiol Aging*, *35*(9), 2072-2078. https://doi.org/10.1016/j.neurobiolaging.2014.03.023

Kuhn, M. (2009). Function and dysfunction of mammalian membrane guanylyl cyclase receptors: lessons from genetic mouse models and implications for human diseases. *Handb Exp Pharmacol*(191), 47-69. https://doi.org/10.1007/978-3-540-68964-5_4

Kujawa, S. G., & Liberman, M. C. (2009). Adding insult to injury: cochlear nerve degeneration after "temporary" noise-induced hearing loss. *J Neurosci*, *29*(45), 14077-14085. https://doi.org/10.1523/JNEUROSCI.2845-09.2009

Kukreja, R. C., Salloum, F. N., & Das, A. (2012). Cyclic guanosine monophosphate signaling and phosphodiesterase-5 inhibitors in cardioprotection. *J Am Coll Cardiol*, *59*(22), 1921-1927. https://doi.org/10.1016/j.jacc.2011.09.086

Lai, B., Li, M., Hu, W., Li, W., & Gan, W. B. (2018). The Phosphodiesterase 9 Inhibitor PF-04449613 Promotes Dendritic Spine Formation and Performance Improvement after Motor Learning. *Dev Neurobiol*, *78*(9), 859-872. https://doi.org/10.1002/dneu.22623

Lambert, K., & Kinsley, C. H. (2011). *Clinical Neuroscience: Psychopathology and the Brain*. Oxford University Press. https://books.google.de/books?id=-H4XSwAACAAJ

Lau, C. G., Zhang, H., & Murthy, V. N. (2022). Deletion of TrkB in parvalbumin interneurons alters cortical neural dynamics. *J Cell Physiol*, *237*(1), 949-964. https://doi.org/10.1002/jcp.30571

Laumonnier, F., Roger, S., Guerin, P., Molinari, F., M'Rad, R., Cahard, D., Belhadj, A., Halayem, M., Persico, A. M., Elia, M., Romano, V., Holbert, S., Andres, C., Chaabouni, H., Colleaux, L., Constant, J., Le Guennec, J. Y., & Briault, S. (2006). Association of a functional deficit of the BKCa channel, a synaptic regulator of neuronal excitability, with autism and mental retardation. *Am J Psychiatry*, *163*(9), 1622-1629. https://doi.org/10.1176/ajp.2006.163.9.1622

Leal, G., Bramham, C. R., & Duarte, C. B. (2017). BDNF and Hippocampal Synaptic Plasticity. *Vitam Horm*, *104*, 153-195. https://doi.org/10.1016/bs.vh.2016.10.004

Lee, D. I., Zhu, G., Sasaki, T., Cho, G. S., Hamdani, N., Holewinski, R., Jo, S. H., Danner, T., Zhang, M., Rainer, P. P., Bedja, D., Kirk, J. A., Ranek, M. J., Dostmann, W. R., Kwon, C., Margulies, K. B., Van Eyk, J. E., Paulus, W. J., Takimoto, E., & Kass, D. A. (2015). Phosphodiesterase 9A controls nitric-oxide-independent cGMP and hypertrophic heart disease. *Nature*, *519*(7544), 472-476. https://doi.org/10.1038/nature14332

Li-Korotky, H. S. (2012). Age-related hearing loss: quality of care for quality of life. *Gerontologist*, *52*(2), 265-271. https://doi.org/10.1093/geront/gnr159

Liberman, M. C. (1980). Morphological differences among radial afferent fibers in the cat cochlea: an electron-microscopic study of serial sections. *Hear Res*, *3*(1), 45-63. https://doi.org/10.1016/0378-5955(80)90007-6

Liberman, M. C., & Kiang, N. Y. (1978). Acoustic trauma in cats. Cochlear pathology and auditory-nerve activity. *Acta Otolaryngol Suppl*, *358*, 1-63. https://www.ncbi.nlm.nih.gov/pubmed/281107

Lin, F. R., Metter, E. J., O'Brien, R. J., Resnick, S. M., Zonderman, A. B., & Ferrucci, L. (2011). Hearing loss and incident dementia. *Arch Neurol*, *68*(2), 214-220. https://doi.org/10.1001/archneurol.2010.362

Lisman, J., Yasuda, R., & Raghavachari, S. (2012). Mechanisms of CaMKII action in long-term potentiation. *Nat Rev Neurosci*, *13*(3), 169-182. https://doi.org/10.1038/nrn3192

Liu, L., Shen, P., He, T., Chang, Y., Shi, L., Tao, S., Li, X., Xun, Q., Guo, X., Yu, Z., & Wang, J. (2016). Noise induced hearing loss impairs spatial learning/memory and hippocampal neurogenesis in mice. *Sci Rep*, *6*, 20374. https://doi.org/10.1038/srep20374

Livingston, G., Sommerlad, A., Orgeta, V., Costafreda, S. G., Huntley, J., Ames, D., Ballard, C., Banerjee, S., Burns, A., Cohen-Mansfield, J., Cooper, C., Fox, N., Gitlin, L. N., Howard, R., Kales, H. C., Larson, E. B., Ritchie, K., Rockwood, K., Sampson, E. L., . . . Mukadam, N. (2017). Dementia prevention, intervention, and care. *Lancet*, *390*(10113), 2673-2734. https://doi.org/10.1016/S0140-6736(17)31363-6

Lonze, B. E., & Ginty, D. D. (2002). Function and regulation of CREB family transcription factors in the nervous system. *Neuron*, *35*(4), 605-623. https://doi.org/10.1016/s0896-6273(02)00828-0

Loughrey, D. G., Kelly, M. E., Kelley, G. A., Brennan, S., & Lawlor, B. A. (2018). Association of Age-Related Hearing Loss With Cognitive Function, Cognitive Impairment, and Dementia: A Systematic Review and Meta-analysis. *JAMA Otolaryngol Head Neck Surg*, *144*(2), 115-126. https://doi.org/10.1001/jamaoto.2017.2513

Lueptow, L. M., Zhan, C. G., & O'Donnell, J. M. (2016). Cyclic GMP-mediated memory enhancement in the object recognition test by inhibitors of phosphodiesterase-2 in mice. *Psychopharmacology (Berl)*, *233*(3), 447-456. https://doi.org/10.1007/s00213-015-4129-1

Lynch, G., Rex, C. S., & Gall, C. M. (2007). LTP consolidation: substrates, explanatory power, and functional significance. *Neuropharmacology*, *52*(1), 12-23. https://doi.org/10.1016/j.neuropharm.2006.07.027

Malmierca, M. S. (2003). The structure and physiology of the rat auditory system: an overview. *Int Rev Neurobiol*, *56*, 147-211. https://doi.org/10.1016/s0074-7742(03)56005-6

Mann, D. A., Colbert, D. E., Gaspard, J. C., Casper, B. M., Cook, M. L., Reep, R. L., & Bauer, G. B. (2005). Temporal resolution of the Florida manatee (Trichechus manatus latirostris) auditory system. *J Comp Physiol A Neuroethol Sens Neural Behav Physiol*, *191*(10), 903-908. https://doi.org/10.1007/s00359-005-0016-2

Manohar, S., Adler, H. J., Chen, G. D., & Salvi, R. (2020). Blast-induced hearing loss suppresses hippocampal neurogenesis and disrupts long term spatial memory. *Hear Res*, *395*, 108022. https://doi.org/10.1016/j.heares.2020.108022

Manohar, S., Chen, G.-D., Ding, D., Liu, L., Wang, J., Chen, Y.-C., Chen, L., & Salvi, R. (2022). Unexpected Consequences of Noise-Induced Hearing Loss: Impaired Hippocampal Neurogenesis, Memory, and Stress [Review]. *Frontiers in Integrative Neuroscience*, *16*. https://doi.org/10.3389/fnint.2022.871223

Marchetta, P., Eckert, P., Lukowski, R., Ruth, P., Singer, W., Ruttiger, L., & Knipper, M. (2022). Loss of central mineralocorticoid or glucocorticoid receptors impacts auditory nerve processing in the cochlea. *iScience*, *25*(3), 103981. https://doi.org/10.1016/j.isci.2022.103981

Marchetta, P., Möhrle, D., Eckert, P., Reimann, K., Wolter, S., Tolone, A., Lang, I., Wolters, M., Feil, R., Engel, J., Paquet-Durand, F., Kuhn, M., Knipper, M., & Rüttiger, L. (2020). Guanylyl Cyclase A/cGMP Signaling Slows Hidden, Age- and Acoustic Trauma-Induced Hearing Loss [Original Research]. *Frontiers in Aging Neuroscience*, *12*. https://doi.org/10.3389/fnagi.2020.00083

Marchetta, P., Savitska, D., Kubler, A., Asola, G., Manthey, M., Mohrle, D., Schimmang, T., Ruttiger, L., Knipper, M., & Singer, W. (2020). Age-Dependent Auditory Processing Deficits after Cochlear Synaptopathy Depend on Auditory Nerve Latency and the Ability of the Brain to Recruit LTP/BDNF. *Brain Sci*, *10*(10). https://doi.org/10.3390/brainsci10100710

Martin del Campo, H. N., Measor, K. R., & Razak, K. A. (2012). Parvalbumin immunoreactivity in the auditory cortex of a mouse model of presbycusis. *Hear Res*, *294*(1-2), 31-39. https://doi.org/10.1016/j.heares.2012.08.017

Matsuzaki, M., Ellis-Davies, G. C., Nemoto, T., Miyashita, Y., Iino, M., & Kasai, H. (2001). Dendritic spine geometry is critical for AMPA receptor expression in hippocampal CA1 pyramidal neurons. *Nat Neurosci*, *4*(11), 1086-1092. https://doi.org/10.1038/nn736

Matsuzaki, M., Honkura, N., Ellis-Davies, G. C., & Kasai, H. (2004). Structural basis of long-term potentiation in single dendritic spines. *Nature*, *429*(6993), 761-766. https://doi.org/10.1038/nature02617

Matt, L., Eckert, P., Panford-Walsh, R., Geisler, H. S., Bausch, A. E., Manthey, M., Muller, N. I. C., Harasztosi, C., Rohbock, K., Ruth, P., Friauf, E., Ott, T., Zimmermann, U., Ruttiger, L., Schimmang, T., Knipper, M., & Singer, W. (2018). Visualizing BDNF Transcript Usage During Sound-Induced Memory Linked Plasticity. *Front Mol Neurosci*, *11*, 260. https://doi.org/10.3389/fnmol.2018.00260

Mazurek, B., Szczepek, A. J., & Hebert, S. (2015). Stress and tinnitus. *HNO*, *63*(4), 258-265. https://doi.org/10.1007/s00106-014-2973-7

McClaskey, C. M., Dias, J. W., & Harris, K. C. (2019). Sustained envelope periodicity representations are associated with speech-in-noise performance in difficult listening conditions for younger and older adults. *Journal of Neurophysiology*, *122*(4), 1685-1696. https://doi.org/10.1152/jn.00845.2018

Melcher, J. R., & Kiang, N. Y. (1996). Generators of the brainstem auditory evoked potential in cat. III: Identified cell populations. *Hear Res*, *93*(1-2), 52-71. https://doi.org/10.1016/0378-5955(95)00200-6

Mifsud, K. R., & Reul, J. (2018). Mineralocorticoid and glucocorticoid receptor-mediated control of genomic responses to stress in the brain. *Stress*, *21*(5), 389-402. https://doi.org/10.1080/10253890.2018.1456526

Miller, J. P., Moldenhauer, H. J., Keros, S., & Meredith, A. L. (2021). An emerging spectrum of variants and clinical features in KCNMA1-linked channelopathy. *Channels (Austin)*, *15*(1), 447-464. https://doi.org/10.1080/19336950.2021.1938852

Minichiello, L., Calella, A. M., Medina, D. L., Bonhoeffer, T., Klein, R., & Korte, M. (2002). Mechanism of TrkB-mediated hippocampal long-term potentiation. *Neuron*, *36*(1), 121-137. https://doi.org/10.1016/s0896-6273(02)00942-x

Mohrle, D., Ni, K., Varakina, K., Bing, D., Lee, S. C., Zimmermann, U., Knipper, M., & Ruttiger, L. (2016). Loss of auditory sensitivity from inner hair cell synaptopathy can be centrally compensated in the young but not old brain. *Neurobiol Aging*, *44*, 173-184. https://doi.org/10.1016/j.neurobiolaging.2016.05.001

Mohrle, D., Reimann, K., Wolter, S., Wolters, M., Varakina, K., Mergia, E., Eichert, N., Geisler, H. S., Sandner, P., Ruth, P., Friebe, A., Feil, R., Zimmermann, U., Koesling, D., Knipper, M., & Ruttiger, L. (2017). NO-Sensitive Guanylate Cyclase Isoforms NO-GC1 and NO-GC2 Contribute to Noise-Induced Inner Hair Cell Synaptopathy. *Mol Pharmacol*, *92*(4), 375-388. https://doi.org/10.1124/mol.117.108548

Moser, T., Brandt, A., & Lysakowski, A. (2006). Hair cell ribbon synapses. *Cell Tissue Res*, *326*(2), 347-359. https://doi.org/10.1007/s00441-006-0276-3

Murad, F., Mittal, C. K., Arnold, W. P., Katsuki, S., & Kimura, H. (1978). Guanylate cyclase: activation by azide, nitro compounds, nitric oxide, and hydroxyl radical and inhibition by hemoglobin and myoglobin. *Adv Cyclic Nucleotide Res*, *9*, 145-158. https://www.ncbi.nlm.nih.gov/pubmed/27076

Nakajima, S., Numakawa, T., Adachi, N., Ooshima, Y., Odaka, H., Yoshimura, A., & Kunugi, H. (2015). Self-amplified BDNF transcription is a regulatory system for synaptic maturation in cultured cortical neurons. *Neurochem Int*, *91*, 55-61. https://doi.org/10.1016/j.neuint.2015.10.009

Newman, A. J., Hayes, S. H., Rao, A. S., Allman, B. L., Manohar, S., Ding, D., Stolzberg, D., Lobarinas, E., Mollendorf, J. C., & Salvi, R. (2015). Low-cost blast wave generator for studies of hearing loss and brain injury: blast wave effects in closed spaces. *J Neurosci Methods*, *242*, 82-92. https://doi.org/10.1016/j.jneumeth.2015.01.009

Nicholls, R. E., Alarcon, J. M., Malleret, G., Carroll, R. C., Grody, M., Vronskaya, S., & Kandel, E. R. (2008). Transgenic mice lacking NMDAR-dependent LTD exhibit deficits in behavioral flexibility. *Neuron*, *58*(1), 104-117. https://doi.org/10.1016/j.neuron.2008.01.039

Noguchi, J., Matsuzaki, M., Ellis-Davies, G. C., & Kasai, H. (2005). Spine-neck geometry determines NMDA receptor-dependent Ca2+ signaling in dendrites. *Neuron*, *46*(4), 609-622. https://doi.org/10.1016/j.neuron.2005.03.015

Organization, W. H. (2021). *World report on hearing*. World Health Organization. https://books.google.de/books?id=zMRqEAAAQBAJ

Park, M. (2018). AMPA Receptor Trafficking for Postsynaptic Potentiation [Review]. *Frontiers in Cellular Neuroscience*, *12*. https://doi.org/10.3389/fncel.2018.00361

Patel, N. S., Klett, J., Pilarzyk, K., Lee, D. I., Kass, D., Menniti, F. S., & Kelly, M. P. (2018). Identification of new PDE9A isoforms and how their expression and subcellular compartmentalization in the brain change across the life span. *Neurobiol Aging*, *65*, 217-234. https://doi.org/10.1016/j.neurobiolaging.2018.01.019

Peebles, C. L., Yoo, J., Thwin, M. T., Palop, J. J., Noebels, J. L., & Finkbeiner, S. (2010). Arc regulates spine morphology and maintains network stability in vivo. *Proc Natl Acad Sci U S A*, *107*(42), 18173-18178. https://doi.org/10.1073/pnas.1006546107

Penn, A. C., Zhang, C. L., Georges, F., Royer, L., Breillat, C., Hosy, E., Petersen, J. D., Humeau, Y., & Choquet, D. (2017). Hippocampal LTP and contextual learning require surface diffusion of AMPA receptors. *Nature*, *549*(7672), 384-388. https://doi.org/10.1038/nature23658

Peters, A., Reisch, C., & Langemann, D. (2018). LTP or LTD? Modeling the Influence of Stress on Synaptic Plasticity. *eNeuro*, *5*(1). https://doi.org/10.1523/ENEURO.0242-17.2018

Pham, T., Hussein, T., Calis, D., Bischof, H., Skrabak, D., Cruz Santos, M., Maier, S., Spahn, D., Kalina, D., Simonsig, S., Ehinger, R., Groschup, B., Knipper, M., Plesnila, N., Ruth, P., Lukowski, R., & Matt, L. (2023). BK channels sustain neuronal Ca(2+) oscillations to support hippocampal long-term potentiation and memory formation. *Cell Mol Life Sci*, *80*(12), 369. https://doi.org/10.1007/s00018-023-05016-y

Potter, L. R. (2011). Guanylyl cyclase structure, function and regulation. *Cell Signal*, *23*(12), 1921-1926. https://doi.org/10.1016/j.cellsig.2011.09.001

Potter, L. R., Abbey-Hosch, S., & Dickey, D. M. (2006). Natriuretic peptides, their receptors, and cyclic guanosine monophosphate-dependent signaling functions. *Endocr Rev*, *27*(1), 47-72. https://doi.org/10.1210/er.2005-0014

Prickaerts, J., de Vente, J., Honig, W., Steinbusch, H. W., & Blokland, A. (2002). cGMP, but not cAMP, in rat hippocampus is involved in early stages of object memory consolidation. *Eur J Pharmacol*, *436*(1-2), 83-87. https://doi.org/10.1016/s0014-2999(01)01614-4

Rees, A., & Malmierca, M. S. (2005). Processing of dynamic spectral properties of sounds. *Int Rev Neurobiol*, *70*, 299-330. https://doi.org/10.1016/S0074-7742(05)70009-X

Reneerkens, O. A., Rutten, K., Steinbusch, H. W., Blokland, A., & Prickaerts, J. (2009). Selective phosphodiesterase inhibitors: a promising target for cognition enhancement. *Psychopharmacology (Berl)*, *202*(1-3), 419-443. https://doi.org/10.1007/s00213-008-1273-x

Reul, J. M. H. M., & Kloet, E. R. d. (1985). Two receptor systems for corticosterone in rat brain: microdistribution and differential occupation. *Endocrinology*, *117 6*, 2505-2511.

Rial Verde, E. M., Lee-Osbourne, J., Worley, P. F., Malinow, R., & Cline, H. T. (2006). Increased expression of the immediate-early gene arc/arg3.1 reduces AMPA receptor-mediated synaptic transmission. *Neuron*, *52*(3), 461-474. https://doi.org/10.1016/j.neuron.2006.09.031

Rich, M. M., & Wenner, P. (2007). Sensing and expressing homeostatic synaptic plasticity. *Trends Neurosci*, *30*(3), 119-125. https://doi.org/10.1016/j.tins.2007.01.004

Rosch, H., Schweigreiter, R., Bonhoeffer, T., Barde, Y. A., & Korte, M. (2005). The neurotrophin receptor p75NTR modulates long-term depression and regulates the expression of AMPA receptor subunits in the hippocampus. *Proc Natl Acad Sci U S A*, *102*(20), 7362-7367. https://doi.org/10.1073/pnas.0502460102

Rose, J. E., Brugge, J. F., Anderson, D. J., & Hind, J. E. (1967). Phase-locked response to low-frequency tones in single auditory nerve fibers of the squirrel monkey. *J Neurophysiol*, *30*(4), 769-793. https://doi.org/10.1152/jn.1967.30.4.769

Rosenbrock, H., Giovannini, R., Schanzle, G., Koros, E., Runge, F., Fuchs, H., Marti, A., Reymann, K. G., Schroder, U. H., Fedele, E., & Dorner-Ciossek, C. (2019). The Novel Phosphodiesterase 9A Inhibitor BI 409306 Increases Cyclic Guanosine Monophosphate Levels in the Brain, Promotes Synaptic Plasticity, and Enhances Memory Function in Rodents. *J Pharmacol Exp Ther*, *371*(3), 633-641. https://doi.org/10.1124/jpet.119.260059

Roux, L., & Buzsaki, G. (2015). Tasks for inhibitory interneurons in intact brain circuits. *Neuropharmacology*, *88*, 10-23. https://doi.org/10.1016/j.neuropharm.2014.09.011

Rumschlag, J. A., & Razak, K. A. (2021). Age-related changes in event related potentials, steady state responses and temporal processing in the auditory cortex of mice with severe or mild hearing loss. *Hear Res*, *412*, 108380. https://doi.org/10.1016/j.heares.2021.108380

Rutherford, B. R., Brewster, K., Golub, J. S., Kim, A. H., & Roose, S. P. (2018). Sensation and Psychiatry: Linking Age-Related Hearing Loss to Late-Life Depression and Cognitive Decline. *Am J Psychiatry*, *175*(3), 215-224. https://doi.org/10.1176/appi.ajp.2017.17040423

Rutherford, L. C., DeWan, A., Lauer, H. M., & Turrigiano, G. G. (1997). Brain-derived neurotrophic factor mediates the activity-dependent regulation of inhibition in neocortical cultures. *J Neurosci*, *17*(12), 4527-4535. https://doi.org/10.1523/JNEUROSCI.17-12-04527.1997

Ruttiger, L., Panford-Walsh, R., Schimmang, T., Tan, J., Zimmermann, U., Rohbock, K., Kopschall, I., Limberger, A., Muller, M., Fraenzer, J. T., Cimerman, J., & Knipper, M. (2007). BDNF mRNA expression and protein localization are changed in age-related hearing loss. *Neurobiol Aging*, *28*(4), 586-601. https://doi.org/10.1016/j.neurobiolaging.2006.02.008

Ruttiger, L., Singer, W., Panford-Walsh, R., Matsumoto, M., Lee, S. C., Zuccotti, A., Zimmermann, U., Jaumann, M., Rohbock, K., Xiong, H., & Knipper, M. (2013). The reduced cochlear output and the failure to adapt the central auditory response causes tinnitus in noise exposed rats. *PLoS One*, *8*(3), e57247. https://doi.org/10.1371/journal.pone.0057247

Sausbier, U., Sausbier, M., Sailer, C. A., Arntz, C., Knaus, H. G., Neuhuber, W., & Ruth, P. (2006). Ca2+ -activated K+ channels of the BK-type in the mouse brain. *Histochem Cell Biol*, *125*(6), 725-741. https://doi.org/10.1007/s00418-005-0124-7

Savitska, D., Hess, M., Calis, D., Marchetta, P., Harasztosi, C., Fink, S., Eckert, P., Ruth, P., Ruttiger, L., Knipper, M., & Singer, W. (2022). Stress Affects Central Compensation of Neural Responses to Cochlear Synaptopathy in a cGMP-Dependent Way. *Front Neurosci*, *16*, 864706. https://doi.org/10.3389/fnins.2022.864706

Schaette, R., & McAlpine, D. (2011). Tinnitus with a normal audiogram: physiological evidence for hidden hearing loss and computational model. *J Neurosci*, *31*(38), 13452-13457. https://doi.org/10.1523/JNEUROSCI.2156-11.2011

Schalk, T. B., & Sachs, M. B. (1980). Nonlinearities in auditory-nerve fiber responses to bandlimited noise. *The Journal of the Acoustical Society of America*, *67*(3), 903-913.

Schrode, K. M., & Bee, M. A. (2015). Evolutionary adaptations for the temporal processing of natural sounds by the anuran peripheral auditory system. *J Exp Biol*, *218*(Pt 6), 837-848. https://doi.org/10.1242/jeb.115014

Sergeyenko, Y., Lall, K., Liberman, M. C., & Kujawa, S. G. (2013). Age-related cochlear synaptopathy: an early-onset contributor to auditory functional decline. *J Neurosci*, *33*(34), 13686-13694. https://doi.org/10.1523/JNEUROSCI.1783-13.2013

Shaddock Palombi, P., Backoff, P. M., & Caspary, D. M. (2001). Responses of young and aged rat inferior colliculus neurons to sinusoidally amplitude modulated stimuli. *Hear Res*, *153*(1-2), 174-180. https://doi.org/10.1016/s0378-5955(00)00264-1

Shah, K. R., Guan, X., & Yan, J. (2021). Structural and Functional Coupling of Calcium-Activated BK Channels and Calcium-Permeable Channels Within Nanodomain Signaling Complexes. *Front Physiol*, *12*, 796540. https://doi.org/10.3389/fphys.2021.796540

Shimazaki, T., Ichimiya, I., Suzuki, M., & Mogi, G. (2002). Localization of glucocorticoid receptors in the murine inner ear. *Ann Otol Rhinol Laryngol*, *111*(12 Pt 1), 1133-1138. https://doi.org/10.1177/000348940211101213

Shukla, M., Roy, K., Kaur, C., Nayak, D., Mani, K. V., Shukla, S., & Kapoor, N. (2019). Attenuation of adverse effects of noise induced hearing loss on adult neurogenesis and memory in rats by intervention with Adenosine A(2A) receptor agonist. *Brain Res Bull*, *147*, 47-57. https://doi.org/10.1016/j.brainresbull.2019.02.006

Singer, Kasini, K., Manthey, M., Eckert, P., Armbruster, P., Vogt, M. A., Jaumann, M., Dotta, M., Yamahara, K., Harasztosi, C., Zimmermann, U., Knipper, M., & Ruttiger, L. (2018). The glucocorticoid antagonist mifepristone attenuates sound-induced long-term deficits in auditory nerve response and central auditory processing in female rats. *FASEB J*, *32*(6), 3005-3019. https://doi.org/10.1096/fj.201701041RRR

Singer, Manthey, M., Panford-Walsh, R., Matt, L., Geisler, H.-S., Passeri, E., Baj, G., Tongiorgi, E., Leal, G., Duarte, C. B., Salazar, I. L., Eckert, P., Rohbock, K., Hu, J., Strotmann, J., Ruth, P., Zimmermann, U., Rüttiger, L., Ott, T., . . . Knipper, M. (2018). BDNF-Live-Exon-Visualization (BLEV) Allows Differential Detection of BDNF Transcripts in vitro and in vivo [Original Research]. *Frontiers in Molecular Neuroscience*, *11*. https://doi.org/10.3389/fnmol.2018.00325

Singer, W., Zuccotti, A., Jaumann, M., Lee, S. C., Panford-Walsh, R., Xiong, H., Zimmermann, U., Franz, C., Geisler, H. S., Kopschall, I., Rohbock, K., Varakina, K., Verpoorten, S., Reinbothe, T., Schimmang, T., Ruttiger, L., & Knipper, M. (2013). Noise-induced inner hair cell ribbon loss disturbs central arc mobilization: a novel molecular paradigm for understanding tinnitus. *Mol Neurobiol*, *47*(1), 261-279. https://doi.org/10.1007/s12035-012-8372-8

Slade, K., Plack, C. J., & Nuttall, H. E. (2020). The Effects of Age-Related Hearing Loss on the Brain and Cognitive Function. *Trends Neurosci*, *43*(10), 810-821. https://doi.org/10.1016/j.tins.2020.07.005

Soderling, S. H., Bayuga, S. J., & Beavo, J. A. (1998). Identification and characterization of a novel family of cyclic nucleotide phosphodiesterases. *J Biol Chem*, *273*(25), 15553-15558. https://doi.org/10.1074/jbc.273.25.15553

Spencer, R. L., & Deak, T. (2017). A users guide to HPA axis research. *Physiol Behav*, *178*, 43-65. https://doi.org/10.1016/j.physbeh.2016.11.014

Storm, J. F. (1987). Action potential repolarization and a fast after-hyperpolarization in rat hippocampal pyramidal cells. *J Physiol*, *385*, 733-759. https://doi.org/10.1113/jphysiol.1987.sp016517

Stranahan, A. M., Arumugam, T. V., & Mattson, M. P. (2011). Lowering corticosterone levels reinstates hippocampal brain-derived neurotropic factor and Trkb expression without influencing deficits in hypothalamic brain-derived neurotropic factor expression in leptin receptor-deficient mice. *Neuroendocrinology*, *93*(1), 58-64. https://doi.org/10.1159/000322808

Suga, N. (2020). Plasticity of the adult auditory system based on corticocortical and corticofugal modulations. *Neurosci Biobehav Rev*, *113*, 461-478. https://doi.org/10.1016/j.neubiorev.2020.03.021

Sumi, T., & Harada, K. (2020). Mechanism underlying hippocampal long-term potentiation and depression based on competition between endocytosis and exocytosis of AMPA receptors. *Sci Rep*, *10*(1), 14711. https://doi.org/10.1038/s41598-020-71528-3

Tahera, Y., Meltser, I., Johansson, P., & Canlon, B. (2006). Restraint stress modulates glucocorticoid receptors and nuclear factor kappa B in the cochlea. *Neuroreport*, *17*(9), 879-882. https://doi.org/10.1097/01.wnr.0000220131.24468.e7

Tao, X., Finkbeiner, S., Arnold, D. B., Shaywitz, A. J., & Greenberg, M. E. (1998). Ca2+ influx regulates BDNF transcription by a CREB family transcription factor-dependent mechanism. *Neuron*, *20*(4), 709-726. https://doi.org/10.1016/s0896-6273(00)81010-7

ten Cate, W. J., Curtis, L. M., Small, G. M., & Rarey, K. E. (1993). Localization of glucocorticoid receptors and glucocorticoid receptor mRNAs in the rat cochlea. *Laryngoscope*, *103*(8), 865-871. https://doi.org/10.1288/00005537-199308000-00007

ter Horst, J. P., van der Mark, M. H., Arp, M., Berger, S., de Kloet, E. R., & Oitzl, M. S. (2012). Stress or no stress: mineralocorticoid receptors in the forebrain regulate behavioral adaptation. *Neurobiol Learn Mem*, *98*(1), 33-40. https://doi.org/10.1016/j.nlm.2012.04.006

Tonnesen, J., Katona, G., Rozsa, B., & Nagerl, U. V. (2014). Spine neck plasticity regulates compartmentalization of synapses. *Nat Neurosci*, *17*(5), 678-685. https://doi.org/10.1038/nn.3682

Tsien, J. Z., Chen, D. F., Gerber, D., Tom, C., Mercer, E. H., Anderson, D. J., Mayford, M., Kandel, E. R., & Tonegawa, S. (1996). Subregion- and cell type-restricted gene knockout in mouse brain. *Cell*, *87*(7), 1317-1326. https://doi.org/10.1016/s0092-8674(00)81826-7

Tune, S., Alavash, M., Fiedler, L., & Obleser, J. (2021). Neural attentional-filter mechanisms of listening success in middle-aged and older individuals. *Nat Commun*, *12*(1), 4533. https://doi.org/10.1038/s41467-021-24771-9

Tuvikene, J., Pruunsild, P., Orav, E., Esvald, E. E., & Timmusk, T. (2016). AP-1 Transcription Factors Mediate BDNF-Positive Feedback Loop in Cortical Neurons. *J Neurosci*, *36*(4), 1290-1305. https://doi.org/10.1523/JNEUROSCI.3360-15.2016

Typlt, M., Mirkowski, M., Azzopardi, E., Ruettiger, L., Ruth, P., & Schmid, S. (2013). Mice with deficient BK channel function show impaired prepulse inhibition and spatial learning, but normal working and spatial reference memory. *PLoS One*, *8*(11), e81270. https://doi.org/10.1371/journal.pone.0081270

Tzingounis, A. V., & Nicoll, R. A. (2006). Arc/Arg3.1: linking gene expression to synaptic plasticity and memory. *Neuron*, *52*(3), 403-407. https://doi.org/10.1016/j.neuron.2006.10.016

van Bodegom, M., Homberg, J. R., & Henckens, M. J. A. G. (2017). Modulation of the Hypothalamic-Pituitary-Adrenal Axis by Early Life Stress Exposure [Review]. *Frontiers in Cellular Neuroscience*, *11*. https://doi.org/10.3389/fncel.2017.00087

van der Staay, F. J., Rutten, K., Barfacker, L., Devry, J., Erb, C., Heckroth, H., Karthaus, D., Tersteegen, A., van Kampen, M., Blokland, A., Prickaerts, J., Reymann, K. G., Schroder, U. H., & Hendrix, M. (2008). The novel selective PDE9 inhibitor BAY 73-6691 improves learning and memory in rodents. *Neuropharmacology*, *55*(5), 908-918. https://doi.org/10.1016/j.neuropharm.2008.07.005

Van Staveren, W. C., Steinbusch, H. W., Markerink-Van Ittersum, M., Repaske, D. R., Goy, M. F., Kotera, J., Omori, K., Beavo, J. A., & De Vente, J. (2003). mRNA expression patterns of the cGMP-hydrolyzing phosphodiesterases types 2, 5, and 9 during development of the rat brain. *J Comp Neurol*, *467*(4), 566-580. https://doi.org/10.1002/cne.10955

van Weert, L., Buurstede, J. C., Mahfouz, A., Braakhuis, P. S. M., Polman, J. A. E., Sips, H. C. M., Roozendaal, B., Balog, J., de Kloet, E. R., Datson, N. A., & Meijer, O. C. (2017). NeuroD Factors Discriminate Mineralocorticoid From Glucocorticoid Receptor DNA Binding in the Male Rat Brain. *Endocrinology*, *158*(5), 1511-1522. https://doi.org/10.1210/en.2016-1422

Vandael, D. H., Marcantoni, A., Mahapatra, S., Caro, A., Ruth, P., Zuccotti, A., Knipper, M., & Carbone, E. (2010). Ca(v)1.3 and BK channels for timing and regulating cell firing. *Mol Neurobiol*, *42*(3), 185-198. https://doi.org/10.1007/s12035-010-8151-3

Vardigan, J. D., Converso, A., Hutson, P. H., & Uslaner, J. M. (2011). The selective phosphodiesterase 9 (PDE9) inhibitor PF-04447943 attenuates a scopolamine-induced deficit in a novel rodent attention task. *J Neurogenet*, *25*(4), 120-126. https://doi.org/10.3109/01677063.2011.630494

Walton, J. P. (2010). Timing is everything: temporal processing deficits in the aged auditory brainstem. *Hear Res*, *264*(1-2), 63-69. https://doi.org/10.1016/j.heares.2010.03.002

Wang, J., & Puel, J. L. (2020). Presbycusis: An Update on Cochlear Mechanisms and Therapies. *J Clin Med*, *9*(1). https://doi.org/10.3390/jcm9010218

West, A. E., Pruunsild, P., & Timmusk, T. (2014). Neurotrophins: transcription and translation. *Handb Exp Pharmacol*, *220*, 67-100. https://doi.org/10.1007/978-3-642-45106-5_4

Wibrand, K., Messaoudi, E., Havik, B., Steenslid, V., Lovlie, R., Steen, V. M., & Bramham, C. R. (2006). Identification of genes co-upregulated with Arc during BDNF-induced long-term potentiation in adult rat dentate gyrus in vivo. *Eur J Neurosci*, *23*(6), 1501-1511. https://doi.org/10.1111/j.1460-9568.2006.04687.x

Wolter, S., Mohrle, D., Schmidt, H., Pfeiffer, S., Zelle, D., Eckert, P., Kramer, M., Feil, R., Pilz, P. K. D., Knipper, M., & Ruttiger, L. (2018). GC-B Deficient Mice With Axon Bifurcation Loss Exhibit Compromised Auditory Processing. *Front Neural Circuits*, *12*, 65. https://doi.org/10.3389/fncir.2018.00065

Xu, H., Kotak, V. C., & Sanes, D. H. (2010). Normal Hearing Is Required for the Emergence of Long-Lasting Inhibitory Potentiation in Cortex. *The Journal of Neuroscience*, *30*(1), 331-341. https://doi.org/10.1523/jneurosci.4554-09.2010

Yang, J., Vitery, M. D. C., Chen, J., Osei-Owusu, J., Chu, J., & Qiu, Z. (2019). Glutamate-Releasing SWELL1 Channel in Astrocytes Modulates Synaptic Transmission and Promotes Brain Damage in Stroke. *Neuron*, *102*(4), 813-827 e816. https://doi.org/10.1016/j.neuron.2019.03.029

Ying, S. W., Futter, M., Rosenblum, K., Webber, M. J., Hunt, S. P., Bliss, T. V., & Bramham, C. R. (2002). Brain-derived neurotrophic factor induces long-term potentiation in intact adult

hippocampus: requirement for ERK activation coupled to CREB and upregulation of Arc synthesis. *J Neurosci*, *22*(5), 1532-1540. https://doi.org/10.1523/JNEUROSCI.22-05-01532.2002

Yu, Y. F., Zhai, F., Dai, C. F., & Hu, J. J. (2011). The relationship between age-related hearing loss and synaptic changes in the hippocampus of C57BL/6J mice. *Exp Gerontol*, *46*(9), 716-722. https://doi.org/10.1016/j.exger.2011.04.007

Yuen, E. Y., Wei, J., Liu, W., Zhong, P., Li, X., & Yan, Z. (2012). Repeated stress causes cognitive impairment by suppressing glutamate receptor expression and function in prefrontal cortex. *Neuron*, *73*(5), 962-977. https://doi.org/10.1016/j.neuron.2011.12.033

Zhang, J., & Abdullah, J. M. (2013). The role of GluA1 in central nervous system disorders. *Reviews in the Neurosciences*, *24*(5), 499-505. https://doi.org/doi:10.1515/revneuro-2013-0021

Zhao, H., Wang, L., Chen, L., Zhang, J., Sun, W., Salvi, R. J., Huang, Y.-N., Wang, M., & Chen, L. (2018). Temporary conductive hearing loss in early life impairs spatial memory of rats in adulthood. *Brain and Behavior*, *8*(7), e01004. https://doi.org/https://doi.org/10.1002/brb3.1004

Zheng, F., Zhou, X., Moon, C., & Wang, H. (2012). Regulation of brain-derived neurotrophic factor expression in neurons. *Int J Physiol Pathophysiol Pharmacol*, *4*(4), 188-200. https://www.ncbi.nlm.nih.gov/pubmed/23320132

Zhu, M. Y., Wang, W. P., Huang, J., & Regunathan, S. (2007). Chronic treatment with glucocorticoids alters rat hippocampal and prefrontal cortical morphology in parallel with endogenous agmatine and arginine decarboxylase levels. *J Neurochem*, *103*(5), 1811-1820. https://doi.org/10.1111/j.1471-4159.2007.04867.x

6. Appendix

a) Accepted Papers

Savitska, D., Hess, M**., Calis, D.**, Marchetta, P., Harasztosi, C., Fink, S., Eckert, P., Ruth, P., Rüttiger, L., Knipper, M., & Singer, W. (2022). Stress Affects Central Compensation of Neural Responses to Cochlear Synaptopathy in a cGMP-Dependent Way. Frontiers in neuroscience, 16, 864706.

Calis, D.*, Hess, M.*, Marchetta, P., Singer, W., Modro, J., Nelissen, E., Prickaerts, J., Sandner, P., Lukowski, R., Ruth, P., Knipper, M., & Rüttiger, L. (2023). Acute deletion of the central MR/GR steroid receptor correlates with changes in LTP, auditory neural gain, and GC-A cGMP signaling. Frontiers in molecular neuroscience, 16, 1017761.

Pham, T., Hussein, T., **Calis, D**., Bischof, H., Skrabak, D., Cruz Santos, M., Maier, S., Spähn, D., Kalina, D., Simonsig, S., Ehinger, R., Groschup, B., Knipper, M., Plesnila, N., Ruth, P., Lukowski, R., & Matt, L. (2023). BK channels sustain neuronal Ca^{2+} oscillations to support hippocampal long-term potentiation and memory formation. Cellular and molecular life sciences: CMLS, 80(12), 369.

*Equal Contribution

frontiers | Frontiers in Neuroscience

ORIGINAL RESEARCH
published: 29 July 2022
doi: 10.3389/fnins.2022.864706

Stress Affects Central Compensation of Neural Responses to Cochlear Synaptopathy in a cGMP-Dependent Way

Daria Savitska[1], Morgan Hess[1], Dila Calis[1], Philine Marchetta[1], Csaba Harasztosi[1], Stefan Fink[1], Philipp Eckert[1], Peter Ruth[2], Lukas Rüttiger[1], Marlies Knipper[1] and Wibke Singer[1]*

[1] Department of Otolaryngology, Head and Neck Surgery, Tübingen Hearing Research Centre, Molecular Physiology of Hearing, University of Tübingen, Tübingen, Germany, [2] Department of Pharmacology, Toxicology and Clinical Pharmacy, Institute of Pharmacy, University of Tübingen, Tübingen, Germany

In light of the increasing evidence supporting a link between hearing loss and dementia, it is critical to gain a better understanding of the nature of this relationship. We have previously observed that following cochlear synaptopathy, the temporal auditory processing (e.g., auditory steady state responses, ASSRs), is sustained when reduced auditory input is centrally compensated. This central compensation process was linked to elevated hippocampal long-term potentiation (LTP). We further observed that, independently of age, central responsiveness to cochlear synaptopathy can differ, resulting in either a low or high capacity to compensate for the reduced auditory input. Lower central compensation resulted in poorer temporal auditory processing, reduced hippocampal LTP, and decreased recruitment of activity-dependent brain-derived neurotrophic factor (BDNF) expression in hippocampal regions (*low compensators*). Higher central compensation capacity resulted in better temporal auditory processing, higher LTP responses, and increased activity-dependent BDNF expression in hippocampal regions. Here, we aimed to identify modifying factors that are potentially responsible for these different central responses. Strikingly, a poorer central compensation capacity was linked to lower corticosterone levels in comparison to those of *high compensators*. *High compensators* responded to repeated placebo injections with elevated blood corticosterone levels, reduced auditory brainstem response (ABR) wave I amplitude, reduced inner hair cell (IHC) ribbon number, diminished temporal processing, reduced LTP responses, and decreased activity-dependent hippocampal BDNF expression. In contrast, the same stress exposure through injection did not elevate blood corticosterone levels in *low compensators*, nor did it reduce IHC ribbons, ABR wave I amplitude, ASSR, LTP, or BDNF expression as seen in *high compensators*. Interestingly, in *high compensators,* the stress-induced responses, such as a decline in ABR wave I amplitude, ASSR, LTP, and BDNF could be restored through the "memory-enhancing" drug phosphodiesterase 9A inhibitor (PDE9i). In contrast, the same treatment did not improve these aspects in *low compensators*. Thus, central compensation of age-dependent cochlear synaptopathy is a glucocorticoid

OPEN ACCESS

Edited by:
Verena Scheper, Hannover Medical School, Germany

Reviewed by:
Huib Versnel, University Medical Center Utrecht, Netherlands
Jennifer Harre, Hannover Medical School, Germany

***Correspondence:**
Marlies Knipper
marlies.knipper@uni-tuebingen.de

Specialty section:
This article was submitted to Neurodegeneration, a section of the journal Frontiers in Neuroscience

Received: *28 January 2022*
Accepted: *16 June 2022*
Published: *29 July 2022*

Citation:
Savitska D, Hess M, Calis D, Marchetta P, Harasztosi C, Fink S, Eckert P, Ruth P, Rüttiger L, Knipper M and Singer W (2022) Stress Affects Central Compensation of Neural Responses to Cochlear Synaptopathy in a cGMP-Dependent Way. Front. Neurosci. 16:864706. doi: 10.3389/fnins.2022.864706

and cyclic guanosine-monophosphate (cGMP)-dependent neuronal mechanism that fails upon a blunted stress response.

Keywords: long-term potentiation, cochlear synaptopathy, phosphodiesterase 9A inhibitor (PDE9i), cGMP, glucocorticoid, blunted stress response

INTRODUCTION

Hearing loss has been identified as a common risk factor in cognitive decline and Alzheimer's disease (Lin et al., 2011; Livingston et al., 2017; Montero-Odasso et al., 2020). A direct link has not yet been established (Lin et al., 2011; Fortunato et al., 2016; Uchida et al., 2019; Johnson et al., 2021), although numerous studies on animals and humans point to an interaction of auditory processing and the hippocampus, the part of the limbic system engaged in memory, spatial navigation, and possibly also sensory gating (see for a review: Knipper et al., 2022; Zhang et al., 2022).

A loss of afferent auditory fibers (cochlear synaptopathy) can progress with aging or following "non-traumatic" loud sound, even when audiometric thresholds are normal, and can occur independently of a loss of outer hair cells (OHCs), as shown in aging animals (Kujawa and Liberman, 2009; Sergeyenko et al., 2013; Möhrle et al., 2016) and humans (Bharadwaj et al., 2014; Plack et al., 2014; Viana et al., 2015; Kobel et al., 2017; Liberman and Kujawa, 2017). It has been suggested that deficits in auditory nerve fibers following acoustic trauma and/or age lead to temporal auditory discrimination deficits in animals (Kujawa and Liberman, 2009) and humans (Plack et al., 2014; Liberman and Kujawa, 2017; Wu et al., 2019). Aging people often experience difficulties in perceiving speech in a noisy environment even when audiometric thresholds remain normal (Frisina, 2009; Fullgrabe and Moore, 2014). The development of poor suprathreshold speech processing during aging was attributed to progressive cochlear synaptopathy (Bharadwaj et al., 2014; Bramhall et al., 2015).

We have previously observed that cochlear synaptopathy following acoustic trauma is linked to cognitive changes, including hippocampal long-term potentiation (LTP) or memory acquisition (Matt et al., 2018; Marchetta et al., 2020b). Moreover, temporal auditory processing deficits were not necessarily linked to cochlear synaptopathy when auditory brainstem response (ABR) wave IV amplitudes were disproportionally elevated in response to a reduced ABR wave I. This compensatory mechanism was associated with shorter auditory response latencies and preserved auditory steady state responses (ASSRs), despite age-dependent cochlear synaptopathy (Möhrle et al., 2016). ASSRs are used to investigate the integrity of higher-level auditory structures by measuring the synchronous, phase-locked discharge of auditory neurons to the modulation frequency of acoustic stimuli (Kuwada et al., 2002). The ASSR is a clear indicator for proper temporal processing of amplitude-modulated acoustic stimuli in subcortical areas and in the frontocentral cortex (Engelien et al., 2000). Strikingly, this central compensation response can vary in animals independently of age (Marchetta et al., 2020b); it was observed that, over the range of 9–23 months, mice with high and mice with low central compensation capacity (*high* and *low compensators*, respectively) could be identified (Marchetta et al., 2020b). *Low compensators* had delayed and reduced auditory responses, diminished temporal resolution (shown as reduced ASSR), and decreased hippocampal LTP (Marchetta et al., 2020b). *High compensators* did not show delayed responses to auditory stimuli and had normal hippocampal LTP (Marchetta et al., 2020b). As brain-derived neurotrophic factor (BDNF, *Bdnf*) highly contributes to hippocampal LTP and is widely expressed in the adult brain, e.g., the hippocampus, amygdala, cerebellum, and cerebral cortex (Hofer et al., 1990; Timmusk et al., 1993), the BDNF-live-exon-visualization (BLEV) reporter mice (Singer et al., 2018b) were used to determine the activity-dependent usage of *Bdnf* exon-IV and -VI promoters through bi-cistronic coexpression of cyan- and yellow-fluorescent-protein (CFP/YFP), respectively. Interestingly, *low compensators* with decreased LTP levels exhibited a lower ability to recruit activity-dependent *Bdnf* exon-IV-CFP and exon-VI-YFP, while *high compensators* with normal LTP exhibited comparatively higher activity-driven *Bdnf* transcript expression (Marchetta et al., 2020b). Searching for a mechanism that distinguishes *high* from *low compensators*, we reconsidered that activity-dependent BDNF expression was also altered in hippocampal capillaries, making differences in hemodynamic responses a possible contributing factor (Marchetta et al., 2020b). This prompted us in the present study to test brain-active vasodilators like the memory-stimulating phosphodiesterase 9A inhibitor (PDE9i) (Kroker et al., 2012). Since the application method itself-a sequence of placebo or drug injections for 10 consecutive days-was a stressful event for the animals, their corticosterone levels were analyzed. We discovered that successful central adaptation to age-related cochlear synaptopathy in *high compensators* is a cGMP- and stress-dependent process that failed in *low compensators* due to their blunted stress response.

Abbreviations: ABR, Auditory brainstem response; ACSF, artificial cerebrospinal fluid; ANOVA, analysis of variance; ASSR, auditory steady state response; BLEV, *Bdnf*-live-exon-visualization; BDNF/*Bdnf*, brain-derived neurotrophic factor; CFP/YFP, cyan- and yellow-fluorescent protein; cGMP, cyclic guanosine-monophosphate; FV, fiber volley; fEPSPs, field excitatory postsynaptic potentials; GC, glucocorticoid; GR, glucocorticoid receptor; HFS, high-frequency stimulation; IHC, inner hair cell; ISI, interstimulus interval; OHC, outer hair cell; IOR, input-output relationship; LTP, long-term potentiation; MD, mediodorsal thalamus; MR, mineralocorticoid receptor; PPF, paired-pulse facilitation; PV, parvalbumin; PV-IN, parvalbumin-positive interneuron; PDE9A, phosphodiesterase 9A; PDE9i, phosphodiesterase 9A inhibitor; PFC, prefrontal cortex; re thr, relative to threshold; SEM, standard error of the mean; SNR, signal-to-noise ratio.

MATERIALS AND METHODS

Animals

Animal care, procedure, and experimental protocols correspond to national and institutional guidelines and were reviewed and approved by University of Tübingen, Veterinary Care Unit, and the Animal Care and Ethics Committee of the regional board of the Federal State Government of Baden-Württemberg, Germany. All experiments were performed according to the European Union Directive 2010/63/EU for the protection of animals used for experimental and other scientific purposes. In-house bred mice were kept according to the national guidelines for animal care in a specific pathogen-free animal facility at 25°C on a 12 h/12 h-light/dark cycle, with average noise levels of around 50–60 dB SPL_{RMS}.

Female and male homozygous *Bdnf*-live-exon-visualization (BLEV) mice were used and categorized into different age groups. Middle-aged animals were between 9 and 14.7 months, while old animals were between 15.2 and 22.7 months.

The mouse model was generated as described (Singer et al., 2018b). Briefly, the brain-derived neurotrophic factor (BDNF, *Bdnf)* exon-IV and -VI sequences, both including the corresponding promoter sequences, were extended by cyan- and yellow-fluorescent protein (CFP/YFP), respectively, both containing a stop codon. A HA-tag was added to *Bdnf* exon-IV-CFP and a cMyc-tag to *Bdnf* exon-VI-YFP. The translation of the protein-coding *Bdnf* exon-IX was enabled by an internal ribosomal entry site sequence, which keeps the mRNA at the ribosome, despite the presence of a stop codon. Additionally, the growth-associated protein 43 was added to anchor the fluorescent proteins at the site of translation. This allows differential monitoring of the non-coding *Bdnf* exon-IV and *Bdnf* exon-VI by the fluorescent proteins CFP and YFP without interfering with *Bdnf* exon-IX.

Hearing Measurements

Hearing function was studied before and after treatment with either a placebo or phosphodiesterase 9A inhibitor (PDE9i) by measuring auditory brainstem responses (ABR) and auditory steady state responses (ASSR) in a soundproof chamber (IAC 400-A, Industrial Acoustics Company GmbH, Niederkrüchten), as previously described (Zuccotti et al., 2012; Rüttiger et al., 2013). Hearing measurements were done under anesthesia, 75 mg/kg ketamine hydrochloride (Ketavet®, Zoetis GmbH, Berlin, Germany), 5 mg/kg xylazine hydrochloride (Rompun®, Bayer Vital GmbH, Leverkusen, Germany), and 0.2 mg/kg atropine (AtropinsulfatB. Braun, Melsungen, Germany), as previously described (Engel et al., 2006; Rüttiger et al., 2013).

The ABR, evoked by short-duration sound stimuli, represents the summed activity of neurons in distinct anatomical structures along the ascending auditory pathway (Burkard and Don, 2007) recorded from subcutaneous electrodes (one active electrode at the recorded ear, the reference electrode at the vertex, and the grounding electrode at the caudal third of the back of the animal, **Supplementary Figure 1A**). A microphone (Bruel & Kjaer 4939, Naerum, Denmark) was used to calibrate and record the acoustic stimuli. ABR thresholds were elicited with a phase-alternating click (100 microsecond duration with an FFT mean of 5.4 kHz), noise-burst (1 ms duration, FFT mean of 7.9 kHz), or pure-tone stimuli (3 ms duration, including a 1 ms cosine squared rise-and-fall envelope, 2–32 kHz). The stimulus level was increased stepwise from 10 to 100 dB SPL in 5dB steps. The stimuli were generated with an I-O-card (PCIe-6259, National Instruments, Austin, Texas, USA) in an IBM compatible computer. The SPL of the stimuli was modulated by custom-made amplifier and attenuator systems (Wulf Elektronik, Frankfurt). The measured signals were bandpass filtered from 200 Hz to 5 kHz (F1, 6-pole Butterworth hardware filter, Wulf Elektronik) and amplified by 100,000. The analog/digital (A/D) rate was 20 kHz. Each stimulus had a recording interval of 16 ms and was directly repeated and averaged up to 512 times (256 for pure-tone stimuli).

ASSRs were measured with amplitude-modulated sinusoidal stimuli (**Supplementary Figure 1B**), with a carrier frequency of 11.3 kHz, a modulation frequency of 512 Hz, and a maximal (100%) modulation depth. For the growth function, the amplitude-modulated stimuli were presented between –10 and 60 dB relative to the threshold in 5 dB steps. The response on amplitude modulation was tested on the ear with the lower click- and noise-evoked threshold directly after finishing the standard ABR protocol using the same electrode positions (**Supplementary Figure 1A**). ASSR responses to amplitude-modulated tones were recorded in epochs of 1,114 ms, filtered (50–2,000 Hz 6th order band-pass Butterworth), amplified (80 or 100 dB), and sampled at 50 kHz by 16-bit A/D conversion of a 5 or 10 V input range by the I-O-card (National Instruments).

Phosphodiesterase 9A Inhibitor

3 mg of PDE9i (BAY 73-6691, Bayer Vital GmbH, Leverkusen, Germany) was dissolved in 500 µl EtOH and diluted with 9.5 ml of 10% Solutol (BASF, Mannheim, Germany). The placebo solution consisted of a dilution medium without PDE9i.

The placebo or PDE9i was administered to the mice intraperitoneally for 10 consecutive days at approximately the same time.

Field Excitatory Postsynaptic Potential Recordings in Hippocampal Slices

Extracellular field excitatory postsynaptic potential (fEPSP) recordings were performed according to standard methods as previously described (Matt et al., 2011; Chenaux et al., 2016).

In brief, 400 µm-thick coronal brain slices were cut on a vibratome (Leica VT 1000S) in an ice-cold dissection buffer (mM): 127 NaCl, 1.9 KCl, 1.2 KH_2PO_4, 26 $NaHCO_3$, 10 D-glucose, 2 $MgSO_4$, and 1.1 $CaCl_2$, constantly saturated with 5% CO_2 and 95% O_2 (pH 7.4). Slices were incubated in oxygenated artificial cerebrospinal fluid (in mM: 127 NaCl, 1.9 KCl, 1.2 KH_2PO_4, 26 $NaHCO_3$, 10 D-glucose, 1 $MgSO_4$, 2.2 $CaCl_2$; pH 7.4) for 1 h at 30°C and, afterwards, stored at room temperature. Recordings were performed in a submerged-type recording chamber (Warner Instruments). Stimulation (TM53CCINS, WPI) and recording (artificial cerebrospinal fluid-filled glass pipettes, 2–3 MΩ) electrodes were positioned in the stratum radiatum to record Schaffer collateral fEPSPs. Signals were amplified with an Axopatch 200B (Molecular Devices),

digitized at 5 kHz with an ITC-16 (HEKA) and recorded using WinWCP from the Strathclyde Electrophysiology Suite. The stimuli (100 μs) were delivered through a stimulus isolator (WPI). For each individual slice, the strength of the stimulation (typically between 30 and 125 μA) was chosen to evoke 40–60% of the maximal response, defined by an initial fEPSP slope. Only slices that showed stable fiber volley (FV) and fEPSP were used for further recording. The same stimulus intensity was applied during baseline recording (0.067 Hz, 20–30 min) and induction of long-term potentiation (LTP) using 100 stimuli during 1 s (100 Hz, 1 s).

Tissue Preparation

Tissue preparation was carried out as described in detail previously (Singer et al., 2016; Matt et al., 2018). In brief, brains were dissected and fixed in 2% paraformaldehyde for 48 h. For cochlear cross-section immunohistochemistry, cochleae were isolated, fixed by immersion in 2% paraformaldehyde, 125 mM sucrose in 100 mM phosphate-buffered saline (pH 7.4) for 2 h and then decalcified for 45 min in RDO rapid decalcifier (Apex Engineering Products Corporation, Aurora, IL, USA). Cochleae were stored in Sucrose-Hank's solution rotated at 4°C overnight before they were embedded in Tissue-tek and cryosectioned in slices of 10 μm, and mounted on SuperFrost*/plus microscope slides before storage at –20°C.

Immunohistochemistry

Immunohistochemistry was carried out as described in detail previously (Singer et al., 2016). Antibodies against C-terminal-binding protein 2 (CtBP2)/RIBEYE (rabbit, diluted 1:750; ARP American Research Products, Inc.™, Waltham, MA, USA) to detect ribbons (Khimich et al., 2005), neurofilament 200 (NF-200, mouse, 1:3,000; Sigma-Adlrich, St. Louis, MO, USA), parvalbumin (PV, rabbit, diluted 1:2,000; Abcam, Cambridge, UK), Synaptobrevin 2 (mouse, diluted 1:200; Synaptic Systems, GmbH, Berlin, Germany), and desmin (mouse, diluted 1:100; Abcam, Cambridge, UK) were used. Primary antibodies were detected using appropriate Cy3 (1:1,500, Jackson Immuno Research Laboratories, West Grove, PA, USA) or Alexa488 (1:500, Invitrogen Molecular Probes, Paisley, UK) secondary antibodies.

All samples were viewed as previously described (Zampini et al., 2010) using an Olympus BX61 microscope (Olympus, Hamburg, Germany), equipped with epifluorescence illumination and analyzed with CellSens Dimension software (OSIS GmbH, Münster, Germany). To increase spatial resolution, the slices were imaged over a distance of 15 μm within an image stack along the *z*-axis (z-stack), followed by 3-dimensional deconvolution using CellSens Dimension's built-in algorithm.

Corticosterone Analysis

Corticosterone concentration in the blood was assessed using the corticosterone ELISA kit (Catalog Nr. ADI-901-097) from Enzo Life Science Inc. (Farmingdale, NY, USA). An assay buffer and a wash buffer were prepared. The assay buffer solution is prepared by diluting the assay buffer provided (a tris buffered saline containing proteins and sodium azide as a preservative) 1:10 with deionized water; subsequently, a wash buffer solution is made by diluting the wash buffer provided (a tris buffered saline containing detergent) 1:20 with deionized water. Afterwards, 5 standard solutions are prepared: 200,000 pg/ml corticosterone standard solution is diluted 1:10 with the assay buffer in a plastic tube, and serial dilutions are made to have these final concentrations of corticosterone 20,000, 4,000, 800, 160, 32 pg/ml, respectively. Each tube is mixed completely using a vortex mixer (MS2 Minishaker, IKA™, Wilmington, NC, USA) to have a correct concentration. Then, the wash buffer solution is made by diluting the wash buffer provided 1:20 with deionized water. Later, wells (covered with a donkey antibody specific to sheep IgG) are disposed on the microtiter plate (Costar™). 100 μl of standards is pipetted into the appropriate wells. 100 μl of samples previously centrifuged 3,000 x g for 5 min with Heraeus Pico 17 Microcentrifuge (ThermoFisher Scientific, MA, USA) and diluted 1:20 with the assay buffer is pipetted into the specific wells and is run in duplicate. Therefore, 150 μl of the assay buffer solution is pipetted into non-specific-binding (NSB) wells, and 100 μl of the assay buffer is pipetted into positive-control (B_0) wells. NSB and B_0 wells will give a 0% and a 100% binding, respectively, with the antibody when the enzyme conjugated with corticosterone is added into the wells.

Then, 50 μl of corticosterone ELISA Conjugate (a solution of alkaline phosphatase conjugated with corticosterone), which competes with corticosterone in samples and standards to the antibody bound, is pipetted into each well, except the total activity (TA) and blank wells. 50 μl of corticosterone ELISA Antibody (a solution of sheep polyclonal antibody) is pipetted into each well, with the exception of the blank, TA, and NSB wells. Next, the plate is incubated at room temperature and shaken at 300 rpm for 2 h using a Rotamax 120 shaker (Heidolph Instruments, Schwabach, Germany). After that, the wells are washed three times with 400 μl of wash buffer solution per well. 5 μl of corticosterone ELISA Conjugate is pipetted into the TA wells, and 200 μl of the p-nitrophenyl phosphate solution is pipetted into every well. Afterwards, the plate is incubated at room temperature for 1 h without shaking. 50 μl of Stop Solution (trisodium phosphate in water) is added to each well, and the plate is read immediately at 405 nm. The four-parameter logistic curve works as the following: before making the standard curve, the average of the optic density of each duplicate is subtracted from the optic density average of the NSB to obtain the optic density net values, which are then divided by the net B_0 to obtain the percentage binding.

Experimental Design

Hearing function was analyzed 3–5 days prior to placebo or PDE9i application and 1–3 day(s) after the last injection. The animals were separated into one group analyzed for LTP and another group for molecular analyses of brain slices. Blood was taken in the first 15 min of the first anesthesia before and after the 10-day injection protocol. The animals were prepared 1 day after the last hearing measurement. Details for *n* numbers of the single experiments are given in **Supplementary Table 1**.

Data Analyses

Statistics and Numbers

Unless otherwise stated, all data were presented as group mean with standard error of the mean (SEM) for *n* animals per the experimental group. Data were tested for normal distribution (the Shapiro-Wilk normality test, $\alpha = 0.05$). Differences of the means were compared for statistical significance either by ungrouped two-tailed Student's t-test (parametric)/ Mann–Whitney U test (non-parametric), 1-way, or 2-way ANOVA (parametric)/ Kruskal–Wallis test (non-parametric) with $\alpha = 0.05$ and correction for type 1 error after Sidak's test/the Bonferroni's multiple comparisons test (parametric) or the Dunn's multiple comparison's test/the two-stage linear step-up procedure of Benjamini, Krieger, and Yekutieli (non-parametric). In figures, significance is indicated by asterisks [trend (*) $p \leq 0.1$, $^{*}p < 0.05$, $^{**}p < 0.01$, $^{***}p < 0.001$, $^{****}p < 0.0001$]. ns denotes non-significant results ($p > 0.1$). All statistical information and *n* numbers can be found in the figure legends and in **Supplementary Table 1**. Statistical calculations and visualizations were done using GraphPad Prism.

ABR Analysis

The ABR evoked by the click, noise-burst, and pure-tone frequency-specific auditory stimuli was examined as described (Marchetta et al., 2020a). The threshold for all click, noise, and pure-tone ABR measurements was manually defined as the lowest sound level at which a clear signal could be discriminated from the baseline (Valero et al., 2017).

ABR waveforms (**Figure 1A**) were analyzed for consecutive amplitude deflections (peaks), with each wave consisting of a starting negative (n) peak and the following positive (p) peak. Peak amplitudes of ABR waves I and IV were extracted in the present study and defined as follows: wave I: In-to-Ip (0.8–1.8 ms), the summed activity originating from the auditory nerve (Johnson and Kiang, 1976); and wave IV: IVn-to-IVp (4.1–4.9 ms), the synchronous neural activity that arises from the lateral lemniscus and inferior colliculus (IC) (Melcher and Kiang, 1996). A customized program ("PEAK.exe") was used to extract ABR peaks on the basis of these definitions. ABR peak-to-peak (wave) amplitude growth functions were constructed for individual ears on the basis of the extracted peaks. ABR wave amplitude growth functions were calculated for increasing stimulus levels with reference to the ABR thresholds (from 0 to a maximum of 80 dB above the threshold in 5 dB steps). Statistical analysis was performed in a range of 20–55 dB relative to the threshold to ensure a consistent number of data points for all treatment conditions and time points.

In **Figures 1D,E**, the peak input-output function for amplitude of the click-ABR measurements was averaged for intensities between 0 and 40 dB relative to threshold (re thr) for each individual ear and analyzed as previously described (Chumak et al., 2016).

For further analysis, the *strength* of the click-ABR growth function was determined in 5 dB steps until a maximum of ca. 105 dB SPL. Therefore, the three highest amplitude values of the individual ears' supra-threshold amplitude growth function were averaged [described in more detail in Singer et al. (2018a)].

The wave IV/I ratio was calculated using click-ABR data for individual animals at all intensities re thr; the ABR wave IV amplitude was divided by ABR wave I amplitude. For further analyses in **Figure 1F**, the mean between 0 and 40 dB (re thr) was calculated.

To determine the level of central compensation for individual animals, the wave IV/I ratio was plotted against wave I strength (**Figure 1F**), as previously described (Marchetta et al., 2020b). The power function ($y = a^{*}x^{b}$) was inserted as a regression line for each group. Only the animals with wave I strength smaller than 2.19 μV [which is the general wave I strength of all the mice corrected by the limitation value of previous studies (Marchetta et al., 2020b)] were subdivided along the black regression line (each mouse is represented by the average of two ears). The animals below the line were defined as *low compensators*, while the animals above were defined as *high compensators*. The animals that were lying on the line were removed from further analysis.

ASSR Analysis

Response trials (**Supplementary Figure 1C**) from 32 artifact-cleaned epochs of every condition were averaged and spectral power determined by Fast Fourier Transformation (FFT; **Supplementary Figure 1D**). From the spectrum of either condition, the signal response was determined as the spectral peak within a frequency window of ± 8 Hz (range, 16 Hz) around the modulation frequency (first harmonic). Noise levels were determined within the same frequency window using an iterative procedure. For this, first, we calculated the average and standard deviation of the spectral power from the lowest 2 and the highest 2 bins of the 16 Hz-wide FFT window around the modulation frequency. Then, we calculated z scores for each next-highest and next-lowest bin within the FFT window. If the spectral amplitude of both bins fell within the confidence ranges around the noise average (criterion = 1.96), the two bins were enclosed to the new mean and standard deviation. If the z-score of one of the newly considered bins exceeded the criterion, the iterative calculation was aborted and the resulting average and variance of the noise reported for subsequent analyses. Dependent on the spectral noise, on average, 14 points (range, 4–42) did contribute to the calculation of the noise level.

Epochs from alternating and non-alternating-phase stimulus presentation contributed to the average. No differences of spectral amplitudes were found for the alternating-phase stimuli, indicating no residual cochlear microphonic or temporal fine structure responses were confounding the spectral data at the first harmonic of the response. We analyzed results for the first to 6th harmonic (**Supplementary Figure 1D**). We show results for the first harmonic only. Summation of all 6 harmonic amplitudes yielded a result similar to the amplitude for the first harmonic.

fEPSP Recordings in Hippocampal Slices

The fEPSP baseline was determined by averaging fEPSP initial slopes from the period before the tetanic stimulation (at least 15 min of stable recording). The level of LTP was determined by averaging fEPSP slopes from the period between 50 and 60 min after the high-frequency stimulation (HFS). Before the

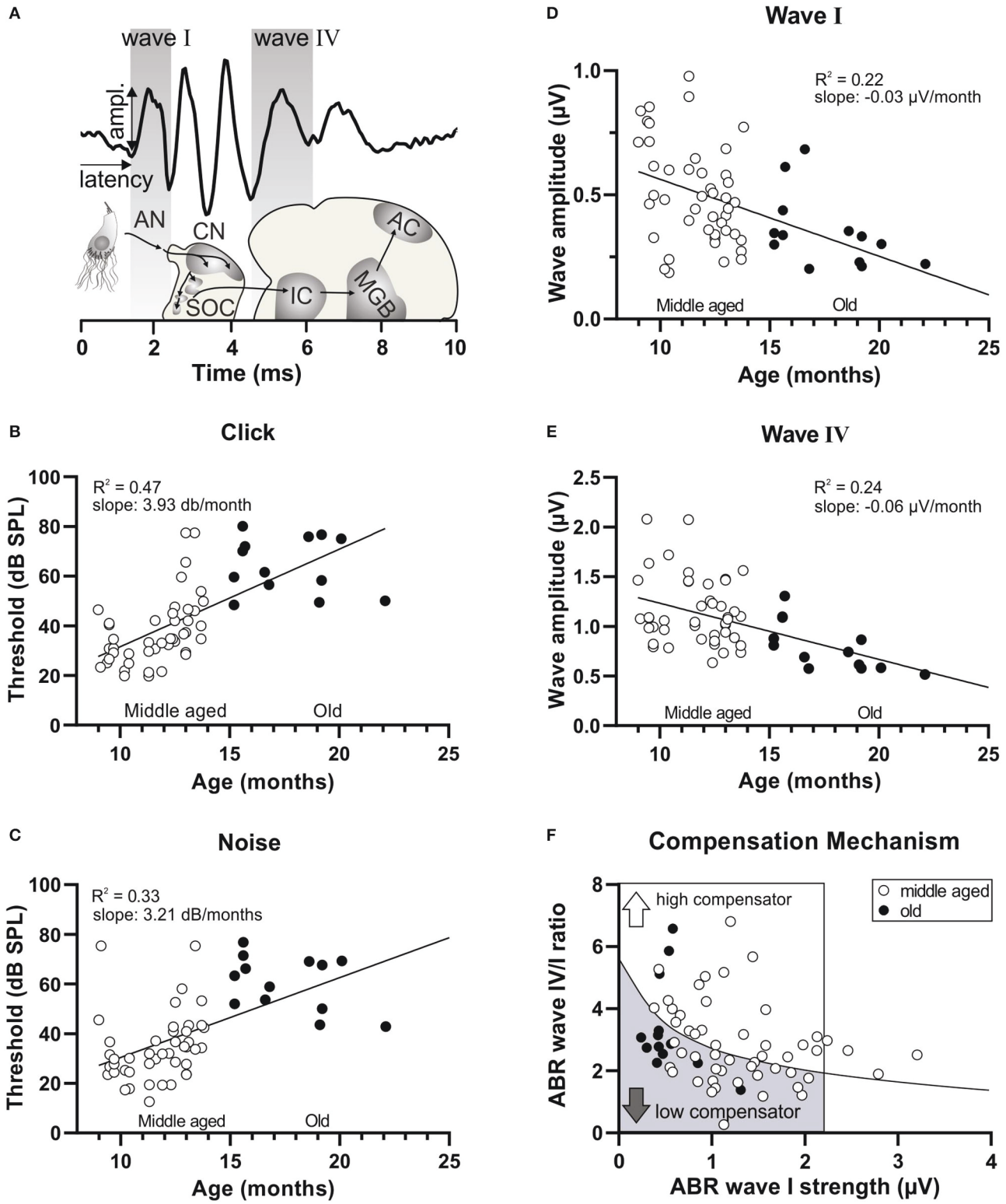

FIGURE 1 | Decrease in hearing function over age and subsequent subdivision by the compensation mechanism. **(A)** Schematic drawing of the auditory pathway and stimulus-evoked deflections of ABR waves correlated with anatomical structures. AN, auditory nerve; CN, cochlear nucleus; SOC, superior olivary complex; IC, inferior colliculus; MGB, medial geniculate body; AC, auditory cortex. **(B)** In a homogenous group of aging animals (white circles < 15 months, middle aged; black circles > 15 months old), increasing age was significantly correlated with an increasing threshold in response to click stimuli and **(C)** noise stimuli. **(D)** In addition, increasing age was significantly correlated with a decreasing amplitude of ABR wave I **(E)** and ABR wave IV. **(F)** A schematic diagram representing animals with reduced ABR wave I (inside the box; ABR wave I < 2.19 µV) subdivided by the black regression line, depending on their central compensation capacity into low compensators (the lower wave IV/I ratio) and high compensators (the higher wave IV/I ratio).

tetanic stimulation, each slice was used to record input-output relationship (IOR, 25–150 μA in 25 μA steps) and paired-pulse facilitation (PPF, 10–20–50–100–200–500 ms interstimulus interval (ISI) at the same stimulation strength as LTP recordings). IOR changes in the fEPSP slope and FV amplitude were normalized within each slice (% from the maximal response at the highest stimulus strength was calculated), and averaged values for each group were plotted against the stimulus intensity. The PPF paired-pulse ratio of the fEPSP2/fEPSP1 slope and amplitude at each ISI was defined per slice, and mean values per group were plotted. fEPSP1 was calculated as an average of fEPSP1s from all interstimulus intervals for each single slice. Four traces were averaged for each single data point analyzed. Data were analyzed and processed using Clampfit 10 (Molecular Devices) and Microsoft Excel.

The data presented per experimental group/condition contained (in addition to mean ± SEM) single dots, showing the fEPSP slope values for each individual brain slice. The *n* indicates the number of slices and animals (slices/animals) used in the analysis (**Figure 6**).

Fluorescence Analysis of Immunohistochemistry

For inner hair cell (IHC) ribbon counting, pictures were taken from all turns of both ears from duplicate immunohistochemical staining.

Pictures acquired from brain sections stained for PV were analyzed using the free Image J software (NIH, Bethesda, MD, USA). For each section, pictures for each single channel (YFP, CFP, PV) were saved and analyzed independently. For the 10× magnified pictures, after conversion to an 8-bit image, background was reduced using the rolling ball algorithm (available as a tool for Image J), with standard parameters in each single channel picture. Afterwards, the integrated density of the fluorescence of CFP, YFP, and PV within the picture was calculated. For each individual animal, both hippocampus hemispheres were analyzed by taking a picture from each side.

Corticosterone Analysis

Calculation of the corticosterone levels was performed using an online data analysis tool (myassays.com). Finally, corticosterone levels were averaged per group/treatment condition and presented as mean ± SEM.

RESULTS

Animals With Age-Related Hearing Loss Differ in the Ability to Centrally Compensate Cochlear Synaptopathy

Previous and present findings document that aging mice could be subdivided into two groups with a higher or lower ability to centrally compensate for a diminished auditory nerve response through a larger or smaller suprathreshold ABR wave IV/I ratio, respectively, and through elevated or attenuated responses to amplitude-modulated tones (Marchetta et al., 2020b). An additional group of 58 animals, subdivided into middle-aged (9–14.7 months, **Figure 1**, white circles) and old (15.2–22.7 months, **Figure 1**, black circles) mice, was analyzed using lower frequency, containing (click) and higher frequency containing (noise-burst) stimuli. Hearing thresholds (**Figures 1B,C**) and the fine structure of suprathreshold ABR waves corresponding to activity in the auditory nerve (wave I, **Figures 1A,D**) and lateral lemniscus and IC (wave IV, **Figures 1A,E**) were analyzed. Upon plotting thresholds to click or noise-burst stimuli as a function of age, we observed a linear correlation (**Figure 1B**, linear regression, $Y = 3.392^*X - 7.781$, $R^2 = 0.047$, $p < 0.0001$, $n = 58$ mice; **Figure 1C**, linear regression, $Y = 3.212^*X - 1.677$, $R^2 = 0.33$, $p < 0.0001$, $n = 58$ mice), indicating that thresholds increased with increasing age. When plotting ABR wave I or wave IV amplitude as a function of age, we observed a significant negative linear correlation, indicating that auditory nerve and brainstem activity decreased with increasing age (**Figure 1D**, linear regression, $Y = -0.03099^*X + 0.08725$, $R^2 = 0.22$, $p = 0.0002$, $n = 58$ mice; **Figure 1E**, linear regression, $Y = -0.05651^*X + 1.798$, $R^2 = 0.24$, $p < 0.0001$, $n = 58$ mice). To define the individual level of compensation, we plotted the ABR wave I strength (average of the three highest wave amplitude values) against the ABR wave IV/I ratio (**Figure 1F**) (see methods). The power function ($y = a^*x^b$) inserted as a regression line was calculated using all available measurements from this mouse line in order to ensure a robust database. The animals characterized by dots lying below the black regression line were assigned to the category *low compensators* (**Figure 1F**, gray arrow), while the animals characterized by dots lying above the black regression line were assigned to *high compensators* (**Figure 1F**, white arrow). We confirmed previous findings (Marchetta et al., 2020b) that both *high* and *low compensator* groups included middle-aged and old mice (**Figure 1F**, bottom, white and black circles). Due to the limited *n*-number in the group of the old mice, especially for the *high compensators* ($n = 3$), we decided to proceed only with the group of the middle-aged mice of $n = 18$ *low compensators* and $n = 26$ *high compensators*.

In conclusion, the process of aging brings about a worsening of hearing function, here reflected in increasing thresholds and decreasing ABR wave amplitudes; however, central compensation abilities are independent of age.

Low Compensators Exhibit Reduced ASSR Response to Amplitude-Modulated Tones

To determine whether the distinction between *high* and *low compensators* is independent of OHC function, hearing thresholds were analyzed and compared. No differences were observed in the thresholds of *high* and *low compensators* in response to click [**Figure 2A**, Mann–Whitney U test, U (30.05, 34.55) = 205.5, $p = 0.50$, low: $n = 18$, high: $n = 26$ mice], noise-burst [**Figure 2B**, Mann–Whitney U test, U (27, 27.35) = 200.5, $p = 0.70$, low: $n = 18$, high: $n = 26$ mice], or 11 kHz pure-tone stimuli [**Figure 2C**, Mann–Whitney U test, U (33, 43) = 197.5, $p = 0.39$, low: $n = 18$, high: $n = 26$ mice]. However, in response to the pure-tone stimuli of increasing frequencies (2–32 kHz, half-octave steps), we observed an increased threshold

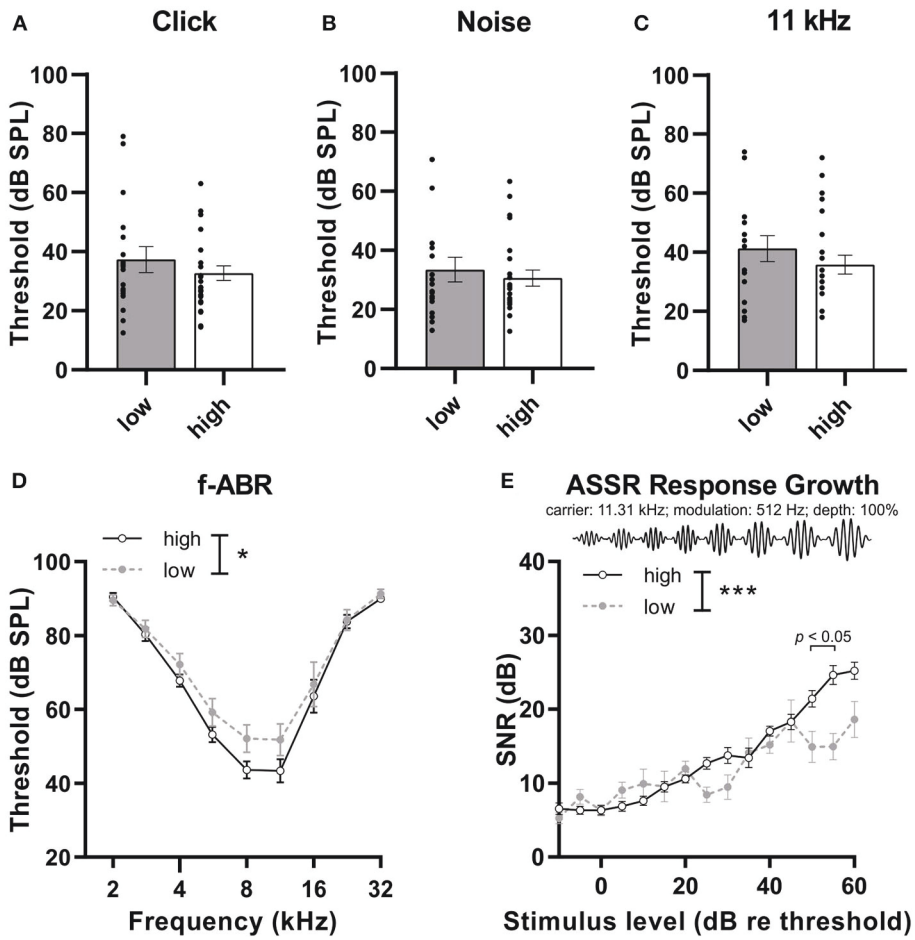

FIGURE 2 | The hearing phenotype of low and high compensators before treatment. **(A)** Low and high compensators showed similar thresholds in response to click and **(B)** noise stimuli. **(C)** High and low compensators showed similar thresholds in response to 11 kHz pure-tone stimuli. **(D)** However, with pure-tone, frequency-specific auditory stimuli (2-32 kHz), low compensators showed elevated thresholds compared to high compensators. **(E)** The temporal auditory resolution was significantly decreased in low compensators in comparison to high compensators. Re threshold, relative to threshold. Mean ± SEM. *p <0.05, ***p <0.001, 2-way ANOVA.

in *low compensators* in comparison to *high compensators* [**Figure 2D**, 2-way ANOVA, $F(1, 325) = 5.00$, $p = 0.03$, Bonferroni's multiple comparisons test, low: $n = 18$, high: $n = 26$ mice]. The hearing phenotypes of *high* and *low compensators* were further characterized by analyzing the auditory temporal resolution through using amplitude-modulated stimuli to obtain ASSRs. In the present study, the growth of the ASSR to amplitude-modulated tones with increasing loudness was tested (carrier frequency, 11.32 kHz; modulation frequency, 512 Hz; modulation depth, 100%) (**Figure 2E**). In the ASSR response-growth function, *low compensators* had a significantly reduced signal-to-noise ratio (SNR) in comparison to *high compensators*, particularly at high sound pressure levels levels [**Figure 2E**, 2-way ANOVA, $F(1, 546) = 13.41$, $p = 0.0003$, Bonferroni's multiple comparisons test, low: $n = 14$, high: $n = 20$ mice].

In conclusion, *high* and *low compensators* do not differ in the threshold, except to pure-tone stimuli, where *low compensators* seem to have higher thresholds in comparison to *high compensators*. In addition, *low compensators* show a temporal auditory processing deficit, particularly for high sound pressure levels.

Low Compensators Exhibit a Reduced Stress Response to Injection-Induced Stress That Is Independent of Hearing Thresholds

We next compared the effect of PDE9i in comparison to a placebo injection on 10 subsequent days. To test whether the placebo treatment alone exerted a possible stress effect that influenced central neuronal activity, we measured the blood-corticosterone levels before and after treatment. Interestingly, *low compensators* showed significantly lower pre-treatment corticosterone levels in comparison to *high compensators* [**Figure 3**, gray bar vs. white bar, two-tailed Student's t-test: t (35) = 2.42, $p = 0.02$, low

pre: $n = 18$, high pre: $n = 19$ mice]. Following 10 days of injection with either placebo or PDE9i, a significant increase in blood-corticosterone levels was observed in *high compensators* after both placebo (**Figure 3**, white bar vs. light blue bar), and PDE9i injection [**Figure 3**, white bar vs. light-orange bar, 1-way ANOVA, $F(5, 63) = 6.79$, $p < 0.001$, Bonferroni's multiple comparisons test, low pre: $n = 18$, high pre: $n = 19$, low placebo: $n = 6$, low PDE9i: $n = 7$, high placebo: $n = 10$, high PDE9i: $n = 9$ mice]. *Low compensators* did not show significant changes in blood-corticosterone levels, following 10 days of injection with either treatment (**Figure 3**, gray bar vs. dark blue bar or dark-orange bar).

As no significant differences between PDE9i or placebo treatment were observed in either *low* or *high compensating* animals, it can be inferred that it is not PDE9i that influences blood corticosterone levels but, rather, the injection itself.

To determine whether the altered stress response between *high* and *low compensators* was reflected in differences in hearing thresholds after treatment, click and noise-burst ABRs were measured (**Supplementary Figure 2**). Neither the injection itself nor treatment with PDE9i had an effect on ABR thresholds for click [**Supplementary Figure 2A**, 1-way ANOVA, $F(3, 24) = 0.19$, $p = 0.91$, pre (gray), and post placebo (dark blue): $n = 6$, pre (gray) and post PDE9i (dark orange): $n = 8$ mice; **Supplementary Figure 2B**, 1-way ANOVA, $F(3, 36) = 0.63$, $p = 0.60$, pre (white) and post placebo (light blue): $n = 9$, pre (white) and post PDE9i (light orange): $n = 11$ mice] and noise-burst stimuli [**Supplementary Figure 2C**, Kruskal–Wallis test, H (3) = 0.49, $p = 0.92$, pre (white) and post placebo (dark blue): $n = 8$, pre (white) and post PDE9i (dark orange): $n = 8$ mice; **Supplementary Figure 2D**, Kruskal–Wallis test, H (3) = 3.47, $p = 0.32$, pre (white) and post placebo (light blue): $n = 9$, pre (white) and post PDE9i (light orange): $n = 11$ mice], suggesting that even profound differences in blood-corticosterone levels had no impact on cochlear mechanics.

In conclusion, in *high compensators* but not *low compensators*, a significant elevation of blood-corticosterone levels is induced by 10 consecutive days of injection with either the placebo or PDE9i. This suggests that *low compensators* exhibit a blunted stress response. Neither the variation in the corticosterone level seen between *high* and *low compensators* nor the placebo or PDE9i treatment had any influence on hearing thresholds.

High Compensators, but Not *Low Compensators*, Exhibit a "Stress-Induced" Drop in Auditory Nerve Response That Can Be Restored by PDE9i Treatment

We next asked whether suprathreshold auditory processing differences might exist independently of the hearing threshold between *low* and *high compensators* that are possibly related to the differences in corticosterone levels. We studied suprathreshold click-ABR wave fine structures and the temporal coding properties (ASSR) in both groups in more detail. Strikingly, in *high compensators* treated with a placebo, the amplitude

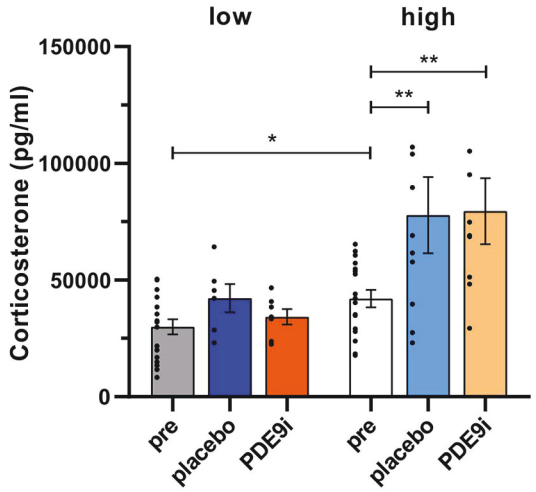

FIGURE 3 | Corticosterone levels in low and high compensators before and after treatment with either placebo or PDE9i. Prior to treatment, low compensators had lower corticosterone levels in comparison to high compensators. Significantly elevated corticosterone levels were found only in high compensators but not in low compensators after treatment with either placebo or PDE9i. However, no significant differences were observed between the two post-treatment conditions in either high or low compensators. Mean ± SEM. *$p < 0.05$ (two-tailed t-test pre low vs. pre high), **$p < 0.01$ (the Bonferroni's multiple comparison test for high compensators).

of ABR wave I showed a significant decrease after treatment [**Figure 4A**, light blue line, repeated measures 2-way ANOVA, $F(1, 138) = 4.92$, $p = 0.03$, Sidak's multiple comparisons test, $n = 20/10$ ears/mice]. However, in *high compensators* treated with PDE9i, the wave I amplitude was preserved [**Figure 4B**, light orange line, repeated measures 2-way ANOVA, $F(1, 124) = 0.15$, $p = 0.70$, $n = 22/11$ ears/mice]. Similar results were observed in ABR wave IV, where *high compensators* showed a decreased amplitude after treatment with placebo, particularly at higher sound pressure levels [**Supplementary Figure 3A**, repeated measures 2-way ANOVA, $F(1, 123) = 5.72$, $p = 0.02$, $n = 20/10$ ears/mice]. After PDE9i treatment, *high compensators* showed no significant change in wave IV amplitude relative to the baseline [**Supplementary Figure 3B**, repeated measures 2-way ANOVA, $F(1, 127) = 2.49$, $p = 0.12$, $n = 22/11$ ears/mice], suggesting that PDE9i treatment continues to preserve auditory responses. In contrast to the change in auditory nerve responses to injection stress in *high compensators*, *low compensators* showed no differences in ABR wave I amplitude after placebo [**Figure 4C**, the dark blue line, repeated measures 2-way ANOVA, $F(1, 44) = 2.04$, $p = 0.16$, $n = 8/4$ ears/mice]; however, after PDE9i treatment, a significant reduction in ABR wave I amplitude was observed [**Figure 4D**, dark orange line, repeated measures, 2-way ANOVA, $F(1, 78) = 4.90$, $p = 0.03$, $n = 12/6$ ears/mice]. ABR wave IV amplitudes were not affected by either PDE9i or placebo treatment in *low compensators* [**Supplementary Figure 3C**, repeated measures 2-way ANOVA, $F(1, 47) = 0.06$, $p = 0.82$, $n = 8/4$ ears/mice; **Supplementary Figure 3D**, repeated

measures 2-way ANOVA, $F(1, 77) = 2.27$, $p = 0.14$, $n = 12/6$ ears/mice].

As a possible rationale for the observed differences in auditory processing between *low* and *high compensators* in response to injection-induced stress, we considered differences in the number of IHC ribbons. To estimate the level of deafferentation, we quantified the number of CtBP2/RIBEYE-immunopositive dots as indicators for ribbon synapses, opposing neurofilament-200 positive auditory fibers of middle-aged, untreated, placebo-, or PDE9i-treated animals.

We observed no differences in number of CtBP2/RIBEYE-immunopositive dots between the groups in the apical turn [**Figure 4E**, two-tailed Student's t-test: $t(10) = 0.16$, $p = 0.88$, low no treatment: $n = 6$, high no treatment: $n = 6$ mice; 1-way ANOVA, $F(2, 18) = 0.01$, $p = 0.99$, low no treatment: $n = 6$, low placebo: $n = 6$, low PDE9i: $n = 9$; 1-way ANOVA, $F(2, 21) = 1.80$, $p = 0.19$, high no treatment: $n = 6$, high placebo: $n = 10$, high PDE9i: $n = 8$ mice]. The number of CtBP2/RIBEYE-immunopositive dots in the medial turn of the cochlea, representing regions coding lower-frequency sounds, was not different between untreated *low* and *high compensators* [**Figure 4F**, two-tailed Student's t-test: $t(10) = 0.73$, $p = 0.48$, low no treatment: $n = 6$, high no treatment: $n = 6$ mice], nor were any significant differences observed in *low compensators* after either treatment [**Figure 4F**, 1-way ANOVA, $F(2, 18) = 1.19$, $p = 0.33$, low no treatment: $n = 6$, low placebo: $n = 6$, low PDE9i: $n = 9$]; however, *high compensators* treated with placebo had significantly lower IHC ribbon numbers in comparison to *high compensators* treated with PDE9i [**Figure 4F**, 1-way ANOVA, $F(2, 21) = 3.54$, $p = 0.048$, Sidak's multiple comparisons test, high no treatment: $n = 6$, high placebo: $n = 10$, high PDE9i: $n = 8$ mice]. In the midbasal cochlear turn, which codes higher frequencies, untreated *low* and *high compensators* did not differ in IHC ribbon number [**Figure 4G**, two-tailed Student's t-test: $t(10) = 0.89$, $p = 0.40$, low no treatment: $n = 6$, high no treatment: $n = 6$ mice]. In addition, despite a trending group effect, no significant differences were observed in *low compensators* after treatment with either placebo or PDE9i [**Figure 4G**, 1-way ANOVA, $F(2, 18) = 3.15$, $p = 0.07$, low no treatment: $n = 6$, low placebo: $n = 6$, low PDE9i: $n = 9$]; however, *high compensators* treated with placebo had significantly lower IHC ribbon numbers in comparison to those treated with PDE9i [**Figure 4F**, 1-way ANOVA, $F(2, 21) = 5.78$, $p = 0.01$, Sidak's multiple comparisons test, high no treatment: $n = 6$, high placebo: $n = 10$, high PDE9i: $n = 8$ mice], reflecting ABR wave I amplitude results.

A similar differential effect in response to placebo or PDE9i treatment between *high* and *low compensators* was observed when we measured the ASSR growth function in response to increasing sound pressure levels. In *high compensators*, a significant decrease of SNR of the ASSR growth function was observed after placebo treatment [**Figure 5A**, light blue line, repeated measures 2-way ANOVA, $F(1, 122) = 44.30$, $p < 0.0001$, Sidak's multiple comparisons test, $n = 10$ mice], a feature that could be prevented by PDE9i treatment [**Figure 5B**, light orange line, repeated measures 2-way ANOVA, $F(1, 106) = 1.52$, $p = 0.22$, $n = 10$ mice]. In contrast, in *low compensators*, the temporal resolution was not affected by either placebo [**Figure 5C**, the dark-blue line, repeated measures, 2-way ANOVA, $F(1, 56) = 1.05$, $p = 0.31$, $n = 6$ mice] or PDE9i treatment [**Figure 5D**, dark orange line, repeated measures 2-way ANOVA, $F(1, 86) = 0.01$, $p = 0.94$, $n = 8$ mice].

This indicates that, in *high compensators*, a glucocorticoid (GC)-sensitive and cyclic guanosine-monophosphate (cGMP)-sensitive component is maintained, and that this component contributes to synchronous auditory nerve responses and temporal coding and could possibly be impaired in *low compensators*.

In conclusion, these results suggest that the stressful placebo injection disrupts discharge rates and/or synchronous auditory nerve responses, as well as temporal coding in *high compensators*, a feature that can be counteracted by PDE9i treatment. *Low compensators*, in contrast, have lost their capacity to respond to stressful events and, therefore, do not profit from treatment with PDE9i.

High Compensators, but Not *Low Compensators*, Exhibit a "Stress-Induced" Drop in Hippocampal LTP That Can Be Preserved by PDE9i Treatment

Stress and noise exposure have been shown to impact cognitive functions, including LTP (Singer et al., 2013; Jafari et al., 2018; Matt et al., 2018; Zhang et al., 2022), motivating us to compare LTP between treated and untreated *high* and *low compensators*. LTP recordings were conducted on acute coronal brain slices of mice without any treatment or after completion of treatment with a placebo or PDE9i (**Figure 6A**, averaged time course). LTP was induced by tetanic stimulation (1 s, 100 Hz) to the CA3 Schaffer's collateral axons, and fEPSPs were recorded from the dendrites of CA1 pyramidal cells that form synaptic contacts with CA3 Schaffer's collateral axons (Matt et al., 2018). The mean of the last 10 min of the 60 min recording was averaged and compared [**Figure 6B**, 1-way ANOVA, $F(6, 49) = 11.17$, $p < 0.0001$]. The post high-frequency stimulation (HFS) fEPSPs of the untreated mice were significantly higher in *high compensators* (**Figures 6B,C**, white, 174.69% ± 9.96%; n = 4/9 animals/slices) in comparison to *low compensators* [**Figure 6B**, gray, 128.35% ± 7.46%, $n = 2/5$ animals/slices; **Figure 6C**, two-tailed Student's t-test: $t(12) = 3.17$, $p = 0.008$], reminiscent of the higher corticosterone levels in *high compensators* in comparison to *low compensators* (**Figure 3**).

Low compensators treated either with placebo (**Figures 6B,C**, dark blue, 142% ± 9%, $n = 2/7$ animals/slices) or PDE9i (**Figures 6B,C**, dark orange, 141% ± 6.2%, $n = 3/9$ animals/slices) showed no significant change in LTP in comparison to the untreated group [**Figures 6B,C**, gray, 1-way ANOVA, $F(2, 18) = 0.81$, $p = 0.46$]. In contrast, in the *high compensators*, placebo treatment caused a significant reduction in the LTP level compared to the untreated mice [**Figure 6B**, light blue, 128.3% ± 5.5%, $n = 3/9$ animals/slices; **Figure 6C**,

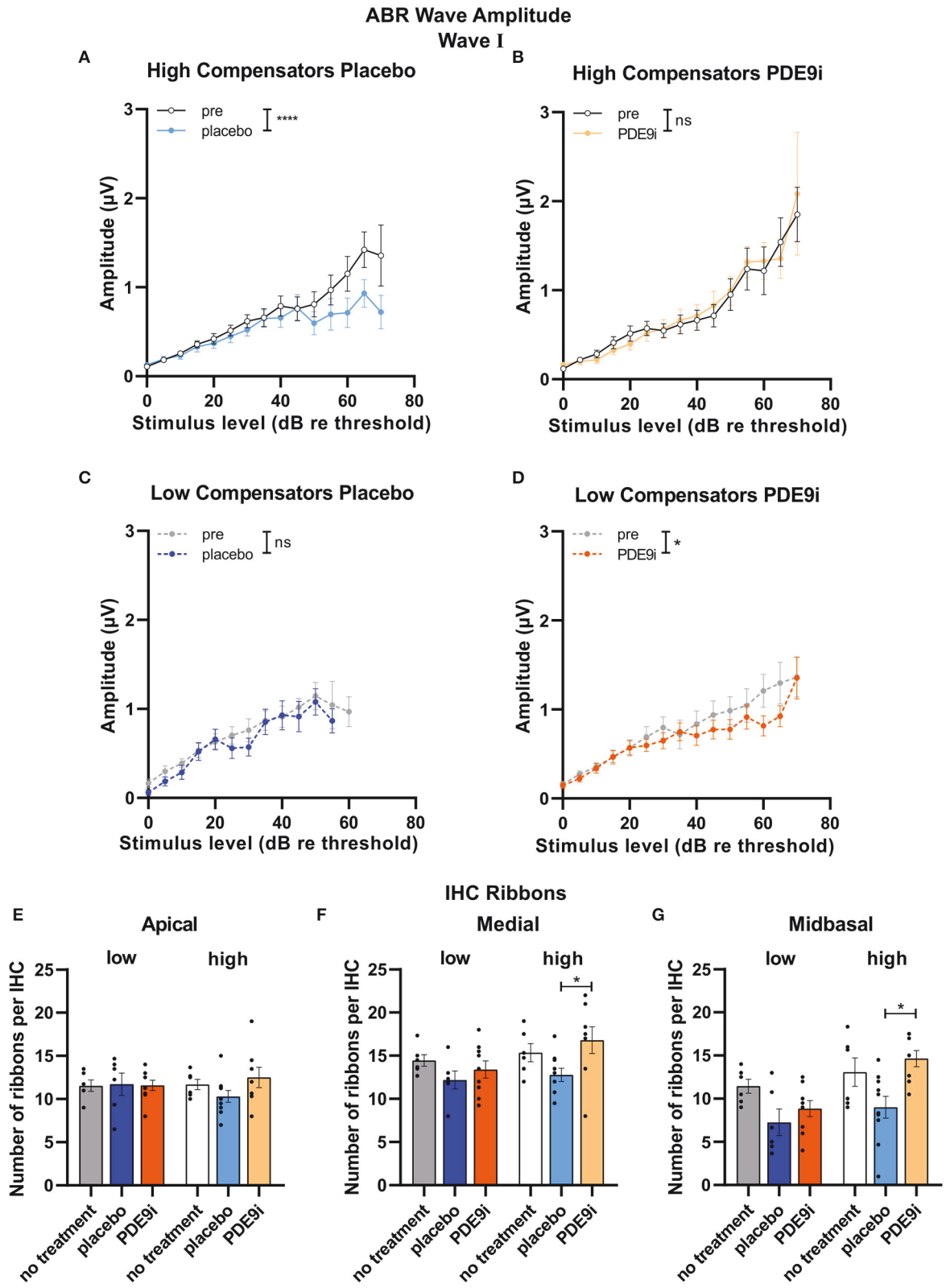

FIGURE 4 | ABR wave I and IHC ribbon numbers in high and low compensators before and after treatment with placebo or PDE9i. **(A)** High compensators showed a significant decrease in ABR wave I amplitude after treatment with placebo. **(B)** However, in high compensators treated with PDE9i, this decrease was not present. Low compensators showed no change in ABR wave I amplitude after treatment with **(C)** placebo **(D)** and a significantly decreased ABR wave I amplitude after

(Continued)

FIGURE 4 | treatment with PDE9i. **(E)** IHC ribbon number in the apical cochlear turn, representing lower-frequency areas, shows no changes between the groups. **(F)** IHC ribbon number in the medial cochlear turn, representing higher-frequency areas, significantly less IHC ribbons were observed in high compensators treated with placebo in comparison to those treated with PDE9i. **(G)** In the midbasal cochlear turn, representing high-frequency areas, a significantly lower IHC ribbon number was found in high compensators treated with placebo in comparison to those treated with PDE9i. Mean ± SEM. ns $p > 0.1$, *$p < 0.05$, ****$p < 0.0001$. For **(A–D)**, results of repeated measures 2-way ANOVA and for **(E–G)** results of the Sidak's multiple comparison test are depicted.

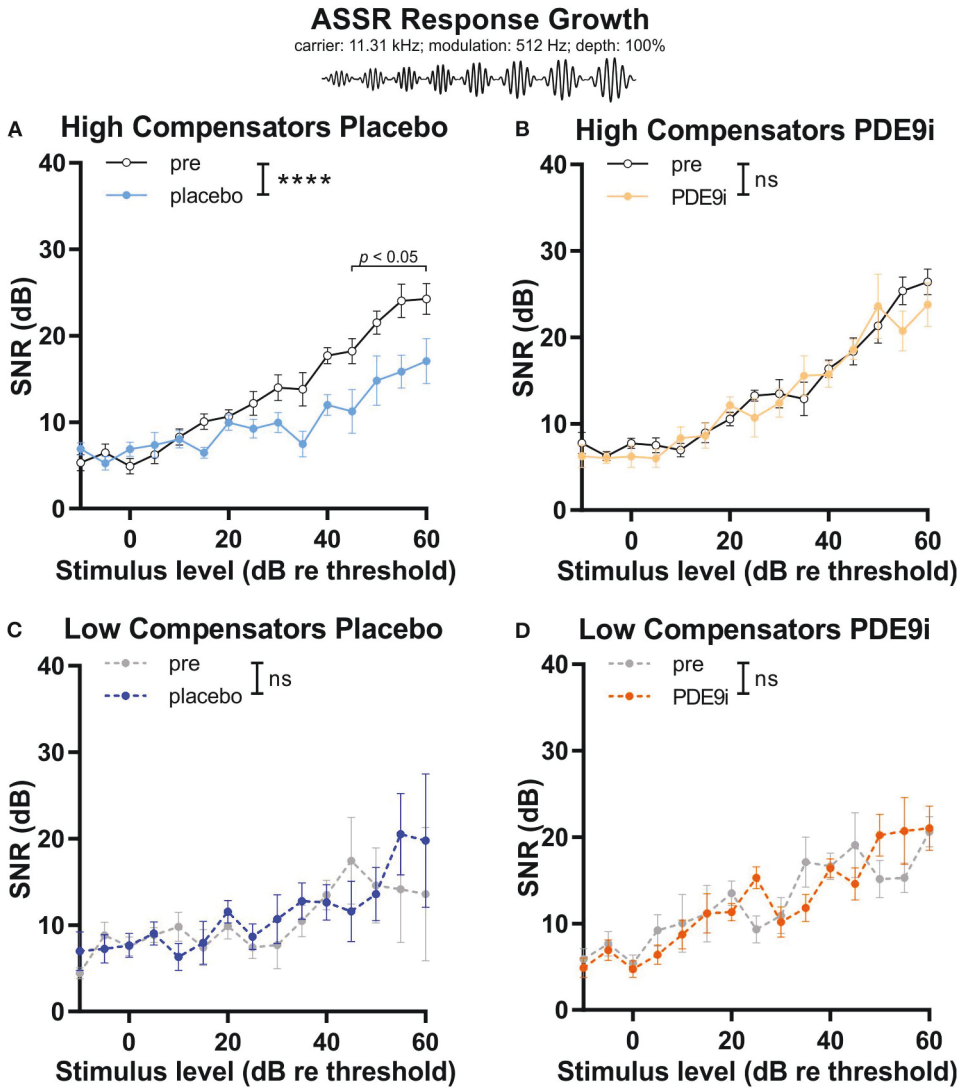

FIGURE 5 | Input–output relationship of auditory steady state responses (carrier frequency: 11.32 kHz; modulation frequency: 512 Hz; modulation depth: 100%) in high and low compensators treated with either placebo or PDE9i. **(A)** High compensators also showed a significant decrease of temporal auditory resolution after treatment with placebo. **(B)** However, in high compensators treated with PDE9i, this decrease was not present. Low compensators showed no change in temporal auditory resolution after treatment with either **(C)** placebo or **(D)** PDE9i. Mean ± SEM. ns $p > 0.1$, ****$p < 0.0001$, repeated measures 2-way ANOVA.

1-way ANOVA, $F(2, 23) = 8.24$, $p = 0.002$, with a two-stage linear step-up procedure of Benjamini, Krieger, and Yekutieli]. Treatment with PDE9i (**Figures 6B,C**, light orange, 153% ± 8.6%, $n = 2/8$ animals/slices) prevented the reduction in LTP caused by the placebo injection, shifting it to a level significantly higher than in the placebo-treated group.

Importantly, basic synaptic transmission is not impaired in *high* or *low compensators* (**Supplementary Figure 4**). Representative traces of fEPSPs with increasing stimulus intensities from 25 μA to 150 μA in 25 μA steps are shown in **Supplementary Figure 4A**. After either placebo or PDE9i treatment in both *high* and *low compensators*, the fEPSP slope and fiber volley (FV) amplitude was increased [**Supplementary Figure 4B**, high compensators: 2-way ANOVA, $F(2, 144) = 10.97$, $p < 0.0001$, a two-stage linear step-up procedure of Benjamini, Krieger, and Yekutieli, high no

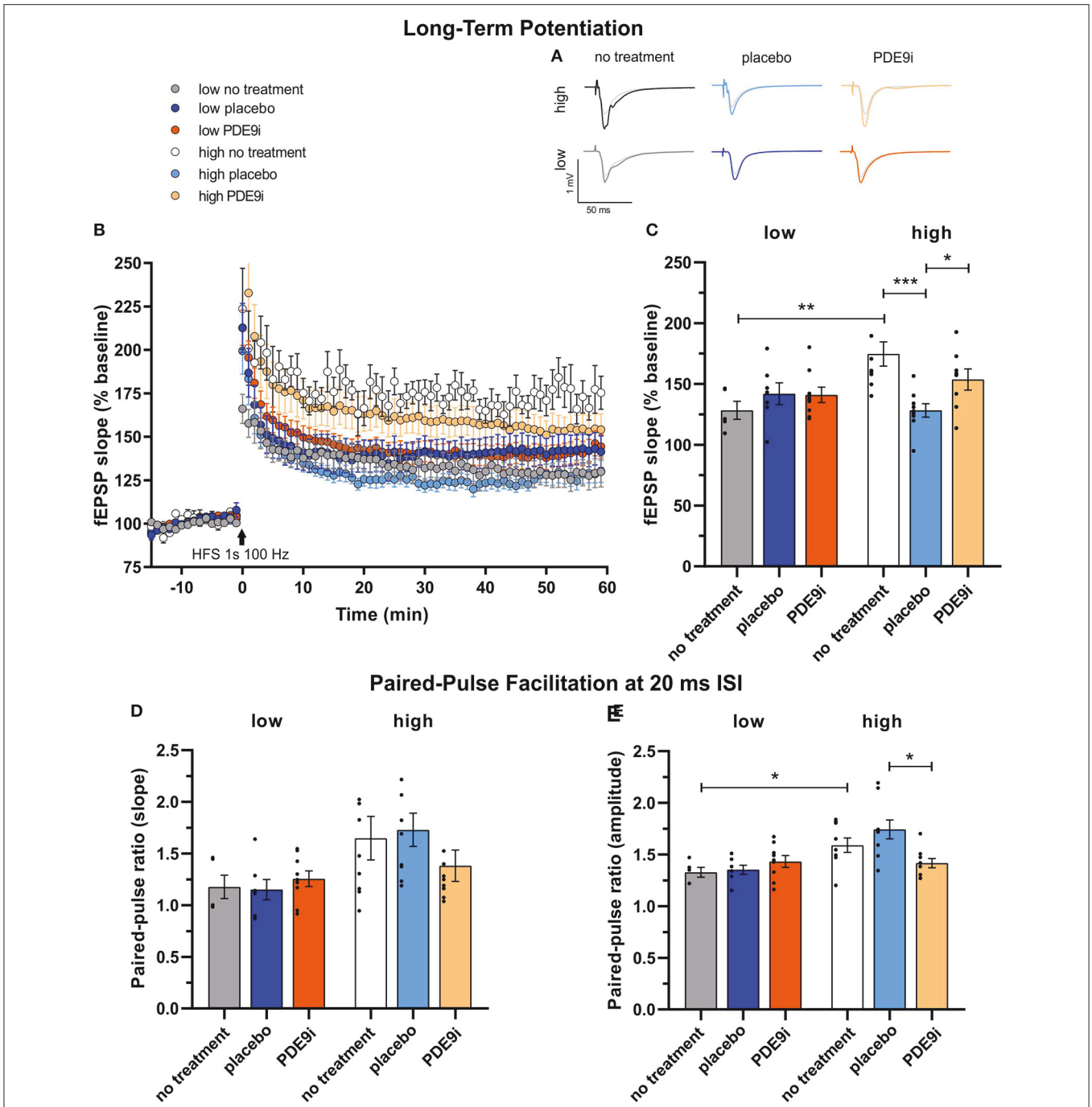

FIGURE 6 | Long-term potentiation (LTP) and paired-pulse facilitation (PPF) of low and high compensators that underwent no treatment, placebo treatment, or PDE9i treatment. **(A)** Representative traces before and after LTP induction and **(B)** averaged time courses of fEPSP slopes in acute coronal brain slices displayed prominent LTP in all animal groups. **(C)** The untreated low compensators had significantly lower LTP in comparison to untreated high compensators. In low compensators, neither a placebo treatment nor PDE9i treatment showed any effect on their already low LTP. In contrast, high compensators treated with a placebo displayed a significantly lower LTP both in comparison to their untreated controls and to high compensators treated with PDE9i. **(D)** The analysis of the paired-pulse ratio of the fEPSP2/fEPSP1 slope at the 20 ms ISI showed no significant differences between high and low compensators before treatment. Neither low compensators nor high compensators treated with either a placebo or PDE9i differed from their untreated controls. Also, no difference in the PPF slope ratio

(Continued)

treatment: $n = 4/9$, high placebo: $n = 3/9$, high PDE9i: $n = 2/8$ animals/slices, low compensators: 2-way ANOVA, $F(2, 108) = 17.72$ $p < 0.0001$, a two-stage linear step-up procedure of Benjamini, Krieger, and Yekutieli, low no

FIGURE 6 | (20 ms ISI) between the treatment conditions of low and high compensators was observed. **(E)** The analysis of the ratio of the paired-pulse ratio of the fEPSP2/fEPSP1 amplitude at the 20 ms interstimulus interval revealed a significantly higher PPF amplitude ratio in untreated high compensators in comparison to untreated low compensators. High compensators treated with placebo had a significantly higher PPF amplitude ratio (ISI 20 ms) in comparison to those treated with PDE9i, but neither placebo- nor PDE9i-treated high compensators significantly differed from their untreated controls. By contrast, low compensators showed no differences after treatment with either a placebo or PDE9i as compared to untreated controls or compared with each other. Mean ± SEM.*$p < 0.05$, **$p < 0.01$, ***$p < 0.001$. For the comparison of the untreated groups in **(C,E)**, results of the two-tailed t-test are depicted. For the comparison of the differentially treated high compensators in **(C,E)**, results of the Sidak's multiple comparison test are depicted.

treatment: $n = 2/5$, low placebo: $n = 2/7$, low PDE9i: $n = 3/9$ animals/slices; **Supplementary Figure 4C**, high compensators: 2-way ANOVA, $F(2, 144) = 59.17$, $p < 0.0001$, a two-stage linear step-up procedure of Benjamini, Krieger, and Yekutieli, high no treatment: $n = 4/9$, high placebo: $n = 3/9$, high PDE9i: $n = 2/8$ animals/slices, low compensators: 2-way ANOVA, $F(2, 108) = 7.71$, $p = 0.0007$, a two-stage linear step-up procedure of Benjamini, Krieger, and Yekutieli, low no treatment: $n = 2/5$, low placebo: $n = 2/7$, low PDE9i: $n = 3/9$ animals/slices]. The fEPSP slope and FV amplitudes were, however, increased at a level that was proportional to one another [**Supplementary Figure 4D**, high compensators: simple linear regression analysis, comparison between slopes of lines, $F(2, 155) = 0.45$, $p = 0.64$, high no treatment: $n = 4/9$, high placebo: $n = 3/9$, high PDE9i: $n = 2/8$ animals/slices, low compensators: simple linear regression analysis, comparison between slopes of lines, $F(2, 120) = 0.04$, $p = 0.96$, low no treatment: $n = 2/5$, low placebo: $n = 2/7$, low PDE9i: $n = 3/9$ animals/slices]. This suggests that the signal transmission was intact in all treatment conditions and compensation groups but operates with a lower ratio at a higher set point after treatment with a placebo or PDE9i. This suggests that the changes in LTP were not due to changes in basic synaptic transmission.

To investigate the effect of compensation group or treatment mechanism on the presynaptic state, we studied paired-pulse facilitation (PPF), a simple form of presynaptic short-term plasticity, which has been explained as a transient increase in the probability of vesicular glutamate release (Satake et al., 2012).

We had studied the time course of PPF in each brain slice before LTP induction in animals that underwent no treatment, placebo injection, or PDE9i treatment using varying interstimulus intervals (ISIs, 10–20–50–100–200–500 ms) and the same stimulation strength used for LTP recordings (**Figures 6D,E**, **Supplementary Figure 5**). Representative traces of fEPSPs with increasing ISIs at the stimulation strength equal to corresponding LTP recordings are shown in **Supplementary Figure 5A**. Specifically, *low compensators* had a significantly lower PPF amplitude ratio for the 20 ms ISI in comparison to *high compensators* [**Figure 6E**, gray vs. white, two-tailed Student's t-test: $t(12) = 2.58$, $p = 0.02$, low no treatment: $n = 2/5$, high no treatment: $n = 4/9$ animals/slices]. In *high compensators*, the PPF amplitude ratio for ISIs up to 20 ms could be even more enhanced by placebo treatment, resulting in a significant increase in comparison to their untreated controls [**Supplementary Figure 5B**, light blue vs. white, 2-way ANOVA, $F(2, 144) = 9.07$, $p = 0.0002$, a two-stage linear step-up procedure of Benjamini, Krieger, and Yekutieli, high no treatment: $n = 4/9$, high placebo: $n = 3/9$, high PDE9i: $n = 2/8$ animals/slices; **Supplementary Figure 5C**, light blue vs. white, 2-way ANOVA, $F(2, 144) = 24.04$, $p < 0.0001$, a two-stage linear step-up procedure of Benjamini, Krieger, and Yekutieli, high no treatment: $n = 4/9$, high placebo: $n = 3/9$, high PDE9i: $n = 2/8$ animals/slices], while PDE9i significantly decreased the PPF amplitude and the slope ratio for ISIs up to 20 ms in comparison to untreated controls (**Supplementary Figures 5B,C**, light orange vs. white). Significant effects on the PPF slope [**Supplementary Figure 5D**, 2-way ANOVA, $F(2, 108) = 4.40$, $p = 0.02$] and the amplitude [**Supplementary Figure 5E**, 2-way ANOVA, $F(2, 108) = 6.09$, $p = 0.003$] ratio were also observed for *low compensators*. In contrast to *high compensators*, *low compensators* showed a significant increase in the PPF amplitude ratio only at the 10 ms ISI both after placebo [**Supplementary Figure 5E**, dark blue, 2-way ANOVA, $F(2, 108) = 6.09$, $p = 0.003$, a two-stage linear step-up procedure of Benjamini, Krieger, and Yekutieli, low no treatment: $n = 2/5$, low placebo: $n = 2/7$, low PDE9i: $n = 3/9$ animals/slices] and PDE9i treatment (**Supplementary Figure 5E**, dark orange) in comparison to their untreated controls (**Supplementary Figure 5E**, gray). Also, in *low compensators,* no difference between placebo and PDE9i treatment conditions was indicated (**Figures 6D,E**, **Supplementary Figure 5E**).

This suggests that a transient increase in the probability of vesicular glutamate release tends to be higher in *high compensators* than in *low compensators*. Only in *high compensators* this feature can be enhanced through injection-induced stress and subsequently lowered through PDE9i treatment. This may suggest that, in *high compensators,* but not *low compensators,* stress-induced facilitated presynaptic release (**Figures 6D,E**, light blue) contributes to the retention of LTP (**Figure 6C**, light blue).

In conclusion, this finding suggests that *low compensators* with a blunted stress response have lower hippocampal LTP and PPF than *high compensators.* As placebo treatment can reduce and PDE9i treatment can restore LTP in *high compensators*, a GC- and cGMP-signaling-dependent facilitation circuit exists in this animal group that is impaired in *low compensators*.

High Compensators, but Not *Low Compensators*, Exhibit a "Stress-Induced" Drop in Levels of Hippocampal BDNF and Inhibitory Markers That Can Be Preserved by PDE9i Treatment

We next investigated the influence of injection-induced stress or application of PDE9i on activity-dependent

changes in *Bdnf* exon-IV and -VI expression, tagged by bi-cistronic expression of CFP or YFP, respectively, monitored in the BLEV reporter mice (**Figure 7A**). We examined *Bdnf* exon-IV-CFP and exon-VI-YFP expression (**Figures 7B–G**, cyan and yellow) as well as parvalbumin (PV) protein staining (**Figures 7B–G**, red) in deconvoluted high-resolution fluorescence stacks in the hippocampus (a framed schematic view in **Figures 7A–G**) (Matt et al., 2018).

We found that *low compensators* had a lower expression level of *Bdnf* exon-IV-CFP and a lower *Bdnf* exon-VI-YFP in CA3 regions of the dorsal hippocampus in comparison to *high compensators*, not always reaching significance [**Figure 7H**, gray vs. white bar, Mann–Whitney U test, U(3.255, 4.197) = 5; $p = 0.07$, low: $n = 5/8$, high: $n = 2/4$ animals/hippocampal hemispheres; **Figure 7I**, gray vs. white bar, Mann–Whitney U test, U(2.749, 5.218) = 0; $p = 0.004$, low: $n = 5/8$, high: $n = 2/4$ animals/hippocampal hemispheres], but their PV expression used to identify changes in fast-spiking GABAergic interneurons (Hu et al., 2014) did not differ [**Figure 7J**, gray vs. white bar, Mann–Whitney U test, U(5.550, 7.208) = 13, $p = 0.68$, low: $n = 5/8$, high: $n = 2/4$ animals/hippocampal hemispheres]. In *low compensators*, treatment with neither placebo nor PDE9i significantly affected the expression of *Bdnf* exon-IV-CFP, *Bdnf* exon-VI-YFP, or PV [**Figure 7H**, gray vs. dark blue and dark orange bars, Kruskal–Wallis test, H (2) = 1.71, $p = 0.43$, low no treatment: $n = 5/8$, low placebo: $n = 5/8$, low PDE9i: $n = 4/7$ animals/hippocampal hemispheres; **Figure 7I**, gray vs. dark blue and dark orange bars, Kruskal–Wallis test, H (2) = 4.83, $p = 0.09$, low no treatment: $n = 5/8$, low placebo: $n = 5/8$, low PDE9i: $n = 4/8$ animals/hippocampal hemispheres; **Figure 7J**, gray vs. dark blue and dark orange bars, Kruskal–Wallis test, H (2) = 0.25, $p = 0.88$, low no treatment: $n = 5/8$, low placebo: $n = 4/8$, low PDE9i: $n = 4/8$ animals/hippocampal hemispheres]. However, in *high compensators*, PDE9i treatment was able to increase the expression of *Bdnf* exon-IV-CFP, *Bdnf* exon-VI-YFP, and PV, in comparison to the placebo treatment where it was slightly diminished [**Figure 7H**, light orange bars vs. light blue bars, Kruskal–Wallis test, H (2) = 9.42, $p = 0.009$, Dunn's multiple comparisons test, high no treatment: $n = 2/4$, high placebo: $n = 2/4$, high PDE9i: $n = 4/8$ animals/hippocampal hemispheres; **Figure 7I**, light orange bars vs. light blue bars, Kruskal–Wallis test, H (2) = 6.05, $p = 0.049$, Dunn's multiple comparisons test, high no treatment: $n = 2/4$, high placebo: $n = 2/4$, high PDE9i: $n = 4/8$ animals/hippocampal hemispheres; **Figure 7J**, light orange bars vs. light blue bars, Kruskal–Wallis test, H (2) = 8.82, $p = 0.01$, Dunn's multiple comparisons test, high no treatment: $n = 2/4$, high placebo: $n = 2/4$, high PDE9i: $n = 4/8$ animals/hippocampal hemispheres]. A significant difference between treatment and untreated controls was not observed (**Figure 7H**, light orange bars/light blue bars vs. white bars).

In conclusion, treatment with a PDE9i can preserve a stress-induced decrease in expression levels of *Bdnf* exon-IV-CFP, *Bdnf* exon-VI-YFP, and PV in hippocampal regions in *high compensators*, but not *low compensators*.

DISCUSSION

The findings of the present study indicate for the first time that central neural responses (neural gain) to age-related cochlear synaptopathy may differ, depending on individual stress responses. Acute high stress induction can reduce increased cochlear and central auditory responses, including hippocampal LTP following cochlear synaptopathy. This stress-induced decrease in central adaptation capacity can be restored by elevating cGMP levels with a PDE9i. However, in case of blunted stress responses, both central neural gain and PDE9i responsiveness fail. This suggests that central neuronal enhancement needed for regular adaptation processes to sensory deprivation depends on proper stress responses and cGMP signaling.

Auditory (Temporal) Processing Deficits in Middle-Aged Animals Differ Between *Low* and *High Compensators* Independent of Hearing Thresholds

In the present study, we confirmed a previously made observation that animals can respond to an age-dependent reduction in auditory nerve amplitude (cochlear synaptopathy) in two different ways: through either lower or higher compensations in the central ABR wave IV responses (Marchetta et al., 2020b). Although during aging, the animals showed a homogenous elevation in hearing threshold (**Figure 1**), the middle-aged animals could be subdivided into two groups based on a better (*high compensators*) or worse (*low compensators*) ability to centrally compensate for the peripheral damage. Between these newly defined groups generated for the present study, hearing thresholds did not differ in response to click, noise, or pure-tone 11 kHz stimuli (**Figures 2A–C**). However, threshold sensitivity in response to pure-tone stimuli over a frequency range of 2–32 kHz was significantly worse in *low compensators* in comparison to *high compensators* in the best frequency range (**Figure 2D**). In addition, temporal auditory resolution was also significantly lower (**Figure 2E**). While this finding confirmed previous observations (Marchetta et al., 2020b), here, we found that the weaker sound responsiveness and lower temporal precision of *low compensators* were related to a significantly lower baseline corticosterone level in comparison to *high compensators* (**Figure 3**). Furthermore, *low compensators* did not respond to injection-induced stress (**Figure 3**), while, in *high compensators,* peripheral and central auditory responsiveness and temporal acuity were reduced by injection-induced stress (**Figures 4**, **5**). Importantly, the differences in corticosterone levels in both groups induced by injection stress did not influence hearing thresholds (**Supplementary Figure 2**).

We hypothesize that this finding discloses two important new features of auditory processing: (i) There is a top-down influence of GCs on peripheral auditory processing, independent of any impact on the electromechanical properties of OHCs, and (ii) auditory processing can profoundly differ depending on the extra-hypothalamic stress control [i.e., modulation through the prefrontal cortex (PFC) or hippocampal regions

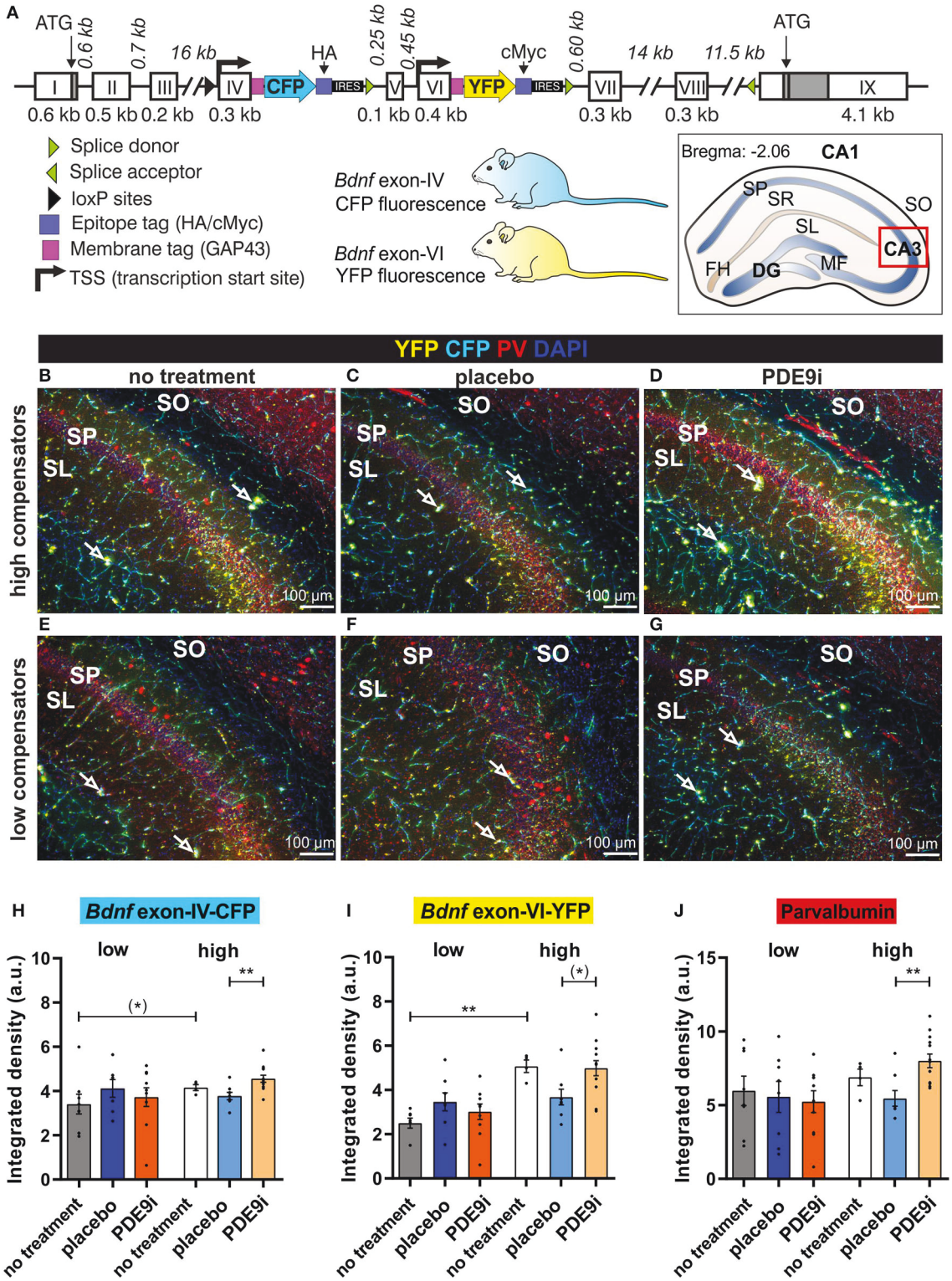

FIGURE 7 | *Bdnf* exon-IV, *Bdnf* exon-VI, and Parvalbumin (PV) expression in the CA3 region of the hippocampus of untreated low and high compensators and animals that received placebo or PDE9i. **(A)** Genetically modified the *Bdnf* gene of the BLEV reporter mouse line in which CFP is expressed with activity-dependent *Bdnf*exon-IV transcription and YFP with activity-dependent *Bdnf*exon-VI transcription. An abstract scheme of a coronal hippocampal section at bregma position

(Continued)

FIGURE 7 | −2.06 mm. The red box indicates the inset seen in **(B–G)** where the integrated density is measured. DG, dentate gyrus; FH, fissura hippocampalis; MF, mossy fiber; SL, stratum lucidum; SO, stratum oriens; SP, stratum pyramidale; SR, stratum radiatum. **(B)** Untreated high compensators showed a strong expression of *Bdnf* exon-IV (CFP), *Bdnf* exon-VI (YFP) (open arrows signify where they are expressed in neighboring structures) and PV (red) in the hippocampal CA3 region (blue = DAPI). **(C)** After placebo treatment, less expression of CFP, YFP, and PV was observed. **(D)** When treated with PDE9i, high compensators showed an increase in CFP, YFP, and PV expression. **(E–G)** CFP, YFP, and PV expression in the hippocampal CA3 region of low compensators, which was slightly weaker than in high compensators, reaching significance for YFP expression in untreated animals, shown in **(I)**. In low compensators, neither placebo nor PDE9i treatment had an effect on CFP, YFP, and PV expression. **(H)** In the SL/SP region of CA3, untreated low compensators showed a lower CFP expression in comparison to untreated high compensators not reaching statistical significance (*). Low compensators treated with placebo or PDE9i did not show any differences in CFP expression to their untreated controls or to each other. By contrast, high compensators treated with PDE9i had significantly higher CFP expression in comparison to those treated with placebo. **(I)** YFP expression in the SL/SP region of CA3 was significantly lower in untreated low compensators in comparison to untreated high compensators. Low compensators showed no difference in YFP expression between treatment groups. However, high compensators treated with PDE9i showed a higher YFP expression in comparison to those treated with placebo not reaching statistical significance. **(J)** PV expression in the SL/SP region of CA3 did not differ between untreated high and low compensators. Low compensators showed no difference in PV expression between treatment groups. High compensators treated with PDE9i showed a significantly higher PV expression compared to those treated with placebo. Mean ± SEM. (*)$p \leq 0.1$, **$p < 0.01$. For the comparison of the untreated groups in **(H–J)**, results of two-tailed t-test are depicted. For the comparison of the differentially treated high compensators in **(H–J)**, results of the Dunn's multiple comparison test are depicted.

(de Kloet et al., 2005, 2019)] of the individual specimen. Central auditory responses can either fall into a group of *low compensators* with characteristics of a so-called blunted or low stress reactivity, possibly being in a state of chronic stress (Turner et al., 2020), or a group of *high compensators* that can maintain stable neuronal activity in central auditory circuits despite auditory deprivation but which risk losing it under acute high-stress conditions.

(i) In line with the present study, a top-down influence of differences in stress responses, independent of hearing thresholds and thus electro mechanical properties of OHCs, has previously been shown. Thus, maintained high levels of endogenous corticosterone or glucocorticoid receptor (GR) antagonists in acoustic trauma did not influence hearing thresholds or the distortion product of otoacoustic emissions in rats (Singer et al., 2018a). Furthermore, posttraumatic or chronic stress has not yet been shown to directly influence hearing thresholds in humans or animals (Kreuzer et al., 2014; Mazurek et al., 2019; Turner et al., 2019; MacGregor et al., 2020), indicating that stressors may influence neuronal rather than mechanical properties of hair cells. When asking how stress could possibly influence neuronal cochlear processes, one should remember that stressors act through GR and mineralocorticoid receptors (MR) in the limbic system, including the PFC and hippocampus, and are suggested to mediate the top-down and bottom-up control of stress, coping with environmental challenges through hypothalamic and extra-hypothalamic pathways (de Kloet et al., 2000, 2019). In a study that performed tamoxifen-induced single or double deletion of MR and GR in the central nervous system of mice, an influence on cochlear sensitivity, as measured by ABR wave I, IHC ribbon number, a compound action-potential threshold, and neural temporal sound processing (ASSR) was shown to occur independently of changes in the mechanics of cochlear OHCs, as measured *via* the distortion-product otoacoustic emissions (Marchetta et al., 2022). This indicates that central stress receptor activation may directly affect cochlear processes.

(ii) Considering that stress receptor activation could modify the neural properties of cochlear auditory processing, higher endogenous corticosterone levels were shown to lower the summed response amplitudes of the auditory nerve and were linked to fewer IHC ribbons in the midbasal cochlear turn of rats (Singer et al., 2018a). Furthermore, an acoustic trauma-induced attenuation of ABR wave I amplitude and diminution of its dynamic range could be counteracted and partially restored by the GR antagonist mifepristone (Singer et al., 2018a). Moreover, differences in auditory nerve processing could be observed, following a deletion of either MR or GR in frontal brain regions (Marchetta et al., 2022). In that study, we deleted MR and GR through a tamoxifen-induced, calmodulin-dependent protein kinase II alpha promoter activation, what restricts the MR/GR deletion to central and frontal brain regions, while leaving MR and GR expression in the cochlea intact (Marchetta et al., 2022). As a consequence, the deletion of MR in the frontal brain regions of the adult mice led to impaired peripheral auditory processing shown by a reduced number of IHC ribbons and ABR wave I amplitudes. This might point to a positive retro-cochlear feedback that is dependent on central MR activation (Marchetta et al., 2022) to preserve auditory processing. As *low compensators* show an overall phenotype of poorer auditory processing and have a low baseline corticosterone level, we may hypothesize that they have an inappropriate MR activation. Additionally, *low compensators* might also have an impaired GR response, in contrast to *high compensators* (**Figure 3**), because also prolonged stress exposure–in this study, 10 days of repeated injections–did not lead to increased corticosterone levels.

While MRs show a high affinity for endogenous GC, which makes them responsive during acute stress events (de Kloet et al., 2005; Joels and de Kloet, 2017; Wirz et al., 2017; Plieger et al., 2018), GRs are typically activated in response to the highest GC level, since GRs, although more widely and extensively expressed, have only one tenth of the affinity for GCs in comparison to MR (de Kloet et al., 1999, 2005; Sapolsky, 2015). *Low compensators* exhibit diminished responsiveness to GCs and thereby the neurons in the auditory pathway would consequently be prevented from adequately responding to even low levels of GCs, which lead to the positive effects of MR

(Marchetta et al., 2022). In humans and rodents with a likewise GC resistance or low and "blunted" stress response, endogenous GCs fail to induce proper responses to stress and circadian cues, which regulate life-sustaining processes, such as metabolism under stressful conditions (Lewis-Tuffin and Cidlowski, 2006; Silverman and Sternberg, 2008; Vitellius et al., 2018; Spies et al., 2021). In future studies, it may thus be interesting if more generalized defects, aside from lower auditory and cognitive performance, may be seen in *low compensators*. In contrast, *high compensators*, which respond to placebo-induced injection stress with a large increase in corticosterone levels (**Figure 3**), show a reduction in ABR wave IV amplitude and decrease in the ASSR after stress, as suggested after activation of central GR (Marchetta et al., 2022).

Future studies should, therefore, discuss central adaptation differences after cochlear synaptopathy in the context of different GR/MR-mediated feedback loops on cochlear processes, which may generally fail upon blunted stress levels.

Short- and Long-Term Potentiation, *Bdnf* Transcript Recruitment, and PDE9i Sensitivity Differ Between *Low* and *High Compensators*

In the present study, *low* and *high compensators* differ in hippocampal LTP responses, as previously described (Marchetta et al., 2020b); here, we have linked this to differences in stress and cGMP signaling.

We suggest a strong relationship between hippocampal processes (i.e., LTP and *Bdnf* transcript levels) and auditory nerve responses, as they respond in the same way to stress and PDE9i-treatment. The *low compensators* are not only insensitive to a stress-induced deterioration of IHC ribbon numbers, ABR wave I amplitude, and ASSR but also to a stress-induced drop in hippocampal LTP (**Figures 6B,C**), to a recruitment of activity-dependent *Bdnf* transcripts (**Figure 7**), as well as to a stress-induced enhancement of the paired-pulse ratio (**Figures 6D,E**). Importantly, *low compensators* are also insensitive to the counteraction of all these effects by PDE9i.

In contrast to *low compensators*, *high compensators* respond to injection-induced stress not only through a drop of hippocampal LTP and *Bdnf* transcripts (**Figure 7**) but also with an enhanced PPF (**Figures 6D,E**), a simple form of pre-synaptically coded short-term plasticity (Neher and Sakaba, 2008). This suggests that, in *high compensators,* injection-induced stress may trigger a transient increase in the probability of vesicular release in Schaffer's collaterals, as previous studies have suggested that PPF results from a prior accumulation of residual Ca^{2+} at the synaptic terminal and a lingering effect of Ca^{2+} on the exocytotic Ca^{2+} sensor of releasable vesicles during the second stimulus [as reviewed in (Thomson, 2000; Zucker and Regehr, 2002)]. The stress-induced enhancement of PPF amplitude and the PPF slope ratio, observed here within the first stimulus intervals (< 100 ms) in *high compensators* (**Supplementary Figures 4B,C**), along with the reduced LTP response seen under the same stress conditions, points to a facilitation of vesicle release and a possible subsequent long-term depletion of releasable vesicles during trains of high-frequency presynaptic stimulation. A stress-induced facilitation of vesicle release may result from stress influences on the mediodorsal thalamus (MD), which, along with the medial PFC, have been shown to interact with the hippocampal formation through topographically complex connectivity patterns (Bueno-Junior and Leite, 2018). Indeed, the inactivation of the MD through tetrodotoxin (Sloan et al., 2011) or chronic unpredictable stress (Jett et al., 2017) has been shown to significantly weaken MD/medial PFC recruitment (Jett et al., 2017), leading to LTP retention, as seen in the present study following injection-induced stress in *high compensators* (**Figure 6**). Importantly, in the present study, the corticosterone level in *high compensators* is increased independently of the treatment condition received (i.e., placebo or PDE9i, **Figure 3**). This indicates that the protective effects of the PDE9i in *high compensators* against the stress-induced diminishment of IHC ribbons, ABR wave I amplitude, ASSR, LTP, BDNF expression, and PPF may not be driven by hypothalamic-pituitary-adrenal (HPA) axis-induced changes in GC levels but, instead, downstream of it.

Consistent with the contrasting influences of stress on central auditory processes presented here in *high* and *low compensators*, acute stress or low corticosterone levels have been shown to exert positive influences on hearing (Meltser and Canlon, 2011; Canlon et al., 2013), while high corticosterone (i.e., posttraumatic or chronic stress) was shown to diminish auditory gating in animal and human studies (Stevens et al., 2001; White et al., 2005; Maxwell et al., 2006; Elling et al., 2011; Kreuzer et al., 2014; Ma et al., 2017; Mazurek et al., 2019; Turner et al., 2019; MacGregor et al., 2020). Moreover, MR activation was shown to exhibit a crucial role in proper neural responses of learning, memory, and selective attention to novel situations (de Kloet et al., 2005; Joels and de Kloet, 2017; Wirz et al., 2017; Plieger et al., 2018), while GR plays an important role in memory consolidation and long-term adaptation to stressful situations (de Kloet et al., 2005). This means that both stress receptors may play a central role in the learning-dependent adaptation processes after cochlear synaptopathy. The connection may lie in a differential influence of stress receptors on the recruitment of activity-dependent *Bdnf* transcripts necessary for adaptation, whose mobilization in *low* and *high compensators* is differentially affected by stress. BDNF has been suggested to bridge GC effects and brain networks by driving the phosphorylation of GRs (Jeanneteau et al., 2018). Impaired GR phosphorylation following a reduced activity-dependent BDNF recruitment has, moreover, been shown to lead to impaired long-term memory acquisition and deficits in forming postsynaptic dendritic spines after, for example, motor-skill training (Arango-Lievano et al., 2019). After stress-inducing acoustic trauma, reduced central compensation was also linked to reduced LTP and reduced levels of activity-dependent BDNF in hippocampal nerve endings and capillaries (Matt et al., 2018), seen here in untreated *low compensators* and *high compensators* treated with placebo (**Figures 6**, **7**). A critical reduction of auditory input was suggested to hamper sufficient recruitment of activity-dependent BDNF to stimulate contrast amplification and distress levels (Matt et al., 2018; Knipper et al., 2020). Important in this context is that we, in

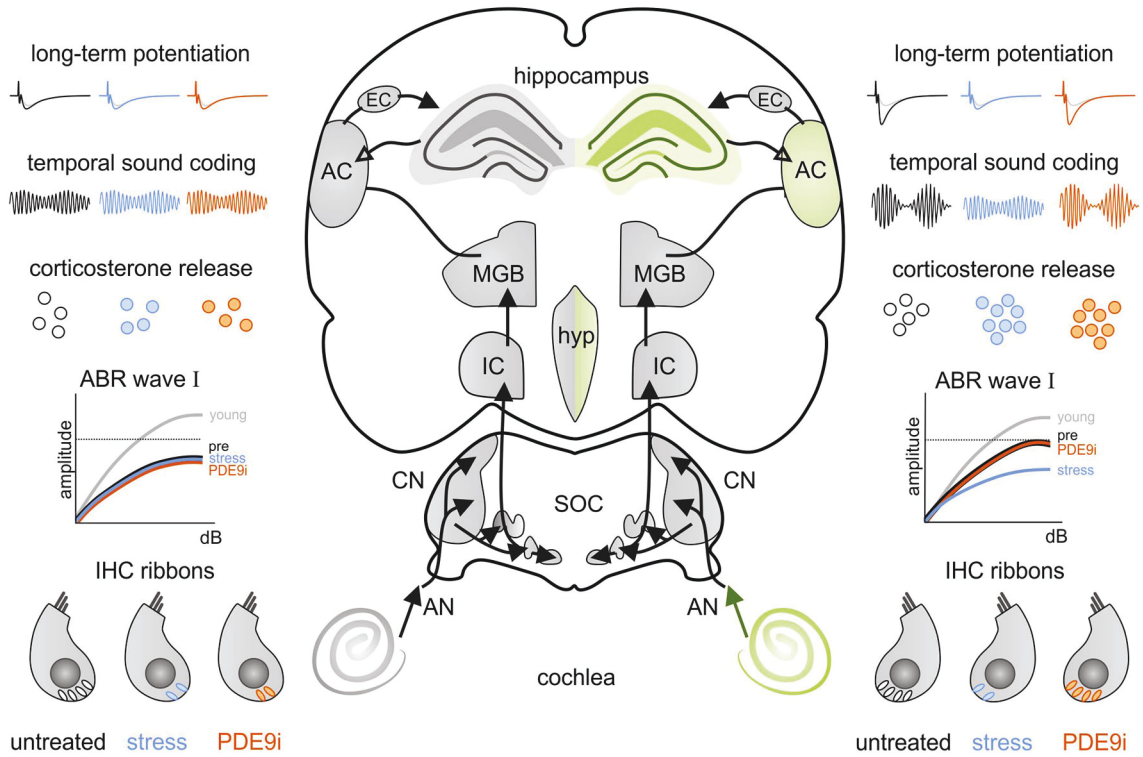

FIGURE 8 | An abstract scheme of the mechanisms in the auditory pathway that are differentially affected by stress or PDE9i application in low compensators (the left side) and high compensators (the right side). Low compensators have a lower baseline corticosterone level (black, left) in comparison to high compensators (black, right). When stress due to repeated injections is applied (blue/orange), high compensators respond in a physiological way, with increased corticosterone release. Low compensators, on the other hand, do not have increased corticosterone levels after application of a stressor, showing characteristics of a blunted stress response. This blunted stress response prevents low compensators from reacting to both a stress-induced drop of long-term potentiation, temporal sound coding, auditory nerve response (ABR wave I), and inner hair cell ribbons, which we see in high compensators. Additionally, where treatment with a PDE9i is able to preserve all of these parameters in high compensators, the blunted stress response of low compensators prevents their restoration. ABR, auditory brainstem response; AC, auditory cortex; AN, auditory nerve; CN, cochlear nucleus; dB, decibels; EC, entorhinal cortex; hyp, hypothalamus; IC, inferior colliculus; IHC, inner hair cell; MGB, medial geniculate body; SOC, superior olivary complex.

line with previous studies analyzing *low compensators* vs. *high compensators* (Marchetta et al., 2020b), observed significantly lower activity-dependent BDNF levels in hippocampal regions in *low compensators* as compared to *high compensators*, which may mirror the low levels observed in *high compensators* after placebo-induced stress (**Figure 7**). This challenges the hypothesis that differences in auditory driving forces between *high* and *low compensators* may contribute to differences in hippocampal LTP through altered recruitment of BDNF-driven GR activation. Differences in activity-driven GR phosphorylation, in analogy to previous observations (Arango-Lievano et al., 2019), may be considered in future studies to be responsible for the observed different adaptive responses between *high* and *low compensators*.

Numerous studies support the notion that stress can impair central processing and task-induced response patterns through impaired neurovascular coupling (Sohal et al., 2009; Lee et al., 2015; Chen et al., 2017; Han et al., 2019). The BLEV reporter mouse, which allows for visualization and identification of activity-dependent *Bdnf* exon-IV and -VI derived expression, is an ideal tool to study molecular correlates of plasticity changes in the hippocampus (Matt et al., 2018). As *Bdnf* exon-IV-CFP is expressed in blood vessels and *Bdnf* exon-VI-YFP is expressed in synaptic nerve terminals, differences in *Bdnf* exon-IV and -VI expression observed between *high* and *low compensators* (**Figures 7H,I**) may reflect differences in hemodynamic hippocampal responses, as has previously been suggested (Marchetta et al., 2020b; Knipper et al., 2022). Considering that specific neuronal activity may tightly regulate blood flow (Hillman, 2014), it was hypothesized that a critically reduced driving force of auditory nerve fibers could lead to less recruitment of activity-driven *Bdnf* exon-VI-YFP transcripts in nerve endings and of *Bdnf* exon-IV-CFP expression in capillaries in *low compensators* in comparison to *high compensators* (Singer et al., 2018b; Marchetta et al., 2020b), which might reveal a chronically lower level of neurovascular coupling in *low compensators* and an acutely depressed level of neurovascular coupling due to stress in *high compensators*.

A loss of fast auditory processing, as seen in *high compensators* after treatment with placebo (**Figure 5A**), is here

also linked to reduced levels of PV-positive interneuron (PV-IN) staining in the hippocampus (**Figure 7J**). Recently, stress has been shown to cause impaired neurovascular coupling and attenuation of cerebral blood flow through a reduction in PV-IN GABAergic signaling, possibly through altered nitric oxide-induced vasodilation (Czeh et al., 2015, 2018; Csabai et al., 2018; Han et al., 2019; Knipper et al., 2022). The differences between *high* and *low compensators* in *Bdnf* exon-IV-CFP expression in capillary vessels within the highly vascularized fissura region in conjunction with the altered PV-IN levels (**Figure 7**) may thus further point to differences in hemodynamic hippocampal responses.

The present study finally demonstrated that PDE9i treatment could ameliorate deficits in peripheral and central auditory processing in *high compensators* but not *low compensators*. Phosphodiesterase 9A (PDE9A) is a phosphodiesterase with high affinity for cGMP that is not only expressed in the brain (Lakics et al., 2010; Kelly, 2012) but also in the adult cochlea (Marchetta et al., 2020a). Preclinical studies have shown that a PDE9i can increase cGMP levels in the rat brain, enhance LTP, and improve memory function in rodent cognition tasks (van der Staay et al., 2008; Hutson et al., 2011; Kleiman et al., 2012; Kroker et al., 2012, 2014). This has also been shown for the PDE9i BAY 73-6691 used in the present study. BAY 73-6691 enhanced LTP in rat hippocampal slices (van der Staay et al., 2008) and stimulated protein synthesis-dependent late LTP in mouse hippocampal slices (Kroker et al., 2012). Furthermore, a PDE9i has been found to ameliorate auditory gating deficits in neurodegenerative diseases, such as Huntington's disease (Nagy et al., 2015). The present study provides new evidence that this PDE9i can ameliorate deficits in peripheral and central auditory processing, as well as in cognition under discrete conditions of preserved GC responsiveness in *high compensators*, but not when stress responses are blunted, as shown for *low compensators*. The results of previous studies suggesting that PDE9A inhibition can improve neurodegenerative diseases (e.g., Nagy et al., 2015; Sanders and Rajagopal, 2020; Sharma et al., 2020) may need to be reconsidered with the knowledge of this new finding.

In conclusion, central compensation following age-dependent cochlear synaptopathy can either be impaired upon a reduced stress response, as evident here in *low compensators* (**Figure 8**, left side), or it can be maintained in *high compensators,* who risk losing it under acute severe stress conditions (**Figure 8**, right side). In *low compensators*, stress induced by successive placebo injections cannot significantly reduce IHC ribbon numbers, ABR wave I amplitudes, ASSR, or LTP, or enhance PPF (**Figure 8**, left side). Under this condition of blunted stress response in *low compensators*, an elevation of cGMP levels by PDE9i cannot occur. In line with neural gain being stress and cGMP dependent in *high compensators*, features lost by stress can be restored through treatment with PDE9i.

Given the growing evidence of a link between hearing loss and dementia (Livingston et al., 2017; Griffiths et al., 2020; Montero-Odasso et al., 2020; Zhang et al., 2022), we sought to gain more insight into the nature of the relationship between cGMP signaling and stress receptors for central brain adaptation to environmental demands based on the present results. We suggest that balanced extra-hypothalamic stress control is a key signature that bridges auditory fiber processing with healthy cognition. We further emphasize that research into age-dependent cochlear synaptopathy and its future therapeutic intervention strategies by the pharmaceutical industry needs to consider individual states of stress response, particularly if aiming to use cognitive stimulators, e.g., PDE9i, as a therapeutic drug to overcome (auditory) cognitive decline.

DATA AVAILABILITY STATEMENT

The original contributions presented in the study are included in the article/**Supplementary Material**, further inquiries can be directed to the corresponding author/s.

ETHICS STATEMENT

The animal study was reviewed and approved by University of Tübingen, Veterinary Care Unit, and the Animal Care and Ethics Committee of the regional board of the Federal State Government of Baden-Württemberg, Germany.

AUTHOR CONTRIBUTIONS

DS, MH, DC, PM, and CH performed the experiments. DS, MH, DC, CH, SF, LR, and WS performed data analyses. MK and PM performed microscopy. MK, LR, and WS contributed to conception and design of the study. PR critically revised the manuscript for intellectual content during this revision process and contributed to the interpretation of the data. All authors contributed to write, read, and approve the resubmitted version of the manuscript.

FUNDING

This work was funded by the Deutsche Forschungsgemeinschaft (DFG, German Research Foundation) Research Training Group (Grant No. 335549539/GRK 2381), FOR 2060 project RU 713/3-2, SPP 1608 RU 316/12-1, KN 316/12-1, and the Sigmund Kiener Stiftung. Each source of funding provided a budget for personnel and material costs.

ACKNOWLEDGMENTS

We thank Hyun-Soon Geisler and Karin Rohbock for excellent technical assistance. English language services were provided by stels-ol.de. We acknowledge support by Open Access Publishing Fund of University of Tübingen.

SUPPLEMENTARY MATERIAL

The Supplementary Material for this article can be found online at: https://www.frontiersin.org/articles/10.3389/fnins.2022.864706/full#supplementary-material

Supplementary Figure 1 | A schematic overview of ASSRs in mice. **(A)** The ASSRs were recorded with similar electrode positions as the ABR measurements,

i.e., the active electrode placed below the pinna, the reference at the vertex and the grounding electrode close to the tail. **(B)** The presented amplitude-modulated stimulus contains a sine wave carrier frequency (CF) at 11.3 kHz, which is modulated by a modulation frequency (MF) of 512 Hz. The modulation of the CF is depicted by the dotted envelope function. **(C)** An example trace of a recorded signal in response to amplitude modulated stimuli; shown in the time-domain. **(D)** Conversion from the time- to the frequency-domain through Fast Fourier Transformation (FFT). Extraction of the signal at the noise floor, 512 Hz and the harmonics.

Supplementary Figure 2 | Changes in hearing thresholds for click and noise ABR after placebo or PDE9i treatment. Neither **(A)** *low compensators* nor **(B)** *high compensators* showed changes in thresholds after treatment with placebo or PDE9i in response to click stimuli. The same result was observed in response to noise stimuli: thresholds of **(C)** *low compensators* and **(D)** *high compensators* remained unchanged with placebo and PDE9i. Mean ± SEM.

Supplementary Figure 3 | ABR wave IV amplitude in *high* and *low* compensators before and after treatment with either placebo or PDE9i. **(A)** *High compensators* showed a significantly lower wave IV amplitude after placebo treatment, but **(B)** the wave IV amplitude of *high compensators* treated with PDE9i remained unchanged after treatment. **(C)** *Low compensators* showed no difference in wave IV amplitude after treatment with placebo or **(D)** with PDE9i. Mean ± SEM. $^{*}p < 0.05$, repeated measures 2-way ANOVA.

Supplementary Figure 4 | Input-output relationship between the fEPSP slope, fiber volley (FV) amplitude, and stimulus intensity. **(A)** Representative traces of fEPSPs with increasing stimulus intensities (from 25 μA to 150 μA in 25 μA steps). **(B)** In high-compensating animals, a significant increase in the fEPSP slope was observed after treatment with either placebo or PDE9i in comparison to their untreated controls at stimulus intensities between 50 and 100 μA. Low compensators treated with placebo and PDE9i also showed significantly increased fEPSP slopes in comparison to their untreated controls at stimulus intensities between 25 and 75 μA. In addition, PDE9i-treated *low compensators* had significantly increased fEPSP slopes at a stimulus intensity of 100 μA, and PDE9i-treated animals and placebo-treated animals were significantly different from one another at the stimulus intensity of 50 μA. **(C)** In *high compensators*, a significant increase in FV amplitude was observed after treatment with either placebo or PDE9i in comparison to untreated controls at stimulus intensities between 25 and 100 μA. In *low compensators*, the animals treated with PDE9i showed a significant increase in FV amplitude in comparison to untreated controls at stimulus intensities of 25 and 50 μA. *Low compensators* treated with placebo showed a significant increase in FV amplitude in comparison to untreated controls only at the stimulus intensity of 25 μA. No difference in FV amplitude between the treatment conditions of low compensators was observed. **(D)** Changes in fEPSP slopes were consistent with changes in FV amplitudes in all treatment groups of both *high* and *low compensators*. nt, no treatment; p, placebo. Mean ± SEM. $^{***}p < 0.001$, $^{****}p < 0.0001$, 2-way ANOVA.

Supplementary Figure 5 | Paired-pulse facilitation (PPF) as an indicator of short-term plasticity. **(A)** Representative traces of fEPSPs with increasing interstimulus intervals (ISIs) at the stimulation strength equal to corresponding LTP recordings. Applied ISIs are indicated by the scale bar above: 10 ms, 20 ms, 50 ms, 100 ms, 200ms, 500 ms (not shown). **(B)** The analysis of PPF in *high compensators* showed a significantly lower paired-pulse ratio of the fEPSP2/fEPSP1 slope after PDE9i treatment in comparison to placebo treatment and to their untreated controls at ISIs of 10 and 20 ms, while placebo-treated high compensators did not differ significantly from their untreated controls. **(C)** *High compensators* treated with PDE9i had a significantly lower paired-pulse ratio of the fEPSP2/fEPSP1 amplitude in comparison to their untreated controls at ISIs of 10 and 20 ms, while placebo injection significantly increased the PPF amplitude ratio in *high compensators* at the same ISIs in comparison to their untreated controls. In addition, the paired-pulse ratio of the fEPSP2/fEPSP1 amplitude of placebo-treated and PDE9i-treated *high compensators* differed from each other at ISIs of 10, 20, and 50 ms. **(D)** The analysis of PPF in *low compensators* showed a significant effect of treatment on the paired-pulse ratio of the fEPSP2/fEPSP1 slope, but this was not significant in the *post hoc* test. **(E)** The paired-pulse ratio of the fEPSP2/fEPSP1 amplitude of *low compensators* treated with both placebo and PDE9i was significantly increased in comparison to the untreated controls at the ISI of 10 ms. No difference in the PPF amplitude ratio between the treatment conditions of *low compensators* was observed. nt, no treatment; p, placebo. Mean ± SEM. $^{*}p < 0.05$, $^{**}p < 0.01$, $^{***}p < 0.001$, $^{****}p < 0.0001$, 2-way ANOVA.

REFERENCES

Arango-Lievano, M., Borie, A. M., Dromard, Y., Murat, M., Desarmenien, M. G., Garabedian, M. J., et al. (2019). Persistence of learning-induced synapses depends on neurotrophic priming of glucocorticoid receptors. *Proc. Natl. Acad. Sci. U. S. A.* 116, 13097–13106. doi: 10.1073/pnas.1903203116

Bharadwaj, H. M., Verhulst, S., Shaheen, L., Liberman, M. C., and Shinn-Cunningham, B. G. (2014). Cochlear neuropathy and the coding of supra-threshold sound. *Front. Syst. Neurosci.* 8, 26. doi: 10.3389/fnsys.2014.00026

Bramhall, N., Ong, B., Ko, J., and Parker, M. (2015). Speech perception ability in noise is correlated with auditory brainstem response wave i amplitude. *J. Am. Acad. Audiol.* 26, 509–517. doi: 10.3766/jaaa.14100

Bueno-Junior, L. S., and Leite, J. P. (2018). Input convergence, synaptic plasticity and functional coupling across hippocampal-prefrontal-thalamic circuits. *Front. Neural. Circuits* 12, 40. doi: 10.3389/fncir.2018.00040

Burkard, R. F., and Don, M. (2007). "The auditory brainstem response," in *Auditory Evoked Potentials: Basic Principles and Clinical Application*, eds. R.F. Burkard, J.J. Eggermont, and M. Don. (Philadelphia: Lippincott Williams and Wilkins).

Canlon, B., Theorell, T., and Hasson, D. (2013). Associations between stress and hearing problems in humans. *Hear. Res.* 295, 9–15. doi: 10.1016/j.heares.2012.08.015

Chen, G., Zhang, Y., Li, X., Zhao, X., Ye, Q., Lin, Y., et al. (2017). Distinct inhibitory circuits orchestrate cortical beta and gamma band oscillations. *Neuron* 96, 1403–1418.e1406. doi: 10.1016/j.neuron.2017.11.033

Chenaux, G., Matt, L., Hill, T. C., Kaur, I., Liu, X.-B., Kirk, L. M., et al. (2016). Loss of SynDIG1 reduces excitatory synapse maturation but not formation *in vivo*. SynDIG1 regulates excitatory synapse maturation. *eNeuro.* 3:ENEURO.0130-16.2016. doi: 10.1523/ENEURO.0130-16.2016

Chumak, T., Rüttiger, L., Lee, S. C., Campanelli, D., Zuccotti, A., Singer, W., et al. (2016). BDNF in lower brain parts modifies auditory fiber activity to gain fidelity but increases the risk for generation of central noise after injury. *Mol. Neurobiol.* 53, 5607–5627. doi: 10.1007/s12035-015-9474-x

Csabai, D., Wiborg, O., and Czeh, B. (2018). Reduced synapse and axon numbers in the prefrontal cortex of rats subjected to a chronic stress model for depression. *Front. Cell. Neurosci.* 12, 24. doi: 10.3389/fncel.2018.00024

Czeh, B., Vardya, I., Varga, Z., Febbraro, F., Csabai, D., Martis, L. S., et al. (2018). Long-term stress disrupts the structural and functional integrity of GABAergic neuronal networks in the medial prefrontal cortex of rats. *Front. Cell. Neurosci.* 12, 148. doi: 10.3389/fncel.2018.00148

Czeh, B., Varga, Z. K., Henningsen, K., Kovacs, G. L., Miseta, A., and Wiborg, O. (2015). Chronic stress reduces the number of GABAergic interneurons in the adult rat hippocampus, dorsal-ventral and region-specific differences. *Hippocampus* 25, 393–405. doi: 10.1002/hipo.22382

de Kloet, E. R., de Kloet, S. F., de Kloet, C. S., and de Kloet, A. D. (2019). Top-down and bottom-up control of stress-coping. *J. Neuroendocrinol.* 31, e12675. doi: 10.1111/jne.12675

de Kloet, E. R., Joels, M., and Holsboer, F. (2005). Stress and the brain: from adaptation to disease. *Nat. Rev. Neurosci.* 6, 463–475. doi: 10.1038/nrn1683

de Kloet, E. R., Oitzl, M. S., and Joels, M. (1999). Stress and cognition: are corticosteroids good or bad guys? *Trends Neurosci.* 22, 422–426. doi: 10.1016/S0166-2236(99)01438-1

de Kloet, E. R., Van Acker, S. A., Sibug, R. M., Oitzl, M. S., Meijer, O. C., Rahmouni, K., et al. (2000). Brain mineralocorticoid receptors and centrally regulated functions. *Kidney Int.* 57, 1329–1336. doi: 10.1046/j.1523-1755.2000.00971.x

Elling, L., Steinberg, C., Brockelmann, A. K., Dobel, C., Bolte, J., and Junghofer, M. (2011). Acute stress alters auditory selective attention in humans

independent of HPA: a study of evoked potentials. *PLoS ONE* 6, e18009. doi: 10.1371/journal.pone.0018009

Engel, J., Braig, C., Rüttiger, L., Kuhn, S., Zimmermann, U., Blin, N., et al. (2006). Two classes of outer hair cells along the tonotopic axis of the cochlea. *Neuroscience* 143, 837–849. doi: 10.1016/j.neuroscience.2006.08.060

Engelien, A., Schulz, M., Ross, B., Arolt, V., and Pantev, C. (2000). A combined functional *in vivo* measure for primary and secondary auditory cortices. *Hear. Res.* 148, 153–160. doi: 10.1016/S0378-5955(00)00148-9

Fortunato, S., Forli, F., Guglielmi, V., De Corso, E., Paludetti, G., Berrettini, S., et al. (2016). A review of new insights on the association between hearing loss and cognitive decline in ageing. *Acta. Otorhinolaryngol. Ital.* 36, 155–166. doi: 10.14639/0392-100X-993

Frisina, R. D. (2009). Age-related hearing loss: ear and brain mechanisms. *Ann. N. Y. Acad. Sci.* 1170, 708–717. doi: 10.1111/j.1749-6632.2009.03931.x

Fullgrabe, C., and Moore, B. C. (2014). Effects of age and hearing loss on stream segregation based on interaural time differences. *J. Acoust. Soc. Am.* 136, EL185–191. doi: 10.1121/1.4890201

Griffiths, T. D., Lad, M., Kumar, S., Holmes, E., McMurray, B., Maguire, E. A., et al. (2020). How can hearing loss cause dementia? *Neuron* 108, 401–412. doi: 10.1016/j.neuron.2020.08.003

Han, K., Min, J., Lee, M., Kang, B. M., Park, T., Hahn, J., et al. (2019). Neurovascular coupling under chronic stress is modified by altered gabaergic interneuron activity. *J. Neurosci.* 39, 10081–10095. doi: 10.1523/JNEUROSCI.1357-19.2019

Hillman, E. M. (2014). Coupling mechanism and significance of the BOLD signal: a status report. *Annu. Rev. Neurosci.* 37, 161–181. doi: 10.1146/annurev-neuro-071013-014111

Hofer, M., Pagliusi, S. R., Hohn, A., Leibrock, J., and Barde, Y. A. (1990). Regional distribution of brain-derived neurotrophic factor mRNA in the adult mouse brain. *EMBO J.* 9, 2459–2464. doi: 10.1002/j.1460-2075.1990.tb07423.x

Hu, H., Gan, J., and Jonas, P. (2014). Interneurons fast-spiking, parvalbumin+ GABAergic interneurons: from cellular design to microcircuit function. *Science* 345, 1255263. doi: 10.1126/science.1255263

Hutson, P. H., Finger, E. N., Magliaro, B. C., Smith, S. M., Converso, A., Sanderson, P. E., et al. (2011). The selective phosphodiesterase 9 (PDE9) inhibitor PF-04447943 (6-[(3S,4S)-4-methyl-1-(pyrimidin-2-ylmethyl)pyrrolidin-3-yl]-1-(tetrahydro-2H-py ran-4-yl)-1,5-dihydro-4H-pyrazolo[3,4-d]pyrimidin-4-one) enhances synaptic plasticity and cognitive function in rodents. *Neuropharmacology* 61, 665–676. doi: 10.1016/j.neuropharm.2011.05.009

Jafari, Z., Kolb, B. E., and Mohajerani, M. H. (2018). Chronic traffic noise stress accelerates brain impairment and cognitive decline in mice. *Exp. Neurol.* 308, 1–12. doi: 10.1016/j.expneurol.2018.06.011

Jeanneteau, F., Borie, A., Chao, M. V., and Garabedian, M. J. (2018). Bridging the gap between brain-derived neurotrophic factor and glucocorticoid effects on brain networks. *Neuroendocrinology* 109, 277–284. doi: 10.1159/000496392

Jett, J. D., Bulin, S. E., Hatherall, L. C., McCartney, C. M., and Morilak, D. A. (2017). Deficits in cognitive flexibility induced by chronic unpredictable stress are associated with impaired glutamate neurotransmission in the rat medial prefrontal cortex. *Neuroscience* 346, 284–297. doi: 10.1016/j.neuroscience.2017.01.017

Joels, M., and de Kloet, E. R. (2017). 30 Years of the mineralocorticoid receptor: the brain mineralocorticoid receptor: a saga in three episodes. *J. Endocrinol.* 234, T49–T66. doi: 10.1530/JOE-16-0660

Johnson, D. H., and Kiang, N. Y. (1976). Analysis of discharges recorded simultaneously from pairs of auditory nerve fibers. *Biophys. J.* 16, 719–734. doi: 10.1016/S0006-3495(76)85724-4

Johnson, J. C. S., Marshall, C. R., Weil, R. S., Bamiou, D. E., Hardy, C. J. D., and Warren, J. D. (2021). Hearing and dementia: from ears to brain. *Brain* 144, 391–401. doi: 10.1093/brain/awaa429

Kelly, M. P. (2012). "Putting together the pieces of phosphodiesterase distribution patterns in the brain: a jigsaw puzzle of cyclic nucleotide regulation," *in Phosphodiesterases in the CNS*, eds. N.J. Brandon and A.R. West. (New York, NY: John Wiley & Sons, Inc).

Khimich, D., Nouvian, R., Pujol, R., Tom Dieck, S., Egner, A., Gundelfinger, E. D., et al. (2005). Hair cell synaptic ribbons are essential for synchronous auditory signalling. *Nature* 434, 889–894. doi: 10.1038/nature03418

Kleiman, R. J., Chapin, D. S., Christoffersen, C., Freeman, J., Fonseca, K. R., Geoghegan, K. F., et al. (2012). Phosphodiesterase 9A regulates central cGMP and modulates responses to cholinergic and monoaminergic perturbation *in vivo*. *J. Pharmacol. Exp. Ther.* 341, 396–409. doi: 10.1124/jpet.111.191353

Knipper, M., Singer, W., Schwabe, K., Hagberg, G. E., Li Hegner, Y., Rüttiger, L., et al. (2022). Disturbed balance of inhibitory signaling links hearing loss and cognition. *Front. Neural. Circuits.* 15:785603. doi: 10.3389/fncir.2021.785603

Knipper, M., van Dijk, P., Schulze, H., Mazurek, B., Krauss, P., Scheper, V., et al. (2020). The neural bases of tinnitus: lessons from deafness and cochlear implants. *J. Neurosci.* 40, 7190–7202. doi: 10.1523/JNEUROSCI.1314-19.2020

Kobel, M., Le Prell, C. G., Liu, J., Hawks, J. W., and Bao, J. (2017). Noise-induced cochlear synaptopathy: Past findings and future studies. *Hear. Res.* 349, 148–154. doi: 10.1016/j.heares.2016.12.008

Kreuzer, P. M., Landgrebe, M., Vielsmeier, V., Kleinjung, T., De Ridder, D., and Langguth, B. (2014). Trauma-associated tinnitus. *J. Head Trauma. Rehabil.* 29, 432–442. doi: 10.1097/HTR.0b013e31829d3129

Kroker, K. S., Mathis, C., Marti, A., Cassel, J. C., Rosenbrock, H., and Dorner-Ciossek, C. (2014). PDE9A inhibition rescues amyloid beta-induced deficits in synaptic plasticity and cognition. *Neurobiol. Aging* 35, 2072–2078. doi: 10.1016/j.neurobiolaging.2014.03.023

Kroker, K. S., Rast, G., Giovannini, R., Marti, A., Dorner-Ciossek, C., and Rosenbrock, H. (2012). Inhibition of acetylcholinesterase and phosphodiesterase-9A has differential effects on hippocampal early and late LTP. *Neuropharmacology* 62, 1964–1974. doi: 10.1016/j.neuropharm.2011.12.021

Kujawa, S. G., and Liberman, M. C. (2009). Adding insult to injury: cochlear nerve degeneration after "temporary" noise-induced hearing loss. *J. Neurosci.* 29, 14077–14085. doi: 10.1523/JNEUROSCI.2845-09.2009

Kuwada, S., Anderson, J. S., Batra, R., Fitzpatrick, D. C., Teissier, N., and D'Angelo, W. R. (2002). Sources of the scalp-recorded amplitude-modulation following response. *J. Am. Acad. Audiol.* 13, 188–204. doi: 10.1055/s-0040-1715963

Lakics, V., Karran, E. H., and Boess, F. G. (2010). Quantitative comparison of phosphodiesterase mRNA distribution in human brain and peripheral tissues. *Neuropharmacology* 59, 367–374. doi: 10.1016/j.neuropharm.2010.05.004

Lee, S., Kang, B. M., Shin, M. K., Min, J., Heo, C., Lee, Y., et al. (2015). Chronic stress decreases cerebrovascular responses during rat hindlimb electrical stimulation. *Front. Neurosci.* 9, 462. doi: 10.3389/fnins.2015.00462

Lewis-Tuffin, L. J., and Cidlowski, J. A. (2006). The physiology of human glucocorticoid receptor beta (hGRbeta) and glucocorticoid resistance. *Ann. N. Y. Acad. Sci.* 1069, 1–9. doi: 10.1196/annals.1351.001

Liberman, M. C., and Kujawa, S. G. (2017). Cochlear synaptopathy in acquired sensorineural hearing loss: Manifestations and mechanisms. *Hear. Res.* 349, 138–147. doi: 10.1016/j.heares.2017.01.003

Lin, F. R., Metter, E. J., O'Brien, R. J., Resnick, S. M., Zonderman, A. B., and Ferrucci, L. (2011). Hearing loss and incident dementia. *Arch. Neurol.* 68, 214–220. doi: 10.1001/archneurol.2010.362

Livingston, G., Sommerlad, A., Orgeta, V., Costafreda, S. G., Huntley, J., Ames, D., et al. (2017). Dementia prevention, intervention, and care. *Lancet* 390, 2673–2734. doi: 10.1016/S0140-6736(17)31363-6

Ma, L., Li, W., Li, S., Wang, X., and Qin, L. (2017). Effect of chronic restraint stress on inhibitory gating in the auditory cortex of rats. *Stress* 20, 312–319. doi: 10.1080/10253890.2017.1323861

MacGregor, A. J., Joseph, A. R., Walker, G. J., and Dougherty, A. L. (2020). Co-occurrence of hearing loss and posttraumatic stress disorder among injured military personnel: a retrospective study. *BMC Public Health* 20, 1076. doi: 10.1186/s12889-020-08999-6

Marchetta, P., Eckert, P., Lukowski, R., Ruth, P., Singer, W., Ruttiger, L., et al. (2022). Loss of central mineralocorticoid or glucocorticoid receptors impacts auditory nerve processing in the cochlea. *iScience* 25, 103981. doi: 10.1016/j.isci.2022.103981

Marchetta, P., Mohrle, D., Eckert, P., Reimann, K., Wolter, S., Tolone, A., et al. (2020a). Guanylyl cyclase A/cGMP signaling slows hidden, age- and acoustic trauma-induced hearing loss. *Front. Aging Neurosci.* 12, 83. doi: 10.3389/fnagi.2020.00083

Marchetta, P., Savitska, D., Kubler, A., Asola, G., Manthey, M., Mohrle, D., et al. (2020b). Age-dependent auditory processing deficits after cochlear synaptopathy depend on auditory nerve latency and the ability of the brain to recruit LTP/BDNF. *Brain Sci.* 10, 710. doi: 10.3390/brainsci 10100710

Matt, L., Eckert, P., Panford-Walsh, R., Geisler, H. S., Bausch, A. E., Manthey, M., et al. (2018). Visualizing BDNF transcript usage during sound-induced memory linked plasticity. *Front. Mol. Neurosci.* 11, 260. doi: 10.3389/fnmol.2018.00260

Matt, L., Michalakis, S., Hofmann, F., Hammelmann, V., Ludwig, A., Biel, M., et al. (2011). HCN2 channels in local inhibitory interneurons constrain LTP in the hippocampal direct perforant path. *Cell. Mol. Life Sci.* 68, 125–137. doi: 10.1007/s00018-010-0446-z

Maxwell, C. R., Ehrlichman, R. S., Liang, Y., Gettes, D. R., Evans, D. L., Kanes, S. J., et al. (2006). Corticosterone modulates auditory gating in mouse. *Neuropsychopharmacology* 31, 897–903. doi: 10.1038/sj.npp.1300879

Mazurek, B., Boecking, B., and Brueggemann, P. (2019). Association between stress and tinnitus-new aspects. *Otol. Neurotol.* 40, e467–e473. doi: 10.1097/MAO.0000000000002180

Melcher, J. R., and Kiang, N. Y. (1996). Generators of the brainstem auditory evoked potential in cat. III: Identified cell populations. *Hear. Res.* 93, 52–71. doi: 10.1016/0378-5955(95)00200-6

Meltser, I., and Canlon, B. (2011). Protecting the auditory system with glucocorticoids. *Hear. Res.* 281, 47–55. doi: 10.1016/j.heares.2011.06.003

Möhrle, D., Ni, K., Varakina, K., Bing, D., Lee, S. C., Zimmermann, U., et al. (2016). Loss of auditory sensitivity from inner hair cell synaptopathy can be centrally compensated in the young but not old brain. *Neurobiol. Aging* 44, 173–184. doi: 10.1016/j.neurobiolaging.2016.05.001

Montero-Odasso, M., Ismail, Z., and Livingston, G. (2020). One third of dementia cases can be prevented within the next 25 years by tackling risk factors. The case "for" and "against". *Alzheimers Res. Ther.* 12, 81. doi: 10.1186/s13195-020-00646-x

Nagy, D., Tingley, F. D. 3rd, Stoiljkovic, M., and Hajos, M. (2015). Application of neurophysiological biomarkers for Huntington's disease: evaluating a phosphodiesterase 9A inhibitor. *Exp. Neurol.* 263, 122–131. doi: 10.1016/j.expneurol.2014.10.001

Neher, E., and Sakaba, T. (2008). Multiple roles of calcium ions in the regulation of neurotransmitter release. *Neuron* 59, 861–872. doi: 10.1016/j.neuron.2008.08.019

Plack, C. J., Barker, D., and Prendergast, G. (2014). Perceptual consequences of "hidden" hearing loss. *Trends Hear.* 4:2331216514550621. doi: 10.1177/2331216514550621

Plieger, T., Felten, A., Splittgerber, H., Duke, E., and Reuter, M. (2018). Corrigendum to "The role of genetic variation in the glucocorticoid receptor (NR3C1) and mineralocorticoid receptor (NR3C2) in the association between cortisol response and cognition under acute stress" [Psychoneuroendocrinology 87 (2018) 173-180]. *Psychoneuroendocrinology* 94, 169–170. doi: 10.1016/j.psyneuen.2018.05.009

Rüttiger, L., Singer, W., Panford-Walsh, R., Matsumoto, M., Lee, S. C., Zuccotti, A., et al. (2013). The reduced cochlear output and the failure to adapt the central auditory response causes tinnitus in noise exposed rats. *PLoS ONE* 8, e57247. doi: 10.1371/journal.pone.0057247

Sanders, O., and Rajagopal, L. (2020). Phosphodiesterase inhibitors for Alzheimer's disease: a systematic review of clinical trials and epidemiology with a mechanistic rationale. *J. Alzheimers Dis. Rep.* 4, 185–215. doi: 10.3233/ADR-200191

Sapolsky, R. M. (2015). Stress and the brain: individual variability and the inverted-U. *Nat. Neurosci.* 18, 1344–1346. doi: 10.1038/nn.4109

Satake, S., Inoue, T., and Imoto, K. (2012). Paired-pulse facilitation of multivesicular release and intersynaptic spillover of glutamate at rat cerebellar granule cell-interneurone synapses. *J. Physiol.* 590, 5653–5675. doi: 10.1113/jphysiol.2012.234070

Sergeyenko, Y., Lall, K., Liberman, M. C., and Kujawa, S. G. (2013). Age-related cochlear synaptopathy: an early-onset contributor to auditory functional decline. *J. Neurosci.* 33, 13686–13694. doi: 10.1523/JNEUROSCI.1783-13.2013

Sharma, V. K., Singh, T. G., and Singh, S. (2020). Cyclic nucleotides signaling and phosphodiesterase inhibition: defying Alzheimer's disease. *Curr. Drug Targets* 21, 1371–1384. doi: 10.2174/1389450121666200727104728

Silverman, M. N., and Sternberg, E. M. (2008). Neuroendocrine-immune interactions in rheumatoid arthritis: mechanisms of glucocorticoid resistance. *Neuroimmunomodulation* 15, 19–28. doi: 10.1159/000135620

Singer, W., Geisler, H. S., Panford-Walsh, R., and Knipper, M. (2016). Detection of excitatory and inhibitory synapses in the auditory system using fluorescence immunohistochemistry and high-resolution fluorescence microscopy. *Methods Mol. Biol.* 1427, 263–276. doi: 10.1007/978-1-4939-3615-1_15

Singer, W., Kasini, K., Manthey, M., Eckert, P., Armbruster, P., Vogt, M. A., et al. (2018a). The glucocorticoid antagonist mifepristone attenuates sound-induced long-term deficits in auditory nerve response and central auditory processing in female rats. *FASEB J.* 32, 3005–3019. doi: 10.1096/fj.201701041RRR

Singer, W., Manthey, M., Panford-Walsh, R., Matt, L., Geisler, H. S., Passeri, E., et al. (2018b). BDNF-live-exon-visualization (BLEV) allows differential detection of BDNF transcripts *in vitro* and *in vivo*. *Front. Mol. Neurosci.* 11, 325. doi: 10.3389/fnmol.2018.00325

Singer, W., Zuccotti, A., Jaumann, M., Lee, S. C., Panford-Walsh, R., Xiong, H., et al. (2013). Noise-induced inner hair cell ribbon loss disturbs central arc mobilization: a novel molecular paradigm for understanding tinnitus. *Mol. Neurobiol.* 47, 261–279. doi: 10.1007/s12035-012-8372-8

Sloan, D. M., Zhang, D., and Bertram, E. H. III. (2011). Excitatory amplification through divergent-convergent circuits: the role of the midline thalamus in limbic seizures. *Neurobiol. Dis.* 43, 435–445. doi: 10.1016/j.nbd.2011.04.017

Sohal, V. S., Zhang, F., Yizhar, O., and Deisseroth, K. (2009). Parvalbumin neurons and gamma rhythms enhance cortical circuit performance. *Nature* 459, 698–702. doi: 10.1038/nature07991

Spies, L. L., Verhoog, N. J. D., and Louw, A. (2021). Acquired glucocorticoid resistance due to homologous glucocorticoid receptor downregulation: a modern look at an age-old problem. *Cells* 10, 2529. doi: 10.3390/cells10102529

Stevens, K. E., Bullock, A. E., and Collins, A. C. (2001). Chronic corticosterone treatment alters sensory gating in C3H mice. *Pharmacol. Biochem. Behav.* 69, 359–366. doi: 10.1016/S0091-3057(01)00523-8

Thomson, A. M. (2000). Facilitation, augmentation and potentiation at central synapses. *Trends Neurosci.* 23, 305–312. doi: 10.1016/S0166-2236(00)01580-0

Timmusk, T., Palm, K., Metsis, M., Reintam, T., Paalme, V., Saarma, M., et al. (1993). Multiple promoters direct tissue-specific expression of the rat BDNF gene. *Neuron* 10, 475–489. doi: 10.1016/0896-6273(93)90335-O

Turner, A. I., Smyth, N., Hall, S. J., Torres, S. J., Hussein, M., Jayasinghe, S. U., et al. (2020). Psychological stress reactivity and future health and disease outcomes: a systematic review of prospective evidence. *Psychoneuroendocrinology* 114, 104599. doi: 10.1016/j.psyneuen.2020.104599

Turner, H. A., Mitchell, K. J., Jones, L. M., Hamby, S., Wade, R. Jr., and Beseler, C. L. (2019). Gun violence exposure and posttraumatic symptoms among children and youth. *J. Trauma Stress* 32, 881–889. doi: 10.1002/jts.22466

Uchida, Y., Sugiura, S., Nishita, Y., Saji, N., Sone, M., and Ueda, H. (2019). Age-related hearing loss and cognitive decline - the potential mechanisms linking the two. *Auris Nasus Larynx* 46, 1–9. doi: 10.1016/j.anl.2018.08.010

Valero, M. D., Burton, J. A., Hauser, S. N., Hackett, T. A., Ramachandran, R., and Liberman, M. C. (2017). Noise-induced cochlear synaptopathy in rhesus monkeys (Macaca mulatta). *Hear. Res.* 353, 213–223. doi: 10.1016/j.heares.2017.07.003

van der Staay, F. J., Rutten, K., Barfacker, L., Devry, J., Erb, C., Heckroth, H., et al. (2008). The novel selective PDE9 inhibitor BAY 73-6691 improves learning and memory in rodents. *Neuropharmacology* 55, 908–918. doi: 10.1016/j.neuropharm.2008.07.005

Viana, L. M., O'Malley, J. T., Burgess, B. J., Jones, D. D., Oliveira, C. A., Santos, F., et al. (2015). Cochlear neuropathy in human presbycusis: Confocal analysis of hidden hearing loss in post-mortem tissue. *Hear. Res.* 327, 78–88. doi: 10.1016/j.heares.2015.04.014

Vitellius, G., Trabado, S., Bouligand, J., Delemer, B., and Lombes, M. (2018). Pathophysiology of glucocorticoid signaling. *Ann. Endocrinol.* 79, 98–106. doi: 10.1016/j.ando.2018.03.001

White, P. M., Kanazawa, A., and Yee, C. M. (2005). Gender and suppression of mid-latency ERP components during stress. *Psychophysiology* 42, 720–725. doi: 10.1111/j.1469-8986.2005.00365.x

Wirz, L., Reuter, M., Wacker, J., Felten, A., and Schwabe, L. (2017). A haplotype associated with enhanced mineralocorticoid receptor expression facilitates the stress-induced shift from "cognitive" to "habit" learning. *eNeuro* 4:ENEURO.0359-17.2017. doi: 10.1523/ENEURO.0359-17.2017

Wu, P. Z., Liberman, L. D., Bennett, K., de Gruttola, V., O'Malley, J. T., and Liberman, M. C. (2019). Primary neural degeneration in the human cochlea: evidence for hidden hearing loss in the aging ear. *Neuroscience* 407, 8–20. doi: 10.1016/j.neuroscience.2018.07.053

Zampini, V., Johnson, S. L., Franz, C., Lawrence, N. D., Munkner, S., Engel, J., et al. (2010). Elementary properties of CaV1.3 Ca(2+) channels expressed in mouse cochlear inner hair cells. *J. Physiol.* 588, 187–199. doi: 10.1113/jphysiol.2009.181917

Zhang, L., Wang, J., Sun, H., Feng, G., and Gao, Z. (2022). Interactions between the hippocampus and the auditory pathway. *Neurobiol. Learn Mem.* 189, 107589. doi: 10.1016/j.nlm.2022.107589

Zuccotti, A., Kuhn, S., Johnson, S. L., Franz, C., Singer, W., Hecker, D., et al. (2012). Lack of brain-derived neurotrophic factor hampers inner hair cell synapse physiology, but protects against noise-induced hearing loss. *J. Neurosci.* 32, 8545–8553. doi: 10.1523/JNEUROSCI.1247-12.2012

Zucker, R. S., and Regehr, W. G. (2002). Short-term synaptic plasticity. *Annu. Rev. Physiol.* 64, 355–405. doi: 10.1146/annurev.physiol.64.092501.114547

Conflict of Interest: The authors declare that the research was conducted in the absence of any commercial or financial relationships that could be construed as a potential conflict of interest.

The handling editor VS declared a past collaboration with the authors, LR, MK, and WS.

frontiers | Frontiers in Molecular Neuroscience

TYPE Original Research
PUBLISHED 17 February 2023
DOI 10.3389/fnmol.2023.1017761

OPEN ACCESS

EDITED BY
Clint L. Makino,
Boston University,
United States

REVIEWED BY
Clive R. Bramham,
University of Bergen,
Norway
Jenna Penney,
University of Guelph,
Canada

*CORRESPONDENCE
Marlies Knipper
✉ marlies.knipper@uni-tuebingen.de

†These authors have contributed equally to this work

SPECIALTY SECTION
This article was submitted to Molecular Signalling and Pathways, a section of the journal Frontiers in Molecular Neuroscience

RECEIVED 12 August 2022
ACCEPTED 18 January 2023
PUBLISHED 17 February 2023

CITATION
Calis D, Hess M, Marchetta P, Singer W, Modro J, Nelissen E, Prickaerts J, Sandner P, Lukowski R, Ruth P, Knipper M and Rüttiger L (2023) Acute deletion of the central MR/GR steroid receptor correlates with changes in LTP, auditory neural gain, and GC-A cGMP signaling.
Front. Mol. Neurosci. 16:1017761.
doi: 10.3389/fnmol.2023.1017761

Acute deletion of the central MR/GR steroid receptor correlates with changes in LTP, auditory neural gain, and GC-A cGMP signaling

Dila Calis[1†], Morgan Hess[1†], Philine Marchetta[1], Wibke Singer[1], Julian Modro[1], Ellis Nelissen[2], Jos Prickaerts[2], Peter Sandner[3], Robert Lukowski[4], Peter Ruth[4], Marlies Knipper[1*] and Lukas Rüttiger[1]

[1]Department of Otolaryngology, Head and Neck Surgery, Tübingen Hearing Research Centre, Molecular Physiology of Hearing, University of Tübingen, Tübingen, Germany, [2]Department of Psychiatry and Neuropsychology, School for Mental Health and Neuroscience (MHeNS), Maastricht University, Maastricht, Netherlands, [3]Bayer Health Care Pharmaceuticals, Global Drug Discovery Pharma Research Centre Wuppertal, Wuppertal, Germany, [4]Institute of Pharmacy, Pharmacology, Toxicology and Clinical Pharmacy, University of Tübingen, Tübingen, Germany

The complex mechanism by which stress can affect sensory processes such as hearing is still poorly understood. In a previous study, the mineralocorticoid (MR) and/or glucocorticoid receptor (GR) were deleted in frontal brain regions but not cochlear regions using a CaMKIIα-based tamoxifen-inducible *Cre*^{ERT2}/loxP approach. These mice exhibit either a diminished (MR^{TMX}cKO) or disinhibited (GR^{TMX}cKO) auditory nerve activity. In the present study, we observed that mice differentially were (MR^{TMX}cKO) or were not (GR^{TMX}cKO) able to compensate for altered auditory nerve activity in the central auditory pathway. As previous findings demonstrated a link between central auditory compensation and memory-dependent adaptation processes, we analyzed hippocampal paired-pulse facilitation (PPF) and long-term potentiation (LTP). To determine which molecular mechanisms may impact differences in synaptic plasticity, we analyzed Arc/Arg3.1, known to control AMPA receptor trafficking, as well as regulators of tissue perfusion and energy consumption (NO-GC and GC-A). We observed that the changes in PPF of MR^{TMX}cKOs mirrored the changes in their auditory nerve activity, whereas changes in the LTP of MR^{TMX}cKOs and GR^{TMX}cKOs mirrored instead the changes in their central compensation capacity. Enhanced GR expression levels in MR^{TMX}cKOs suggest that MRs typically suppress GR expression. We observed that hippocampal LTP, GC-A mRNA expression levels, and ABR wave IV/I ratio were all enhanced in animals with elevated GR (MR^{TMX}cKOs) but were all lower or not mobilized in animals with impaired GR expression levels (GR^{TMX}cKOs and MRGR^{TMX}cKOs). This suggests that GC-A may link LTP and auditory neural gain through GR-dependent processes. In addition, enhanced NO-GC expression levels in MR, GR, and MRGR^{TMX}cKOs suggest that both receptors suppress NO-GC; on the other hand, elevated Arc/Arg3.1 levels in MR^{TMX}cKOs and MRGR^{TMX}cKOs but not GR^{TMX}cKOs suggest that MR suppresses Arc/Arg3.1 expression levels. Conclusively, MR through GR inhibition may define the threshold for hemodynamic responses for LTP and auditory neural gain associated with GC-A.

KEYWORDS

glucocorticoid receptor, mineralocorticoid receptor, NO-GC, GC-A, cognition

Highlights

- Baseline MR suppresses GR levels.
- Enhanced GR suppresses presynaptic hippocampal excitability.
- Baseline MR and GR suppress hippocampal NO-GC.
- Baseline MR inhibits Arc/Arg3.1.
- Enhanced GR increases GC-A, LTP, and auditory neural gain.

Introduction

Hearing dysfunction in response to age, acoustic trauma, or posttraumatic stress has been linked with different stress responses possibly influencing cognitive functions (Meltser and Canlon, 2011; Canlon et al., 2013; Basner et al., 2014; Jafari et al., 2019; Mazurek et al., 2019; Wang and Puel, 2020; Nadhimi and Llano, 2021). During stress, the naturally occurring glucocorticoid hormones (corticosterone in rodents and cortisol in humans) activate two different receptors. Besides aldosterone, the mineralocorticoid receptor (MR) shows high affinity to glucocorticoids, while the glucocorticoid receptor (GR) gradually becomes occupied by stress-induced high glucocorticoid concentrations (see for a review de Kloet et al., 2018). Both MR and GR actions need to be in balance for maintenance of homeostasis and health (see for a review de Kloet et al., 2018). The expression of MR dominates in glutamatergic neurons of the hippocampus, while GR is more ubiquitously expressed in the CNS (Reul and de Kloet, 1985; Chao et al., 1989; de Kloet et al., 2005; McEwen et al., 2016). To better understand the thus far elusive relationship between balanced stress receptor activity, hearing, and cognition, we previously employed a Cre/loxP-based approach in which a tamoxifen (TMX)-inducible Cre is expressed in the forebrain and hippocampus *via* the CaMKIIα promoter (Dragatsis and Zeitlin, 2000; Wang et al., 2013). The resulting MRGR^{CaMKIIαCreERT2} double knockout (MRGR^{TMX}cKO) lacked MR and GR expression in frontal brain and in the hippocampal region, while cochlear MR and GR expression was unchanged (Marchetta et al., 2022). Remarkably, the examination of MR^{CaMKIIαCreERT2} single knockout (MR^{TMX}cKO), GR^{CaMKIIαCreERT2} single knockout (GR^{TMX}cKO), and MRGR^{TMX}cKO mice unraveled unfavorable effects of central MR deletion and favorable effects of central GR deletion on peripheral auditory nerve processing (Marchetta et al., 2022), suggesting a top-down effect of central MR and GR activities. We reconsidered that the coordinated function of central MR and GR are predominantly predicted to influence the extinction (MR) and consolidation (GR) of long-term potentiation (LTP; see for a review de Kloet et al., 2018). Any adaptive central auditory responses following sound enrichment or acoustic trauma were found to be accompanied by increased hippocampal LTP levels (Matt et al., 2018; Likhtik and Johansen, 2019; Knipper et al., 2020; Marchetta et al., 2020b; Knipper et al., 2022; Manohar et al., 2022; Savitska et al., 2022; Zhang et al., 2022). The association between adaptive central auditory responses following sound enrichment or auditory trauma and LTP changes is suggested to be triggered through corticothalamic feedforward and feedback circuits (Antunes and Malmierca, 2021; Knipper et al., 2022). This encouraged us to investigate the influence of changed peripheral auditory processing in MR^{TMX}cKO and GR^{TMX}cKO (Marchetta et al., 2022) on central auditory responses of these animals in relation to short- and long-term hippocampal plasticity responses. Since the stress-induced drop in central adaptive auditory responses is restorable by inhibition of 3′,5′-cyclic guanosine monophosphate (cGMP) hydrolyzing phosphodiesterase 9A (Savitska et al., 2022), we additionally asked to what extent cGMP-producing nitric oxide (NO)-sensitive (NO-GC), encoded by the mammalian *Gucy1a1*, *Gucy1a2,* and *Gucy1b1* genes, and membrane-bound (GC-A) guanylyl cyclase, encoded by the mammalian *Npr1* gene, may correlate with changes in auditory or hippocampal circuits acutely induced by MR and/or GR deletion. This is of particular interest because cGMP plays an important role in AMPA and NMDA receptor signaling, facilitating synaptic plasticity and memory formation (Giesen et al., 2022), specifically including functions of NO-GC (Koesling et al., 2016; Nelissen et al., 2021, 2022) and possibly also GC-A (Kroker et al., 2012). As AMPA receptor surface diffusion during LTP was shown to be changed by GR activation (Groc et al., 2008), the mRNA of activity-regulated cytoskeletal protein (Arc, also known as Arg3.1) that controls AMPA receptor trafficking during LTP/long-term depression (LTD; Guzowski et al., 1999; Plath et al., 2006; Kuipers et al., 2016) was analyzed.

Based on the herein presented findings, we conclude that balanced basal MR and GR activities play a critical role in setting the threshold for presynaptic reactivities in the hippocampus. Basal MR expression may suppress GR expression levels, which enables higher levels of LTP. This dynamic setting of MR and GR activity appears to keep the threshold for presynaptic excitability (PPF through GR), the NO-GC level (through MR and GR), and neuronal Arc/Arg3.1 level (through MR) low. The elevation of GR levels may lead to elevated hippocampal GC-A and Arc/Arg3.1, elevated LTP, and elevated central auditory neural gain. We conclusively suggest that GR-induced changes in GC-A activity are involved in auditory neural gain, and thus may provide a means for altering corticofugal top-down feedback.

Materials and methods

Animals

Animal care, use, and experimental protocols correspond to national and institutional guidelines and were reviewed and approved by University of Tübingen, Veterinary Care Unit, and the Animal Care and Ethics Committee of the regional board of the Federal State Government of Baden-Württemberg, Germany. All experiments were performed according to the European Union Directive 2010/63/EU for the protection of animals used for experimental and other scientific purposes. In-house bred mice were kept in a specified pathogen free

Abbreviations: Arc/Arg3.1, activity regulated cytoskeletal protein; ABR, auditory brainstem response; BW, body weight; cGMP, 3′,5′-cyclic guanosine monophosphate; FV, fiber volley; fEPSP, field excitatory postsynaptic potential; GC, glucocorticoids; GR, glucocorticoid receptor; GRE, glucocorticoid response element; GR^{TMX}cKO, GR^{CaMKIIαCreERT2} knockout; GC-A, guanylyl cyclase A; HFS, high-frequency stimulation; HPA, hypothalamus-pituitary–adrenal; ISI, interstimulus interval; LTD, long-term depression; LTP, long-term potentiation; MR, mineralocorticoid receptors; NO-GC, nitric oxide (NO)-sensitive (soluble) guanylyl cyclase; MR^{TMX}cKO, MR^{CaMKIIαCreERT2} knockout; MRGR^{TMX}cKO, MRGR^{CaMKIIαCreERT2} knockout; PPF, paired-pulse facilitation; SEM, standard error of the mean; TMX, tamoxifen.

facility at 25°C on a 12/12 h light/dark cycle with average noise levels of around 50–60 dB SPL. The weight of the animals was recorded on each experimental day.

In the present study, three TMX-inducible conditional knockout mouse lines were studied, in which MR and/or GR were deleted mainly in the forebrain. MRGR^{TMX}cKO, MR^{TMX}cKO, GR^{TMX}cKO and corresponding control animals were generated as previously described (Marchetta et al., 2022). In brief, homozygous floxed MR, GR (Berger et al., 2006; Erdmann et al., 2007), or MRGR lines, in which exon 3 of *Mr* and/or *Gr* is flanked by *loxP* sites, were crossed with a CaMKIIα CreERT2 line (kindly provided by Prof. Günther Schütz). After confirmation of normal hearing function, all mice received an intraperitoneal injection of 1 mg TMX in 100 µL TMX-solution (Sigma-Aldrich, T-5648, Munich) twice a day for five consecutive days at the lowest age of approximately eight weeks. 50 mg TMX were dissolved in 500 µL Ethanol abs. (Merck, Darmstadt) and 4.5 mL sunflower oil (Sigma-Aldrich, S-5007). After the last injection, animals were allowed to recover in their home cages for four weeks before experiments started. For the respective transgenic mouse line, homozygous floxed Cre-negative littermates, which also received TMX injections, were used as controls. For all lines, mice of both sexes ranging between 1.8 months (beginning of the experiment) and 7.9 months (end of the experiment) were used. The genetic status of all mouse lines was confirmed by genotyping using gene-specific PCR protocols.

Hearing measurements

Mice were anesthetized with an intraperitoneal injection of a mixture of Fentanyl (0.05 mg/kg bodyweight (BW), Fentanyl-Hameln, Hameln Pharma plus, Hameln, Germany), Midazolam (5.0 mg/kg BW, Midazolam-hameln®; Hameln Pharma plus), Medetomidin (0.5 mg/kg BW, Sedator®; Albrecht, Aulendorf, Germany) and atropine sulfate (0.2 mg/kg BW, B. Braun, Melsungen, Germany) diluted with water ad. inj. (Ampuwa, Fresenius KABI, Bad Homburg, Germany) to an injection volume of 10 mL/kg BW. Additional doses of anesthetics were administered if needed. The anesthesia was antagonized after the measurements by a subcutaneously administered mixture of Naloxon (1.2 mg/kg BW, Naloxon-hameln®; Hameln Pharma plus), Flumazenil (0.55 mg/kg BW, Flumazenil®; Fresenius KABI), and Atipazemol (2.5 mg/kg BW, Antisedan®; VETOQUINOL GmbH, Ravensburg, Germany) diluted with water ad. inj. (Ampuwa) to an injection volume of 10 mL/kg BW.

The anesthetized mice lay on a pre-warmed resting pad (37°C) in a soundproof chamber (IAC 400-A, Industrial Acoustics Company GmbH, Niederkrüchten, Germany). Auditory brainstem responses (ABRs) in anesthetized mice were evoked by short-duration sound stimuli with the same stimulus parameters for all groups. The ABRs represent the summed activity of neurons in distinct anatomical structures along the ascending auditory pathway recorded from subcutaneous cranial electrodes. A microphone (Bruel & Kjaer 4191, Naerum, Denmark) was used to calibrate and record the acoustic stimuli. ABR thresholds were elicited with click stimuli (100 µs duration with an FFT mean of 5.4 kHz). The stimulus level was increased stepwise from 10 to 100 dB SPL in 5 dB steps. Stimuli were generated with an I-O-card (PCI-6052E, PCI-6251, or PCIe-6259, National Instruments, Austin, Texas, United States) in an IBM compatible computer. The SPL of the stimuli was modulated by custom-made amplifier and attenuator systems (Wulf Elektronik, Frankfurt, Germany). The measured signals were band-pass filtered from 200 Hz to 5 kHz (F1, 6-pole Butterworth hardware Filter, Wulf Elektronik) and amplified by 100,000. The analog/digital (A/D) rate was 20 kHz. Each stimulus had a recording interval of 16 ms and was directly repeated and averaged up to 512 times.

Field excitatory postsynaptic potential recordings in hippocampal slices

Extracellular field excitatory postsynaptic potential (fEPSP) recordings were performed according to standard methods as previously described (Matt et al., 2011; Chenaux et al., 2016). In brief, 400 µm thick hippocampal brain slices were coronally sectioned on a vibratome (Leica VT 1000S, Wetzlar, Germany) in ice-cold dissection buffer (mM): 127 NaCl, 1.9 KCl, 1.2 KH2PO4, 26 NaHCO3, 10 D-glucose, 2 MgSO4, and 1.1 CaCl2, constantly saturated with 5% CO2 and 95% O2 (pH 7.4). Slices were incubated in carbogenated artificial cerebrospinal fluid (in mM: 127 NaCl, 1.9 KCl, 1.2 KH2PO4, 26 NaHCO3, 10 D-glucose, 1 MgSO4, 2.2 CaCl2; pH 7.4) for 1 h at 30°C and afterwards stored at room temperature. Recordings were performed in a submerged-type recording chamber (Warner Instruments, Holliston, MA, United States). Stimulation (TM53CCINS, WPI, Sarasota, FL, United States) and recording (artificial cerebrospinal fluid-filled glass pipettes, 2–3 MΩ) electrodes were positioned in the stratum radiatum to record Schaffer collateral fEPSPs. Signals were amplified with an Axopatch 200B (Molecular Devices, San Jose, CA, United States), digitized at 5 kHz with an ITC-16 (HEKA, Reutlingen, Germany) and recorded using WinWCP from the Strathclyde Electrophysiology Suite. Stimuli (100 µs) were delivered through the stimulus isolator (WPI). For each individual slice the strength of the stimulation (typically between 30 and125 µA) was chosen to evoke 40%–60% of the maximal response, defined by initial fEPSP slope. Only slices that showed stable fiber volley (FV) and fEPSP were used for further recording. The same stimulus intensity was applied during baseline recording (0.067 Hz, 20–30 min) and during induction of long-term potentiation (LTP) using 100 stimuli during 1 s (100 Hz). The baseline was determined by averaging fEPSP initial slopes from the period before the tetanic stimulation (at least 15 min of stable recording). The level of LTP was determined by averaging fEPSP slopes from the period between 50 and 60 min after the high-frequency stimulation (HFS). Before the tetanic stimulation, each slice was used to record paired-pulse facilitation [PPF, 10–20–50–100–200–500 ms interstimulus interval (ISI) at the same stimulation strength as LTP recordings]. The paired-pulse ratio of EPSP2/EPSP1 slope and amplitude at each ISI were defined per slice and mean values per group were plotted. EPSP1 was calculated as an average of EPSP1s from all ISIs for each single slice.

Four traces were averaged for each single data point analyzed.

Riboprobe synthesis

To amplify Arc/Arg3.1, we used the following primers: for: 5′-CGA AGT GTC CAA GCA GGT G-3′; and rev: 5′-TGA TGG CAT AGG GGC TAA CA-3′. To amplify NO-GC, we used the following primers: for: 5′-ATC CTC TTC AGC GGC ATT GTG-3′ and rev: 5′-TGC ATT

GGT TCC TTC TTG CCC-3′. To amplify GC-A, we used the following primers: for: 5′-TGT GAA ACG TGT GAA CCG GA-3′ and rev: 5′-AGG CGG ATC GTT GAA AGG G-3′. To amplify GR, we used the following primers: for: 5′-TCC CCC TGG TAG AGA CGA AG-3′ and rev: 5′-GGC TGG TCG ACC TAT TGA GG-3′. To amplify MR, we used the following primers: for: 5′-GAG ATG AGG CTT CTG GGT GT-3′ and rev: 5′-CAG GAT CAT GGA CGG GGA TG-3′. These fragments were cloned into the pCR II Topo vector (Invitrogen, Karlsruhe, Germany) and their nucleotide sequences were verified by an automated sequencer. Plasmids were isolated using QIAprep Spin Miniprep Kit from Qiagen (Hilden, Germany). Complementary strands for sense and antisense riboprobes were transcribed from either Sp6 or T7 RNA polymerases and labeled using rNTP mix containing digoxigenin labeled uridine triphosphates. All restriction enzymes, RNA polymerases and digoxigenin-labeled rNTP were purchased from Roche Diagnostics (Mannheim, Germany).

Co-localization of mRNA and protein in brain sections

A separate subset of mice from those used for *in vitro* electrophysiology measurements was deeply anesthetized with CO2 and then sacrificed by decapitation. Brain tissue was prepared and sectioned with a vibratome at 60 µm, as previously described (Singer et al., 2013a, 2016). mRNA and protein were co-localized on free-floating brain sections as previously described (Singer et al., 2013a). In brief, following prehybridization for 1 h at 37°C, sections were incubated overnight with NO-GC, GC-A, Arc/Arg3.1, MR, or GR riboprobes at 56°C, incubated with anti-digoxigenin antibody conjugated to alkaline phosphatase (anti-Dig-AP, Roche, 11093274910), and developed as previously described (Singer et al., 2013a). For protein detection, streptavidin–biotin was blocked according to the manufacturer's instructions (Streptavidin–Biotin Blocking Kit, Vector Laboratories, Newark, CA, United States) after blocking endogenous peroxidase. Sections were incubated overnight at 4°C with the primary antibody against parvalbumin (Abcam, Berlin, Germany, anti-rabbit, 1:500, ab11427) as a marker for inhibitory neurons, followed by incubation with the secondary antibody (biotinylated goat anti-rabbit, Vector Laboratories, BA-1000) and chromogenic detection (AEC, 3-amino-9-ethylcarbazole, Vector Laboratories, SK-4200). For microscopy (BX61 microscope, Olympus, Hamburg, Germany) evaluation photographs of the hippocampus and auditory cortex were taken at a bregma position between −1.58 and −2.18 with a bright-field camera (DP 71, Olympus) for detection of mRNA and protein, without adjusting the picture frame or the plane of focus.

Identification of GRE binding sites in NO-GC and GC-A upstream regions

To identify potential glucocorticoid-responsive elements (GRE) binding sites in NO-GC and GC-A upstream regions, Benchling was used to import and annotate the following genes: *Gucy1a1*, *Gucy1a2, Gucy1b1,* and *Npr1*. Subsequently, known sequences for GRE binding sites were aligned (see Supplementary Methods). These sequences were based on JASPAR and sequences previously identified by Meijsing et al. (2009), Polman et al. (2013), and van Weert et al. (2017).

Quantification and statistical analysis

All statistical information and *n*-numbers can be found in the results section and in Supplementary Table S1. Data was tested for a normal distribution (the Shapiro–Wilk normality test, $\alpha = 0.05$). Differences of the means were compared for statistical significance either by unpaired two-tailed Student's *t*-test (parametric)/Mann–Whitney *U*-test (non-parametric), repeated measurement (RM) 2-way ANOVA, 2-way ANOVA (parametric) with $\alpha = 0.05$ and correction for type 1 error using Sidak's and Bonferroni's multiple comparisons tests.

In figures, significance and a trend for significance is indicated by asterisks [(*) $p < 0.08$, * $p < 0.05$, ** $p < 0.01$, *** $p < 0.001$]. n.s. denotes non-significant results ($p \geq 0.08$). The *p*-values of the 2-way ANOVAs refer to the main effect of the genotype.

ABR analysis

For each individual ear, the peak input–output function for amplitude of the click-ABR measurements were averaged for intensities between 0 and 40 dB relative to threshold (re thr) and analyzed as previously described (Chumak et al., 2016).

Two peak classes were selected: (1) early peaks (at 1.2–1.8 ms, wave I), interpreted as the sum of the first stimulus-related action potential within the auditory nerve, and (2) delayed peaks (at 4.1–4.9 ms, wave IV), the response from the auditory midbrain.

Wave IV/I ratio was calculated by dividing the ABR wave IV amplitude by ABR wave I amplitude for individual animals at all intensities higher than 5 dB (re thr). For each individual ear, stimulus levels of 10–30 dB, 35–55 dB, and 60–80 dB re thr were averaged to yield three repeated measurements for fibers of different sensitivity and spontaneous rate [high-spontaneous rate (SR) low-threshold fibers, middle-SR, and low-SR high-threshold fibers; Bharadwaj et al., 2014]. Inter-peak latency growth functions were calculated by subtracting the ABR wave I latency from the ABR wave IV amplitudes for individual animals for increasing stimulus levels with reference to the ABR thresholds (from higher than 5 dB to a maximum of 80 dB re thr) and grouped into stimulus level ranges as described (10–30 dB, 35–55 dB, and 60–80 dB). For statistical analyses, single ears are used as sample size.

fEPSP recordings in hippocampal slices

Data was analyzed and processed using Clampfit 10 (Molecular Devices) and Excel (Microsoft). The data presented per experimental group/condition contained (in addition to mean ± SEM) single dots showing the fEPSP slope values for each individual brain slice. The *n* indicates the number of slices and animals (slices/animals) used in the analysis. Recordings which did not show stable baseline or shifting ±2% from the average in the baseline recording were not included in the statistical analysis. For statistical analyses, single slices are used as sample size.

Co-localization of mRNA and protein and immunohistochemistry in brain sections

Brain sections were quantified by integrating density values of color pixels for each single specimen using ImageJ software (NIH, Bethesda,

MD; United States). Quantification of the mRNA from the double method staining was performed by artificially separating the image into three defined color "channels," which were selected as the average signal from all groups of the background, the protein staining, and the mRNA staining. A detection threshold was then defined in the mRNA color "channel" which was consistent across all groups and genotypes. The integrated density was then calculated for each image and all images are averaged for one animal. The density values of all specimens stained within the same experiment were then normalized to the group mean (i.e., all hippocampal brain sections stained in the same experiment gave an average value of 1.0). This correction allowed for compensation of the high intertrial variation of staining intensity. All sections from one mouse were then averaged and entered the statistical evaluation as $n = 1$. When no quantifiable staining could be measured, the group was excluded from analysis.

Results

Acute deletion of MR in adult mice leads to elevated GR expression levels

Global and conditional MR deletion affected the expression profiles of GR in central neurons (Berger et al., 2006; Erdmann et al., 2007). We questioned if comparable effects are observed after TMX-induced acute deletion in MR and GR^{TMX}cKOs. Brain sections of MR and GR^{TMX}cKOs were exposed to GR- or MR-specific riboprobes. Data was evaluated quantitively as previously described (Singer et al., 2013a; Eckert et al., 2021). As exemplarily shown in Figure 1A, MR^{TMX}cKOs had a significantly higher expression of GR mRNA in the hippocampus in comparison to their WT controls [Figure 1A, unpaired two-tailed student's *t*-test, $t(6) = 3.530$, $p = 0.0124$, $n = 4$ mice each]. In contrast, conditional ablation of GR did not significantly affect the MR mRNA abundance in the hippocampus in comparison to WT controls [Figure 1B, unpaired two-tailed student's *t*-test, $t(8) = 1.993$, $p = 0.0814$, $n = 5$ mice each]. The finding confirms that the differential GR expression which was observed in global and conditional MR/GR double- and single-KOs (Berger et al., 2006; Erdmann et al., 2007) is also observed in TMX-induced MR^{TMX}cKOs. This proves the validity of the CaMKIIα-based TMX-inducible *Cre*^{ERT2}/*loxP* approach for central deletion of MR and GR.

This also means that the MR^{TMX}cKO phenotype should not only be interpreted with respect to the central MR deletion but also from the perspective of increased GR expression levels.

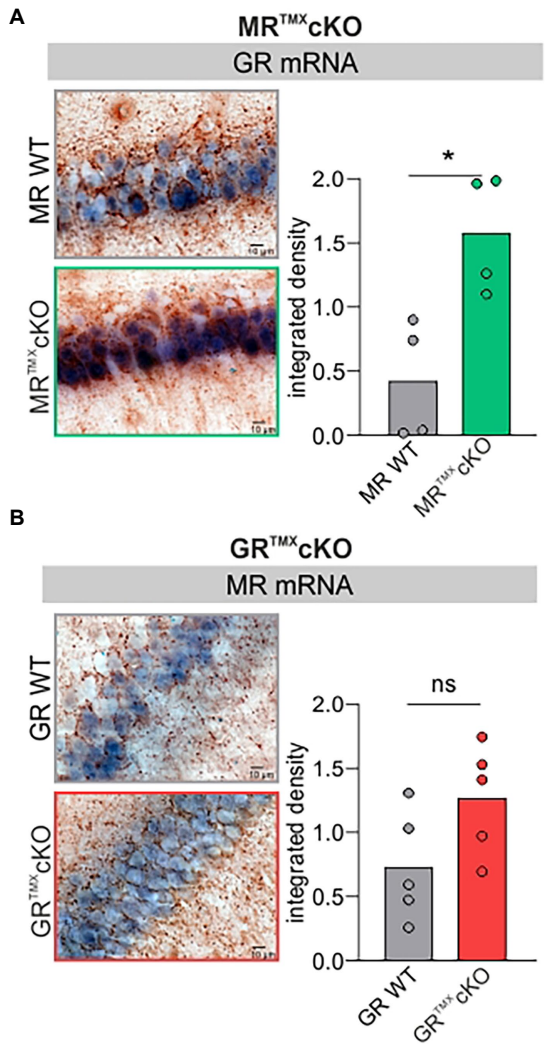

FIGURE 1
GR and MR mRNA expression level (blue) in the CA1 region of the hippocampus of MR and GR^{TMX}cKO mice. **(A)** MR^{TMX}cKO (green) mice showed significantly higher GR mRNA expression levels in comparison to their WT controls (gray). **(B)** GR^{TMX}cKO (red) mice showed no difference in MR mRNA expression levels in comparison to their WT controls (gray). Mean±SEM. ns=p>0.08, *=p<0.05.

Differential impact of central MR and/or GR deletion on central auditory neural gain, PPF, and LTP

We next analyzed the central auditory responses (ABR wave IV) relative to the altered cochlear auditory processing (ABR wave I) of MR^{TMX}cKOs, GR^{TMX}cKOs, and MRGR^{TMX}cKOs mice (Figure 2, left). Raw ABR wave amplitude and latency values were consistent with previously-reported data for all genotypes (data not shown; Marchetta et al., 2022). ABR wave IV/I ratio (input/output function) analysis for stimulus ranges corresponding to auditory fibers of different sensitivity and response range [10–30 dB, 35–55 dB, and 60–80 dB re thr for high-spontaneous rate (SR), middle-SR, and low-SR auditory fibers, respectively (Bharadwaj et al., 2014)] revealed that the reduced auditory nerve response of MR^{TMX}cKOs could be centrally compensated through neural gain [higher ABR wave IV/I ratio; Figure 2A, left, repeated measurement (RM) 2-way ANOVA, $F(1, 49) = 7.652$, $p = 0.008$, Sidak's multiple comparisons test, MR WT: $n = 30$ ears from 16 mice, MR^{TMX}cKO: $n = 21$ ears from 14 mice]. Accordingly, the inter-peak latency of MR^{TMX}cKO mice reached similar values in comparison to their WT controls (Supplementary Figure S2A). On the other hand, the TMX-mediated deletion of central GR resulted in slightly reduced ABR wave IV/I ratio indicating less neural gain, although this effect was not statistically significant (Figure 2B, left, RM 2-way ANOVA, $F(1, 28) = 3.284$, $p = 0.0807$, Sidak's multiple comparisons test, GR WT: $n = 14$ ears from 8 mice, GR^{TMX}cKO: $n = 16$ ears from 8 mice), despite the enhanced/disinhibited ABR wave amplitudes in these conditional mutants (Marchetta et al., 2022). The inter-peak latency of GR^{TMX}cKO mice was significantly shorter in comparison to their WT controls, particularly above 30 dB (Supplementary Figure S2B). Finally, the

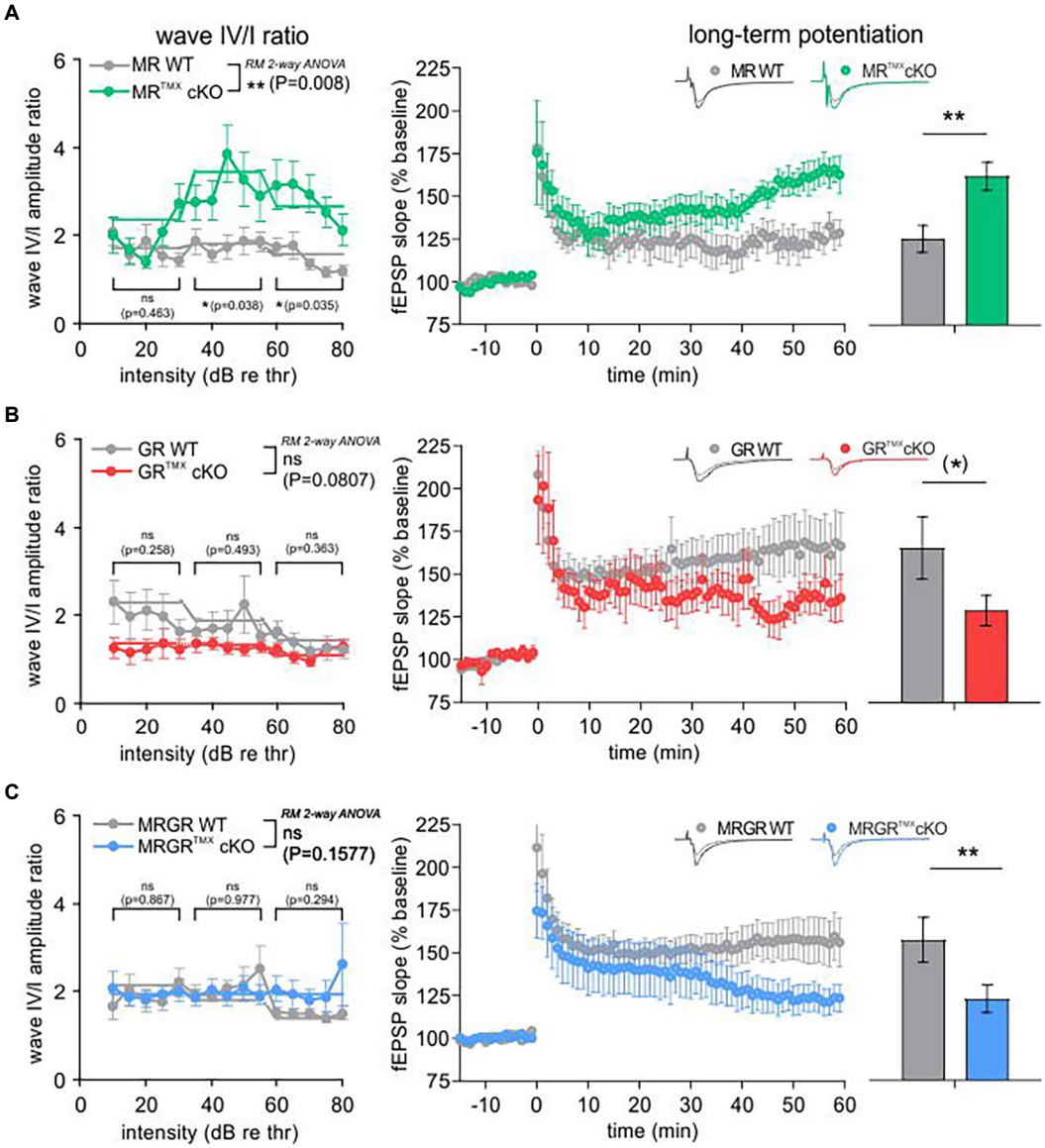

FIGURE 2
ABR wave IV/I amplitude ratio and LTP of MR^{TMX}cKO, GR^{TMX}cKO, and MRGR^{TMX}cKO in comparison to their WT controls. **(A)** MR^{TMX}cKOs (green) had a significantly higher wave IV/I ratio in comparison to their WT controls (gray). The MR^{TMX}cKOs had significantly higher LTP in comparison to their WT controls. **(B)** GR^{TMX}cKOs (red) had a slightly, non-significantly lower wave IV/I ratio compared to their WT controls (gray). GR^{TMX}cKOs had a trend toward lower LTP in comparison to their WT controls. **(C)** MRGR^{TMX}cKOs (blue) did not show a significant difference of wave IV/I ratio in comparison to their WT controls (gray). Contrary to this, MRGR^{TMX}cKOs had significantly lower LTP in comparison to their WT controls. Mean±SEM. ns=p>0.08, (*)=p<0.08, *=p<0.05, **=p<0.01.

conditional deletion of both MR and GR in the MRGR^{TMX}cKOs, resulted in an unchanged ABR wave IV/I ratio (Figure 2C, left, RM 2-way ANOVA, $F(1, 42) = 0.1546$, $p = 0.6962$, MRGR WT: $n = 19$ ears from 11 mice, MRGR^{TMX}cKO: $n = 25$ ears from 14 mice). We interpret this as an intermediate response resulting from counterbalancing effects of the individual cKOs. In addition, the inter-peak latency of MRGR^{TMX}cKO mice was equally long as for their WT controls (Supplementary Figure S2C). As we assume that in our mouse model MR and GR are not deleted in the ascending auditory pathway (cochlea, brainstem), the alterations observed in auditory neural gain are likely a top-down effect resulting from the forebrain deletion of MR and/or GR, as also described to be the case for blood pressure changes resulting from MR overexpression under the CamKIIα promoter (Lai et al., 2007).

The predicted influence of stress and hippocampal LTP on central auditory adaptive responses (Singer et al., 2013b; Jafari et al., 2018; Matt et al., 2018; Savitska et al., 2022; Zhang et al., 2022) motivated us to study hippocampal LTP on acute coronal brain slices in the individual and compound MR and GR^{TMX}cKO models (Figure 2, right). LTP was induced by tetanic stimulation (1 s, 100 Hz) of CA3 Schaffer's collateral axons, and fEPSPs were recorded from the dendrites of CA1 pyramidal cells that form synaptic contacts with CA3 neurons (Matt et al., 2018). LTP, determined by averaging fEPSP slopes from the period between 50 and 60 min after the high-frequency stimulation (HFS), was significantly higher after 50–60 min with changes seen from ~35 min onwards in MR^{TMX}cKOs (Figure 2A, right, green; 162.16% ± 8.25%, $n = 9$ slices from 5 animals) in comparison to WT controls [Figure 2A, right, gray;

125.44% ± 7.90%, $n = 7$ slices from 4 animals; Mann–Whitney U-test, $U(117.8, 167.9) = 6$, $p = 0.0093$], while the GR^{TMX}cKOs had a trend toward lower LTP in comparison to WT controls [Figure 2B, right, GR^{TMX}cKO, red, 128.96% ± 8.98%, $n = 9$ slices from 6 animals, WT, gray, 165.52% ± 18.27%, $n = 7$ slices from 5 animals; Mann–Whitney U-test, $U(151.0, 124.0) = 12$, $p = 0.0721$]. On the other hand, MRGR^{TMX}cKOs exhibited significantly lower LTP in comparison to their respective WT controls [Figure 2C, right, MRGR^{TMX}cKO, blue, 122.88% ± 8.12%, $n = 13$ slices from 7 animals, WT, gray, 157.30% ± 13.18%, $n = 12$ slices from 6 animals; Mann–Whitney U-test, $U(160.7, 121.3) = 45$, $p = 0.0076$].

To investigate to what extent the differences in central compensation or LTP are associated with differences in the presynaptic state of Schaffer's collaterals in the hippocampus, we studied paired-pulse facilitation (PPF), an indication of presynaptic activity underlying short-term plasticity. PPF, a transient increase in the probability of glutamate release (Zucker and Regehr, 2002), was studied in MR^{TMX}cKO, GR^{TMX}cKO, and MRGR^{TMX}cKO brain slices as described in methods and previous studies (Satake et al., 2012).

The PPF was investigated in each brain slice prior to LTP induction using varying ISIs of 10, 20, 50, 100, 200, and 500 ms and the same stimulation strength that was also used for LTP recordings (Figure 3). The MR^{TMX}cKO mice had a significantly lower PPF, seen in its slope ratio, in comparison to their WT controls [Figure 3A, green vs. gray circles, 2-way ANOVA, $F(1, 78) = 14.48$, $p = 0.0003$, Sidak's multiple comparisons test, MR^{TMX}cKO: $n = 8$ slices from 5 animals, WT: $n = 7$ slices from 4 animals]. In contrast, in GR^{TMX}cKO mice, the PPF slope ratio was not significantly different from their respective controls [Figure 3B, red vs. gray circles, 2-way ANOVA, $F(1, 78) = 2.172$, $p = 0.1446$, GR^{TMX}cKO: $n = 9$ slices from 6 animals, WT: $n = 7$ slices from 5 animals]. In MRGR^{TMX}cKO mice also, no difference in PPF slope ratio was observed in comparison to their WT controls [Figure 3C, blue vs. gray circles, 2-way ANOVA, $F(1, 138) = 2.217$, $p = 0.1388$, MRGR^{TMX}cKO: $n = 13$ slices from 7 animals, WT: $n = 12$ slices from 6 animals].

We further examined the fEPSP slopes and fiber volley (FV) amplitudes of individual cKOs, in order to ensure that the effects observed in the LTP and PPF were not due to a change in the basal synaptic transmission properties. fEPSP slope or FV amplitudes in MR^{TMX}cKOs (Supplementary Figure S3A), GR^{TMX}cKOs (Supplementary Figure S3B), and MRGR^{TMX}cKOs (Supplementary Figure S3C) were not different from their respective WT controls. Further, the increase in fEPSP slope remained proportional to FV amplitudes and did not differ between the different genotypes (Supplementary Figure S3A–C, bottom). Overall, the findings suggest that basal synaptic transmission properties were unchanged by cKO of MR and/or GR.

In conclusion, the reduced PPF in MR^{TMX}cKO implies that MR coordinates the release probability in the presynapse of hippocampal neurons, possibly through elevation of GR expression levels. We further conclude that the enhanced LTP and ABR wave IV/I ratio in MR^{TMX}cKOs are linked to the reduced suppression of GR expression levels in these mice. In that sense, GR expression levels regulate LTP and auditory neural gain. The lack of effect in GR^{TMX}cKOs and MRGR^{TMX}cKOs is consistent with this notion.

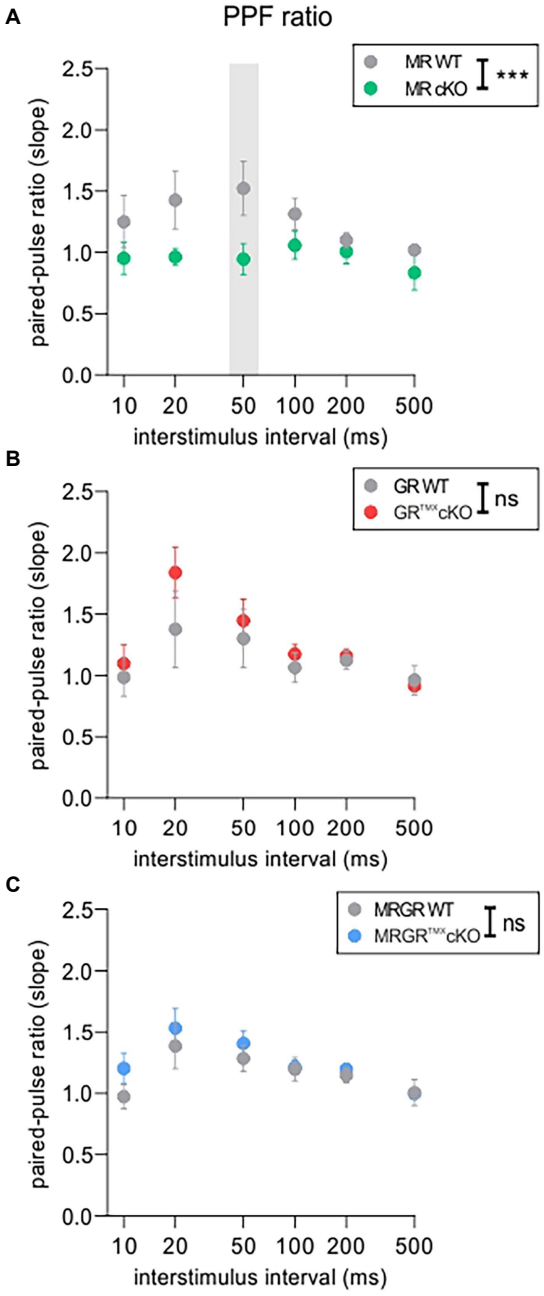

FIGURE 3
PPF as an indicator of short-term plasticity. **(A)** The analysis of PPF in MR^{TMX}cKOs (green) showed a significantly lower paired-pulse ratio of the EPSP2/EPSP1 slope in comparison to WT controls (gray) with a significant post-hoc test at 50ms ISI. **(B)** GR^{TMX}cKOs (red) showed no difference in paired-pulse ratio of the EPSP2/EPSP1 slope in comparison to WT controls (gray). **(C)** MRGR^{TMX}cKOs (blue) showed no difference in paired-pulse ratio of the EPSP2/EPSP1 slope in comparison to WT controls (gray). Mean±SEM. ns=p>0.08, ***=p<0.001.

Deletion of MR and/or GR in the hippocampus differentially affects NO-GC, GC-A, and Arc/Arg3.1 mRNA levels

To better understand the differential impact of acute deletion of MR and GR function on hippocampal LTP and auditory processing, we tested for altered cGMP generator expression profiles, previously hypothesized to provide the missing link between auditory processing and LTP. The mRNA expression profiles of a crucial NO-GC subunit and membrane-bound GC-A were analyzed in the CA1 region of the hippocampus. Two isoforms of NO-GC exist: the more widely expressed NO-GC1 and NO-GC2. Both isoforms build a heterodimer complex with the beta-1 subunit (Koesling et al., 2016), the changes of which parallel that of the alpha subunit (Mergia et al., 2006; Koesling et al.,

2016). Therefore, we targeted NO-GC β1 mRNA for analysis of expression profiles. The recently observed potentiating influence of altered cGMP generator activity on LTP and synaptic AMPA receptor transport activity (Nelissen et al., 2021, 2022) moreover motivated us to correlate levels of cGMP generators with changes of cytoplasmic Arc/Arg3.1, the mRNA of which is targeted to dendrites during LTP/LTD changes in response to neuronal activity (Korb and Finkbeiner, 2011; Goel et al., 2019). *In situ* hybridizations of NO-GC β1, GC-A, and Arc/Arg3.1 mRNA were analyzed in brain sections and quantified in the CA1 region of the hippocampus according to previously established protocols (Matt et al., 2018; Eckert et al., 2021; Figure 4). MR^{TMX}cKOs exhibited significantly higher levels of NO-GC, Arc/Arg3.1, and GC-A mRNA in comparison to their WT controls [Figure 4A, NO-GC left, unpaired two-tailed student's *t*-test, $t(10) = 3.651$, $p = 0.0045$, $n = 6$ mice each; Arc/Arg3.1 mRNA middle, unpaired two-tailed student's *t*-test, $t(6) = 53.63$, $p < 0.0001$, $n = 4$ mice each; GC-A mRNA right, unpaired two-tailed student's *t*-test, $t(8) = 6.874$, $p = 0.0001$, $n = 5$ mice each]. GR^{TMX}cKOs also had significantly higher levels of NO-GC mRNA [Figure 4B, left, unpaired two-tailed student's *t*-test, $t(8) = 3.924$, $p = 0.0044$, $n = 5$ mice each] but strikingly showed no significant differences in levels of Arc/Arg3.1 and GC-A mRNA in comparison to their WT controls [Figure 4B, Arc/Arg3.1 mRNA middle, unpaired two-tailed student's *t*-test, $t(6) = 0.4093$, $p = 0.6965$, $n = 4$ mice each; GC-A mRNA right, unpaired two-tailed student's *t*-test, $t(8) = 0.3671$, $p = 0.7231$, $n = 5$ mice each]. MRGR^{TMX}cKO displayed significantly higher levels of NO-GC mRNA and Arc/Arg3.1 mRNA, as also observed in MR^{TMX}cKOs [Figure 4C, NO-GC, left, unpaired two-tailed student's *t*-test, $t(4) = 11.17$, $p = 0.0004$, $n = 3$ mice each; Arc/Arg3.1 mRNA middle, unpaired two-tailed student's *t*-test, $t(4) = 2.883$, $p = 0.0449$, $n = 3$ mice each]. On the other hand, the GC-A expression levels in the MRGR^{TMX}cKO were significantly reduced [Figure 4C, right, unpaired two-tailed student's *t*-test, $t(4) = 5.941$, $p = 0.0040$, $n = 3$ mice each].

We additionally tested for altered cGMP generator expression levels in the auditory cortex of MR^{TMX}cKO and GR^{TMX}cKO mice in neurons of all cortical layers (layer I–VI). We found that GC-A expression levels in the auditory cortex for both MR^{TMX}cKO and GR^{TMX}cKO mice mirror the findings in the hippocampus (Supplementary Figure S4), hypothalamus, and amygdala (data not shown). NO-GC expression levels in MR^{TMX}cKO and GR^{TMX}cKO mice were also both significantly higher in the auditory cortex in comparison to their respective WT controls (Supplementary Figure S4), as also observed in the hippocampus; however, NO-GC levels throughout the rest of the brain were more variable (data not shown).

In order to test whether MR or GR directly influence NO-GC or GC-A *via* their classical transcriptional cis-activation GR element binding motifs, a search was carried out for MR/GR-specific binding

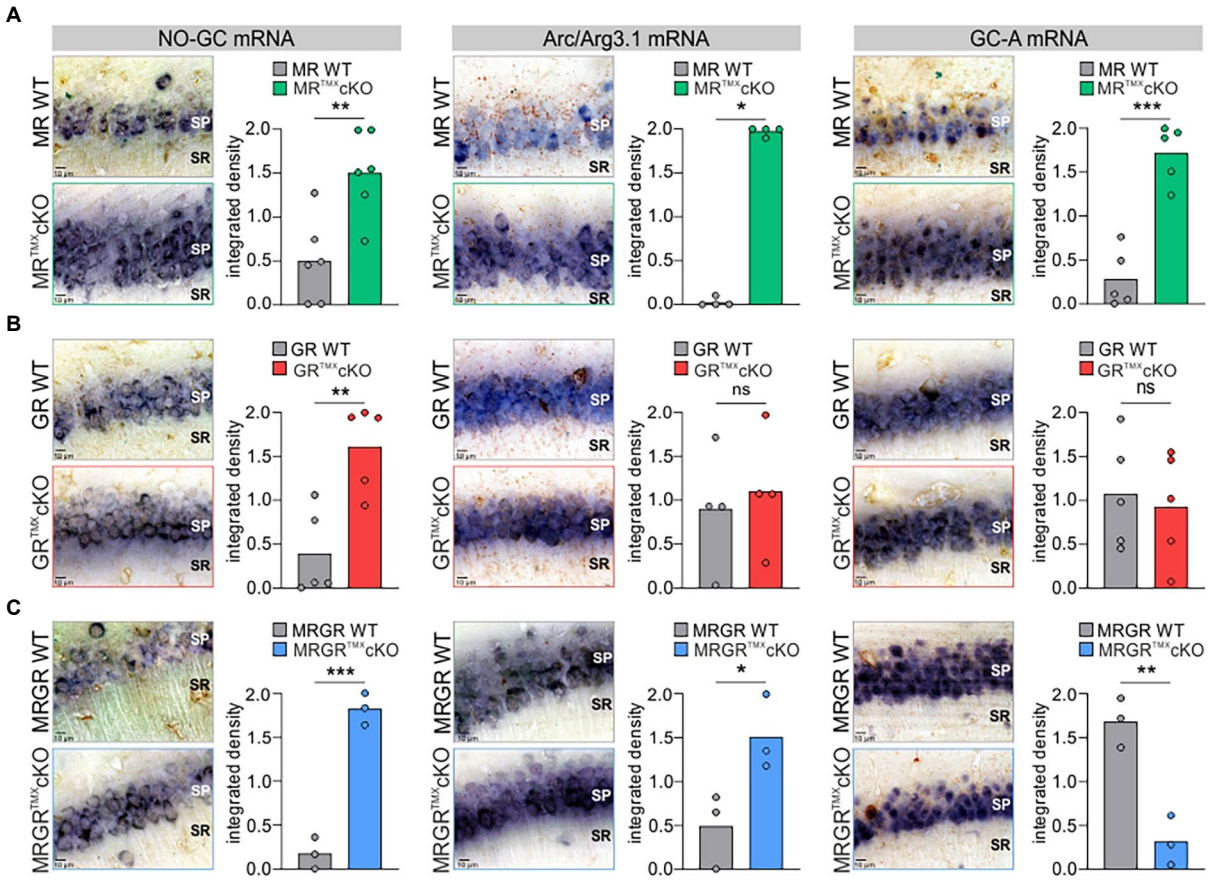

FIGURE 4
NO-GC, Arc/Arg3.1, and GC-A expression in the CA1 region of the hippocampus in MR, GR, and MRGR^{TMX}cKO mice. **(A)** MR^{TMX}cKO (green) mice showed significantly higher levels of NO-GC mRNA expression, Arc/Arg3.1 mRNA expression, and GC-A mRNA expression in comparison to their WT controls (gray). **(B)** GR^{TMX}cKO (red) mice showed significantly higher NO-GC mRNA expression levels, equal Arc/Arg3.1 mRNA expression levels, and equal GC-A mRNA expression levels in comparison to their WT controls (gray). **(C)** MRGR^{TMX}cKO (blue) mice showed significantly higher levels of NO-GC mRNA expression levels and Arc/Arg3.1 mRNA expression, but significantly lower GC-A mRNA expression levels in comparison to their WT controls (gray). Mean. ns=p>0.08, *=p<0.05, **=p<0.01, ***=p<0.001.

motifs (GRE sequences) in the genes encoding NO-GC (i.e., *Gucy1a1*, *Gucy1a2*, *Gucy1b1*) and GC-A (*Npr1*). No relevant GRE sequences could be detected in *Gucy1b1* or *Npr1*. For *Gucy1a1* and *Gucy1a2*, each gene was found to contain a conserved GRE sequence (Supplementary Figures S5, S6). Specifically, for *Gucy1a1*, this GRE sequence (5′-AGGAACACCATGTTCTG-3′) was found to span across the start codon of the transcribed part of the gene. This also included an Atoh sequence (5′-CAGAAGG-3′) 25 bp upstream of the GRE sequence. For *Gucy1a2*, the GRE sequence was a palindrome (5′-AGAACA AACTGTTCT-3′) located near multiple regulatory regions in the intron between exons 3 and 4.

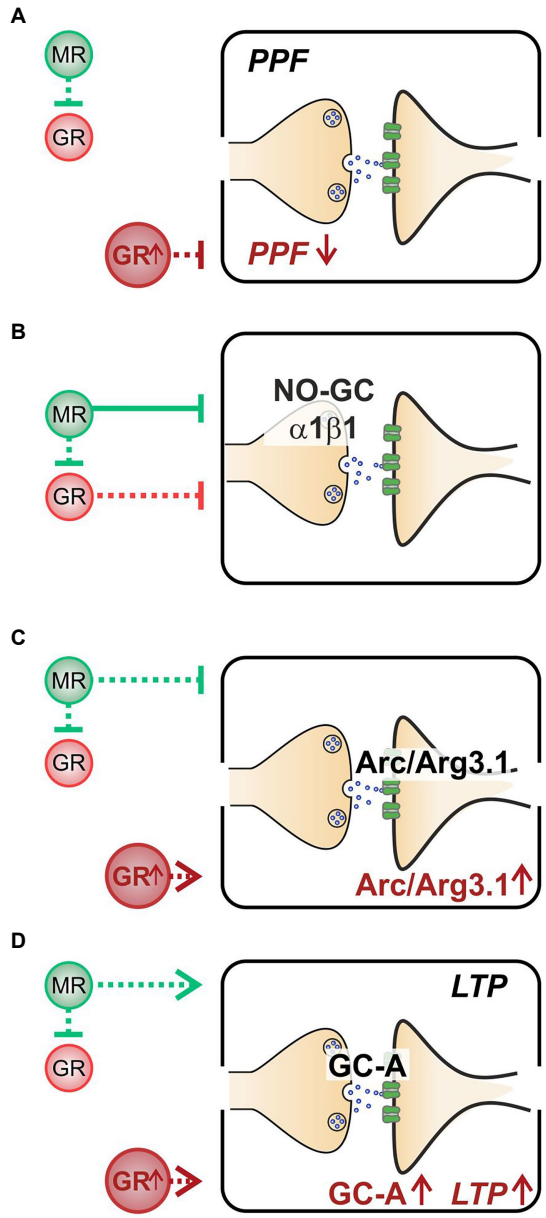

FIGURE 5
A summary of the hypothesized effects of MR and GR in a physiological state and stress state (GR↑). **(A)** When at a normal level, MR inhibits GR (green dashed line, upper half). However, neither MR nor GR affect PPF when at physiological levels. At elevated GR conditions (lower half), PPF is low. **(B)** Both stress receptors exhibit an inhibitory effect on NO-GC expression levels, though the inhibitory effect of MR (green solid line) is stronger than that of GR (red dashed line). **(C)** MR inhibits Arc/Arg3.1 expression levels (green dashed line, upper half); however, when GR is elevated, Arc/Arg3.1 is stimulated (lower half). **(D)** Basal MR stimulates GC-A expression levels and LTP (green dashed line, upper half). Elevated GR expression also leads to elevated GC-A and to elevated LTP (lower half).

Altogether, we here demonstrate that (i) decreased PPF in MR^{TMX}cKOs may be linked to elevated GR expression levels (Figure 5A). (ii) Enhanced NO-GC expression levels in MR, GR, and MRGR^{TMX}cKOs, imply that both receptors' activity is required to effectively suppress NO-GC in hippocampal neurons under physiological conditions, which may be supported by GRE elements responding to both MR and GR (Figure 5B). (iii) Increased Arc/Arg3.1 expression levels in MR^{TMX}cKOs and MRGR^{TMX}cKOs but not in GR^{TMX}cKOs (Figure 5C) do not correlate to LTP as simply. The changes of Arc/Arg3.1 in MRGR^{TMX}cKOs rather point to basal MR activity but not GR activity as being inhibitory to Arc/Arg3.1 levels (Figure 5C). Further, the gradient of Arc/Arg3.1 changes in MR^{TMX}cKOs and MRGR^{TMX}cKOs suggests that elevated GR expression may stimulate Arc/Arg3.1 (Figure 6B). (iv) MR^{TMX}cKOs exhibited an increased GR expression, suggesting that under physiological conditions MR suppresses GR expression. When this suppression is removed in MR^{TMX}cKOs, animals exhibit elevated LTP, GC-A, and ABR wave IV/I ratio. This is not seen in GR^{TMX}cKOs, suggesting that GR may contribute to the empowerment of central neural gain during auditory adaption by controlling the energization through GC-A (Figure 5D).

Discussion

By investigating TMX-induced conditional single or combined deletion of MR and GR in forebrain regions, we show for the first time that central MR and GR activity must be balanced in order to set thresholds for presynaptic activity and central auditory compensation (auditory neural gain). Changes in MR and GR activities result in significant alterations of cGMP generator expression levels in hippocampal neurons. In detail, we suggest (i) baseline hippocampal MR expression levels suppress GR expression. (ii) MR-induced control of GR may set a threshold for presynaptic plasticity. (iii) Basal MR may set a threshold for AMPA receptor trafficking by Arc/Arg3.1, while elevated GR levels may enhance Arc/Arg3.1 expression levels. (iv) Elevated GR may enhance LTP and GC-A expression levels and thereby contribute to LTP-dependent neural auditory gain.

Basal MR activities suppress GR expression

Until now, insights into the physiological function of stress receptors in the adult brain have been limited because global GR KOs (Cole et al., 1995) or early Cre-mediated deletion of GR (Erdmann et al., 2008) is lethal in mice. Also, a global lack of MR induces early postnatal death linked with bodily dehydration (exsiccosis) due to massive renal sodium and water loss (Berger et al., 1998). Early Cre-induced conditional MR deletion is expected to allow long-term adaptation processes to compensate for the absence of MR (Erdmann et al., 2008). Some of these limitations were avoided by the acute TMX-induced deletion of MR and GR studied here. Although in Marchetta et al., 2022, a TMX-induced deletion of MR and GR protein was only shown for the MRGR^{TMX}cKO and not for the single MR^{TMX}cKO and GR^{TMX}cKO, the observed higher GR expression levels in MR^{TMX}cKOs, also previously reported in global or conditional MR^{TMX}cKO mice (Berger et al., 2006; Erdmann et al., 2007), may point

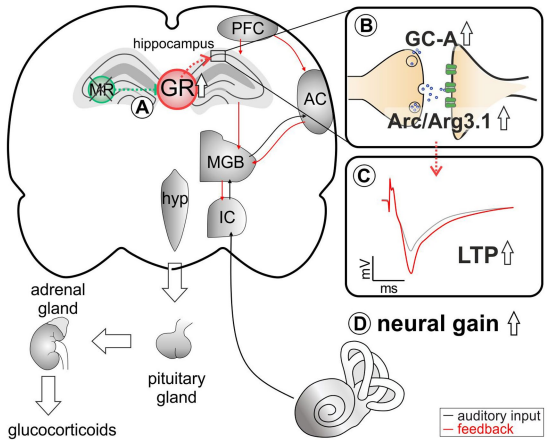

FIGURE 6
An abstract scheme of the pathways that can be concluded from the acute deletion of MR (green). **(A)** MR deletion leads to elevated GR expression levels. **(B)** As a result of elevated GR, an increase in GC-A and Arc/Arg3.1 expression levels in the hippocampus can be observed. **(C)** This change in expression pattern may be functionally related to higher hippocampal LTP. **(D)** Elevated GC-A and Arc/Arg3.1 expression levels and elevated LTP potentially provide a means for top-down mechanisms allowing for auditory neural gain.

to successful targeting of individual receptor expression. We however cannot entirely exclude that the receptor protein may not have been completely deleted (knocked out), at the time of the experiments. Nevertheless, it can be assumed that an upregulation of GR in MR^{TMX}cKOs reflects the previously-described balancing effect of MR on the hypothalamic-pituitary-adrenal (HPA) axis, which stems from central neurons (see for a review de Kloet et al., 2018). Thus, elevated corticosterone levels were reported in conditional GR but not MR mutants (Erdmann et al., 2007), and consistently higher corticosterone levels were measured in GR^{TMX}cKOs but not in MR^{TMX}cKOs (Marchetta et al., 2022). In line with this, normal corticosterone levels—occurring when HPA axis feedback regulation is balanced—are the result of physiologically lower GR levels when baseline MR activities prevent excessive GR expression (Harris et al., 2013), as also concluded from the findings of the present study. This tight control of the HPA axis was recently demonstrated in heterozygous GR mutants that had an enhanced HPA axis activity in response to restraint stress (Harris et al., 2013). Interestingly, the HPA axis overshoot in heterozygous GR mutants in response to stress was counterbalanced through an overexpression of MR in these heterozygous GR mutants (Harris et al., 2013). Apparently, MR exerts a tonic inhibitory influence on HPA axis activity, and thereby determines the threshold of reactivity during stress (see for a review de Kloet et al., 2018).

In conclusion, we suggest that the predicted tonic inhibitory influence of MR on the HPA axis is severely disturbed upon the acute MR or GR deletion.

GR may suppress plasticity in presynaptic hippocampal activity

The TMX-induced deletion of MR in hippocampal regions of MR^{TMX}cKOs resulted in reduced PPF (Figures 3, 5A). Because PPF results from a prior accumulation of residual Ca^{2+} at the synaptic terminal and a lingering effect of Ca^{2+} on the exocytotic Ca^{2+} sensor of releasable vesicles during the second stimulus (as reviewed in Thomson, 2000; Zucker and Regehr, 2002), we expect the probability of vesicular release to be transiently decreased in MR^{TMX}cKOs. This is likely due to increased GR expression in these mutants, as can be concluded from the absence of PPF effects in GR^{TMX}cKO and MRGR^{TMX}cKO (Figure 5A). We thus assume that baseline MR or GR activity alone do not strongly affect presynaptic excitability, but rather that increased GR activity, as occurs in the MR^{TMX}cKOs, suppresses PPF (Figures 1A, 3A, 5A). This finding may contrast findings in which corticosterone application in hippocampal CA1 neurons resulted in a brief increase in miniature excitatory postsynaptic current frequency, a feature described to occur through MR activities (Sarabdjitsingh et al., 2016; de Kloet et al., 2018; Joels, 2018). Further studies are required to clarify this controversy. It is noteworthy to consider the findings in our previous study, which implied a reduced activity at the inner hair cell synapse in the MR^{TMX}cKO (Marchetta et al., 2022). The peripheral depression of activity in MR^{TMX}cKOs is comparable to the here-observed more central changes of reduced release probability in the presynapse of hippocampal neurons (Figure 3; Marchetta et al., 2022). Overall, it gives credence to the hypothesis that balanced central MR and GR activities set the threshold for sensory activity centrally and peripherally by targeting presynaptic mechanisms, possibly through tuning reactivity of top-down auditory feedback loops, which would need to be examined in future studies.

Baseline MR and GR activity keeps NO-GC expression levels low in neurons

It was previously suggested that the complementary functions of MR and GR on presynaptic excitability in hippocampal brain neurons may be the result of distinct transcriptional networks activated by the glucocorticoid receptors (Reul and de Kloet, 1985; de Kloet et al., 2000; Obradovic et al., 2004; Mifsud and Reul, 2016; McCann et al., 2021).

Considering a possible MR/GR driven transcriptional control of pre- or post-synaptic activity by NO-GC, we searched for respective GREs that bind to MR and GR (Shimba and Ikuta, 2020) in the upstream regions of NO-GC subtypes (Shimba and Ikuta, 2020). GREs constitute a palindromic consensus sequence AGAACAnnnTGTTCT (Polman et al., 2013); however, several other GRE-like sequence motifs have been identified (Meijsing et al., 2009; van Weert et al., 2017). We found a GRE in the start codon region of *Gucy1a1* but not in the β1 subunit. In addition to a GRE sequence in *Gucy1a1,* the detection of a 25 bp Atoh sequence moreover suggests that this GRE binding motif is potentially used as a MR-specific recognition site, since GRE sequences that coincide with an Atoh consensus sequence within 400 bp of the GRE have been defined to be MR-specific (van Weert et al., 2017). Additionally, a GRE motif was found in *Gucy1a2* in an intron between exons 3 and 4, apparently completely outside of known regulatory regions, questioning the significance of this potential GRE motif. Regarding the observation of elevated *Gucy1b1* NO-GC expression levels both in single MR^{TMX}cKOs and GR^{TMX}cKOs as well as in double MRGR^{TMX}cKOs, we must question how a potential GRE in the start codon region of *Gucy1a1*, but not β1 subunit may be interpreted in the context of the findings in the present study. While it is necessary to confirm expression changes of *Gucy1a1* in MRGR^{TMX}cKOs in future studies, it is important to consider that changes in β1 subunits went along with changes in α1 expression (Mergia et al., 2006; Koesling et al., 2016). Further, expression levels of NO-GC1 and NO-GC2 in the brain mirror each other (Koesling et al., 2016). Thus, we hypothesize that

under physiological conditions, NO-GC1 (α1, β1) or NO-GC2 (α2, β1) is suppressed by MR and GR (Figure 5B). The elevation of NO-GC expression in MRGR^{TMX}cKOs in comparison to MR^{TMX}cKOs, which exhibit elevated GR expression levels. This may suggest that the inhibitory effect of MR on NO-GC may outweigh that of GR. Using NO-GC1 and NO-GC2 KO mice, the differential localization of NO-GC1 in hippocampal presynapses and NO-GC2 in postsynapses was shown to contribute to LTP through facilitation of presynaptic (NO-GC1) and postsynaptic (NO-GC2) excitability of hippocampal neurons (see for a review Koesling et al., 2016). Although more detailed studies are needed to validate the functionality of the GRE binding motifs, the data nevertheless suggest one possible pathway of how MR and GR could influence NO-GC1 (Figure 5B). This is in line with the observation that steroid hormone receptors exert positive or negative effects on the expression of target genes (Beato and Klug, 2000). Thereby, our findings suggest that baseline MR and GR activity could control the NO-GC abundance, which may be relevant for sensing NO released from eNOS- and nNOS-producing hippocampal cells to influence plasticity events (Son et al., 1996; Hopper and Garthwaite, 2006).

In conclusion, baseline MR and GR activity may keep NO-GC expression levels in neurons low. The target of a specific GRE element found in upstream regions of *Gucy1a1* NO-GC1, the dominant NO-GC isoform in hippocampal presynapses, may need further specification.

Baseline MR may keep Arc/Arg3.1 levels low in neurons

TMX-induced deletion of MR in frontal brain regions resulted in increased Arc/Arg3.1 expression levels in the hippocampus (Figure 4A). As Arc/Arg3.1 expression levels in the hippocampus are elevated in MRGR^{TMX}cKOs but not GR^{TMX}cKOs (Figure 4C), we hypothesize that basal activity of MR but not GR keeps Arc/Arg3.1 expression levels in hippocampal neurons low (Figure 5C). While we hypothesize that basal levels of GR have no effect on Arc/Arg3.1 expression levels, higher levels of GR (as seen in MR^{TMX}cKOs) enhance it (Figure 6B).

Arc/Arg3.1 expression changes have been shown to influence the strength of individual synapses, during both LTP (Rodriguez et al., 2005) and LTD (Guzowski et al., 1999; Plath et al., 2006; Tzingounis and Nicoll, 2006; Park et al., 2008; Waung et al., 2008; Bramham et al., 2010; Yilmaz-Rastoder et al., 2011; Wall and Correa, 2018; Zhang and Bramham, 2021). Moreover it is important to consider that neuronal stimuli induce the rapid transcription of the Arc/Arg3.1 gene (within 5 min; Ramirez-Amaya et al., 2005) and translocation of its mRNA from the nucleus to the cytoplasm (within 30 min; Guzowski et al., 1999). From the cytoplasm, Arc/Arg3.1 mRNA incorporates into a large ribonucleoprotein complex that is actively transported along the dendrite (Dynes and Steward, 2007). From the pre-existing Arc/Arg3.1 mRNA pool in dendrites, a selected pool is translated rapidly by acute neuronal activity, changing surface expression of AMPA receptors (Hedde et al., 2021). The present study may indicate that baseline MR levels influence the level of Arc/Arg3.1 mRNA in the cytoplasm of pyramidal neurons. In addition, when the control of GR expression by MR is lost (as in MR^{TMX}cKOs), Arc/Arg3.1 expression levels are enhanced more than in MRGR^{TMX}cKOs. This indicates that elevated GR levels may stimulate the level of Arc/Arg3.1 mRNA in the cytoplasm of pyramidal neurons. This makes sense considering that previous studies demonstrated that a selective activation of glucocorticoid receptors promotes lateral diffusion and enhanced surface expression of AMPA receptors in CA1 neurons (Karst and Joels, 2005; Groc et al., 2008; Martin et al., 2009), a feature linked with LTP (Groc et al., 2008). It is therefore feasible that MR—both at basal levels and through control of GR—sets the reactivity for Arc/Arg3.1 mobilization in dendrites and its rapid translation in spines through defining the cytoplasmatic Arc/Arg3.1 mRNA pool.

Elevated GR activity relates to elevated LTP, elevated GC-A, and elevated auditory neural gain

A strong association has been suggested between critical auditory nerve activity and central auditory neural gain, measured *via* enhanced ABR wave IV/I ratio, and plasticity changes in LTP, assessed both through *in vitro* electrophysiology (Marchetta et al., 2020b; Savitska et al., 2022) and through a hippocampus-dependent learning test in animal models (Matt et al., 2018). It has been speculated that a critical input of auditory activity is necessary for the recruitment of a reinforcement process that interacts between the auditory thalamus, prefrontal cortex (PFC), and the hippocampus. Thus, the dorsal aspect of the MGB, which receives input from the primary auditory cortex and projects to higher-order auditory regions (Antunes and Malmierca, 2021; Mease and Gonzalez, 2021), is likely part of the topographically complex connectivity pattern projecting between the medio-dorsal thalamus, the medial PFC, and the hippocampal formation (Bueno-Junior and Leite, 2018). These corticofugal projections from the PFC influence auditory processing at lower levels of the cortical sensory hierarchy and often include activation of mesolimbic areas, such as the basolateral amygdala, the activation of which is involved in top-down feedback reinforcement processes (Asilador and Llano, 2020; Suga, 2020).

The medio-dorsal thalamus/PFC/hippocampal connectivity (see Figure 6) is not only sensitive to stress responses (for review, see Jett et al., 2017), but is also part of the extra-hypothalamic pathways involved in stress-control, emotional states, attention, and vigilance influenced by glucocorticoids (de Kloet et al., 2000, 2019; Wingenfeld and Otte, 2019; Antunes and Malmierca, 2021; Knipper et al., 2022). Interestingly, the TMX-induced deletion of MR in frontal brain regions resulted in enhanced ABR wave IV/I ratio (neural gain) and LTP. If this response were due to increased GR expression resulting from the loss of MR, an acute deletion of GR should result in opposite changes of ABR wave IV/I ratio and LTP. In line, when GR is deleted (as in GR^{TMX}cKOs and MRGR^{TMX}cKOs), animals do not have higher wave IV/I ratio and their LTP is unchanged or lower, respectively, indicating that GR elevation – but not baseline GR levels – contributes to elevated neural gain and LTP. Interestingly, the higher wave IV/I ratio and LTP in MR^{TMX}cKO occurred with an elevation of GC-A expression levels. Also, lower LTP occurred with lower GC-A, as can be seen from MRGR^{TMX}cKOs (Figure 5D). Comparable changes in GC-A were detected not only in the hippocampus but also in the auditory cortex (Supplementary Figure S4) and amygdala. Differences in GC-A activity may thus provide a means for altering corticofugal top-down feedback facilitation processes (Asilador and Llano, 2020; Suga, 2020) and thereby contribute to auditory neural gain.

Oitzl and de Kloet were the first to demonstrate that MRs and GRs mediate the storage of spatial information in a coordinated manner (Oitzl and de Kloet, 1992). Their study suggested that MR promotes the extinction of information, while GR is essential for consolidation. Supporting this, memory storage was impaired when progesterone and

the glucocorticoid antagonist mifepristone was given immediately after the learning trial (Oitzl and de Kloet, 1992), while the MR antagonist spironolactone under the same condition did not affect consolidation but rather retrieval (Oitzl and de Kloet, 1992). Meanwhile, memory storage was shown to be impaired in numerous studies, e.g., when GRs are deleted in the amygdala or hippocampus or when GR antagonists are administered in the hippocampus immediately after learning, prior to consolidation (see for a review de Kloet et al., 1999; Rodrigues et al., 2009; Luksys and Sandi, 2011; Roozendaal and McGaugh, 2011; Schwabe et al., 2012; de Kloet et al., 2018).

Very recently, the treatment of WT mice with a phosphodiesterase 9A inhibitor restored a stress-induced drop of temporal auditory processing and hippocampal LTP (Savitska et al., 2022). This finding can now possibly be linked to elevated auditory neural gain, LTP, and GC-A expression levels. Increased GC-A expression levels here corresponded with elevated GR expression levels when the inhibition of GR was removed in MR^{TMX}cKOs, while expression levels were not elevated in GR^{TMX}cKOs (Figure 4). Indeed, the memory-enhancing phosphodiesterase 9A inhibitor (Kroker et al., 2012) has been suggested to regulate a pool of cGMP that is independent of nNOS (Harms et al., 2019). Other findings suggest that the phosphodiesterase 9A in the brain even preferentially regulates nuclear- and membrane-proximal pools of cGMP, which include the GC-A generated cGMP pools (Patel et al., 2018). Within this framework, the present study links for the first time the recognized function of the GR stress receptors in LTP (de Kloet et al., 2018; Joels, 2018) with the perfusion and blood supply driven metabolism-promoting function of the transmembrane GC-A. GC-A is activated through the atrial natriuretic peptide and brain natriuretic peptide (Potter, 2011) and has meanwhile emerged as a key regulator of energy consumption and metabolism counteracting vasoconstriction by inducing vasodilation (Kuhn, 2016). This role of GC-A has also been linked with neurogenesis (Muller et al., 2009) and angiogenesis (Kuhn et al., 2009), two processes which are essential for proper memory-dependent processes (Anacker and Hen, 2017). A critical role of GC-A for central auditory processing has been suggested through the use of global GC-A KO mice, which are unable to maintain proper central auditory processing following auditory trauma (Marchetta et al., 2020a).

Conclusion

Our data suggest that under physiological conditions, MR suppresses GR expression to keep the threshold for memory consolidation high (Figure 6A). The threshold of LTP is implemented *via* MR-induced control of postsynaptic Arc/Arg3.1 levels for optimized AMPA-receptor trafficking (Figure 6B), *via* MR- and GR-induced control of NO-GC (Figure 5B) and neuronal GC-A levels (Figure 6B) for optimized energy supply during hemodynamic responses.

Hemodynamic responses take place within a glutamatergic neural feedforward signaling, that includes a neuronal-derived nitric oxide (NO) release from the glutamatergic synapses as well as endothelial-derived NO from blood vessels (Sohal et al., 2009; Czeh et al., 2015; Lee et al., 2015; Chen et al., 2017; Csabai et al., 2018; Czeh et al., 2018; Han et al., 2019). This is followed by a metabolic feedback signal in the smooth muscle cells of parenchymal arterioles, which results in vasodilation (for a review see Attwell et al., 2010; Kisler et al., 2017; Ledo et al., 2021). cGMP signaling plays an integral role for the LTP results of the present study (Sanderson and Sher, 2013; Bradley and Steinert, 2016; Dorner-Ciossek et al., 2017; Borovac et al., 2018). We conclude that GR inhibition by MR may define the threshold for hemodynamic responses through the control of GC-A levels (Figure 6B). Through lowering GR expression levels *via* MR, the threshold for metabolically-demanding neuronal responses and vasodilation (possibly requiring GC-A) would be kept high. In future studies, it would be of particular interest to investigate how the suppression of NO-GC by MR and GR and the elevation of GC-A by increased GR levels contribute to LTP and related auditory neural gain (Figure 6).

Limitations of the study

The search for GRE- and MR-specific binding motifs requires experimental validation of the functionality of the binding sites. Moreover, the observation that the *in silico* prediction tools did not identify GRE motifs in the promoter regions of GC-A or Arc/Arg3.1 does not rule out their existence. Adequate validation of the function of GC-A for LTP-dependent auditory processing and its explicit relation to balanced stress levels is also pending and requires inducible deletion of GC-A under conditions comparable to those shown here for MR/GR deletion.

Data availability statement

The datasets generated and/or analyzed during the current study are available from the corresponding author upon reasonable request.

Ethics statement

The animal study was reviewed and approved by University of Tübingen, Veterinary Care Unit and the Animal Care and Ethics Committee of the regional board of the Federal State Government of Baden-Württemberg, Germany. Written informed consent was obtained from the owners for the participation of their animals in this study.

Author contributions

MK and LR conceived the study. DC, MH, PM, JM, and WS performed the experiments and analyzed the data. EN and JP performed data sequencing analysis. MK, LR, RL, PR, JP, and PS wrote the manuscript. MK, WS, and LR supervised the work. MK, LR, RL, PR, PS, EN, and JP reviewed and edited the manuscript. All authors contributed to the article and approved the submitted version.

Funding

This work was funded by the Deutsche Forschungsgemeinschaft (DFG, German Research Foundation) – DC, PM, MK, RL, and PR are members of the Research Training Group [grant number 335549539/GRK 2381]; FOR 2060 project RU 713/3-2, SPP 1608 RU 316/12-1, KN 316/12-1. JM was supported by the Interdisziplinäres Promotionskolleg Medizin of the University of Tübingen. EN and JP are supported by a restricted research grant from BAYER. Each source of funding provided a budget for personnel and material costs. We acknowledge support by Open Access Publishing Fund of University of Tübingen. BAYER was not

involved in the study design, collection, analysis, interpretation of data, the writing of this article, or the decision to submit it for publication.

Acknowledgments

We acknowledge support by Open Access Publishing Fund of University of Tübingen.

Conflict of interest

PS was employed by the company BAYER.

The remaining authors declare that the research was conducted in the absence of any commercial or financial relationships that could be construed as a potential conflict of interest.

Publisher's note

Supplementary material

The Supplementary material for this article can be found online at: https://www.frontiersin.org/articles/10.3389/fnmol.2023.1017761/full#supplementary-material

References

Anacker, C., and Hen, R. (2017). Adult hippocampal neurogenesis and cognitive flexibility—linking memory and mood. *Nat. Rev. Neurosci.* 18, 335–346. doi: 10.1038/nrn.2017.45

Antunes, F. M., and Malmierca, M. S. (2021). Corticothalamic pathways in auditory processing: recent advances and insights from other sensory systems. *Front. Neural Circuits* 15:721186. doi: 10.3389/fncir.2021.721186

Asilador, A., and Llano, D. A. (2020). Top-down inference in the auditory system: potential roles for Corticofugal projections. *Front. Neural Circuits* 14:615259. doi: 10.3389/fncir.2020.615259

Attwell, D., Buchan, A. M., Charpak, S., Lauritzen, M., Macvicar, B. A., and Newman, E. A. (2010). Glial and neuronal control of brain blood flow. *Nature* 468, 232–243. doi: 10.1038/nature09613

Basner, M., Babisch, W., Davis, A., Brink, M., Clark, C., Janssen, S., et al. (2014). Auditory and non-auditory effects of noise on health. *Lancet* 383, 1325–1332. doi: 10.1016/S0140-6736(13)61613-X

Beato, M., and Klug, J. (2000). Steroid hormone receptors: an update. *Hum. Reprod. Update* 6, 225–236. doi: 10.1093/humupd/6.3.225

Berger, S., Bleich, M., Schmid, W., Cole, T. J., Peters, J., Watanabe, H., et al. (1998). Mineralocorticoid receptor knockout mice: pathophysiology of Na+ metabolism. *Proc. Natl. Acad. Sci. U. S. A.* 95, 9424–9429. doi: 10.1073/pnas.95.16.9424

Berger, S., Wolfer, D. P., Selbach, O., Alter, H., Erdmann, G., Reichardt, H. M., et al. (2006). Loss of the limbic mineralocorticoid receptor impairs behavioral plasticity. *Proc. Natl. Acad. Sci. U. S. A.* 103, 195–200. doi: 10.1073/pnas.0503878102

Bharadwaj, H. M., Verhulst, S., Shaheen, L., Liberman, M. C., and Shinn-Cunningham, B. G. (2014). Cochlear neuropathy and the coding of supra-threshold sound. *Front. Syst. Neurosci.* 8:26. doi: 10.3389/fnsys.2014.00026

Borovac, J., Bosch, M., and Okamoto, K. (2018). Regulation of actin dynamics during structural plasticity of dendritic spines: signaling messengers and actin-binding proteins. *Mol. Cell. Neurosci.* 91, 122–130. doi: 10.1016/j.mcn.2018.07.001

Bradley, S. A., and Steinert, J. R. (2016). Nitric oxide-mediated posttranslational modifications: impacts at the synapse. *Oxid. Med. Cell. Longev.* 2016, 5681036–5681039. doi: 10.1155/2016/5681036

Bramham, C. R., Alme, M. N., Bittins, M., Kuipers, S. D., Nair, R. R., Pai, B., et al. (2010). The arc of synaptic memory. *Exp. Brain Res.* 200, 125–140. doi: 10.1007/s00221-009-1959-2

Bueno-Junior, L. S., and Leite, J. P. (2018). Input convergence, synaptic plasticity and functional coupling across hippocampal-prefrontal-thalamic circuits. *Front. Neural Circuits* 12:40. doi: 10.3389/fncir.2018.00040

Canlon, B., Theorell, T., and Hasson, D. (2013). Associations between stress and hearing problems in humans. *Hear. Res.* 295, 9–15. doi: 10.1016/j.heares.2012.08.015

Chao, H. M., Choo, P. H., and McEwen, B. S. (1989). Glucocorticoid and mineralocorticoid receptor mRNA expression in rat brain. *Neuroendocrinology* 50, 365–371. doi: 10.1159/000125250

Chen, G., Zhang, Y., Li, X., Zhao, X., Ye, Q., Lin, Y., et al. (2017). Distinct inhibitory circuits orchestrate cortical beta and gamma band oscillations. *Neuron* 96, 1403–1418.e6. doi: 10.1016/j.neuron.2017.11.033

Chenaux, G., Matt, L., Hill, T. C., Kaur, I., Liu, X.-B., Kirk, L. M., et al. (2016). Loss of SynDIG1 reduces excitatory synapse maturation but not formation *in vivo*. SynDIG1 regulates excitatory synapse maturation. *eNeuro* 3, ENEURO.0130–ENEU16.2016. doi: 10.1523/ENEURO.0130-16.2016

Chumak, T., Ruttiger, L., Lee, S. C., Campanelli, D., Zuccotti, A., Singer, W., et al. (2016). BDNF in lower brain parts modifies auditory fiber activity to gain Fidelity but increases the risk for generation of central noise after injury. *Mol. Neurobiol.* 53, 5607–5627. doi: 10.1007/s12035-015-9474-x

Cole, T. J., Blendy, J. A., Monaghan, A. P., Krieglstein, K., Schmid, W., Aguzzi, A., et al. (1995). Targeted disruption of the glucocorticoid receptor gene blocks adrenergic chromaffin cell development and severely retards lung maturation. *Genes Dev.* 9, 1608–1621. doi: 10.1101/gad.9.13.1608

Csabai, D., Wiborg, O., and Czeh, B. (2018). Reduced synapse and axon numbers in the prefrontal cortex of rats subjected to a chronic stress model for depression. *Front. Cell. Neurosci.* 12:24. doi: 10.3389/fncel.2018.00024

Czeh, B., Vardya, I., Varga, Z., Febbraro, F., Csabai, D., Martis, L. S., et al. (2018). Long-term stress disrupts the structural and functional integrity of GABAergic neuronal networks in the medial prefrontal cortex of rats. *Front. Cell. Neurosci.* 12:148. doi: 10.3389/fncel.2018.00148

Czeh, B., Varga, Z. K., Henningsen, K., Kovacs, G. L., Miseta, A., and Wiborg, O. (2015). Chronic stress reduces the number of GABAergic interneurons in the adult rat hippocampus, dorsal-ventral and region-specific differences. *Hippocampus* 25, 393–405. doi: 10.1002/hipo.22382

de Kloet, E. R., de Kloet, S. F., de Kloet, C. S., and de Kloet, A. D. (2019). Top-down and bottom-up control of stress-coping. *J. Neuroendocrinol.* 31:e12675. doi: 10.1111/jne.12675

de Kloet, E. R., Joels, M., and Holsboer, F. (2005). Stress and the brain: from adaptation to disease. *Nat. Rev. Neurosci.* 6, 463–475. doi: 10.1038/nrn1683

de Kloet, E. R., Meijer, O. C., de Nicola, A. F., de Rijk, R. H., and Joels, M. (2018). Importance of the brain corticosteroid receptor balance in metaplasticity, cognitive performance and neuro-inflammation. *Front. Neuroendocrinol.* 49, 124–145. doi: 10.1016/j.yfrne.2018.02.003

de Kloet, E. R., Oitzl, M. S., and Joels, M. (1999). Stress and cognition: are corticosteroids good or bad guys? *Trends Neurosci.* 22, 422–426. doi: 10.1016/s0166-2236(99)01438-1

de Kloet, E. R., Van Acker, S. A., Sibug, R. M., Oitzl, M. S., Meijer, O. C., Rahmouni, K., et al. (2000). Brain mineralocorticoid receptors and centrally regulated functions. *Kidney Int.* 57, 1329–1336. doi: 10.1046/j.1523-1755.2000.00971.x

Dorner-Ciossek, C., Kroker, K. S., and Rosenbrock, H. (2017). Role of PDE9 in cognition. *Adv. Neurobiol.* 17, 231–254. doi: 10.1007/978-3-319-58811-7_9

Dragatsis, I., and Zeitlin, S. (2000). CaMKIIalpha-Cre transgene expression and recombination patterns in the mouse brain. *Genesis* 26, 133–135. doi: 10.1002/(sici)1526-968x(200002)26:2<133::aid-gene10>3.0.co;2-v

Dynes, J. L., and Steward, O. (2007). Dynamics of bidirectional transport of arc mRNA in neuronal dendrites. *J. Comp. Neurol.* 500, 433–447. doi: 10.1002/cne.21189

Eckert, P., Marchetta, P., Manthey, M. K., Walter, M. H., Jovanovic, S., Savitska, D., et al. (2021). Deletion of BDNF in Pax2 lineage-derived interneuron precursors in the hindbrain hampers the proportion of excitation/inhibition, learning, and behavior. *Front. Mol. Neurosci.* 14:642679. doi: 10.3389/fnmol.2021.642679

Erdmann, G., Schutz, G., and Berger, S. (2007). Inducible gene inactivation in neurons of the adult mouse forebrain. *BMC Neurosci.* 8:63. doi: 10.1186/1471-2202-8-63

Erdmann, G., Schutz, G., and Berger, S. (2008). Loss of glucocorticoid receptor function in the pituitary results in early postnatal lethality. *Endocrinology* 149, 3446–3451. doi: 10.1210/en.2007-1786

Giesen, J., Mergia, E., Koesling, D., and Russwurm, M. (2022). Hippocampal AMPA- and NMDA-induced cGMP signals are mainly generated by NO-GC2 and are under tight control by PDEs 1 and 2. *Eur. J. Neurosci.* 55, 18–31. doi: 10.1111/ejn.15564

Goel, A., Cantu, D. A., Guilfoyle, J., Chaudhari, G. R., Newadkar, A., Todisco, B., et al. (2019). Author correction: impaired perceptual learning in a mouse model of fragile X

syndrome is mediated by parvalbumin neuron dysfunction and is reversible. *Nat. Neurosci.* 22:143. doi: 10.1038/s41593-018-0273-3

Groc, L., Choquet, D., and Chaouloff, F. (2008). The stress hormone corticosterone conditions AMPAR surface trafficking and synaptic potentiation. *Nat. Neurosci.* 11, 868–870. doi: 10.1038/nn.2150

Guzowski, J. F., McNaughton, B. L., Barnes, C. A., and Worley, P. F. (1999). Environment-specific expression of the immediate-early gene arc in hippocampal neuronal ensembles. *Nat. Neurosci.* 2, 1120–1124. doi: 10.1038/16046

Han, K., Min, J., Lee, M., Kang, B. M., Park, T., Hahn, J., et al. (2019). Neurovascular coupling under chronic stress is modified by altered GABAergic interneuron activity. *J. Neurosci.* 39, 10081–10095. doi: 10.1523/JNEUROSCI.1357-19.2019

Harms, J. F., Menniti, F. S., and Schmidt, C. J. (2019). Phosphodiesterase 9A in brain regulates cGMP signaling independent of nitric-oxide. *Front. Neurosci.* 13:837. doi: 10.3389/fnins.2019.00837

Harris, A. P., Holmes, M. C., de Kloet, E. R., Chapman, K. E., and Seckl, J. R. (2013). Mineralocorticoid and glucocorticoid receptor balance in control of HPA axis and behaviour. *Psychoneuroendocrinology* 38, 648–658. doi: 10.1016/j.psyneuen.2012.08.007

Hedde, P. N., Malacrida, L., Barylko, B., Binns, D. D., Albanesi, J. P., and Jameson, D. M. (2021). Membrane remodeling by arc/Arg3.1. *Front. Mol. Biosci.* 8:630625. doi: 10.3389/fmolb.2021.630625

Hopper, R. A., and Garthwaite, J. (2006). Tonic and phasic nitric oxide signals in hippocampal long-term potentiation. *J. Neurosci.* 26, 11513–11521. doi: 10.1523/JNEUROSCI.2259-06.2006

Jafari, Z., Kolb, B. E., and Mohajerani, M. H. (2018). Chronic traffic noise stress accelerates brain impairment and cognitive decline in mice. *Exp. Neurol.* 308, 1–12. doi: 10.1016/j.expneurol.2018.06.011

Jafari, Z., Kolb, B. E., and Mohajerani, M. H. (2019). Age-related hearing loss and tinnitus, dementia risk, and auditory amplification outcomes. *Ageing Res. Rev.* 56:100963. doi: 10.1016/j.arr.2019.100963

Jett, J. D., Bulin, S. E., Hatherall, L. C., McCartney, C. M., and Morilak, D. A. (2017). Deficits in cognitive flexibility induced by chronic unpredictable stress are associated with impaired glutamate neurotransmission in the rat medial prefrontal cortex. *Neuroscience* 346, 284–297. doi: 10.1016/j.neuroscience.2017.01.017

Joels, M. (2018). Corticosteroids and the brain. *J. Endocrinol.* 238, R121–R130. doi: 10.1530/JOE-18-0226

Karst, H., and Joels, M. (2005). Corticosterone slowly enhances miniature excitatory postsynaptic current amplitude in mice CA1 hippocampal cells. *J. Neurophysiol.* 94, 3479–3486. doi: 10.1152/jn.00143.2005

Kisler, K., Nelson, A. R., Montagne, A., and Zlokovic, B. V. (2017). Cerebral blood flow regulation and neurovascular dysfunction in Alzheimer disease. *Nat. Rev. Neurosci.* 18, 419–434. doi: 10.1038/nrn.2017.48

Knipper, M., Singer, W., Schwabe, K., Hagberg, G. E., Li Hegner, Y., Rüttiger, L., et al. (2022). Disturbed balance of inhibitory signaling links hearing loss and cognition. *Front. Neural Circuits* 15, 1–25. doi: 10.3389/fncir.2021.785603

Knipper, M., van Dijk, P., Schulze, H., Mazurek, B., Krauss, P., Scheper, V., et al. (2020). The neural bases of tinnitus: lessons from deafness and Cochlear implants. *J. Neurosci.* 40, 7190–7202. doi: 10.1523/JNEUROSCI.1314-19.2020

Koesling, D., Mergia, E., and Russwurm, M. (2016). Physiological functions of NO-sensitive Guanylyl Cyclase isoforms. *Curr. Med. Chem.* 23, 2653–2665. doi: 10.2174/0929867323666160812145050

Korb, E., and Finkbeiner, S. (2011). Arc in synaptic plasticity: from gene to behavior. *Trends Neurosci.* 34, 591–598. doi: 10.1016/j.tins.2011.08.007

Kroker, K. S., Rast, G., Giovannini, R., Marti, A., Dorner-Ciossek, C., and Rosenbrock, H. (2012). Inhibition of acetylcholinesterase and phosphodiesterase-9A has differential effects on hippocampal early and late LTP. *Neuropharmacology* 62, 1964–1974. doi: 10.1016/j.neuropharm.2011.12.021

Kuhn, M. (2016). Molecular physiology of membrane Guanylyl Cyclase receptors. *Physiol. Rev.* 96, 751–804. doi: 10.1152/physrev.00022.2015

Kuhn, M., Volker, K., Schwarz, K., Carbajo-Lozoya, J., Flogel, U., Jacoby, C., et al. (2009). The natriuretic peptide/guanylyl cyclase--a system functions as a stress-responsive regulator of angiogenesis in mice. *J. Clin. Invest.* 119, 2019–2030. doi: 10.1172/JCI37430

Kuipers, S. D., Trentani, A., Tiron, A., Mao, X., Kuhl, D., and Bramham, C. R. (2016). BDNF-induced LTP is associated with rapid arc/Arg3.1-dependent enhancement in adult hippocampal neurogenesis. *Sci. Rep.* 6:21222. doi: 10.1038/srep21222

Lai, M., Horsburgh, K., Bae, S. E., Carter, R. N., Stenvers, D. J., Fowler, J. H., et al. (2007). Forebrain mineralocorticoid receptor overexpression enhances memory, reduces anxiety and attenuates neuronal loss in cerebral ischaemia. *Eur. J. Neurosci.* 25, 1832–1842. doi: 10.1111/j.1460-9568.2007.05427.x

Ledo, A., Lourenco, C. F., Cadenas, E., Barbosa, R. M., and Laranjinha, J. (2021). The bioactivity of neuronal-derived nitric oxide in aging and neurodegeneration: switching signaling to degeneration. *Free Radic. Biol. Med.* 162, 500–513. doi: 10.1016/j.freeradbiomed.2020.11.005

Lee, S., Kang, B. M., Shin, M. K., Min, J., Heo, C., Lee, Y., et al. (2015). Chronic stress decreases cerebrovascular responses during rat Hindlimb electrical stimulation. *Front. Neurosci.* 9:462. doi: 10.3389/fnins.2015.00462

Likhtik, E., and Johansen, J. P. (2019). Neuromodulation in circuits of aversive emotional learning. *Nat. Neurosci.* 22, 1586–1597. doi: 10.1038/s41593-019-0503-3

Luksys, G., and Sandi, C. (2011). Neural mechanisms and computations underlying stress effects on learning and memory. *Curr. Opin. Neurobiol.* 21, 502–508. doi: 10.1016/j.conb.2011.03.003

Manohar, S., Chen, G. D., Ding, D., Liu, L., Wang, J., Chen, Y. C., et al. (2022). Unexpected consequences of noise-induced hearing loss: impaired hippocampal neurogenesis, memory, and stress. *Front. Integr. Neurosci.* 16:871223. doi: 10.3389/fnint.2022.871223

Marchetta, P., Eckert, P., Lukowski, R., Ruth, P., Singer, W., Ruttiger, L., et al. (2022). Loss of central mineralocorticoid or glucocorticoid receptors impacts auditory nerve processing in the cochlea. *iScience* 25:103981. doi: 10.1016/j.isci.2022.103981

Marchetta, P., Mohrle, D., Eckert, P., Reimann, K., Wolter, S., Tolone, A., et al. (2020a). Guanylyl Cyclase a/cGMP signaling slows hidden, age- and acoustic trauma-induced hearing loss. *Front. Aging Neurosci.* 12:83. doi: 10.3389/fnagi.2020.00083

Marchetta, P., Savitska, D., Kubler, A., Asola, G., Manthey, M., Mohrle, D., et al. (2020b). Age-dependent auditory processing deficits after Cochlear Synaptopathy depend on auditory nerve latency and the ability of the brain to recruit LTP/BDNF. *Brain Sci.* 10. doi: 10.3390/brainsci10100710

Martin, S., Henley, J. M., Holman, D., Zhou, M., Wiegert, O., van Spronsen, M., et al. (2009). Corticosterone alters AMPAR mobility and facilitates bidirectional synaptic plasticity. *PLoS One* 4:e4714. doi: 10.1371/journal.pone.0004714

Matt, L., Eckert, P., Panford-Walsh, R., Geisler, H. S., Bausch, A. E., Manthey, M., et al. (2018). Visualizing BDNF transcript usage during sound-induced memory linked plasticity. *Front. Mol. Neurosci.* 11:260. doi: 10.3389/fnmol.2018.00260

Matt, L., Michalakis, S., Hofmann, F., Hammelmann, V., Ludwig, A., Biel, M., et al. (2011). HCN2 channels in local inhibitory interneurons constrain LTP in the hippocampal direct perforant path. *Cell. Mol. Life Sci.* 68, 125–137. doi: 10.1007/s00018-010-0446-z

Mazurek, B., Boecking, B., and Brueggemann, P. (2019). Association between stress and tinnitus-new aspects. *Otol. Neurotol.* 40, e467–e473. doi: 10.1097/MAO.0000000000002180

McCann, K. E., Lustberg, D. J., Shaughnessy, E. K., Carstens, K. E., Farris, S., Alexander, G. M., et al. (2021). Novel role for mineralocorticoid receptors in control of a neuronal phenotype. *Mol. Psychiatry* 26, 350–364. doi: 10.1038/s41380-019-0598-7

McEwen, B. S., Nasca, C., and Gray, J. D. (2016). Stress effects on neuronal structure: hippocampus, amygdala, and prefrontal cortex. *Neuropsychopharmacology* 41, 3–23. doi: 10.1038/npp.2015.171

Mease, R. A., and Gonzalez, A. J. (2021). Corticothalamic pathways from layer 5: emerging roles in computation and pathology. *Front. Neural Circuits* 15:730211. doi: 10.3389/fncir.2021.730211

Meijsing, S. H., Pufall, M. A., So, A. Y., Bates, D. L., Chen, L., and Yamamoto, K. R. (2009). DNA binding site sequence directs glucocorticoid receptor structure and activity. *Science* 324, 407–410. doi: 10.1126/science.1164265

Meltser, I., and Canlon, B. (2011). Protecting the auditory system with glucocorticoids. *Hear. Res.* 281, 47–55. doi: 10.1016/j.heares.2011.06.003

Mergia, E., Friebe, A., Dangel, O., Russwurm, M., and Koesling, D. (2006). Spare guanylyl cyclase NO receptors ensure high NO sensitivity in the vascular system. *J. Clin. Invest.* 116, 1731–1737. doi: 10.1172/JCI27657

Mifsud, K. R., and Reul, J. M. (2016). Acute stress enhances heterodimerization and binding of corticosteroid receptors at glucocorticoid target genes in the hippocampus. *Proc. Natl. Acad. Sci. U. S. A.* 113, 11336–11341. doi: 10.1073/pnas.1605246113

Muller, D., Hida, B., Guidone, G., Speth, R. C., Michurina, T. V., Enikolopov, G., et al. (2009). Expression of guanylyl cyclase (GC)-a and GC-B during brain development: evidence for a role of GC-B in perinatal neurogenesis. *Endocrinology* 150, 5520–5529. doi: 10.1210/en.2009-0490

Nadhimi, Y., and Llano, D. A. (2021). Does hearing loss lead to dementia? A review of the literature. *Hear. Res.* 402:108038. doi: 10.1016/j.heares.2020.108038

Nelissen, E., Argyrousi, E. K., Van Goethem, N. P., Zhao, F., Hines, C. D. G., Swaminath, G., et al. (2021). Soluble Guanylate Cyclase stimulator Vericiguat enhances long-term memory in rats without altering cerebral blood volume. *Biomedicine* 9, 1–20. doi: 10.3390/biomedicines9081047

Nelissen, E., Possemis, N., Van Goethem, N. P., Schepers, M., Mulder-Jongen, D. A. J., Dietz, L., et al. (2022). The sGC stimulator BAY-747 and activator runcaciguat can enhance memory in vivo via differential hippocampal plasticity mechanisms. *Sci. Rep.* 12:3589. doi: 10.1038/s41598-022-07391-1

Obradovic, D., Tirard, M., Nemethy, Z., Hirsch, O., Gronemeyer, H., and Almeida, O. F. (2004). DAXX, FLASH, and FAF-1 modulate mineralocorticoid and glucocorticoid receptor-mediated transcription in hippocampal cells--toward a basis for the opposite actions elicited by two nuclear receptors? *Mol. Pharmacol.* 65, 761–769. doi: 10.1124/mol.65.3.761

Oitzl, M. S., and de Kloet, E. R. (1992). Selective corticosteroid antagonists modulate specific aspects of spatial orientation learning. *Behav. Neurosci.* 106, 62–71. doi: 10.1037//0735-7044.106.1.62

Park, S., Park, J. M., Kim, S., Kim, J. A., Shepherd, J. D., Smith-Hicks, C. L., et al. (2008). Elongation factor 2 and fragile X mental retardation protein control the dynamic translation of arc/Arg3.1 essential for mGluR-LTD. *Neuron* 59, 70–83. doi: 10.1016/j.neuron.2008.05.023

Patel, N. S., Klett, J., Pilarzyk, K., Lee, D. I., Kass, D., Menniti, F. S., et al. (2018). Identification of new PDE9A isoforms and how their expression and subcellular compartmentalization in the brain change across the life span. *Neurobiol. Aging* 65, 217–234. doi: 10.1016/j.neurobiolaging.2018.01.019

Plath, N., Ohana, O., Dammermann, B., Errington, M. L., Schmitz, D., Gross, C., et al. (2006). Arc/Arg3.1 is essential for the consolidation of synaptic plasticity and memories. *Neuron* 52, 437–444. doi: 10.1016/j.neuron.2006.08.024

Polman, J. A., de Kloet, E. R., and Datson, N. A. (2013). Two populations of glucocorticoid receptor-binding sites in the male rat hippocampal genome. *Endocrinology* 154, 1832–1844. doi: 10.1210/en.2012-2187

Potter, L. R. (2011). Regulation and therapeutic targeting of peptide-activated receptor guanylyl cyclases. *Pharmacol. Ther.* 130, 71–82. doi: 10.1016/j.pharmthera.2010.12.005

Ramirez-Amaya, V., Vazdarjanova, A., Mikhael, D., Rosi, S., Worley, P. F., and Barnes, C. A. (2005). Spatial exploration-induced arc mRNA and protein expression: evidence for selective, network-specific reactivation. *J. Neurosci.* 25, 1761–1768. doi: 10.1523/JNEUROSCI.4342-04.2005

Reul, J. M., and de Kloet, E. R. (1985). Two receptor systems for corticosterone in rat brain: microdistribution and differential occupation. *Endocrinology* 117, 2505–2511. doi: 10.1210/endo-117-6-2505

Rodrigues, S. M., LeDoux, J. E., and Sapolsky, R. M. (2009). The influence of stress hormones on fear circuitry. *Annu. Rev. Neurosci.* 32, 289–313. doi: 10.1146/annurev.neuro.051508.135620

Rodriguez, J. J., Davies, H. A., Silva, A. T., De Souza, I. E., Peddie, C. J., Colyer, F. M., et al. (2005). Long-term potentiation in the rat dentate gyrus is associated with enhanced arc/Arg3.1 protein expression in spines, dendrites and glia. *Eur. J. Neurosci.* 21, 2384–2396. doi: 10.1111/j.1460-9568.2005.04068.x

Roozendaal, B., and McGaugh, J. L. (2011). Memory modulation. *Behav. Neurosci.* 125, 797–824. doi: 10.1037/a0026187

Sanderson, T. M., and Sher, E. (2013). The role of phosphodiesterases in hippocampal synaptic plasticity. *Neuropharmacology* 74, 86–95. doi: 10.1016/j.neuropharm.2013.01.011

Sarabdjitsingh, R. A., Pasricha, N., Smeets, J. A., Kerkhofs, A., Mikasova, L., Karst, H., et al. (2016). Hippocampal fast Glutamatergic transmission is transiently regulated by Corticosterone Pulsatility. *PLoS One* 11:e0145858. doi: 10.1371/journal.pone.0145858

Satake, S., Inoue, T., and Imoto, K. (2012). Paired-pulse facilitation of multivesicular release and intersynaptic spillover of glutamate at rat cerebellar granule cell-interneurone synapses. *J. Physiol.* 590, 5653–5675. doi: 10.1113/jphysiol.2012.234070

Savitska, D., Hess, M., Calis, D., Marchetta, P., Harasztosi, C., Fink, S., et al. (2022). Stress affects central compensation of neural responses to Cochlear Synaptopathy in a cGMP-dependent way. *Front. Neurosci.* 16:864706. doi: 10.3389/fnins.2022.864706

Schwabe, L., Joels, M., Roozendaal, B., Wolf, O. T., and Oitzl, M. S. (2012). Stress effects on memory: an update and integration. *Neurosci. Biobehav. Rev.* 36, 1740–1749. doi: 10.1016/j.neubiorev.2011.07.002

Shimba, A., and Ikuta, K. (2020). Control of immunity by glucocorticoids in health and disease. *Semin. Immunopathol.* 42, 669–680. doi: 10.1007/s00281-020-00827-8

Singer, W., Geisler, H. S., and Knipper, M. (2013a). The Geisler method: tracing activity-dependent cGMP plasticity changes upon double detection of mRNA and protein on brain slices. *Methods Mol. Biol.* 1020, 223–233. doi: 10.1007/978-1-62703-459-3_15

Singer, W., Geisler, H. S., Panford-Walsh, R., and Knipper, M. (2016). Detection of excitatory and inhibitory synapses in the auditory system using fluorescence immunohistochemistry and high-resolution fluorescence microscopy. *Methods Mol. Biol.* 1427, 263–276. doi: 10.1007/978-1-4939-3615-1_15

Singer, W., Zuccotti, A., Jaumann, M., Lee, S. C., Panford-Walsh, R., Xiong, H., et al. (2013b). Noise-induced inner hair cell ribbon loss disturbs central arc mobilization: a novel molecular paradigm for understanding tinnitus. *Mol. Neurobiol.* 47, 261–279. doi: 10.1007/s12035-012-8372-8

Sohal, V. S., Zhang, F., Yizhar, O., and Deisseroth, K. (2009). Parvalbumin neurons and gamma rhythms enhance cortical circuit performance. *Nature* 459, 698–702. doi: 10.1038/nature07991

Son, H., Hawkins, R. D., Martin, K., Kiebler, M., Huang, P. L., Fishman, M. C., et al. (1996). Long-term potentiation is reduced in mice that are doubly mutant in endothelial and neuronal nitric oxide synthase. *Cells* 87, 1015–1023. doi: 10.1016/s0092-8674(00)81796-1

Suga, N. (2020). Plasticity of the adult auditory system based on corticocortical and corticofugal modulations. *Neurosci. Biobehav. Rev.* 113, 461–478. doi: 10.1016/j.neubiorev.2020.03.021

Thomson, A. M. (2000). Facilitation, augmentation and potentiation at central synapses. *Trends Neurosci.* 23, 305–312. doi: 10.1016/s0166-2236(00)01580-0

Tzingounis, A. V., and Nicoll, R. A. (2006). Arc/Arg3.1: linking gene expression to synaptic plasticity and memory. *Neuron* 52, 403–407. doi: 10.1016/j.neuron.2006.10.016

van Weert, L., Buurstede, J. C., Mahfouz, A., Braakhuis, P. S. M., Polman, J. A. E., Sips, H. C. M., et al. (2017). NeuroD factors discriminate mineralocorticoid from glucocorticoid receptor DNA binding in the male rat brain. *Endocrinology* 158, 1511–1522. doi: 10.1210/en.2016-1422

Wall, M. J., and Correa, S. A. L. (2018). The mechanistic link between arc/Arg3.1 expression and AMPA receptor endocytosis. *Semin. Cell Dev. Biol.* 77, 17–24. doi: 10.1016/j.semcdb.2017.09.005

Wang, J., and Puel, J. L. (2020). Presbycusis: an update on Cochlear mechanisms and therapies. *J. Clin. Med.* 9, 1–22. doi: 10.3390/jcm9010218

Wang, X., Zhang, C., Szabo, G., and Sun, Q. Q. (2013). Distribution of CaMKIIalpha expression in the brain in vivo, studied by CaMKIIalpha-GFP mice. *Brain Res.* 1518, 9–25. doi: 10.1016/j.brainres.2013.04.042

Waung, M. W., Pfeiffer, B. E., Nosyreva, E. D., Ronesi, J. A., and Huber, K. M. (2008). Rapid translation of arc/Arg3.1 selectively mediates mGluR-dependent LTD through persistent increases in AMPAR endocytosis rate. *Neuron* 59, 84–97. doi: 10.1016/j.neuron.2008.05.014

Wingenfeld, K., and Otte, C. (2019). Mineralocorticoid receptor function and cognition in health and disease. *Psychoneuroendocrinology* 105, 25–35. doi: 10.1016/j.psyneuen.2018.09.010

Yilmaz-Rastoder, E., Miyamae, T., Braun, A. E., and Thiels, E. (2011). LTP- and LTD-inducing stimulations cause opposite changes in arc/arg3.1 mRNA level in hippocampal area CA1 in vivo. *Hippocampus* 21, 1290–1301. doi: 10.1002/hipo.20838

Zhang, H., and Bramham, C. R. (2021). Arc/Arg3.1 function in long-term synaptic plasticity: emerging mechanisms and unresolved issues. *Eur. J. Neurosci.* 54, 6696–6712. doi: 10.1111/ejn.14958

Zhang, L., Wang, J., Sun, H., Feng, G., and Gao, Z. (2022). Interactions between the hippocampus and the auditory pathway. *Neurobiol. Learn. Mem.* 189:107589. doi: 10.1016/j.nlm.2022.107589

Zucker, R. S., and Regehr, W. G. (2002). Short-term synaptic plasticity. *Annu. Rev. Physiol.* 64, 355–405. doi: 10.1146/annurev.physiol.64.092501.114547

Cellular and Molecular Life Sciences (2023) 80:369
https://doi.org/10.1007/s00018-023-05016-y

ORIGINAL ARTICLE

BK channels sustain neuronal Ca^{2+} oscillations to support hippocampal long-term potentiation and memory formation

Thomas Pham[1] · Tamara Hussein[1] · Dila Calis[2] · Helmut Bischof[1] · David Skrabak[1] · Melanie Cruz Santos[1] · Selina Maier[1] · David Spähn[1] · Daniel Kalina[1] · Stefanie Simonsig[1] · Rebekka Ehinger[1] · Bernhard Groschup[3] · Marlies Knipper[2] · Nikolaus Plesnila[3,4] · Peter Ruth[1] · Robert Lukowski[1] · Lucas Matt[1]

Received: 15 May 2023 / Revised: 25 September 2023 / Accepted: 24 October 2023 / Published online: 21 November 2023

Abstract

Mutations of large conductance Ca^{2+}- and voltage-activated K^+ channels (BK) are associated with cognitive impairment. Here we report that CA1 pyramidal neuron-specific conditional BK knock-out (cKO) mice display normal locomotor and anxiety behavior. They do, however, exhibit impaired memory acquisition and retrieval in the Morris Water Maze (MWM) when compared to littermate controls (CTRL). In line with cognitive impairment in vivo, electrical and chemical long-term potentiation (LTP) in cKO brain slices were impaired in vitro. We further used a genetically encoded fluorescent K^+ biosensor and a Ca^{2+}-sensitive probe to observe cultured hippocampal neurons during chemical LTP (cLTP) induction. cLTP massively reduced intracellular K^+ concentration ($[K^+]_i$) while elevating L-Type Ca^{2+} channel- and NMDA receptor-dependent Ca^{2+} oscillation frequencies. Both, $[K^+]_i$ decrease and Ca^{2+} oscillation frequency increase were absent after pharmacological BK inhibition or in cells lacking BK. Our data suggest that L-Type- and NMDAR-dependent BK-mediated K^+ outflow significantly contributes to hippocampal LTP, as well as learning and memory.

Keywords Large-conductance Ca^{2+}- and voltage-activated potassium channel · BK · Synaptic plasticity · Long-term potentiation (LTP) · Intracellular K^+ dynamics

Introduction

Mutations in *KCNMA1*, the human gene encoding the pore forming α subunit of the large-conductance calcium ion (Ca^{2+})- and voltage-activated potassium ion (K^+) channel BK (maxi K^+, $K_{Ca}1.1$, Slo1) are linked to a growing number of clinically relevant phenotypes. Besides movement disorders and epileptic seizures, these mutations are accompanied by cognitive impairments like developmental delay and intellectual disability [1], which are also linked to autism spectrum disorders and schizophrenia [2, 3].

Throughout the mammalian central nervous system [4], the ubiquitously expressed BK was found in pre- as well as postsynaptic locations [5, 6], where it associates closely with voltage-gated Ca^{2+} channels [7] and *N*-methyl-D-aspartate (NMDA)-type glutamate receptors (NMDAR; [8]). These act as Ca^{2+} sources to provide high local $[Ca^{2+}]_i$ of more than 10 µM necessary for BK activation in the physiologically relevant voltage range of − 50 to 0 mV [7, 9, 10], reviewed in [11]. In presynaptic terminals, massive K^+ outflow in response to BK activation and the ensuing membrane

Robert Lukowski and Lucas Matt have contributed equally to the study.

Lucas Matt: Lead contact.

✉ Lucas Matt
lucas.matt@uni-tuebingen.de

[1] Department of Pharmacology, Toxicology and Clinical Pharmacy, Institute of Pharmacy, University of Tübingen, Tübingen, Germany

[2] Department of Otolaryngology, Head and Neck Surgery, Molecular Physiology of Hearing, Tübingen Hearing Research Centre, University of Tübingen, Tübingen, Germany

[3] Laboratory of Experimental Stroke Research, Institute for Stroke and Dementia Research (ISD), University Hospital, Ludwig-Maximilians-University Munich (LMU), Munich, Germany

[4] Munich Cluster for Systems Neurology (SyNergy), Munich, Germany

hyperpolarization limits synaptic transmission by reducing Ca^{2+} influx through voltage-gated Ca^{2+} channels [12]. In some postsynaptic cells, BK was described to decrease activity levels through hyperpolarization-mediated inhibition of voltage-gated cation channels [13]. In other cell populations like hippocampal CA1 pyramidal cells, however, BK increases firing rate by contributing to the fast repolarization after individual action potentials (AP) [14–16].

Brain development [17] as well as learning and memory aspects of cognition essentially depend on NMDAR-dependent plasticity of α-amino-3-hydroxy-5-methyl-4-isoxazolepropionic acid (AMPA)-type glutamate receptor (AMPAR)-dependent glutamatergic transmission [18]. High frequency stimulation (HFS) of AMPAR provokes postsynaptic Ca^{2+} influx through NMDAR and voltage-activated L-Type Ca^{2+} channels (LTCC; [19, 20]). The resulting increase in $[Ca^{2+}]_i$ strengthens synapses by increasing AMPAR conductance and exocytosis-mediated integration of additional postsynaptic AMPAR. This process of synaptic strengthening is called long-term potentiation (LTP). The converse mechanism termed long-term depression (LTD) reduces synaptic strength by AMPAR endocytosis [21].

Synaptic plasticity in the form of LTP and LTD has been most intensively studied in the hippocampus, a brain region involved in spatial and declarative learning and memory [22], where it is compromised in different models of cognitive impairment [23–26]. So far, however, little is known about the role of postsynaptic BK in hippocampal synaptic plasticity. Reportedly, BK-mediated afterhyperpolarization (fAHP) in hippocampal CA1 pyramidal cells is modulated in response to learning [27]. Additionally, global BK knock-out mice (BK KO or $BK^{-/-}$) suffer from delayed acquisition of hippocampus-dependent spatial memory in the Morris Water Maze (MWM) [28].

Combining behavioral, electrophysiological and biochemical approaches, we found impaired hippocampal learning and LTP in hippocampus-specific conditional BK KO (cKO) mice as well as reduced Ca^{2+} oscillations and K^+ loss in dissociated neurons lacking BK function during chemically induced LTP (cLTP) in vitro. Hence, we propose that BK-mediated hyperpolarizing K^+-currents support postsynaptic Ca^{2+} activity necessary for hippocampal LTP expression.

Materials and methods

Animals

All experimental studies were approved by the local ethics Committee for Animal Research (Regierungspräsidium Tübingen, Germany) and performed according to the guidelines of the German Animal Welfare Act. Animals were kept in standardized cages on a 12/12 h light/dark cycle (lights on 6 a.m.–6 p.m.) under controlled temperature and humidity with access to food and water ad libitum.

8–12 weeks-old animals of both sexes used for characterization by PCR, Western blot and immunofluorescence as well as behavioral, electrophysiological and cLTP experiments were generated by mating the T29-1 transgenic subline expressing Cre recombinase under control of the CaMKII promoter in CA1 pyramidal neurons (B6.Cg-Tg(Camk2a-cre)T29-1Stl/J, JAX #005359) [29] with mice heterozygous for the floxed ($BK^{fl/+}$; B6-Kcnma1$^{tm2.1Ruth}$) or the BK KO allele ($BK^{-/+}$; (B6-Kcnma1^{tm1Ruth}) [30]. Subsequent intercrossing to floxed BK ($BK^{fl/fl}$) mice produced age- and litter-matched CA1 pyramidal neuron-specific conditional BK knockouts (cKO, *genotype*: $Cre^{tg/+}$; $BK^{fl/-}$) and respective controls (CTRL, *genotype*: $Cre^{tg/+}$; $BK^{fl/+}$). Primary hippocampal neurons for cultures were obtained from homozygous P0–P1 wildtype ($BK^{+/+}$) or KO ($BK^{-/-}$) animals bred from either homozygous $BK^{+/+}$ or heterozygous ($BK^{-/+}$) breeders, respectively. Genetic status of neuronal cultures prepared from individual pups was determined by genotyping PCR of biopsies obtained from originating animals. Primer sequences are listed in Table S6.

Antibodies and reagents

All primary antibodies used in the present study are listed in Table S7. All secondary antibodies were isotype-specific and conjugated to Alexa Fluor 488- or Alexa Fluor 555 (Thermo Fisher Scientific). DL-2-Amino-5-phosphonopentanoic acid sodium salt (AP-5, #105), Forskolin (#1099), and Paxilline (#2006) were from Tocris. Nifedipine (#N7634), Picrotoxin (#P1675) and Rolipram (#R6520) were from Sigma-Aldrich. DNA oligonucleotide primers used in this study are listed in Table S6. If not specifically stated, all other reagents were of standard quality and from the usual vendors.

DNA Extraction and PCR

DNA was isolated from freshly dissected hippocampi of T29.1-Cre^{tg}; $BK^{fl/+}$ using High Pure PCR Template Preparation Kit (Roche #11796828,001) according to manufacturer specifications. BKα-null allele (132 bp) was amplified using KAPA HotStart Mouse-Genotyping Kit (Roche #KK7352) and BK forward-1 5′-TGG TCT TCT TCA TCC TCG GG-3′; BK forward-2 5′-AAG GGC CAT TTT GAA GAC GTC-3′ and BK reverse 5′-CCA GCC ACG TGT TTG TTG G-3′ primers to confirm hippocampus specific recombination of BK.

Immunofluorescence

Mice were euthanized with CO_2 and transcardially perfused with 20 mL Dulbecco's Balanced Salt Solution

(DPBS, Thermo Scientific #14190144) followed by 20 mL 4% (wt/vol) paraformaldehyde in DPBS to fix the tissue. Brains were isolated, snap frozen in -40 to -60 °C cold isopentane and stored at − 80 °C. Brains were transferred to − 20 °C 2 h before 8 µm thick coronal sections were obtained. Slices from CTRL, cKO and $BK^{-/-}$ were collected on the same glass slides (epredia Superfrost™ Plus Adhesion Microscope Slides #J1800AMNZ) together with additional sections from $BK^{+/+}$ that served as positive controls. Blocking buffer (BB) consisting of DPBS supplemented with 2% Glycerol, 5% NGS, 0.3% Triton-X-100, 2% (wt/vol) BSA and 50 mM NH_4Cl was used for permeabilization and blocking of unspecific antibody binding. Primary antibodies against BK were diluted 1:1000 in BB and incubated overnight at 4 °C. Sections were then washed thrice with 0.01% Triton-X-100 in DPBS and blocked again with BB for 1 h before incubation with secondary antibody (1:2500) and Hoechst 33342 (1:1000) for 2 h. After three washes with 0.01% Triton-X-100 in DPBS, DPBS and water, sections were mounted with Permafluor (Fisher Scientific, #TA-030-FM). Primary antibodies are listed in Table S7.

Tissue lysis and western blot

Upon dissection, tissues were suspended in RIPA buffer (in mM: 50 Tris, 150 NaCl, 5 EGTA, 10 EDTA, final pH 7.4) containing protease inhibitors (in µg/ml; 1 phenylmethanesulfonyl fluoride, 1 pepstatin A, 10 leupeptin, 20 aprotinin), 1% NP-40, 10% glycerol, 0.05% sodium dodecyl sulfate (SDS), 0.4% deoxycholate and phosphatase inhibitors (Sigma Phosphatase Inhibitor Cocktail 2 and 3) and homogenized with a hand disperser (Polytron).

Protein concentration was measured using BCA assay (Thermo Scientific #23227). 80 µg total protein were incubated with SDS sample buffer at 95 °C for 5 min, separated by electrophoresis in 10% polyacrylamide gels, transferred to polyvinylidene fluoride (PVDF) membranes (Merck #IPFL00010) using a semi-dry blotting system (Carl Roth, 110 mA per membrane for 90 min), probed with the indicated primary antibodies (Table S7) and detected with fluorescently labelled secondary antibodies. Immunosignals were visualized using an Amersham Imager 600 (General Electrics). To simultaneously label multiple proteins of different molecular weight on the membrane using antibodies, the membranes were cut with a little safety margin, according to the size of the proteins of interest. The contrast of the displayed blots was increased to improve visibility of the bands. Importantly, however, densiometric quantification using ImageJ was performed with unprocessed raw images.

Blinding procedures

During the in vivo experiments (beam-walk, open-field and water-maze) as well as electrophysiology, the experimenter was unaware of the animals' genotype. To mask the genotypes, a person other than the experimenter blinded genotypes prior to each experiment by assigning a randomized number to each mouse that did not provide the experimenter with any information about the genotype. Only after data analysis, the experimenter was informed about genotypes.

Beam-Walk

As previously described [31], mice were trained for 3 consecutive days with four trials per day on a rectangular beam of 1 m length with 12 mm edge length suspended in 0.5 m height. The area below the beam was cushioned to prevent fall injuries. On test day, latency to traverse rectangular (28, 12 and 5 mm edge length) and circular beams (28, 17 and 11 mm diameter) was recorded and analyzed offline by an observer unaware of the genotype for latency to cross beam, hind paw foot slips and number of falls.

Open-Field

Open-Field was performed as previously described [31]. Mice were recorded while freely exploring a circular arena with a diameter of 112 cm for 30 min using a suspended camera. Latency to enter border zone (15 cm from the edge), relative time spent in the border zone, total distance travelled, resting time and mean speed were quantified and analyzed using Smart 3.0 tracking software (Panlab). Additionally, the number of rearings during the first 5 min was quantified.

Spatial acquisition and reversal (Water-Maze)

As previously described [31], a 112 cm diameter pool was filled with 30 cm of water (25 °C) made opaque by milk powder. A transparent cylindrical escape platform of 12 cm diameter was submerged 0.5 cm beneath the water surface. The maze was virtually divided into 4 quadrants NE, SE, SW and NW. Swimming trials were recorded with a camera suspended above center of the pool and processed via Smart 3.0 tracking software (Panlab). Mice were trained for 5 consecutive days with four trials per day to find the platform submerged in the NW quadrant using visual cues. For every trial, mice were released into the pool from a different starting location. On day 6, the platform was removed for probe trial. Mice were released into SE quadrant opposite of the target and their movement was tracked for 60 s. After acquisition probe trial, a reversal phase was performed in which the cognitive

flexibility was queried. For this purpose, the platform was positioned in the opposite SE quadrant and insertion locations were mirrored. Training days and number of trials as well as probe trial were otherwise performed identically to the initial acquisition phase.

Electrophysiology

Extracellular fEPSP were recorded as previously described [38]. In brief, brains were quickly isolated and immersed in ice-cold slicing buffer (in mM: 127 NaCl, 1.9 KCl, 26 $NaHCO_3$, 1.2 KH_2PO_4, 10 D-glucose, 2 $MgSO_4$, and 1.1 $CaCl_2$, saturated with 5% CO_2 and 95% O_2, final pH 7.4). 400 µM thick forebrain sections were coronally cut on a vibrating microtome (Leica VT 1000S) and stored in artificial cerebrospinal fluid (ACSF, in mM: 127 NaCl, 1.9 KCl, 26 $NaHCO_3$, 1.2 KH_2PO_4, 2.2 $CaCl_2$, 1 $MgSO_4$ and 10 D-glucose, oxygenated with 95% O_2 plus 5% CO_2, final pH 7.4) at 30 °C for at least 1 h before remaining at room temperature until measurement. Sections were transferred to a measurement chamber constantly perfused with oxygenated warm ACSF at 30 °C. Stimulation (bipolar concentric, TM53CCINS, WPI) and recording (ACSF-filled glass pipettes, 2–3 MΩ) electrodes were positioned in the *stratum radiatum* to measure Schaffer collateral fEPSPs. Signals were amplified using an Axopatch 200B amplifier (Molecular Devices), digitized by a LIH 8 + 8 (HEKA) at 5 kHz and recorded using WinWCP from the *Strathclyde Electrophysiology Suite*. Stimuli (100 µs) were applied through a stimulus isolator (WPI). For each individual slice the strength of the stimulation (typically between 50 and 100 µA) was chosen to evoke approximately 50% of the maximal response, defined by initial fEPSP slope. LTP was induced by high-frequency stimulation (HFS; 100 Hz, 1 s) at the same intensity as baseline. Baseline and LTP levels were determined by average fEPSP initial slopes from the period between −10 to 1 min before and 45 and 60 min after HFS, respectively. Paired Student's T-test was used to determine whether LTP was induced within a genotype (mean baseline vs. mean LTP levels). Two-way ANOVA was used to compare LTP levels (45 to 60 min after HFS) between CTRL and cKO. Before each LTP measurement, input–output ratio (IOR) was determined for stimulus intensities between 25–150 µA and paired-pulse facilitation (PPF) for inter-stimulus intervals of 10, 20, 50, 100, 200, and 500 ms (with the same intensity as for the LTP measurement) for each slice. The stimulation interval was 1/15 s, with 4 traces being averaged to one data point. Data were analyzed and processed using Clampfit 10 (Molecular Devices) and Microsoft Excel. Statistics and visualization were performed with GraphPad Prism. Two-way ANOVA with Sidak's multiple comparison was used to compare IOR and PPF between CTRL and cKO.

Chemically induced LTP (cLTP)

Freshly isolated brains were immediately transferred into ice cold sucrose dissection buffer (SACSF, in mM: 254 sucrose, 1.9 KCl, 1.2 KH_2PO_4, 26 $NaHCO_3$, 10 D-glucose, 2 $MgSO_4$ and 1.1 $CaCl_2$, saturated with 5% CO_2 and 95% O_2, final pH 7.4). Hippocampi were isolated and cut into 350 µM transversal sections using a McIlwain Tissue chopper and incubated in oxygenated ACSF (see above) for 30 min at room temperature. cLTP was induced by adding 20 µM forskolin, 0.1 µM rolipram 50 µM picrotoxin for 10 min in the presence or absence of 5 µM paxilline [32]. This treatment increases cAMP levels [32] and subsequently increases network activity leading to tetanic-like bulk stimulation potentiating a majority of excitatory synapses [33]. Stimulation was terminated by subsequently storing slices in oxygenated ACSF for an additional 10 min.

cLTP induction was evaluated by Western immunoblot using the indicated antibodies (Table S7) as described above. After detection of phospho-specific GluA1 signals, membranes were stripped using Re-blot Plus Strong Antibody Stripping Solution (Millipore) before incubation with GluA1-specific antibodies and detection with secondary antibodies labelled with a fluorescent dye different from the one used for detection of phospho signals (all primary antibodies are listed in Table S7).

Primary dissociated hippocampal neurons

Primary hippocampal neurons were cultured from P0 $BK^{+/+}$ and $BK^{-/-}$ as previously described [34]. In summary, hippocampi were isolated in dissection medium (DM) consisting of Hank's Balanced Salt Solution (Invitrogen #14175095) supplemented with 1 mM sodium pyruvate, 0.1% (wt/vol) Glucose and 10 mM HEPES) and cleared of meninges. After washing thrice with DM, hippocampi were trypsinized (0.25% (wt/vol) in DM for 20 min at 37 °C) and subsequently incubated with 0.1% (wt/vol) Deoxyribonuclease I (Sigma #DN25) for 5 min at room temperature. After washing twice with DM, trypsin was deactivated by washing twice with plating medium (PM) consisting of BME medium (Invitrogen #21010046) supplemented with 10% FCS, 0.45% (wt/vol) glucose, 1 mM sodium pyruvate, 2 mM glutamine and 100 U/ml penicillin/streptomycin. Neurons were dissociated by triturating several times using a fire-polished glass pipette, counted and seeded (700,000 cells) onto 30 mm circular poly-L-lysine coated (Sigma #P2636) glass coverslips. After 2 h, PM was replaced with maintenance medium (MM; Neurobasal; Invitrogen #21103049) supplemented with B-27 (Invitrogen #17504044), 2 mM glutamine and 100 U/ml penicillin/streptomycin. Cells were maintained at 37 °C in a humidified environment with 5% CO_2/95% air. Half of the MM was replaced every 3–4 days.

K^+ imaging

FRET-based recordings of $[K^+]_i$ were performed as previously described [35]. Neurons were transduced after 7 days in vitro (DIV) at a multiplicity of infection (MOI) of 100 with an adeno associated virus -DJ/8 vector system encoding a cytosol targeted K^+ sensitive lc-LysM GEPII 1.0 FRET-based biosensor [36] under control of a CAG promoter. At 9 DIV, coverslips were mounted in a PC30 perfusion chamber (NGFI GmbH, Graz, Austria), perfused with imaging buffer (IB, in mM: 126.5 NaCl, 5 KCl, 2 $CaCl_2$, 2 $MgCl_2$, 10 HEPES, 30 D-glucose, 10 sodium pyruvate, final pH 7.4) through a gravity-based perfusion system (NGFI GmbH, Graz, Austria) which was also used for drug application. Single cell live imaging was conducted on a Zeiss Observer Z.1 (Wetzlar, Germany) with an external light source (2200114 LED-Hub, Omicron Laserage, Rodgau-Dudendorf, Germany) and a Plan-Neofluar 40x/1.30 Oil immersion objective as previously described [37]. Emissions were simultaneously collected at 480 and 535 nm using an Optosplit II (Cairn Research, Faversham, UK). The LED hub (Omicron Laserage, Rodgau-Dudendorf, Germany) featured a 340 nm, 380 nm and 455 nm, LED with 340×, 380× and 427/10 bandpass filters, respectively (AHF Analysentechnik, Tübingen, Germany). Emissions were recorded using a 459/526/596 dichroic with a 475/543/702 emission filter (AHF Analysentechnik, Tübingen, Germany). Images were recorded using a pco.panda 4.2 bi sCMOS camera (PCO, Kelheim, Germany). VisiView software (Visitron Systems, Puchheim, Germany) was used to acquire images and to control the microscope. During live cell imaging, drugs were applied 10 min prior to the start of the recording. Background subtraction was performed using a background ROI. The ratio, which is proportional to $[K^+]_i$ levels, was calculated from the corrected values of the YFP images to those of CFP. First 5 min of basal FRET ratio signal were used for normalization.

Ca^{2+} imaging

Ca^{2+}-sensitive live cell imaging was conducted as described before [38]. 9 DIV neurons were loaded with 2.5 µM of the ratiometric dye Fura-2AM (AAT Bioquest, Sunnyvale, USA) in IB for 20 min at 37 °C followed by a washing step in IB for 10 min at room temperature. Excitation at 340 nm (Ca^{2+} bound to Fura-2) and 380 nm (Ca^{2+} free) induced emissions which were recorded on the same setup as K^+ signals. Background subtraction was performed using a background ROI. The ratio, which is proportional to $[Ca^{2+}]_i$ levels, was calculated from the corrected values of the images at 340 nm to those taken at 380 nm. Only spikes with at least 10% of the height of the glutamate peak were considered in the analysis.

Membrane potential imaging

Membrane potential was visualized by live cell fluorescence imaging using membrane potential sensitive dye Bis-(1,3-dibutylbarbituric acid)trimethine oxonol ($DiBAC_4(3)$) [39]. 9 DIV neurons were loaded with a 1:40,000 dilution of a 10 mg/mL stock of $DiBAC_4(3)$ for 30 min at RT in IB. During recordings $DiBAC_4(3)$ in the indicated concentration was present in all buffers used. cLTP induction, recording of induced emissions at 516 nm and background subtraction by background ROI were performed as described for K^+- and Ca^{2+} -sensitive recordings.

Statistical analysis

Statistical analyses were performed using GraphPad Prism 9.4.1. Data are expressed as mean ± standard error of mean (SEM). After data sets passed the Shapiro–Wilk test for Gaussian normal distribution, an unpaired (Figs. 1B; 2E and S3B, D) or paired (Figs. 2F, G) t-test was performed. Comparisons consisting of more than 2 data sets were tested with either one- or two-way ANOVA followed by a Dunnett's (Fig. 4H), Sidak's (Fig. 2A, B, F, G, 3; S1B-D and S2) or Tukey's (Figs. 5F; S4K; S5C and S6F) multiple comparison test. The specific statistical tests used are explained in the respective legends. For an exact description, see also Tables S1–S5. P-values of ≤ 0.05 were represented with *, $p \leq 0.01$ with **, and $p \leq 0.001$ with ***, indicating comparisons between genotypes. Statistically significant differences to corresponding $BK^{+/+}$ condition (Figs. 4H and 5F) were indicated by † = $p \leq 0.05$; § = $p \leq 0.01$; # = $p \leq 0.001$.

Results

Characterization of conditional CA1-specific BK KO mice

Impaired MWM memory acquisition in $BK^{-/-}$ was previously reported [28]. $BK^{-/-}$ were also observed to suffer from cerebellar ataxia [30, 40], which could impact their MWM swimming performance. In order to determine whether memory performance is affected independently of motor performance, we generated a conditional KO line lacking the pore-forming BKα subunit in hippocampal CA1 pyramidal cells (cKO), the postsynaptic neurons of hippocampal Schaffer-collateral CA3 to CA1 synapses. Plasticity of these synapses is generally agreed to correlate with the animal's performance in spatial learning tasks [41]. Ablation of the floxed BKα ($BK^{fl/+}$) pore exon in CA1 pyramidal cells was achieved by intercrossing mice carrying the floxed allele to a transgenic subline (T29-1) expressing Cre recombinase under control of CaMKII ($Cre^{tg/+}$) in CA1 pyramidal cells

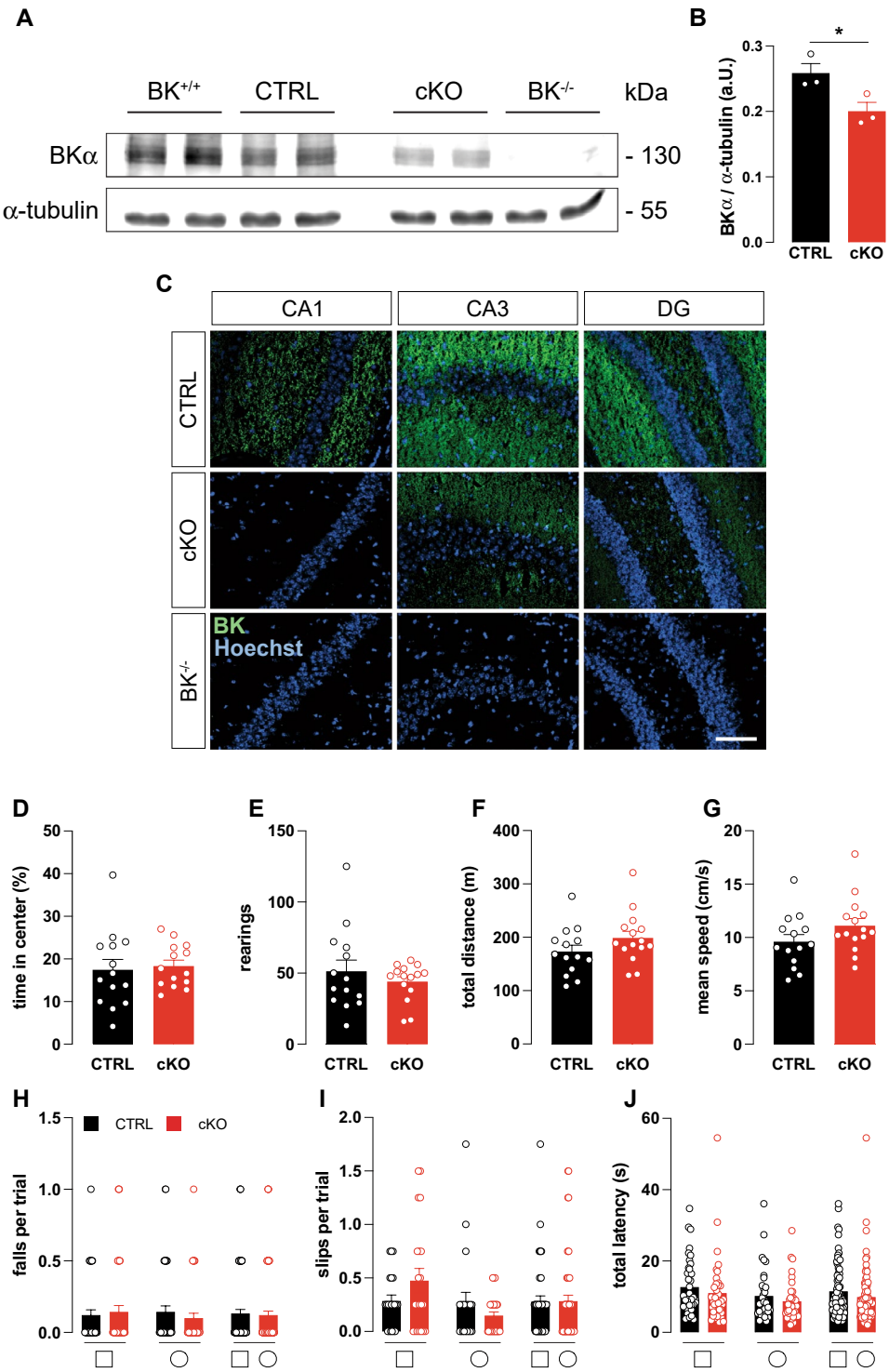

[29] to generate age- and litter-matched cKO (*genotype*: $Cre^{tg/+}$; $BK^{fl/-}$) and the corresponding controls (CTRL, *genotype*: $Cre^{tg/+}$; $BK^{fl/+}$). T29-1 was used in many studies to achieve recombination in CA1 pyramidal cells [42, 43]. It is one of several Cre-expressing sublines originally created by the Tonegawa lab under control of the CamKIIα promoter. All original founder lines display different expression patterns [29], with T29-1 causing very high recombination efficiency and also a remarkable selectivity in CA1 pyramidal cells. First, specific hippocampal recombination in cKO was confirmed by polymerase chain reaction (PCR) (Fig. S1A). Additionally, Western blots demonstrated significantly reduced immunoreactivity to a validated BKα antibody [44] in the hippocampus of cKO

◂**Fig. 1** Characterization of conditional hippocampus-specific BK KO mice. **A** Representative immunoblot of whole hippocampal lysates from wildtype ($BK^{+/+}$), conditional BK control (CTRL), conditional (cKO) and global BK KO ($BK^{-/-}$) mice probed using BKα-specific antibodies revealed that BK protein levels were comparable between $BK^{+/+}$ and CTRL, but significantly reduced in cKO. Compared to CTRL no BKα immunoreactivity was obtained in $BK^{-/-}$ samples. α-Tubulin immunoreactivity serves as loading control. **B** Quantification of BK protein band intensities normalized to α-tubulin. n = 3 independent samples from N = 3 mice. **C** Representative immunofluorescence labelling of cryosections from CTRL, cKO and $BK^{-/-}$ mice using specific antibodies against the pore forming α-subunit of BK (BKα, green). Nuclei were stained with Hoechst 33342 (blue). In CTRL, BKα immunosignals were detected in all hippocampal regions. In cKO, BK immunosignals were virtually absent in CA1, but were present in CA3 and DG. No BK immunosignals were detected in $BK^{-/-}$ mice. n = 3 protein samples obtained from N = 3 mice per genotype. Scale bar is 100 µm. **D–G** During 30 min of observation in the open field experiment, time spent in center of the arena (**D**), number of rearings (**E**), total distance travelled (**F**) and mean velocity (**G**) did not differ between cKO and CTRL (N = 14). **H–J** cKO and CTRL performed similar in the beam walk test as assessed by falls per trial (**H**), missteps per trial (**I**) and latency to cross the bar (**J**). Diagrams depict averages of all bar diameters of the square (□, left), round (○, middle) or both (□○, right) cross-sections indicated below (N = 10–14). Statistics: Unpaired Student's t-test (**D–G**), Two-way ANOVA with Sidak's multiple comparison test (**H–J**). All bar diagrams presented as means ± SEM. See also Fig. S1 and Table S1

compared to CTRL (Fig. 1A, B) with tissue from wildtype ($BK^{+/+}$) and $BK^{-/-}$ serving as positive and negative controls, respectively. Consistent with the Cre expression pattern [29], BKα immunofluorescence was consistently reduced in CA1 but not CA3 or the dentate gyrus (DG) of cKO compared to CTRL as shown in hippocampal sections of adult mice. Again, absence of BKα immunoreactivity in slices from global $BK^{-/-}$ confirmed antibody specificity (Fig. 1C). While Cre-mediated recombination is not completely restricted to CA1 pyramidal cells, cKO mice do not seem to express any BK in these cells. Therefore, these mice are well suited to test BK's role in hippocampal synaptic plasticity and hippocampus-dependent learning paradigms [41].

Anxiety behavior and motor abilities are normal in cKO

Comparison of learning behavior between genotypes in the MWM can be perturbed by differences in anxiety and motor abilities. Thus, open field and beam walk tests were performed to assess if cKO suffer from corresponding impediments. Both paradigms examine test subjects' motor abilities [45, 46], while mouse behavior in the open field additionally represents an important indicator of anxiety levels [47, 48]. cKO and CTRL did not differ in anxiety and exploratory behavior as evidenced by similar amounts of time spent in the center of the open field arena (Fig. 1D) and similar number of rearings (Fig. 1E). During their time in the open field, animals from both genotypes did not differ in total distance travelled (Fig. 1F) and mean movement speed (Fig. 1G). These equivalent motor abilities of cKO and CTRL were further confirmed by the more complex beam walk test in which animals walk over round- and square-shaped beams of decreasing diameter and increasing difficulty. Neither falls or missteps nor the time to cross the beam differed between genotypes (Fig. 1H–J and Fig. S1B–D). Additionally, results from the beam walk test do not suggest any defects in the visual abilities of cKO. This is expected, as in T29.1 Cre activity is only sparsely detected in retinal bipolar, amacrine, and ganglion cells [49] and global BK knockout mice display unaltered electroretinography results under normal lighting conditions [50]. In summary we conclude that BKα is specifically depleted from hippocampal CA1 pyramidal cells of cKO mice, which do not display altered anxiety levels or locomotor abilities in comparison to their age- and litter-matched CTRLs.

Hippocampal learning, memory and Schaffer collateral LTP is impaired in cKO

To test hippocampus-dependent spatial learning and cognitive performance, cKO and CTRL mice were subjected to a MWM task [51]. Over the course of five training days with four training sessions per day, mice learned to remember the hidden platform's position in the NE quadrant. On the first day, CTRL and cKO exhibit similar latencies (Fig. 2A). On the second day already, performance in CTRL improved more quickly than in cKO. As evidenced by continuous shortening of the latency, cKO also learned the platform location over the course of 5 training days, but never reached the performance of CTRL (Fig. 2A). During probe trial on day 6, cKO latency to the platform location was similar to CTRL, but cKO showed significantly less target quadrant preference while spending significantly more time in the opposite SW quadrant than CTRL (Fig. 2B). The lack of target quadrant preference was evident when observing the animals' swimming path. While CTRL focused on examining the target quadrant (Fig. 2C), cKO kept randomly scanning the arena (Fig. 2D). Swim speed as evaluated at the acquisition probe trial was similar between CTRL and cKO (Fig. 2E), ruling out swimming abilities as source for different latencies to reach the platform as well as quadrant preferences.

Schaffer collateral LTP is defective in cKO

Acquisition of spatial memory in the MWM was repeatedly shown to correlate with NMDAR- dependent LTP of hippocampal Schaffer collateral synapses [41, 52]. Therefore, we measured hippocampal LTP by recording extracellular field potentials (fEPSP) in acute hippocampal slices.

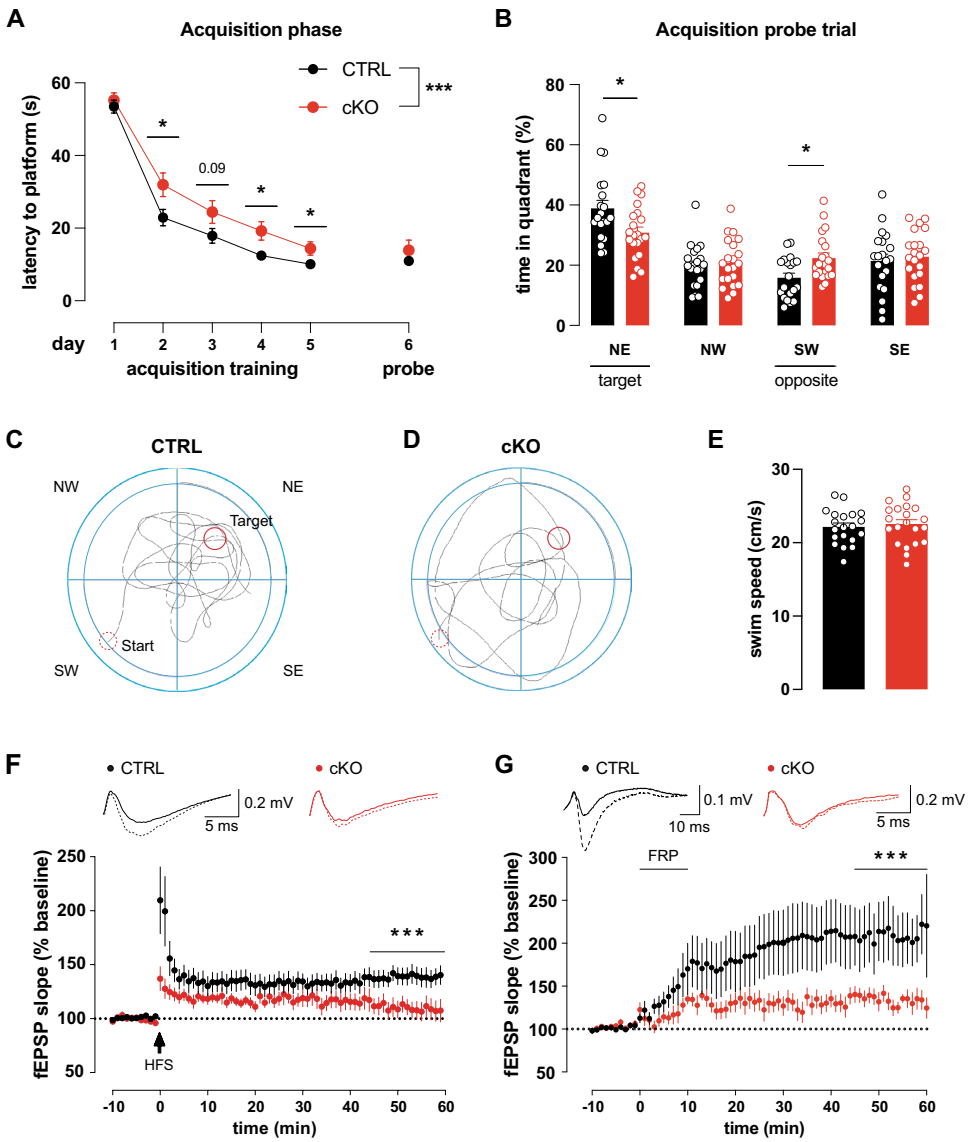

Fig. 2 Impaired MWM performance and hippocampal LTP in cKO. **A**–**C** Compared to CTRL (N = 20), cKO (N = 21) exhibit delayed learning and reduced memory in the MWM task. **A** Mean latencies to reach the hidden platform or original platform position over 5 training days (4 training sessions per day). Latency was similar on day 1 but decreased quicker in CTRL than cKO during the following trainings days. Since the hidden platform was removed, latency during probe trial on day 6 was measured for reaching the former platform position. The latency of the probe is offset, as it is not part of the acquisition phase. **B** CTRL but not cKO showed significant target quadrant (NE) preference during probe trial and also significantly avoided the opposing quadrant (SW). **C** Representative paths traveled by the CTRL and **D** cKO during acquisition probe trial. Start and finish indicated by dashed and solid red circle, respectively. **E** Swim speed of CTRL (N = 20) and cKO (N = 21) during acquisition probe trial were comparable. **F** Schaffer-collateral fEPSP initial slopes recorded from forebrain slices. 100 Hz 1 s high frequency stimulation (HFS) induced significantly more LTP in CTRL (n = 7 slices from N = 4 animals) than cKO (n = 8 slices from N = 4 animals). Top: Representative traces before (solid) and after (dashed) LTP induction. **G** Schaffer-collateral fEPSP initial slopes recorded from forebrain slices. 10 min perfusion of 20 µM forskolin, 50 µM picrotoxin and 0.1 µM rolipram (FRP) induced significantly more cLTP in CTRL (n = 10 slices from N = 4 animals) than cKO (n = 10 slices from N = 5 animals). Top: Representative traces before (solid) and after (dashed) LTP induction. Statistics: Two-way ANOVA (**F**, **G**) with Sidak's multiple comparison test (**A**, **B**), unpaired Student's t-test (**E**). All bar diagrams presented as means ± SEM. See also Fig. S2 and Table S2

In accordance with MWM observations, HFS elicited stable LTP in CTRL, while initially potentiated fEPSP slopes dropped to baseline levels in cKO within 60 min (Fig. 2F, Table S2F). We could not find any indications that altered LTP is due to changes in basal synaptic transmission, as both genotypes displayed similar fEPSP amplitudes in response to a range of input strengths (Fig. S2D). Importantly, similar levels of paired-pulse facilitation (PPF) also indicated unaltered presynaptic function between CTRL and cKO (Fig. S2C).

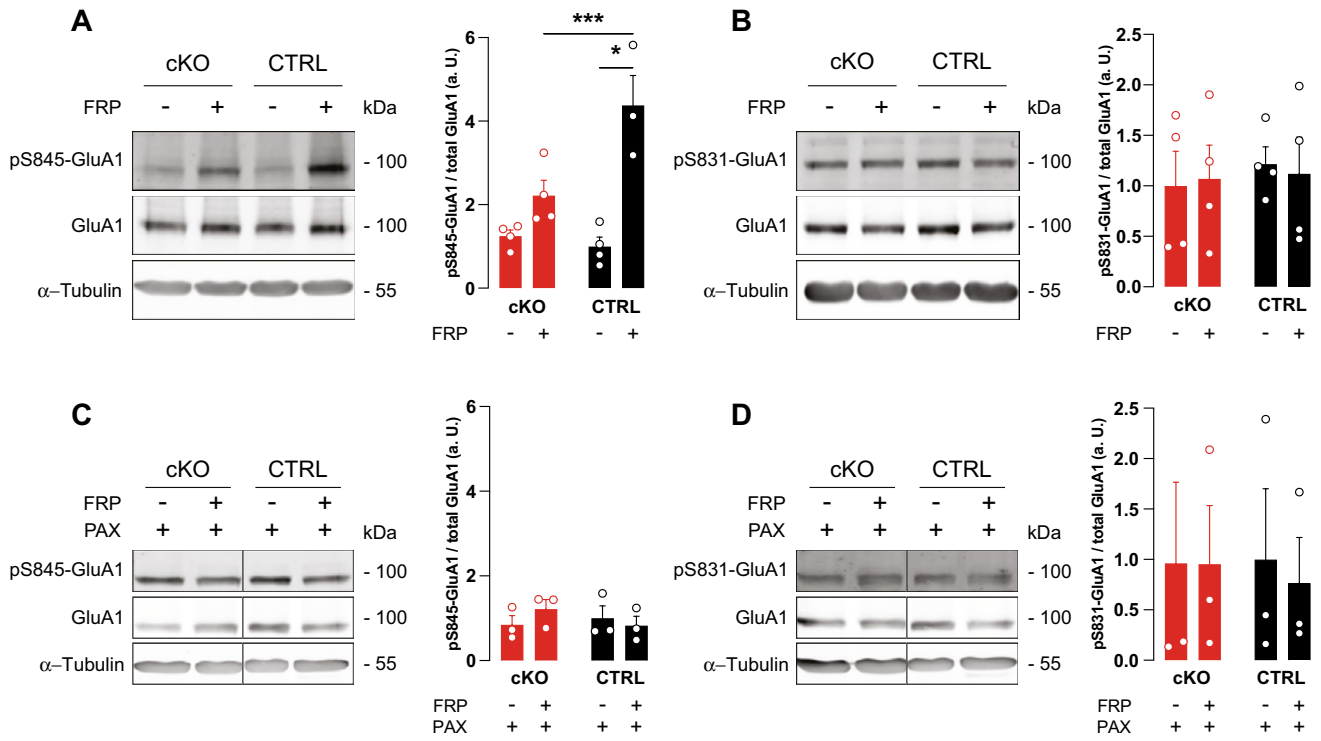

Fig. 3 BK deficiency precludes GluA1 S845 phosphorylation after LTP induction. Acute hippocampal slices from 8–12 weeks-old mice were treated with vehicle or 20 µM forskolin, 0.1 µM rolipram and 50 µM picrotoxin for 10 min to chemically elicit LTP in the presence or absence of the BK channel blocker PAX (5 µM). 10 min after cLTP induction, slices were lysed for immunodetection of phosphorylation at GluA1 residues S845 and S831. Blots were stripped and reprobed for total GluA1. Loading control: α-Tubulin. Representative blots on the left, densitometric quantification on the right. Relative expression was normalized to the mean of the respective untreated CTRL group not stimulated by cLTP to better represent the ratios. **A** cLTP significantly increased GluA1 S845 phosphorylation in CTRL but not cKO (N = 4 animals per genotype), **B** while S831 phosphorylation levels were not altered. **C** Presence of PAX precludes changes in S845 phosphorylation levels. **D** S831 phosphorylation remains unchanged after cLTP in both CTRL (N = 3) and cKO (N = 3) also in the presence of PAX. Statistics: Two-way ANOVA with Sidak's multiple comparison test. All bar diagrams presented as means ± SEM. See also Table S3

Additionally, we also observed reduced LTP in a chemically induced LTP (cLTP) paradigm, in which synapses are not potentiated electrically, but chemically. We tested this key mechanism in cKO by applying cLTP, a model in which LTP is induced by application of 20 µM forskolin, to activate adenylyl cyclases, 0.1 µM rolipram to inhibit phosphodiesterase 4 (PDE4) and 50 µM picrotoxin, to block $GABA_A$ receptors [32, 53, 54]. Interestingly, forskolin/rolipram/picrotoxin (FRP)-induced LTP was previously demonstrated to depend on NMDAR [32]. 10 min FRP perfusion of hippocampal slices sustainably increased initial fEPSP slopes in both genotypes to levels significantly higher than the respective baselines. This potentiation, however, was significantly less pronounced in cKO than CTRL (Fig. 2G, Table S2G). In both genotypes, FRP-induced comparatively more potentiation than HFS. This is probably the result of a more complete activation of the total neuronal population by the cLTP cocktail, while electrical stimulation is restricted to tissue directly adjacent to the stimulation electrode.

Hippocampal LTP is generally associated with MWM learning ability, while hippocampal LTD is linked to cognitive flexibility as observed during MWM reversal training [55, 56]. Recently, defective hippocampal LTD and an associated reduction in reversal learning and cognitive flexibility were described in mice lacking the Na^+-activated K^+ channel Slack (Sequence Like a Ca^{2+}-activated K^+ Channel, $K_{Na}1.1$, Slo2.2) which is highly homologous to BK [31, 38]. We therefore conducted reversal training subsequent to the acquisition phase of the MWM by placing the platform on the opposite SW side and by mirroring the animals' insertion points. As compared to the last acquisition trial(s) and the acquisition probe trials, both genotypes took longer to locate the new platform position in the reversal phase (Fig. S2A), but latencies were comparable between CTRL and cKO throughout of the reversal phase. Apparently, both cKO and CTRL were able to effectively update their memory of the new platform location (Fig. S2B), indicating comparable memory flexibility in both genotypes.

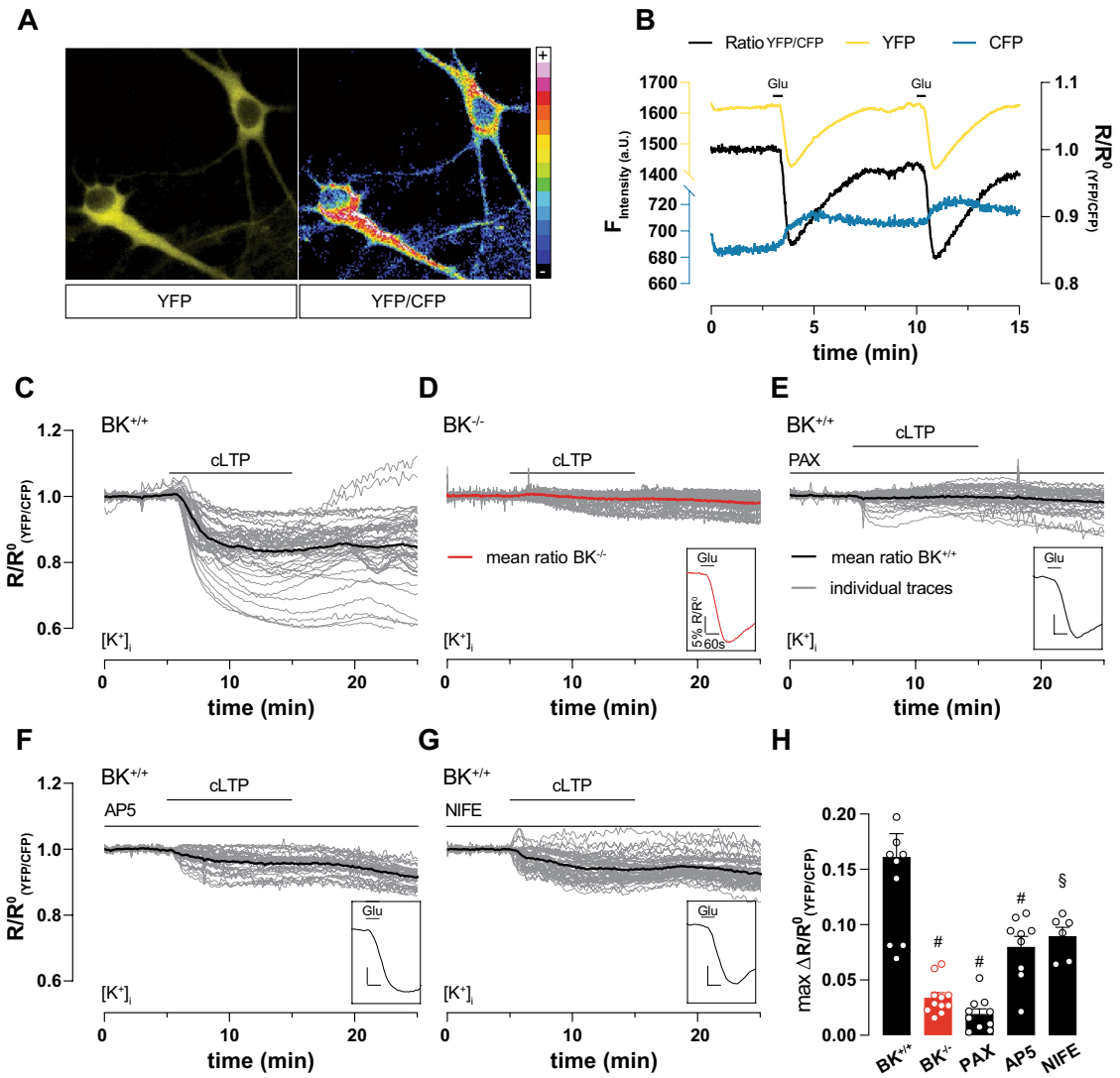

Fig. 4 cLTP induction causes massive K^+ outflow depending on BK, NMDAR and LTCC. Live imaging of 9 DIV hippocampal neuronal cultures (representative cells in **A**), virally transduced at 7 DIV with the FRET-based K^+-sensitive sensor (GEPII), allowed single-cell live recording of $[K^+]_i$ in response to external stimuli. (**B**) Representative time course of ratio between single fluorescence intensities (YFP/CFP, black) highlights reduction of $[K^+]_i$ after repeated application of 20 µM glutamate. Single fluorescence intensities shown in yellow and blue as indicated. **C**–**G** Individual (gray) and averaged (black or red in (**D**)) YFP/CFP in response to cLTP induction in neurons. Glutamate (20 µM) application at the end of each measurement verified cell viability (inset on lower right of each panel). **C** cLTP strongly and persistently decreased $[K^+]_i$ in $BK^{+/+}$ (n = 11 independent experiments from a total of n = 54 neurons obtained from N = 6 preparations). **D** cLTP induction failed to decrease $[K^+]_i$ in $BK^{-/-}$ (n = 9 independent experiments with a total of n = 48 neurons obtained from N = 5 preparations). **E** BK inhibition by PAX (5 µM) prevented decrease of $[K^+]_i$ during cLTP (n = 10) independent experiments from a total of n = 43 neurons obtained from from N = 5 preparations). **F** Compared to vehicle, NMDAR inhibition by AP5 (100 µM) significantly reduced K^+ efflux during cLTP (n = 9 independent experiments with a total of n = 37 neurons obtained from N = 5 preparations). **G** Compared to vehicle, LTCC inhibition by NIFE (5 µM) significantly reduced K^+ efflux during cLTP (n = 6 independent experiments with a total of n = 52 neurons obtained from N = 4 preparations). **H** Maximum differences between average baseline and minimum YFP/CFP during cLTP recordings in panels C-G to corresponding $BK^{+/+}$ condition: § = p ≤ 0.01; # = p ≤ 0.001. Statistics: One-way ANOVA with Dunnett's multiple comparison test. All bar diagrams presented as means ± SEM. See also Fig. S4 and Table S4

Together, our behavioral and electrophysiological data suggest that BK is necessary for normal hippocampal synaptic plasticity in the form of MWM learning and Schaffer collateral LTP.

BK deletion does not alter glutamate receptor subunit composition

Function of heterotetrameric NMDA- [57] and AMPA- [21] receptor complexes necessary for synaptic

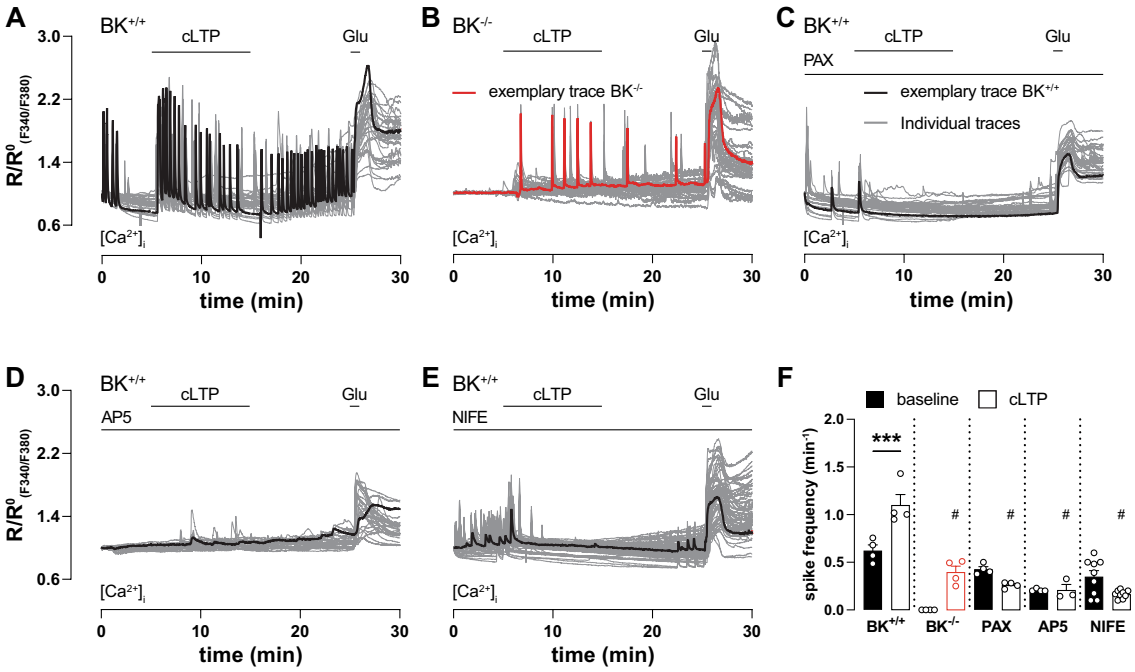

Fig. 5 Ca^{2+} oscillations during cLTP induction depend on BK, NMDAR and LTCC. **A**–**E** Time course of ratio between fluorescence intensities at 340 nm and 380 nm ($R_{F340/F380}$) in 9 DIV hippocampal neuronal cultures loaded with the Ca^{2+}-sensitive dye Fura-2-AM. Traces recorded from individual neurons during multiple measurements are plotted in grey, representative traces in black except for (**B**) which is in red. Glutamate (20 µM) application at the end of each measurement verified cell viability and served as positive control. **A**, **B** Neuronal Ca^{2+} oscillations spontaneously occurred under control conditions in $BK^{+/+}$ (**A**; n = 4 independent experiments with a total of n = 31 neurons obtained from 4 preparations) but not $BK^{-/-}$ neurons (**B**; n = 4 independent experiments with a total of n = 35 neurons obtained from 3 preparations). In $BK^{+/+}$, cLTP induction increased oscillation frequency to a significantly higher degree than in $BK^{-/-}$. **C**–**E** Inhibition of BK, NMDAR, and LTCC by 10 min pre-incubation with 5 µM PAX (**C**; n = 4 independent experiments with a total of n = 29 neurons obtained from 3 preparations), 100 µM AP5 (**D**; n = 4 independent experiments with a total of n = 29 neurons obtained from 3 preparations) and 5 µM NIFE (**E**; n = 4 independent experiments with a total of n = 69 neurons obtained from 5 preparations), respectively, reduced spontaneous Ca^{2+} oscillations and prevented the cLTP-induced rise in frequency. **F** Spiking frequency before and after cLTP induction in indicated conditions. cLTP increased Ca^{2+} oscillation frequency in $BK^{+/+}$ neurons. Genetically or pharmacological BK inhibition as well as AP5 and NIFE prevented frequency increase. Compared with corresponding $BK^{+/+}$ condition: # = p ≤ 0.001. Statistics: Two-way ANOVA with Tukey's multiple comparison test. All bar diagrams presented as means ± SEM. See also Table S5

transmission and plasticity is crucially determined by their respective subunit composition. It was previously reported that animals lacking the closely related Na^+-activated K^+ channel Slack show decreased hippocampal GluN2B expression and impaired hippocampal synaptic plasticity [38]. We therefore examined protein levels of the most prevalent hippocampal NMDAR and AMPAR subunits [58, 59] in adult cKO and CTRL prior to or after completion of the MWM task. Expression levels were not different between cKO and CTRL for GluN1, GluN2A, GluN2B, GluA1 and GluA2 in the naïve state (Fig. S3A) nor for GluN2A, GluN2B and GluA1 after completion of the MWM task (Fig. S3B). GluN1 and GluA2 could not be analyzed due to low sample availability. Taken together, this suggests that defective hippocampal learning, memory and LTP in cKO is not due to altered glutamate receptor subunit expression.

Reduced GluA1-S845 phosphorylation in cKO after LTP induction

Induction of LTP by NMDAR stimulation initiates a signaling cascade resulting in GluA1 phosphorylation at S845, which is a crucial step to allow LTP expression by regulated AMPAR exocytosis [60–62]. We used cLTP to test this key mechanism in cKO. Compared to vehicle-treated controls, cLTP induction for 10 min with FRP (20 µM/0.1 µM/50 µM) significantly increased S845 phosphorylation in hippocampal slices of CTRL but not cKO (Fig. 3A). As shown earlier [54], cLTP induction by FRP did not influence GluA1 S831 phosphorylation confirming specificity of the elicited signaling (Fig. 3B). Interestingly, however, acute pharmacological blockade of BK channels with paxilline (PAX; 5 µM) effectively prevented cLTP-induced GluA1 S845 phosphorylation in CTRL, while PAX was less effective in cKO (Fig. 3C). In both genotypes, pharmacological BK blockade did not

influence GluA1 S831 phosphorylation levels (Fig. 3D). This confirms our electrophysiological and MWM studies that suggest a pivotal role for BK in the cellular signaling mechanisms necessary for the expression of hippocampal LTP as well as hippocampus-dependent spatial learning and memory.

BK-mediated K^+ efflux sustains neuronal Ca^{2+} oscillations during cLTP

To examine in detail how BK supports hippocampal LTP and, in turn, hippocampus-dependent memory formation, we next performed live cell imaging of dissociated hippocampal neuronal cultures generated from homozygous $BK^{+/+}$ and $BK^{-/-}$ pups. Neurons were virally transduced with the genetically encoded potassium ion indicator (GEPII) NES lc-lysM GEPII 1.0 [35, 36] (Fig. 4A) or loaded with the Ca^{2+}-sensitive dye Fura-2-AM (Fig. 5). For NES lc-LysM GEPII 1.0, the ratio of Förster resonance energy transfer (FRET) fluorescence divided by cyan fluorescent protein (CFP) fluorescence is directly proportional to $[K^+]_i$. GEPII sensitivity to $[K^+]_i$ changes was verified by reproducible rapid decrease of the FRET/CFP ratio after repeated perfusion of 20 µM glutamate for 10 s presumably in response to neuronal depolarization (Fig. 4B). Additionally, we observed antiparallel progression of single fluorescent protein fluorescence intensity traces recorded over time, which indicates a valid FRET signal (Figs. 4B and S4A–E). cLTP induction by FRP application massively reduced $[K^+]_i$ in $BK^{+/+}$ (Fig. 4C and H). This drop in $[K^+]_i$ was not observed after cLTP induction in $BK^{-/-}$ neurons (Fig. 4D and H) or after BK inhibition by PAX in $BK^{+/+}$ (Fig. 4E and H). Neuron viability and physiological functionality was verified by glutamate application after each measurement (insets in Fig. 4C–G). This suggests that BK channels are necessary for sustained $[K^+]_i$ depression during and after cLTP induction. Surprisingly, inhibition of both, NMDAR (Fig. 4F) as well as LTCC (Fig. 4G) prevented $[K^+]_i$ reduction during cLTP by about 50% (Fig. 4H). This indicates that K^+ outflow during cLTP depends on LTCC and NMDAR as sources for the high local $[Ca^{2+}]_i$ required for BK activation. Comparison of the mean baseline between non-normalized curves of all K^+ sensitive measurements (Fig. S4F–J) revealed a comparable basal $[K^+]_i$ in both genotypes (Fig. S4K).

The sustained reduction of $[K^+]_i$ after cLTP induction (Fig. 4C) was surprising. To evaluate whether it might affect the neuronal resting membrane potential, we elicited cLTP in the presence of the membrane potential-sensitive dye $DiBAC_4(3)$ [39]. The dye enters depolarized cells leading to increased fluorescence. Upon cLTP induction by FRP, $DiBAC_4(3)$ fluorescence was not significantly affected in either $BK^{+/+}$ and PAX-inhibited $BK^{+/+}$, while glutamate application provoked a rapid and profound increase in $DiBAC_4(3)$ fluorescence (Fig. S5A–C). The fact that the membrane potential hardly changes despite a sustained K^+ efflux (Fig. 4C) might be a consequence of sustained Ca^{2+} influx through Ca^{2+} oscillations during cLTP and washout (Fig. 5A), which could offset the increased K^+ permeability to result in a constant net membrane potential.

BK supports Ca^{2+} oscillations during LTP

Although high local $[Ca^{2+}]_i$ is necessary for BK activation, BK channel activity also supports Ca^{2+} entry by rapidly repolarizing the plasma membrane to return voltage-gated Na^+ or Ca^{2+} channels into an activatable state to support fast AP firing rates [14–16]. To test this reciprocal relationship, we induced cLTP in hippocampal neurons loaded with the Ca^{2+}-sensitive dye Fura-2-AM (Fig. 5). In line with previous observations [63], spontaneous Ca^{2+} spikes were observed under basal conditions in 86% of all $BK^{+/+}$ neurons (Fig. 5A). In all $BK^{+/+}$ neurons, however, cLTP led to a significant increase in Ca^{2+} oscillation frequency that was preserved after wash-out (Fig. 5A and F). Interestingly, no spontaneous basal activity was observed in neurons lacking BK (Fig. 5B) while spiking activity in these cells was also increased by cLTP albeit at a significantly lower frequency than in $BK^{+/+}$ (Fig. 5F). When BK activity was pharmacologically blocked in $BK^{+/+}$, basal Ca^{2+} oscillations were only observed in 45% of these neurons and their frequency did not increase during or after cLTP induction (Fig. 5C and F). As expected, blocking neuronal Ca^{2+} entry through NMDAR and LTCC, by AP5 and NIFE, respectively, prevented FRP cLTP-induced increases in Ca^{2+} spiking frequency (Fig. 5D–F). Spontaneous activity was observed under NIFE, but not AP5. Comparison of mean baselines from non-normalized curves of all Ca^{2+} sensitive measurements (Fig. S6A–E) indicates equivalent basal $[Ca^{2+}]_i$ in both genotypes (Fig. S6F).

In conclusion, cLTP-provoked Ca^{2+} spikes require NMDAR and LTCC in addition to functional BK expression. Hence, the low-frequency activity of hippocampal neurons lacking BK lays basis for the impaired expression of hippocampal LTP and deficits in spatial learning and memory performances in cKO.

Discussion

Here we report efficient hippocampus-specific conditional BK deletion (cKO. Figs. 1A–C and S1A) by Cre-mediated recombination under control of the CA1-selective T29-1 Cre subline [29]. Impairment of spatial learning and memory performance in the MWM as well as reduced electrically and chemically induced hippocampal LTP in cKO (Fig. 2) confirms an earlier report of restricted MWM learning in

$BK^{-/-}$ global BK KO mice [28]. Unlike $BK^{-/-}$, however, cKO do not display motor deficits like tremor and ataxia (Fig. 1D–J and S1B–D) previously reported to affect $BK^{-/-}$ [30, 40] that might interfere with their performance in behavioral assays.

LTP expression relies on activation of postsynaptic signaling mechanisms by Ca^{2+} entry through NMDAR and LTCC [64]. This increased postsynaptic $[Ca^{2+}]_i$, in turn, promotes insertion of additional AMPAR into postsynaptic sites after phosphorylation of the GluA1 subunit at either S831 or S845 to ultimately enhance synaptic transmission efficiency [19–21, 52]. In accordance with lack of hippocampal LTP, cLTP induction in cKO failed to increase phosphorylation levels at S845 of the AMPAR subunit GluA1, while phosphorylation at S831 remained unaffected (Fig. 3A, B). Additionally, S845 phosphorylation during cLTP was sensitive to acute BK inhibition by PAX (Fig. 3C). This suggests that BK activity during LTP induction is necessary for LTP expression through GluA1 phosphorylation at S845 that, in turn, increases AMPAR conductance and exocytosis of AMPAR from intracellular compartments [21]. BK might affect protein kinase A (PKA)-mediated S845 phosphorylation by supporting postsynaptic Ca^{2+} entry through NMDAR or LTCC to activate Ca^{2+}-dependent adenylyl cyclase [65]. Alternative explanations for impaired hippocampal LTP were ruled out by confirming normal synaptic function (Fig. S2C, D) as well as AMPAR and NMDAR subunit composition in cKO (Fig. S3). Interestingly, cKO performed equal to CTRL in the reversal phase of the MWM (Fig. S2A), which tests the memory flexibility of the experimental animals. Many studies suggest that physiological LTD may be the base for proper memory flexibility [55, 56]. This stands in contrast to adult Slack KO, which are deficient in MWM reversal learning [31] and display normal LTP [38]. Thus, even as BK and Slack share high sequence homology and several topological features, both channels seem to serve very different functions in hippocampal synaptic plasticity. In addition to BK and Slack, small-conductance Ca^{2+}-activated K^+ channels (SK), which are also gated by Ca^{2+} to cause an efflux of K^+ yielding a single channel conductance of 10–20 pS, are widely expressed in central neurons including the postsynaptic membrane of glutamatergic synapses [66]. Blocking SK channels with apamin promoted hippocampal synaptic plasticity and improved spatial learning in the MWM task by reducing SK-mediated AHP to disinhibit NMDAR [67–69]. In contrast to post-synaptic BK function, these findings suggest that the repolarizing conductance provided by SK activation decreases hippocampal glutamate receptor-mediated depolarization and thereby synaptic plasticity, neuronal excitability, and memory formation [66, 70, 71]. However, apamin-sensitive SK channels are also present at intracellular sites, and they are widely distributed throughout the surface of hippocampal neurons as well as in interneurons. Thus, multiple SK channel pools may indirectly contribute to LTP expression and thereby to learning performance [72–74].

Patients carrying both gain- and loss-of-function (LOF) mutations of BK suffer from multifaceted combinations of movement and seizure disorders as well as developmental delay and intellectual disability [1]. Cognitive development and neuronal functions like learning and memory are associated with synaptic plasticity [17, 18]. Thus, our finding of impaired hippocampal LTP might explain cognitive impairment in these patients, particularly in the case of LOF mutations. Additionally interesting in this context is that reduced BK expression was associated with Alzheimer's disease (AD), while reduced LTP was demonstrated in synapses from AD patients and related mouse models [75, 76]. Accordingly, pharmacological BK activation not only rescues hippocampal LTP in a mouse model of AD but also recovers cognitive function as assessed by behavioral assays [76].

How could BK influence hippocampal synaptic plasticity in the form of LTP? LTP induction depends on postsynaptic Ca^{2+} entry. Accordingly, we observe that the frequency of spontaneous Ca^{2+} oscillations in dissociated hippocampal neuronal cultures was greatly raised by cLTP induced signaling (Fig. 5A). Concomitant to this increased Ca^{2+} spike activity, we observed a massive BK-dependent reduction in $[K^+]_i$ (Fig. 4C). We assume that this outflow of K^+ through BK is triggered by Ca^{2+} entry through NMDAR and LTCC (Fig. 4F and G). Both of these channels were previously demonstrated to physically interact with postsynaptic BK channels [7, 8] and to provide elevated local $[Ca^{2+}]_i$ necessary for BK activation [7, 9–11]. It is therefore tempting to speculate that BK activation is one of the mechanisms by which both NMDAR and LTCC exert their essential contribution to the expression of hippocampal LTP [19, 20]. In contrast, inhibition of each NMDAR and LTCC substantially reduced Ca^{2+} during cLTP (Fig. 5D and E), while the reduction of $[K^+]_i$ was still at about half the amplitude of the control (Fig. 4F–H). It is conceivable that this drop in $[K^+]_i$ is due to Ca^{2+}-independent BK activation e.g. by direct phosphorylation of BK [77] or due to altered assembly with auxiliary subunits [78]. Alternatively, each Ca^{2+} source (NMDAR and LTCC) might activate a locally associated BK population. This would slightly reduce cellular $[K^+]_i$, but not sufficiently to support LTP. Only the simultaneous activity of both Ca^{2+} sources raises global $[Ca^{2+}]_i$ sufficiently to trigger LTP and to efficiently activate BK channels.

While Ca^{2+} entry activates BK channels, we were surprised to discover that BK activity, in contrast to SK activity [70, 79], seems to support neuronal Ca^{2+} oscillations (Fig. 4C and D). This seems contradictory, as neuronal hyperpolarization by K^+ channels in general and BK in particular is thought to inhibit NMDAR as well as voltage-gated

cation channels [8, 80]. It has, however, also been proposed that BK is involved in fast repolarization after APs [14–16]. Consistent with our observations, BK inhibition was previously shown to slow the firing rate of hippocampal CA1 pyramidal cells, GABAergic neurons, and intracardiac autonomic neurons [15, 81, 82]. Others, however, reported increased firing frequencies after BK blockade in CA1 pyramidal neurons of the rat [83].

So far, we assumed neurons to act as single functional units despite their well-known morphological subdivision into different compartments. An increasing body of evidence, however, suggests specialized functions of dendritic compartments, particularly in respect to synaptic plasticity [84–87]. Fear learning-induced increases in local Ca^{2+}, for example, were found in apical but not basal dendrites of layer 2/3 (L2/3) pyramidal neurons in the mouse auditory cortex [88]. Paradoxically, just in those apical dendrites an inactivating function of BK could be observed [89], which consequently leads to decrease in neuronal excitation as BK is activated by Ca^{2+} spikes mediated by NMDAR [90] and voltage-gated Ca^{2+} channels [91]. This contrasts with our findings suggesting positive feedback involvement of somatic BK in LTP through fAHP (Figs. 4C and 5A). While this seems like a contradiction at first glance, dendritic BK may nevertheless support increased plasticity through three factors. First, by hyperpolarizing the membrane potential, BK could impede the triggering of action potentials by synaptic inputs [89]. This could increase the specificity of synaptic potentiation, as only closely tuned inputs can cross the increased threshold [92]. Next, excessive and thus neurotoxic Ca^{2+} accumulation may be prevented, so that fewer synapses or dendrites perish [12]. Lastly, hyperpolarization in apical dendrites by BK may influence the timing of postsynaptic potentials and Ca^{2+} spikes to optimize temporal coding and signal summation, which might facilitate coincidence detection and thus also the occurrence of LTP [93].

Based on the presented data we propose a mechanism by which BK is activated by Ca^{2+} entry through both NMDAR and LTCC in postsynaptic membranes. BK-mediated K^+ outflow, in turn, amplifies Ca^{2+} spiking frequency, which facilitates Ca^{2+} entry in support of the Ca^{2+}-mediated mechanisms ultimately leading to AMPAR phosphorylation and LTP expression.

Supplementary Information The online version contains supplementary material available at https://doi.org/10.1007/s00018-023-05016-y.

Acknowledgements We thank John Dempster for WinWCP as well as Clement Kabagema-Bilan and Michael Glaser for excellent technical support.

Author contributions TP, HB, LM and RL designed experiments, TP, TH, DC, DSp, DK and SS performed experiments. TP, TH, DC, DSp, DK, SS and LM analyzed data. HB, DSk, MCS, SM, MK, BG, RE and NP contributed resources, materials and protocols. PR, RL and LM contributed to discussions. TP and LM wrote the manuscript. TP, RL and LM edited the manuscript. PR, RL and LM obtained funding. RL and LM supervised the project. All authors approved the content and submission of the paper.

Funding Open Access funding enabled and organized by Projekt DEAL. This work was supported by the Deutsche Forschungsgemeinschaft (DFG) with individual grants to LM and RL. TP, TH, DC, MCS, MK, PR and RL were supported by GRK2381: "cGMP: From Bedside to Bench", DFG Grant Number 335549539. HB is a fellow of the Austrian Science Fund (FWF) funded Erwin-Schrödinger-Program, project number J4457. LM received support from the Wilhelm Schuler-Stiftung of the University of Tübingen.

Availability of data and materials All data generated or analyzed during this study that are not included in this published article and its supplementary information files are available from the corresponding authors on reasonable request. Further information and requests for resources and reagents should be directed to and will be fulfilled either by the Lead Contact, Lucas Matt (lucas.matt@uni-tuebingen.de) or by Robert Lukowski (robert.lukowski@uni-tuebingen.de). This study includes no data deposited in external repositories.

Declarations

Conflict of interest RL has a cooperation with Cyclerion Therapeutics Inc. on a topic not directly related to this study. All other authors authors have stated explicitly that there are no conflicts of interest in connection with this article.

Ethical approval All experimental procedures were conducted in accordance with the animal protection laws in Germany and were approved by the local Ethics Committee for Animal Research (Regierungspräsidium Tübingen).

References

1. Miller JP, Moldenhauer HJ, Keros S, Meredith AL (2021) An emerging spectrum of variants and clinical features in KCNMA1-linked channelopathy. Channels (Austin) 15(1):447–464. https://doi.org/10.1080/19336950.2021.1938852
2. Laumonnier F, Roger S, Guerin P, Molinari F, M'Rad R, Cahard D et al (2006) Association of a functional deficit of the BKCa channel, a synaptic regulator of neuronal excitability, with autism and mental retardation. Am J Psychiatry 163(9):1622–1629. https://doi.org/10.1176/ajp.2006.163.9.1622
3. Zhang L, Li X, Zhou R, Xing G (2006) Possible role of potassium channel, big K in etiology of schizophrenia. Med Hypotheses 67(1):41–43. https://doi.org/10.1016/j.mehy.2005.09.055

4. Sausbier U, Sausbier M, Sailer CA, Arntz C, Knaus H-G, Neuhuber W et al (2005) Ca^{2+}-activated K^+ channels of the BK-type in the mouse brain. Histochem Cell Biol 125(6):725. https://doi.org/10.1007/s00418-005-0124-7
5. Misonou H, Menegola M, Buchwalder L, Park EW, Meredith A, Rhodes KJ et al (2006) Immunolocalization of the Ca^{2+}-activated K^+ channel Slo1 in axons and nerve terminals of mammalian brain and cultured neurons. J Compar Neurol 496(3):289–302. https://doi.org/10.1002/cne.20931
6. Sailer CA, Kaufmann WA, Kogler M, Chen L, Sausbier U, Ottersen OP et al (2006) Immunolocalization of BK channels in hippocampal pyramidal neurons. Eur J Neurosci 24(2):442–454. https://doi.org/10.1111/j.1460-9568.2006.04936.x
7. Berkefeld H, Sailer CA, Bildl W, Rohde V, Thumfart JO, Eble S et al (2006) BKCa-Cav channel complexes mediate rapid and localized Ca^{2+}-activated K^+ signaling. Science 314(5799):615–620. https://doi.org/10.1126/science.1132915
8. Zhang J, Guan X, Li Q, Meredith AL, Pan HL, Yan J (2018) Glutamate-activated BK channel complexes formed with NMDA receptors. Proc Natl Acad Sci USA 115(38):E9006–E9014. https://doi.org/10.1073/pnas.1802567115
9. Berkefeld H, Fakler B (2013) Ligand-gating by Ca^{2+} is rate limiting for physiological operation of BK(Ca) channels. J Neurosci 33(17):7358–7367. https://doi.org/10.1523/JNEUROSCI.5443-12.2013
10. Perez GJ, Bonev AD, Nelson MT (2001) Micromolar Ca(2+) from sparks activates Ca(2+)-sensitive K(+) channels in rat cerebral artery smooth muscle. Am J Physiol Cell Physiol 281(6):C1769–C1775. https://doi.org/10.1152/ajpcell.2001.281.6.C1769
11. Shah KR, Guan X, Yan J (2021) Structural and functional coupling of calcium-activated BK channels and calcium-permeable channels within nanodomain signaling complexes. Front Physiol 12:796540. https://doi.org/10.3389/fphys.2021.796540
12. Hu H, Shao LR, Chavoshy S, Gu N, Trieb M, Behrens R et al (2001) Presynaptic Ca^{2+}-activated K^+ channels in glutamatergic hippocampal terminals and their role in spike repolarization and regulation of transmitter release. J Neurosci 21(24):9585–9597. https://doi.org/10.1523/JNEUROSCI.21-24-09585.2001
13. Contet C, Goulding SP, Kuljis DA, Barth AL (2016) BK channels in the central nervous system. Int Rev Neurobiol 128:281–342. https://doi.org/10.1016/bs.irn.2016.04.001
14. Storm JF (1987) Action potential repolarization and a fast after-hyperpolarization in rat hippocampal pyramidal cells. J Physiol 385:733–759. https://doi.org/10.1113/jphysiol.1987.sp016517
15. Gu N, Vervaeke K, Storm JF (2007) BK potassium channels facilitate high-frequency firing and cause early spike frequency adaptation in rat CA1 hippocampal pyramidal cells. J Physiol 580(Pt.3):859–882. https://doi.org/10.1113/jphysiol.2006.126367
16. Jin W, Sugaya A, Tsuda T, Ohguchi H, Sugaya E (2000) Relationship between large conductance calcium-activated potassium channel and bursting activity. Brain Res 860(1–2):21–28. https://doi.org/10.1016/s0006-8993(00)01943-0
17. Volk L, Chiu SL, Sharma K, Huganir RL (2015) Glutamate synapses in human cognitive disorders. Annu Rev Neurosci 38:127–149. https://doi.org/10.1146/annurev-neuro-071714-033821
18. Takeuchi T, Duszkiewicz AJ, Morris RG (2014) The synaptic plasticity and memory hypothesis: encoding, storage and persistence. Philos Trans R Soc Lond B Biol Sci 369(1633):20130288. https://doi.org/10.1098/rstb.2013.0288
19. Freir DB, Herron CE (2003) Inhibition of l-type voltage dependent calcium channels causes impairment of long-term potentiation in the hippocampal CA1 region in vivo. Brain Res 967(1–2):27–36. https://doi.org/10.1016/s0006-8993(02)04190-2
20. Malenka RC (1991) Postsynaptic factors control the duration of synaptic enhancement in area CA1 of the hippocampus. Neuron 6(1):53–60. https://doi.org/10.1016/0896-6273(91)90121-f
21. Diering GH, Huganir RL (2018) The AMPA receptor code of synaptic plasticity. Neuron 100(2):314–329. https://doi.org/10.1016/j.neuron.2018.10.018
22. Lisman J, Buzsaki G, Eichenbaum H, Nadel L, Ranganath C, Redish AD (2017) Viewpoints: how the hippocampus contributes to memory, navigation and cognition. Nat Neurosci 20(11):1434–1447. https://doi.org/10.1038/nn.4661
23. Kim JH, Lee HK, Takamiya K, Huganir RL (2003) The role of synaptic GTPase-activating protein in neuronal development and synaptic plasticity. J Neurosci 23(4):1119–1124
24. Komiyama NH, Watabe AM, Carlisle HJ, Porter K, Charlesworth P, Monti J et al (2002) SynGAP regulates ERK/MAPK signaling, synaptic plasticity, and learning in the complex with postsynaptic density 95 and NMDA receptor. J Neurosci 22(22):9721–9732
25. Nadif Kasri N, Nakano-Kobayashi A, Malinow R, Li B, Van Aelst L (2009) The Rho-linked mental retardation protein oligophrenin-1 controls synapse maturation and plasticity by stabilizing AMPA receptors. Genes Dev 23(11):1289–1302. https://doi.org/10.1101/gad.1783809
26. Nadif Kasri N, Nakano-Kobayashi A, Van Aelst L (2011) Rapid synthesis of the X-linked mental retardation protein OPHN1 mediates mGluR-dependent LTD through interaction with the endocytic machinery. Neuron 72(2):300–315. https://doi.org/10.1016/j.neuron.2011.09.001
27. Matthews EA, Disterhoft JF (2009) Blocking the BK channel impedes acquisition of trace eyeblink conditioning. Learn Mem 16(2):106–109. https://doi.org/10.1101/lm.1289809
28. Typlt M, Mirkowski M, Azzopardi E, Ruettiger L, Ruth P, Schmid S (2013) Mice with deficient BK channel function show impaired prepulse inhibition and spatial learning, but normal working and spatial reference memory. PLoS One 8(11):e81270. https://doi.org/10.1371/journal.pone.0081270
29. Tsien JZ, Chen DF, Gerber D, Tom C, Mercer EH, Anderson DJ et al (1996) Subregion- and cell type-restricted gene knockout in mouse brain. Cell 87(7):1317–1326. https://doi.org/10.1016/s0092-8674(00)81826-7
30. Sausbier M, Hu H, Arntz C, Feil S, Kamm S, Adelsberger H et al (2004) Cerebellar ataxia and Purkinje cell dysfunction caused by Ca^{2+}-activated K^+ channel deficiency. Proc Natl Acad Sci USA 101(25):9474–9478. https://doi.org/10.1073/pnas.0401702101
31. Bausch AE, Dieter R, Nann Y, Hausmann M, Meyerdierks N, Kaczmarek LK et al (2015) The sodium-activated potassium channel Slack is required for optimal cognitive flexibility in mice. Learn Mem 22(7):323–335. https://doi.org/10.1101/lm.037820.114
32. Otmakhov N, Khibnik L, Otmakhova N, Carpenter S, Riahi S, Asrican B et al (2004) Forskolin-induced LTP in the CA1 hippocampal region is NMDA receptor dependent. J Neurophysiol 91(5):1955–1962. https://doi.org/10.1152/jn.00941.2003
33. Kopec CD, Li B, Wei W, Boehm J, Malinow R (2006) Glutamate receptor exocytosis and spine enlargement during chemically induced long-term potentiation. J Neurosci 26(7):2000–2009. https://doi.org/10.1523/JNEUROSCI.3918-05.2006
34. Beaudoin GM 3rd, Lee SH, Singh D, Yuan Y, Ng YG, Reichardt LF et al (2012) Culturing pyramidal neurons from the early postnatal mouse hippocampus and cortex. Nat Protoc 7(9):1741–1754. https://doi.org/10.1038/nprot.2012.099
35. Ehinger R, Kuret A, Matt L, Frank N, Wild K, Kabagema-Bilan C et al (2021) Slack K(+) channels attenuate NMDA-induced excitotoxic brain damage and neuronal cell death. FASEB J 35(5):e21568. https://doi.org/10.1096/fj.202002308RR
36. Bischof H, Rehberg M, Stryeck S, Artinger K, Eroglu E, Waldeck-Weiermair M et al (2017) Novel genetically encoded fluorescent probes enable real-time detection of potassium in vitro

and in vivo. Nat Commun 8(1):1422. https://doi.org/10.1038/s41467-017-01615-z
37. Bischof H, Burgstaller S, Springer A, Matt L, Rauter T, Bachkonig OA et al (2021) Potassium ions promote hexokinase-II dependent glycolysis. iScience 24(4):102346. https://doi.org/10.1016/j.isci.2021.102346
38. Matt L, Pham T, Skrabak D, Hoffmann F, Eckert P, Yin J et al (2021) The Na^+-activated K^+ channel Slack contributes to synaptic development and plasticity. Cell Mol Life Sci 78(23):7569–7587. https://doi.org/10.1007/s00018-021-03953-0
39. Bräuner T, Hülser DF, Strasser RJ (1984) Comparative measurements of membrane potentials with microelectrodes and voltage-sensitive dyes. Biochim Biophys Acta 771(2):208–216. https://doi.org/10.1016/0005-2736(84)90535-2
40. Chen X, Kovalchuk Y, Adelsberger H, Henning HA, Sausbier M, Wietzorrek G et al (2010) Disruption of the olivo-cerebellar circuit by Purkinje neuron-specific ablation of BK channels. Proc Natl Acad Sci USA 107(27):12323–12328. https://doi.org/10.1073/pnas.1001745107
41. Morris RG, Anderson E, Lynch GS, Baudry M (1986) Selective impairment of learning and blockade of long-term potentiation by an *N*-methyl-D-aspartate receptor antagonist, AP5. Nature 319(6056):774–776. https://doi.org/10.1038/319774a0
42. Tsien JZ, Huerta PT, Tonegawa S (1996) The essential role of hippocampal CA1 NMDA receptor-dependent synaptic plasticity in spatial memory. Cell 87(7):1327–1338. https://doi.org/10.1016/s0092-8674(00)81827-9
43. Goto A, Bota A, Miya K, Wang J, Tsukamoto S, Jiang X et al (2021) Stepwise synaptic plasticity events drive the early phase of memory consolidation. Science 374(6569):857–863. https://doi.org/10.1126/science.abj9195
44. Lu R, Lukowski R, Sausbier M, Zhang DD, Sisignano M, Schuh CD et al (2014) BKCa channels expressed in sensory neurons modulate inflammatory pain in mice. Pain 155(3):556–565. https://doi.org/10.1016/j.pain.2013.12.005
45. Carter RJ, Morton J, Dunnett SB (2001) Motor coordination and balance in rodents. Curr Protoc Neurosci. https://doi.org/10.1002/0471142301.ns0812s15
46. Gould TD, Dao DT, Kovacsics CE. The open field test. Mood and anxiety related phenotypes in mice: characterization using behavioral tests. 2009;42:1–20.https://doi.org/10.1007/978-1-60761-303-9_1
47. Prut L, Belzung C (2003) The open field as a paradigm to measure the effects of drugs on anxiety-like behaviors: a review. Eur J Pharmacol 463(1–3):3–33. https://doi.org/10.1016/s0014-2999(03)01272-x
48. Choleris E, Thomas AW, Kavaliers M, Prato FS (2001) A detailed ethological analysis of the mouse open field test: effects of diazepam, chlordiazepoxide and an extremely low frequency pulsed magnetic field. Neurosci Biobehav Rev 25(3):235–260. https://doi.org/10.1016/s0149-7634(01)00011-2
49. Ivanova E, Hwang GS, Pan ZH (2010) Characterization of transgenic mouse lines expressing Cre recombinase in the retina. Neuroscience 165(1):233–243. https://doi.org/10.1016/j.neuroscience.2009.10.021
50. Tanimoto N, Sothilingam V, Euler T, Ruth P, Seeliger MW, Schubert T (2012) BK channels mediate pathway-specific modulation of visual signals in the in vivo mouse retina. J Neurosci 32(14):4861–4866. https://doi.org/10.1523/jneurosci.4654-11.2012
51. Vorhees CV, Williams MT (2006) Morris water maze: procedures for assessing spatial and related forms of learning and memory. Nat Protoc 1(2):848–858. https://doi.org/10.1038/nprot.2006.116
52. Citri A, Malenka RC (2008) Synaptic plasticity: multiple forms, functions, and mechanisms. Neuropsychopharmacology 33(1):18–41. https://doi.org/10.1038/sj.npp.1301559
53. Nelissen E, Argyrousi EK, Van Goethem NP, Zhao F, Hines CDG, Swaminath G et al (2021) Soluble guanylate cyclase stimulator vericiguat enhances long-term memory in rats without altering cerebral blood volume. Biomedicines. https://doi.org/10.3390/biomedicines9081047
54. Diering GH, Heo S, Hussain NK, Liu B, Huganir RL (2016) Extensive phosphorylation of AMPA receptors in neurons. Proc Natl Acad Sci USA 113(33):E4920–E4927. https://doi.org/10.1073/pnas.1610631113
55. Nicholls RE, Alarcon JM, Malleret G, Carroll RC, Grody M, Vronskaya S et al (2008) Transgenic mice lacking NMDAR-dependent LTD exhibit deficits in behavioral flexibility. Neuron 58(1):104–117. https://doi.org/10.1016/j.neuron.2008.01.039
56. Collingridge GL, Peineau S, Howland JG, Wang YT (2010) Long-term depression in the CNS. Nat Rev Neurosci 11(7):459–473. https://doi.org/10.1038/nrn2867
57. Hansen KB, Yi F, Perszyk RE, Menniti FS, Traynelis SF (2017) NMDA receptors in the central nervous system. Methods Mol Biol 1677:1–80. https://doi.org/10.1007/978-1-4939-7321-7_1
58. Traynelis SF, Wollmuth LP, McBain CJ, Menniti FS, Vance KM, Ogden KK et al (2010) Glutamate receptor ion channels: structure, regulation, and function. Pharmacol Rev 62(3):405–496. https://doi.org/10.1124/pr.109.002451
59. Zhao Y, Chen S, Swensen AC, Qian WJ, Gouaux E (2019) Architecture and subunit arrangement of native AMPA receptors elucidated by cryo-EM. Science 364(6438):355–362. https://doi.org/10.1126/science.aaw8250
60. Lee HK, Takamiya K, Han JS, Man H, Kim CH, Rumbaugh G et al (2003) Phosphorylation of the AMPA receptor GluR1 subunit is required for synaptic plasticity and retention of spatial memory. Cell 112(5):631–643. https://doi.org/10.1016/s0092-8674(03)00122-3
61. Oh MC, Derkach VA, Guire ES, Soderling TR (2006) Extrasynaptic membrane trafficking regulated by GluR1 serine 845 phosphorylation primes AMPA receptors for long-term potentiation. J Biol Chem 281(2):752–758. https://doi.org/10.1074/jbc.M509677200
62. Esteban JA, Shi SH, Wilson C, Nuriya M, Huganir RL, Malinow R (2003) PKA phosphorylation of AMPA receptor subunits controls synaptic trafficking underlying plasticity. Nat Neurosci 6(2):136–143. https://doi.org/10.1038/nn997
63. Dravid SM, Murray TF (2004) Spontaneous synchronized calcium oscillations in neocortical neurons in the presence of physiological [Mg(2+)]: involvement of AMPA/kainate and metabotropic glutamate receptors. Brain Res 1006(1):8–17. https://doi.org/10.1016/j.brainres.2004.01.059
64. Malenka RC (1991) The role of postsynaptic calcium in the induction of long-term potentiation. Mol Neurobiol 5(2–4):289–295. https://doi.org/10.1007/BF02935552
65. Lu HC, She WC, Plas DT, Neumann PE, Janz R, Crair MC (2003) Adenylyl cyclase I regulates AMPA receptor trafficking during mouse cortical 'barrel' map development. Nat Neurosci 6(9):939–947. https://doi.org/10.1038/nn1106
66. Adelman JP, Maylie J, Sah P (2012) Small-conductance Ca^{2+}-activated K^+ channels: form and function. Annu Rev Physiol 74(1):245–269. https://doi.org/10.1146/annurev-physiol-020911-153336
67. Norris CM, Halpain S, Foster TC (1998) Reversal of age-related alterations in synaptic plasticity by blockade of L-type Ca^{2+} channels. J Neurosci 18(9):3171–3179. https://doi.org/10.1523/JNEUROSCI.18-09-03171.1998
68. Stackman RW, Hammond RS, Linardatos E, Gerlach A, Maylie J, Adelman JP et al (2002) Small conductance Ca^{2+}-activated K^+

channels modulate synaptic plasticity and memory encoding. J Neurosci 22(23):10163–10171. https://doi.org/10.1523/JNEUROSCI.22-23-10163.2002
69. Kramar EA, Lin B, Lin CY, Arai AC, Gall CM, Lynch G (2004) A novel mechanism for the facilitation of theta-induced long-term potentiation by brain-derived neurotrophic factor. J Neurosci 24(22):5151–5161. https://doi.org/10.1523/JNEUROSCI.0800-04.2004
70. Ngo-Anh TJ, Bloodgood BL, Lin M, Sabatini BL, Maylie J, Adelman JP (2005) SK channels and NMDA receptors form a Ca2+-mediated feedback loop in dendritic spines. Nat Neurosci 8(5):642–649. https://doi.org/10.1038/nn1449
71. Tigaret CM, Olivo V, Sadowski J, Ashby MC, Mellor JR (2016) Coordinated activation of distinct Ca(2+) sources and metabotropic glutamate receptors encodes Hebbian synaptic plasticity. Nat Commun 7:10289. https://doi.org/10.1038/ncomms10289
72. Behnisch T, Reymann KG (1998) Inhibition of apamin-sensitive calcium dependent potassium channels facilitate the induction of long-term potentiation in the CA1 region of rat hippocampus in vitro. Neurosci Lett 253(2):91–94. https://doi.org/10.1016/s0304-3940(98)00612-0
73. McKay BM, Oh MM, Disterhoft JF (2013) Learning increases intrinsic excitability of hippocampal interneurons. J Neurosci 33(13):5499–5506. https://doi.org/10.1523/JNEUROSCI.4068-12.2013
74. Lujan R, Merchan-Perez A, Soriano J, Martin-Belmonte A, Aguado C, Alfaro-Ruiz R et al (2021) Neuron class and target variability in the three-dimensional localization of SK2 channels in hippocampal neurons as detected by immunogold FIB-SEM. Front Neuroanat 15:781314. https://doi.org/10.3389/fnana.2021.781314
75. Prieto GA, Trieu BH, Dang CT, Bilousova T, Gylys KH, Berchtold NC et al (2017) Pharmacological rescue of long-term potentiation in Alzheimer diseased synapses. J Neurosci 37(5):1197–1212. https://doi.org/10.1523/JNEUROSCI.2774-16.2016
76. Wang L, Kang H, Li Y, Shui Y, Yamamoto R, Sugai T et al (2015) Cognitive recovery by chronic activation of the large-conductance calcium-activated potassium channel in a mouse model of Alzheimer's disease. Neuropharmacology 92:8–15. https://doi.org/10.1016/j.neuropharm.2014.12.033
77. Reinhart P, Chung S, Martin B, Brautigan D, Levitan I (1991) Modulation of calcium-activated potassium channels from rat brain by protein kinase A and phosphatase 2A. J Neurosci 11(6):1627–1635. https://doi.org/10.1523/jneurosci.11-06-01627.1991
78. Li Q, Yan J (2016) Modulation of BK channel function by auxiliary beta and gamma subunits. Int Rev Neurobiol 128:51–90. https://doi.org/10.1016/bs.irn.2016.03.015
79. Titley HK, Brunel N, Hansel C (2017) Toward a neurocentric view of learning. Neuron 95(1):19–32. https://doi.org/10.1016/j.neuron.2017.05.021
80. Gomez R, Maglio LE, Gonzalez-Hernandez AJ, Rivero-Perez B, Bartolome-Martin D, Giraldez T (2021) NMDA receptor-BK channel coupling regulates synaptic plasticity in the barrel cortex. Proc Natl Acad Sci USA 118(35):e2107026118. https://doi.org/10.1073/pnas.2107026118
81. Gittis AH, Moghadam SH, du Lac S (2010) Mechanisms of sustained high firing rates in two classes of vestibular nucleus neurons: differential contributions of resurgent Na, Kv3, and BK currents. J Neurophysiol 104(3):1625–1634. https://doi.org/10.1152/jn.00378.2010
82. Perez GJ, Desai M, Anderson S, Scornik FS (2013) Large-conductance calcium-activated potassium current modulates excitability in isolated canine intracardiac neurons. Am J Physiol Cell Physiol 304(3):C280–C286. https://doi.org/10.1152/ajpcell.00148.2012
83. Matthews EA, Weible AP, Shah S, Disterhoft JF (2008) The BK-mediated fAHP is modulated by learning a hippocampus-dependent task. Proc Natl Acad Sci USA 105(39):15154–15159. https://doi.org/10.1073/pnas.0805855105
84. Beaulieu-Laroche L, Toloza EHS, van der Goes M-S, Lafourcade M, Barnagian D, Williams ZM et al (2018) Enhanced dendritic compartmentalization in human cortical neurons. Cell 175(3):643–51.e14. https://doi.org/10.1016/j.cell.2018.08.045
85. Poirazi P, Brannon T, Mel BW (2003) Pyramidal neuron as two-layer neural network. Neuron 37(6):989–999. https://doi.org/10.1016/S0896-6273(03)00149-1
86. Petreanu L, Mao T, Sternson SM, Svoboda K (2009) The subcellular organization of neocortical excitatory connections. Nature 457(7233):1142–1145. https://doi.org/10.1038/nature07709
87. Makino H, Komiyama T (2015) Learning enhances the relative impact of top-down processing in the visual cortex. Nat Neurosci 18(8):1116–1122. https://doi.org/10.1038/nn.4061
88. Godenzini L, Shai AS, Palmer LM (2022) Dendritic compartmentalization of learning-related plasticity. Eneuro 9(3):ENEURO.0060-22.2022. https://doi.org/10.1523/eneuro.0060-22.2022
89. Bock T, Stuart GJ (2016) The impact of BK channels on cellular excitability depends on their subcellular location. Front Cell Neurosci 10:206. https://doi.org/10.3389/fncel.2016.00206
90. Antic SD, Zhou WL, Moore AR, Short SM, Ikonomu KD (2010) The decade of the dendritic NMDA spike. J Neurosci Res 88(14):2991–3001. https://doi.org/10.1002/jnr.22444
91. Westenbroek RE, Hell JW, Warner C, Dubel SJ, Snutch TP, Catterall WA (1992) Biochemical properties and subcellular distribution of an N-type calcium channel alpha 1 subunit. Neuron 9(6):1099–1115. https://doi.org/10.1016/0896-6273(92)90069-p
92. Sjöström PJ, Rancz EA, Roth A, Häusser M (2008) Dendritic excitability and synaptic plasticity. Physiol Rev 88(2):769–840. https://doi.org/10.1152/physrev.00016.2007
93. Xu N-l, Ye C-q, Poo M-m, Zhang X-h (2006) Coincidence detection of synaptic inputs is facilitated at the distal dendrites after long-term potentiation induction. J Neurosci 26(11):3002–3009. https://doi.org/10.1523/jneurosci.5220-05.2006